Khadijeh Nekoueian

MODIFICATION OF CARBON-BASED ELECTRODES USING METAL NANOSTRUCTURES: APPLICATION TO VOLTAMMETRIC DETERMINATION OF SOME PHARMACEUTICAL AND BIOLOGICAL COMPOUNDS

ACTA UNIVERSITATIS LAPPEENRANTAENSIS 862

Khadijeh Nekoueian

MODIFICATION OF CARBON-BASED ELECTRODES USING METAL NANOSTRUCTURES: APPLICATION TO VOLTAMMETRIC DETERMINATION OF SOME PHARMACEUTICAL AND BIOLOGICAL COMPOUNDS

Dissertation for the degree of Doctor of Science (Technology) to be presented with due permission for public examination and criticism in the Auditorium in Mikkeli University Consortium, MUC at Lappeenranta-Lahti University of Technology LUT, Mikkeli, Finland on the 16th of August, 2019, at noon.

Acta Universitatis
Lappeenrantaensis 862

Supervisors Professor Mika Sillanpää
LUT School of Engineering Science
Lappeenranta-Lahti University of Technology LUT
Finland

Professor Mandana Amiri
Department of Chemistry
University of Mohaghegh Ardabili
Iran

Reviewers Professor Sabine Szunerits
Department of Chemistry
Institute of Electronic, Microelectronic Nanotechnology
University of Lille 1
France

Professor Jay D. Wadhawan
Department of Science and Engineering
University of Hull
United Kingdom

Opponent Doctor Sara Dale
Department of Physics
University of Bath
United Kingdom

ISBN 978-952-335-394-7
ISBN 978-952-335-395-4 (PDF)
ISSN-L 1456-4491
ISSN 1456-4491

Lappeenranta-Lahti University of Technology LUT
LUT University Press 2019

Abstract

Khadijeh Nekoueian
Modification of carbon-based electrodes using metal nanostructures: Application to voltammetric determination of some pharmaceutical and biological compounds
Mikkeli 2019
95 pages
Acta Universitatis Lappeenrantaensis 862
Diss. Lappeenranta-Lahti University of Technology LUT
ISBN 978-952-335-394-7, ISBN 978-952-335-395-4 (PDF), ISSN-L 1456-4491, ISSN 1456-4491

In this study, new modified carbon-based electrodes were fabricated and applied in the detection and determination of several medicines and water pollutants. Modification enhanced the use of these electrodes for analytical measurements. A modified carbon paste electrode and modified glassy carbon electrode were applied as desired working electrodes. Different modifiers such as KolliphorEL, gold/palladium/multi-walled carbon nanotubes nanocomposite, palladium nanoparticles and carbon-modified titanium dioxide nanocomposite were synthesised using chemical and electrochemical methods and were characterised using different techniques such as scanning electron microscopy (SEM), X-ray photoelectron spectroscopy (XPS), X-ray diffraction (XRD) and Fourier transform infrared techniques (FTIR). Then, these prepared modifiers were employed to modify the surface or matrix of the carbon-based electrodes. Electrochemical impedance spectroscopy and cyclic voltammetry methods were utilised to investigate the effect of the modification on the rate of the electron transfer at the modified electrodes.

The modified carbon-based electrodes were employed efficiently to determine trace amounts of pharmaceutical and biological compounds by using voltammetric methods such as differential pulse voltammetry. The experimental conditions of the voltammetric measurements such as the pH of the buffered solutions and potential sweep rate were optimised to obtain a well-defined response signal.

Keywords: modified carbon-based electrodes, cobalt/polyaniline nanocomposite, kolliphorEL, gold/palladium/multi-walled carbon nanotubes nanocomposite, palladium nanoparticles, carbon-modified titanium dioxide nanocomposite, voltammetric determination, ferrocene derivatives, methylene blue.

Acknowledgements

This work was carried out at the School of Engineering Science at Lappeenranta University of Technology, Finland, between 2013 and 2018.

I would like to express my sincere gratitude to Prof. Mika Sillanpää who believed in me and gave me a valuable opportunity to work in the Department of Green Chemistry, complete my PhD studies and develop my skills. I am grateful for his support, guidance and supervision.

I would like to sincerely thank Dr. Mandana Amiri for her endless support, encouragement, supervision and help. I am very grateful to her as she guided and helped me with kindness at all stages of my studies. Dear Mandana, many thanks!

I would also like to express my sincere thanks to Prof. Frank Marken who gave me a valuable chance to visit his laboratory and learn electrochemical impedance spectroscopy. The time that I worked with him was so worthwhile. I am so grateful for his impressive support during my visit.

I would like to thank all my colleagues and friends at the Department of Green Chemistry, the Marken group at Bath University and the Amiri group at Mohaghegh Ardebili University. Special thanks also to Mikko Rantalankila, Dr. Ali Ayati, Dr. Bahareh Tanhaee, Dr. Heikki Särkkä and Dr. Shila Jafari who were very supportive and helpful during my stay abroad. Their support and friendship were invaluable.

I would sincerely like to thank Dr. Christopher Edward Hotchen for his contribution toward KolliphorEL monolayer modified electrode, Mrs. Yasaman Sefidehkhan for her work on the modification of the carbon paste electrode using palladium NPs and Dr. Shila Jafari for synthesising the carbon-modified TiO_2 nanostructures.

I would like to express my special appreciation and thanks to my parents for their unconditional love and support during these years, and to my brother and sister who were always helpful. My warmest thanks go to my husband, Masoud, who supported me and encouraged me to continue despite difficulties. I would also like to extend my warmest thanks to my lovely son, Ryan, who is my happiness. I would not have been able to complete my PhD without their love, help and sacrifices.

Khadijeh Nekoueian
August 2019
Mikkeli, Finland

Contents

List of publications

This dissertation is based on the following papers. The rights have been granted by publishers to include the papers in dissertation.

I. Nekoueian, K., Hotchen, CE., Amiri, M., Sillanpää, M., Nelson, GW. Foord, JS., Holdway, P., Buchard, A., Parker, SC., Marken, F. (2015). Interfacial electron-shuttling processes across KolliphorEL monolayer grafted electrodes. *Applied Materials & Interfaces*, 7, pp.15458-15465.

II. Nekoueian, K., Amiri,M., Sillanpää, M. (2017). Carbon paste electrode with Au/Pd/MWCNT nanocomposite for nanomolar determination of Timolol. *International Journal of Electrochemical Science*, 12, PP.1612-1624.

III. Sefid-sefidehkhan[1], Y., Nekoueian[1], K., Amiri, M., Sillanpää, M., Eskandari, H. (2017). Palladium nanoparticles in electrochemical sensing of trace terazosin in human serum and pharmaceutical preparations. *Materials Science and Engineering C*, 75 pp. 368–374.
[1] Y. S and K. N are both first authors with equal contribution

IV. Nekoueian, K., Jafari, S., Amiri, M., Sillanpää, M. (2018). Pre adsorbed Methylene blue at carbon-modified TiO_2 electrode: application for lead sensing in water. IEEE Sensors Journal, 18(23), pp. 9477-9485.

Other publications are:

I. Amiri, M., Nekoueian, K., Bezaatpour, A. (2012). Nanomolar determination of penicillamine by using a novel cobalt /polyaniline/carbon paste nanocomposite electrode. *Electroanalysis*, 24, pp. 2186.

II. Amiri, M., Bezaatpour, A., Pakdel, Z., Nekoueian, K. (2012). Simultaneous voltammetric determination of uric acid and ascorbic acid using carbon paste/cobalt Schiff base composite electrode. *Journal of solid state electrochemistry*, 16, PP.2178.

III. Amiri, M., Alimoradi, M., Nekoueian, K., Bezaatpour, A. (2012). Cobalt flower like nanostructure as modifier for voltammetric determination of chloropheniramine. *Industrial and Engineering Chemistry Research*. 51, PP. 14317.

IV. Amiri, M., Alimoradi, M., Nekoueian, K. (2012). Voltammetric determination of acetaminophen by using carbon paste electrode modified by hierarchically structured cobalt. *Journal of Semnan Applied Chemistry (In Persian)*, 7, PP. 9-19.

V. Nekoueian, K., Amiri, M., Sillanpää, M., Marken, F., Boukherroub, R., Szunerits, S. (2019). Carbon-Based Quantum Particles: An Electroanalytical and Biomedical Perspective. *Chemical Society Reviews.*

Author's contribution

K. N did most of the experiments, analysed the data of papers I –IV and wrote the first draft of papers II –IV. Prof. Frank Marken wrote the first draft of paper I. C. H kindly contributed to analysing the data of paper I and Y. S contributed in paper III.

Nomenclature

Latin alphabet

A	electrode area	cm^2
a	constant	–
C	concentration of the analyte	mol cm^{-3}
D	diffusion coefficient	cm^2 s^{-1}
d	diameter	m
$E_{p,a}$	cyclic voltammetric anodic peak potential	V
$E_{p,c}$	cyclic voltammetric cathodic peak potential	V
f	frequency	Hz
$I_{p,a}$	cyclic voltammetric anodic peak current	A
$I_{p,c}$	cyclic voltammetric cathodic peak current	A
L	characteristic length	m
N	number of particles	–
n	numbers of moles of electro involved in the redox reaction	
R_{et}	electron transfer resistance	Ω
r	radius	m
T	temperature	K
t	time	s
V	volume	m^3
Z	impedance value	Ω

Greek alphabet

Δ	separation	
v	scan rate	V s^{-1}
φ	phase shift	
Ω	Ohms	

Abbreviations

AFM	atomic force microscopy
C	capacitors
CFMs	carbon fibre microelectrodes
CMEs	chemically modified electrodes
CMTN	carbon-modified titanium dioxide nanostructured
Co	cobalt
CPE	carbon paste electrode
CPE	constant phase element
CPs	conducting polymers
Cu	copper
YHA	Algerian humic acid
EDA	ethylenediamine
TETA	triethylenetetramine
CV	cyclic voltammetry
D	dimensions
DPV	differential pulse voltammetry
EDS	energy-dispersive X-Ray spectroscopy
EIS	electrochemical impedance spectroscopy
Fc	ferrocene
FTIR	fourier transform infrared

GCE	glassy carbon electrode
I	inductors
M	metal
MB	methylene blue
MIP	molecularly imprinted polymer
MPS	mesoporous silica
MWCNT	multi wall carbon nanotube
NPs	nanoparticles
PANI	polyaniline
PA	penicillamine
PBS	phosphate buffer solution
Pd	palladium
R	resistors
RGO	reduced graphene oxide
R_{et}	electron transfer resistance
SCE	saturated calomel electrode
SEM	scanning electron microscopy
SWCNT	single wall carbon nanotube
TEM	transmission electron microscopy
TR	terazosin
TM	timolol maleate
WE	Warburg element
XOD	xanthine oxidase enzyme
XRD	X-ray diffraction
XPS	X-ray photoelectron spectroscopy

1 Introduction

Electrode modification plays a pivotal role in the fabrication of novel and high-performance voltammetric sensors. Modification is performed on the surface or in the body of the working electrode to boost the electron transfer rate, prevent undesired reactions, enhance sensitivity and selectivity, decrease response time and reduce over-voltage [1]. Various factors orient the modification method, such as the simplicity of the method, the presentation of a favourable redox behaviour, the low expenses and non-toxicity or low-toxicity of the chemicals and apparatuses [2].

Nanotechnology has played a significant role in the development of carbon-based electrodes. Novel modified electrodes based on the modification with various forms of nano-scaled metal such as metal oxide and metal nanoparticles (NPs), metal NPs-carbon nanotubes nanocomposites and metal oxide-polymer nanocomposites have been constructed. The large surface-to-volume ratio of the metal nano-sized structures gives remarkable properties to the modified electrode such as a high electron transfer rate, significant sensitivity and good selectivity. In order to cover all targeted factors for modification, recent studies have concentrated on the preparation of inexpensive, environmentally-friendly and high-performance carbon-based modified electrodes.

Nanomaterials have played an important role in the flourishing of the technology in recent years. They have been considered in a wide range of studies including electrocatalysts, fuel cells, photonic processes and electroanalytical techniques due to their excellent physical and chemical characteristics that originate from their small dimensions (nanomaterials have a high surface area to volume ratio). Nanostructured materials can be classified in accordance with dimensions (D) such as [3]:

(a) 0D: spheres and clusters (e.g. Quantum dots)

(b) 1D: nanofibres, nanowires, and nanorods (e.g. surface films)

(c) 2D: films, plates, and networks (e.g. strands or fibres)

(d) 3D: nanomaterials (e.g. particles)

In recent years, metal NPs have been studied and utilised significantly in the design and fabrication of novel modified electrodes due to their unique electronic, optical, magnetic and electrocatalytic properties that make them an effective electron mediator in redox processes [4].

The surface of carbon-based electrodes can be modified with metallic films and conductive materials such as palladium film [5, 6], gold film [7] and silver film [8]. It was reported that surface-modified carbon-based electrodes with metallic films and well established solid electrodes are very similar in performance. In addition, the easy, low-cost preparation and mechanical resistance of surface-modified carbon-based electrodes with metallic films are very advantageous for electrochemical purpose [2].

Various analytical methods have been suggested for environmental monitoring, industrial quality control, and biomedical analysis [1]. Among them, electrochemical methods perform well and show significant advantages such as sensitivity, accuracy, precision, wide linear dynamic range, relatively low-cost instrumentation, easy operational procedures and portability [9].

Electrochemical methods investigate electrical parameters, including the potential of the oxidation or reduction process, the number of electrons that participate in the oxidation or reduction process and current versus chemical parameters such as pH and concentration [1]. Overall, the factors in interfacial transport of charge across the chemical phases include the area between an electronic conductor (an electrode) and an ionic conductor (an electrolyte) [10].

Modified electrodes with metal NPs have been applied widely in the detection and determination of organic and inorganic compounds, pharmaceutical and biological compounds. It is important that the consumed dose is kept within the relevant pharmaco-toxicological limits. Usually, the standard dosage of the medicaments is adjusted depending on the age and weight of the patients. An excessive dose of the medicament has lethal effects. However, an insufficient dose of the medicament is not efficient. Thus, developing highly sensitive, low-cost, simple, portable, environmentally-friendly, a solvent-free and rapid response technique is vital. The response of electrochemical methods to this essential demand of medication quantification utilising a suitably modified electrodes is good. In this regard, timolol maleate, terazosin and methylene blue are investigated as pharmaceutical samples.

2 State-of-the-art research improvements in modified carbon-based electrodes

The performance of electrochemical methods is strongly related to the working electrode material. Fabrication of suitable and efficient working electrodes is important for experimental success. Several factors affect the selection of a favourable working electrode such as a wide potential window (anodic and cathodic potential range), high conductivity, low resistance, low background current, cost-effectiveness, renewability of the surface and ease of preparation and utilisation.

Jaroslav Heyrovsky conducted the classical electrochemical measurements utilising the dropping mercury electrode in 1922. Mercury-based electrodes demonstrate good advantages such as high reproducibility and surface renewability. The utilisation of mercury-based electrodes has gradually decreased due to drawbacks such as its restricted potential window and toxic nature, which are extremely harmful to people and the environment. On the other hand, the application of solid working electrodes including metal electrodes (gold and platinum) and carbon-based electrodes has increased significantly. However, the utilisation of platinum and gold electrodes is limited due to their drawbacks such as high cost and a restricted practical potential window (negative potentials because of the reduction of H^+ at the platinum electrode and positive potentials because of the surface oxidation of the gold electrode) [11].

The essential demand for investigating an efficient electrode, which can make up for the drawbacks of mercury-based electrodes and metal electrodes, led to the emergence of carbon-paste electrodes. Carbon has interesting advantages including a chemically inert nature, low cost, high compatibility with various materials and good conductivity. Carbon-based electrodes also have the benefit of a wide potential range window, low background signal, low electrical resistance, good conductivity and suitability for modification with various modifiers with high compatibility [11]. The first application of carbon-based electrodes (carbon paste electrode) as an effective alternative to mercury-based electrodes dates back to the late 1950s by Professor Ralph Norman Adams.

The most popular forms of carbon are graphite, glassy carbon, diamond, fullerenes, carbon nanotubes (CNTs), carbon nanofibres and graphene, which have been studied and applied widely in the fabrication of new biosensors and sensors since their appearance in 1950s. Carbon-based electrodes have been known as the most practical working electrodes for decades [12, 13]. Carbon-based electrodes show different electrochemical performances depending on their structure, hybridisation (for example; the hybridisation of carbyne, graphite, fullerenes (distorted) and diamond are sp^1, sp^2, sp^2 and sp^3) and surface functional groups. However, most of the carbon-based materials structures are established from stacked sheets of graphene (graphite) [14].

In this regard, the main activities in the fabrication of new carbon-based electrodes have been summarised in investigations of new forms of carbon, the study of their electrochemical performances, development of their electrochemical properties and the study of their possible sensing applications. In the following sections, types of carbon-

based electrodes, fabrication methods, properties and the pros and cons of utilising carbon-based electrodes are discussed briefly.

2.1 Carbon paste electrodes (CPEs)

CPEs with interesting advantages such as good electrical conductivity, ease of fabrication, ease of modification and ease of cleaning have been applied widely in the determination of pharmaceutical and biological compounds since Ralph Norman Adams introduced this kind of electrode in the late 1950s, which was originally designed as an alternative to the dropping mercury electrode [15].

CPE is prepared by thoroughly mixing graphite powder and a binder such as paraffin oil, mineral oil or ionic liquids. Then, the resulting homogeneous paste is packed into the cave of an inert electrode body such as a Teflon tube. A copper wire is then placed into the electrode body for connecting with the external circuit. Smooth and fresh electrode surfaces are obtained by polishing them against weighing paper until the surface becomes shiny. The activity of the CPE is strongly related to the amount of binder. An excess amount of binder reduces the electron transport kinetics.

CPEs have all the carbon advantages including a chemically inert nature, simple fabrication method from inexpensive materials, low cost, high compatibility with various materials and good conductivity. In addition, CPEs possess special features such as a renewable electrode surface which leads to a fresh electrode surface, the clearing of all history effects, the easy achievement of reproducible peak currents just by polishing the weighing paper, a wide potential window to investigate charge transport mechanisms in the cathodic potentials, as well as the anodic potentials range. However, beyond +1.4 V, a large background current appears and the analyte peak and background signals overlap each other. CPEs demonstrate high compatibility with various modifiers. The matrix and surface of CPE can be easily modified to fabricate a modified CPE with developed electrochemical properties such as charge transfer rate, selectivity and sensitivity. The need of an expert operator to calibrate CPE for conducting measurements and recording reproducible response signals is the major disadvantage of CPEs compared with other commercial carbon-based electrodes. CPEs compared with glassy carbon electrodes are prepared more easily and demonstrate a wider potential window and lower residual currents. However, the sensitivity of glassy carbon electrodes is higher than CPE due to the uniform structure of glassy carbon [16].

2.2 Glassy carbon electrodes (GCEs)

GCE with higher sensitivity was introduced after the emergence of CPEs and has been greatly employed in sensing various bio-molecules, medicines, water pollutants and metal ions.

Glassy carbon is fabricated by a controlled heating program of a pre-modelled polymeric (phenol-formaldehyde) resin body in an inert atmosphere. The structure of the glassy carbon involves thin, tangled ribbons of cross-linked graphite-like sheets. Due to significant conductivity, good mechanical characteristics and a chemically inert structure, glassy carbon can be applied to the fabrication of a high-performance electrode. Some pre-treatment is required to increase the analytical performance of GCE

and obtain a fresh surface such as polishing the surface of GCE with alumina powder (smaller than 0.05 µm) on a polishing cloth to achieve a shiny (mirror-like) surface and rinsing with deionised water before use. The high resistance of glassy carbon to chemical attack makes it possible to apply GCE in highly acidic and alkaline media [1, 2].

The electrochemical properties of GCE can be developed or changed by surface modification of GCE. In this regard, various surface modification methods have been employed such as drop casting [17], electro-grafting [18] and solvent evaporation methods [19].

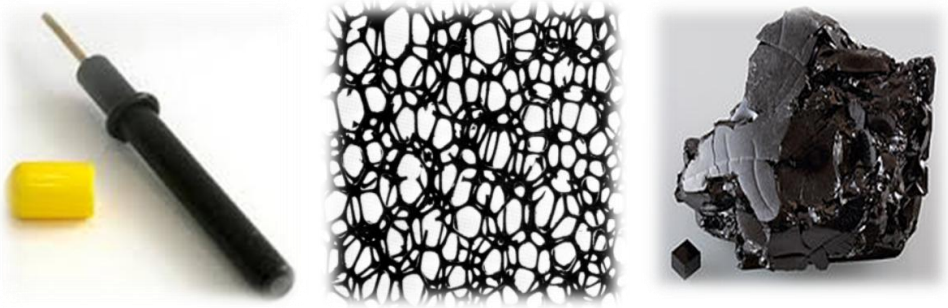

Figure 2.1: The structure of GCE [16].

2.3 Diamond electrodes

Diamond is another form of carbon material existing in nature. It was synthesised by applying a high-pressure/high-temperature technique in the 1950s. However, development of other synthesising methods has been continued for decades. For example, diamond polycrystalline films and diamond powder were synthesised by low-pressure chemical vapour deposition (CVD) and shock waves in the 1960s. The unique properties of diamond such as hardness, high thermal conductivity and high chemical stability are strongly related to the tetrahedral structure and sp^3 hybridisation of the diamond crystal. The electrical conductivity of the diamond is too low, which is counted as its major disadvantage. In this regard, the improvement of diamond electrical conductivity is an essential step for the utilisation of diamond as an electrode material. The doping process amplified the electrical conductivity of diamond significantly. The positive effect of doping agents such as boron and nitrogen on the electrically conductivity of diamond was studied by Pleskov *et al* [20]. Among diamond-doped electrodes, boron-doped diamond electrodes (BDDEs) showed interesting advantages such as a wide potential window, low background signal, metal-like electrical conductivity (for a high doping grade), a well-defined response signal (dissolving oxygen in electrolyte does not make any interference) and high performance in analytical measurements [21]. CVD methods and combined methods with CVD such as microwave plasma-assisted CVD or hot filament have been applied successfully in the preparation of BDD by introducing boron compounds (for example, diborane or trimethyl borane) when mixed with deposition gas to the growing diamond film [22]. The atmosphere utilised during the CVD process leads to different terminated surface groups at BDDE, which have various advantages. For example, the hydrogen terminated surface BDDE demonstrated multiplied electrical conductivity, the oxygen

terminated surface BDDE had a wider potential window, better stability and compatibility and the fluorine-terminated surface BDDE presented the widest potential window. In comparison, with metal electrode (for example; gold, platinum) BDDEs presented the widest potential window [23].

2.4 Screen-printed electrodes

Screen printing electrodes (SPEs) have been employed as one of the most popular methods in the fabrication of biosensors and sensors [24]. SPEs showed high potential in the detection of a wide range of analysts from bio-molecules such as riboflavin, glucose, vitamin C and DNA to water and environmental contaminates such as organophosphate and metal ions [25, 26].

Over the last couple of decades since the appearance of SPEs, much effort has been put into investigating and developing various features and utilities of SPEs. The SPE materials are mostly carbon, gold, platinum and other metals [24]. Based on the research need, SPEs can be prepared in different sizes, dimensions, geometrics and materials that make the research experiment simpler and faster (no need for electrode surface pre-treatment or maintenance). Carbon materials among other electrode materials possess interesting properties such as low cost, good conductivity, a wide redox potential window, inertness and high compatibility [27]. Screen printing carbon electrodes (SPCEs) demonstrate interesting advantages such as accurate and reproducible results (the electrode surface area and the thickness of deposited carbon are easily controllable), high versatility, easy operation (no need for an expert operator) and are easy to carry anywhere to conduct experiments, even by car, which eliminate the need for a central laboratory. The substrate in SPCE is flat, which counts as its major disadvantage. The procedure of SPCE fabrication is simply conducted by putting carbon ink on an inert and flat support such as plastic, glass or ceramic. The applied solvent in the preparation of carbon-based ink should demonstrate high purity, electrochemical inertness and volatility. The electrical conductivity of the carbon can be boosted by modification with different modifiers such as carbon active, nano-materials and catalysts (enzymes).

2.5 Carbon fibre microelectrodes (CFMs)

The first application of CFMs was introduced at Mark Wightman's laboratory in the determination of different concentration of dopamine in the 1980s [16]. Carbon nanofibres are the products of the decomposition of selected hydrocarbons and carbon monoxide over hot metal surfaces [28]. CFMs are typically constructed from placing a single carbon fibre on the inside of a glass tube pulled to a fine taper, or from a polyimide-coated capillary that is 90 μm in outer diameter [29]. Due to the interesting properties of CFMs such as a wide-ranging positive potential window, simplicity of construction and low cost, CFMs have been used widely in various analytical measurements ranging from the determination of different pesticides in different samples [30], to anodic measurements in different microenvironments [31] and CFMs are also employed in neurotransmitter-based electrochemistry as they can restrict tissue damage [15].

2.6 Chemically-modified electrodes (CMEs)

CMEs have been applied significantly in the detection and determination of different chemical compounds for decades. Modification is applied to boost the electron transfer rate, prevent undesired reactions, enhance sensitivity and selectivity, decrease response time, reduce over-voltage and increase the efficiency of the unmodified electrodes. In this regard, the surface or matrix of the working electrode is modified to fabricate the CMEs [32].

Different methods have been utilised for the modification of the electrode surface such as drop casting [17], electro-grafting [18], solvent evaporation [19] and electro-polymerisation methods [1]. Nanomaterials have been widely applied in electrode surface modification as well as electrode matrix modification using metallic NPs [33], carbon nanotubes [34] and graphene [35]. In addition, the matrix of the carbon-based electrodes can be modified using different modifiers such as nanomaterials [36], metal complexes [37, 38], zeolites [39], conducting polymers [40], organic compounds [41] and ionic liquids [42]. The employed values of the modifier should be between 5% and 10% (w/w) of the paste because low concentration cannot provoke the desired effect and high concentration may increase background current and ohmic resistivity [2].

Among different modifiers, carbon-based nanomaterials have been investigated and widely used in the preparation of CMEs, due to their significant properties (such as high effective surface area, increased mass transport, multiplied response to noise ratio and electro-catalysis) since their discovery. In addition, the combination of carbon-based nanomaterial such as CNTs and metal NPs such as gold (Au) has been applied widely in the fabrication of CMEs and in monitoring various analytes including proteins, sugars, pharmaceutical compounds and metal ions. Next, the most common synthetic methods and the electroanalytical application of some nanomaterials will be discussed.

2.6.1 Graphene

Graphene is a basic element of popular carbon-based nanomaterial structures such as three-dimensioned graphite, one-dimensioned carbon nanotubes and zero-dimensioned fullerene. Graphene is an important member of the carbon allotropes family, which is established from a single sheet of carbon atoms (with hybridisation of sp^2 linked to each other by a covalent band) organised in a hexagonal lattice. Graphene was discovered and named by Hanns-Peter Boehm in 1962 but a comprehensive study of the graphene was done in 2004 and won the Nobel Prize for Andre Geim and Konstantin Novoselov in 2010. Investigations into the two-dimensioned structure of graphene has had a great effect on expanding technology and science borders. Graphene possesses special advantages compare to graphite and CNTs such as higher surface area, fast charge transporting, higher electrical conductivity, higher thermal conductivity and mechanical stability. Various methods have been applied in the synthesis of graphene such as top-down (from graphite), electrochemical exfoliation and CVD methods [43].

Graphene as an electrode material performs well and demonstrates a higher charge transport rate, lower resistance and the same potential window compared with graphite, glassy carbon and boron-doped diamond. In recent years, graphene has been applied in various fields of technology, in particular the fabrication of biosensors and sensors (Table 2.1).

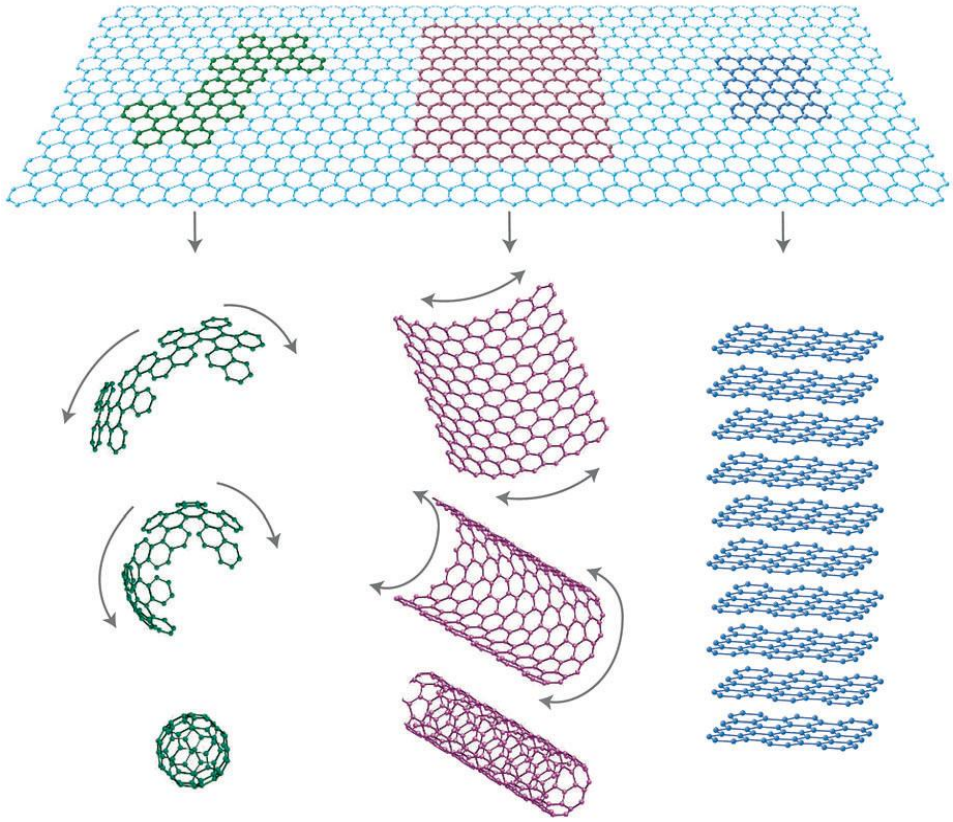

Figure 2.2: Graphene is a basic element of carbon-based nanomaterial structures. Graphite is composed of stacked layers of graphene, CNTs are formed from a single rolled-up graphene layer and fullerene from the closed graphene layer [43]. [Reprinted by permission from Springer Nature, Nature Materials,The rise of graphene, A. K. Geim, K. S. Novoselov, Copyright © 2007, Springer Nature]

2.6.2 **Fullerene**

Fullerene (C_{60}) is known as one of the most important discoveries. It was introduced to the world of science as a new form of symmetric carbon-based nanomaterial by Harry Kroto, Robert Curl and Richard Smalley in 1985. Fullerene is composed of many carbon units (60, 36, 70, 76 and 84 carbon units) with hybridisation of sp^2, which are arranged in the shape of a hollow sphere, ellipse or closed cylinder [44]. The closed cylinder shape fullerene is called carbon nanotubes or carbon buckytubes and its spherical structure is frequently called "buckyballs". The carbon cage structure of fullerene is composed of hexagonal and pentagonal rings with many oxidation/reduction states [45]. Fullerene was synthesised by the laser evaporation of carbon, incomplete combustion of benzene in oxygen [46] and the microwave method [47].

The remarkable properties of fullerene such as high biocompatibility, high surface area, good electrical conductivity, chemical stability and inert nature have attracted much interest from researchers and scientists since its emergence. Fullerenes have been

utilised in various areas of technology and science. In medicinal engineering for example, fullerenes are reported as HIV inhibitors [48].

In addition, the role of fullerene as a homogeneous redox catalyst is remarkable in electrochemical reactions. Fullerenes have been applied as an electro-catalyst to fabricate biosensors such as glucose sensor [49], immunosensor [50] and sensing insulin [51].

It was reported that modification of fullerene with other materials such as noble metal NPs like gold and palladium NPs resulted in a new functional nanomaterial with improved electrochemical properties such as increased electron transport rate, better sensitivity and selectivity [49, 52].

2.6.3 CNTs

CNTs have developed the domains of technology and science significantly and performed well in various fields of technology. CNTs belong to the carbon-based nanomaterial family, which have been constantly developed since their introduction by Sumio Iijima in 1991. CNT is composed of a rolled-up graphene layer and is formed in the shape of a closed cylinder, a cap with the structure of a pentagonal ring and a tube with distinct properties. The structure of CNTs consists of units of carbon with hybridisation of sp^2 linked together by covalent bonds, which have remarkable mechanical properties. CNTs are classified into two types; single-walled CNTs (SWCNTs) and multi-walled CNTs (MWNTs) that are established from the rolling-up of one or more graphene cylinders (diameter: 2-50 nm). CNTs have been studied extensively since their discovery due to their significant electronic, chemical, geometric and mechanical features [53]. In this regard, various methods have been investigated and applied to synthesis CNTs such as arc discharge (MWCNT, SWCNT), laser ablation (SWCNT) and CVD method (MWCNT, SWCNT). CNTs are known as reliable materials for the fabrication of biosensors and sensors due to their significant advantages compared to graphite and glassy carbon such as enlarged surface area, improved charge transfer rate and great sensitivity [54]. In addition, CNTs electrodes demonstrate interesting advantages in electrochemical experiments such as reduced electrode surface contamination, improved peak currents and enhanced heterogeneous charge transport kinetics [55].

The major advantage of CNTs compared to fullerenes and graphene is their great chemical compatibility with bio-molecules. CNTs act as an effective electron catalyser by enhancing the rate charge transport of the related reactions [27].

CNTs can be decorated with other nanomaterials such as metal NPs to improve their performance in areas like catalytic activity. Various methods have been used to decorate metal or metal oxide NPs onto the surface of CNTs [56]. The nanocomposites of CNTs/nanomaterial have been applied on the surface or matrix of carbon-based electrodes to fabricate new modified carbon-based electrodes. Zhang *et al.* fabricated CNT-nickel NPs hybrid paste electrodes for the electrochemical sensing of carbohydrates in 2014 [57]. The surface of the MWCNTs was decorated with Au NPs and the MWCNTs/Au NPs were utilised to modify CPE for the determination of the thiocyanate by Afkhami *et al.* in the same year [58]. The poly (4, 5-dihydro-1, 3-thiazol-2-ylsulfanyl-3-methyl-1, 2-benzenediol)-Au NPs film was applied to the

modified electrode with MWCNTs by Fakharia *et al.* in 2015. This electrochemical sensor was applied for the determination of hydrazine [59].

2.6.4 Au NPs

Among metal NPs, Au NPs have gained huge popularity because of their significant electronic and catalytic characteristics. The unique features of Au NPs relating to their nano-sized structure have led to significant development in various areas of chemistry since the 1990s. Au NPs demonstrate high compatibility with bio-molecules, which have led to their use in a wide range of bio-sensing applications [60]. Au NPs have been employed as a modifier in the fabrication of high-performance modified electrodes due to their excellent characteristics such as high metal conductivity, good stability and good biocompatibility. Au NPs facilitate electron transfer on the electrode surface, improve electrode conductivity and enlarge surface area, which enhance peak current and develop the detection limit [61].

Various methods have been reported to synthesise Au NPs such as the chemical reduction method or "Turkevitch method" applied by Turkevitch *et al.* in 1951. In the Turkevitch method, Au NPs (diameter: 20 nm) were synthesised by reducing $AuCl_4$ with citrate. In another common method, the Brust-Schiffrin method, Au NPs (diameter: 1-5 nm) were synthesised by reducing $AuCl_4$ with $NaBH_4$ in toluene media including dodecanethiol as a stabiliser [62]. In the methods reported next, the procedure of synthesising and its condition were optimised and developed to adjust the uniformity and flavoured diameter. In this regard, stabilisers such as dodecanethiol [62], poly (L-lactide) [63] and β-cyclodextrin [64] have been reported widely. In addition, the way of adding reductant to $AuCl_4$ has been developed such as using the dropwising method [65].

Au NPs can cover the surface of carbon-based electrodes such as a film or can become embedded in the matrix of CPEs. The bulk of CPEs can be modified simply by adding the Au NPs to the graphite or carbon-based composite and a suitable buffer solution being stirred, and then the dried paste can be applied in the fabrication of CMCPE. Regarding the electrode surface modification with Au NPs, other Au NPs synthesising methods have flourished such as the electro-deposition (such as electro-reduction) and physical deposition (such as adsorption) of Au NPs.

The surface of carbon-based electrodes can be coated with a layer of Au NPs using deposition methods such as layer-by-layer assembly and solvent evaporation, which just need the solution of Au NPs in a suitable solvent. The application of chitosan coverage was reported to be effective for controlling binding sits and Au NPs film composition in the layer-by-layer assembly method [66].

The simplest and most reliable method for synthesising Au NPs film is the electro-reduction of $HAuCl_4$ solution, which is easily conducted using chronoamperometry (in potential −200 mV *vs.* SCE for 60 sec), linear sweep voltammetry or cyclic voltammetry (in potential range of −0.18–1.2 V *vs.* SCE, scan rate: 100 mV s^{-1}, for 15 cycles) [67]. The deposited Au NPs film is more stable than other deposition methods and its thickness and conductivity can be investigated, controlled and optimised depending on the purpose of the experiment.

Au NPs play an effective role in fabrication of biosensors. In this regard, Au NPs were synthesised by chemical reducing $AuCl_4$ with $NaBH_4$ and using β-cyclodextrin as a stabilizer. Then the stabilised Au NPs was applied as a support for enzyme of laccase by mixing with each other (1:1, v/v). Then, a homogeneous paste was prepared by mixing graphite, modifier (Au NPs/β-cyclodextrin/laccase) and mineral oil to fabricate a modified CPE as a sensitive biosensor for rutin (flavonoid) (LOD: 0.17 μmol L^{-1}, by using square-wave voltammetry) [68].

Since first applications of Au NPs colloidal solutions for the fabrication of biosensors in 1990, many studies have been performed on designing them. In recent years, Au NPs have been applied significantly in the fabrication of glucose biosensors. In this regard, Au NPs were prepared by the chemical reduction of acidified $HAuCl_4 \cdot 3H_2O$/tannic acid solution using sodium citrate. Then, the synthesised Au NPs were deposited on the graphite electrode surface; the enzyme of glucose oxidase was next deposited on the electrode surface. It was reported that the deposited Au NPs played an effective role in increasing the rate of charge transport between enzyme active sites and the electrode, and acted as a good support for the immobilisation of enzymes. The presence of polypyrrole as a conducting polymer was effective for electron transport and the sensitivity of the glucose biosensors [69]. This work was improved in 2017; the reported glucose biosensors were prepared with the same composition (Au NPs/glucose oxidase/polypyrrole), but with a different preparation method for modifying with Au NPs. In this report, Au NPs were synthesised and deposited on the electrode surface in one step by electrochemical deposition, which conducted more quickly and easily than previous the chemical deposition method [70].

Investigations into the high affinity of Au NPs towards thiol compounds and the linkage of Au-S have revealed many sensing applications of Au NPs. Au NPs act as an effective support to immobilise thiols such as cysteine and penicilamin. On the other hand, the catalytic behaviour of Au NPs can be enhanced in the polymeric bulk of thiols. Cysteine can be oxidised to cysteic acid and polymerised on the GCE surface by employing cyclic voltammetry in the potential window −0.8–2.2 V *vs.* SCE (sweep rate was 100 mV s^{-1}, 20 cycles). Then, Au NPs were synthesised and embedded electrochemically (potential −400 mV for 100 s) into the cysteic acid polymeric substrate. The electrochemical studies on the modified GCE demonstrated the effect of the cysteic acid matrix on the enhancement of the electron transfer kinetic very well. Cysteic acid/Au NPs/GCE was applied successfully for detecting of epinephrine in the presence of uric acid with high sensitivity and selectivity [71].

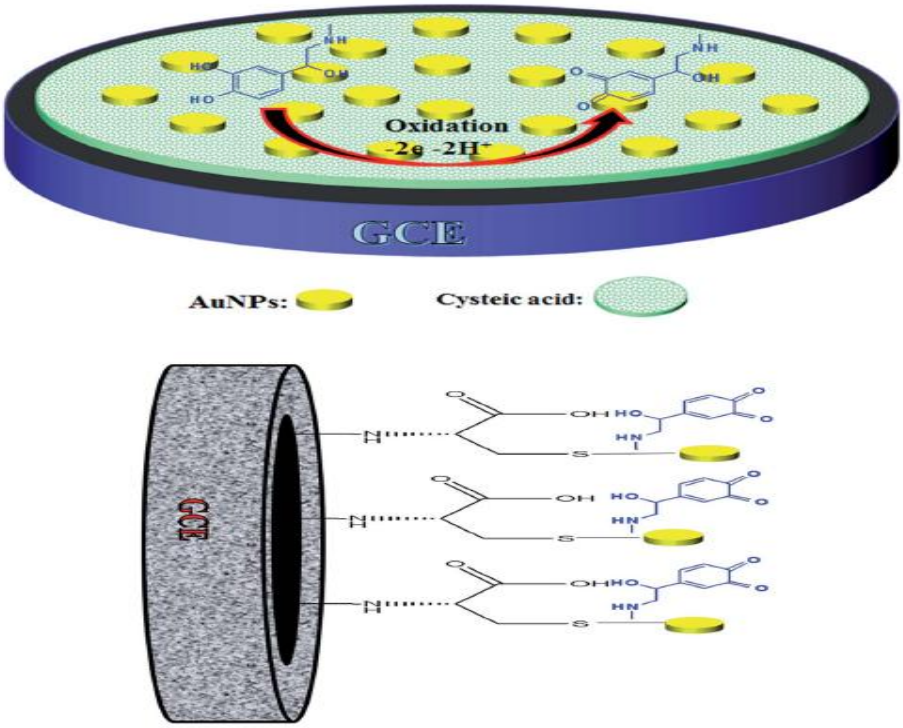

Figure 2.3: Fabrication method of cysteic acid/Au NPs/GCE [71]. [Reprinted by permission from Royal Society of Chemistry, Analytical methods, Selective analysis of epinephrine in the presence of uric acid by using an amplified electrochemical sensor employing a gold nanoparticle decorated cysteic acid film, Karim-Nezhad, G. ; Khorablou, Z. Julkaisussa, Copyright © 2017, Royal Society of Chemistry]

These CMEs have been applied in the determination of various biological molecules and pharmaceutical samples, including cysteine [72-74], carcinoembryonic antigen norepinephrine [74]. Afkhami *et al.* constructed a surface-modified CPE with Au NPs for the determination of cefixime by applying the chronoamperometry method [7]. In the other studies, CPE modified with Au NPs was applied in sensing folic acid in plasma [61], eugenol [75] and acetazolamide [76] in human serum and urine, using differential pulse voltammetry. The German and co-workers modified a graphite electrode with an Au NPs colloid and the enzyme of the glucose oxidase to fabricate a high-performance glucose biosensor [77]. Other samples of the modified electrodes with Au NPs are listed in Table 2.1.

2.6.5 **Pd NPs**

Pd NPs are the most active noble metal because of their interesting properties such as high heterogeneous catalysis and electrocatalysis activity, versatility, no toxicity and relatively low cost [78]. Pd NPs have been utilised in various sensing methods,

especially in electrochemistry. Pd NPs have been employed as a modifying element in the fabrication of different sensors. Carbon-based electrodes have been successfully modified with Pd NPs or Pd nanostructure-based compounds for years. Different synthesising methods have been investigated in the preparation of Pd NPs including chemical reduction, electrochemical reduction, and pulsed laser ablation [79].

The chemical reduction method has been applied widely to generate Pd NPs, and various studies have been conducted to improve the efficiency of this method. One of the most important factors in the preparation of Pd NPs is the size of the generated particles, which plays a major role in the electrocatalytic feature of Pd NPs. Employing stabilisers such as cetyl trimethylammonium bromide, polyvinylpyrrolidone and sodium dodecyl sulphate is a useful way to control the size and distribution of the formed Pd NPs.

The utilisation of a continuous flow microreactor in the chemical reduction of $PdCl_2$ promoted the chemical and physical characteristics of the generated Pd NPs. The size distribution of the generated Pd NPs could be managed and adjusted successfully by changing the rate of flow and the ratio of precursor to reducing agent, which is an advantage of the continuous flow microreactor over the common batch chemical reduction method [80, 81].

Pd NPs can be synthesised chemically by the *in situ* reduction of K_2PdCl_4. In this method, K_2PdCl_4 was electrostatically linked to the surface of modified GC with trimethoxy-silylpropyl-modified polyethyleneimine before facing with reducing agent (formic acid). In this way, Pd NPs (approximately 8 nm) were produced and the sensor was fabricated simply in a one-step process. Then, the designed sensor was successfully employed in the oxidation of ethanol, n-propanol, isopropanol, ethylene glycol, glycerol [82] and dopamine [83]. The application of modified carbon-based electrodes with Pd NPs has been studied in the detection and determination of the various compounds such as catecholamines [84], entacapone, levodopa and carbidopa [85] (other examples listed in Table 2.1).

Pd NPs can be employed alone or embedded in the various substrates, especially carbon-based nano-structures. The deposition of Pd NPs on carbon-based nano-structures (MWCNTs, fullerenes and graphenes) as a support enhanced the electrocatalytic properties significantly and improved the electrochemical performance of the modified electrode. For example; the Pd NPs deposited on the porous graphitised carbon monolith promoted the performance of the modified CPE in determining ascorbic acid and uric acid (in mixed solution) with high sensitivity and good reproducibility [3]. Dopamine, ascorbic acid and uric acid were determined efficiently at the same time by employing Pd NPs loaded on the carbon nanofibres [3]. The Pd NPs deposited on SWCNT thin film and fullerene demonstrated high electrocatalytic activity in nitrite oxidation [78] and methane sensing [52]. In addition, the electrochemically immobilised Pd NPs on the carbon ionic liquid electrode detected isoniazid with high sensitivity [86].

The electro-deposition method has been applied as a simple, fast and promising technique to modify the surface of GCE with Pd NPs. In this method, Pd NPs were synthesised using the CV method (the potential window was −0.50–0.80 V *vs.* Ag/AgCl and 15 cycles scanned) in acidified solution of $PdCl_2$ (1mM). However, the presence of

a fullerene layer on the GCE surface as a support for Pd NPs improved the efficiency of modified GCE significantly. The fabricated CME was employed in the detection of methane [87]. SPCEs can be modified by the same method in the potential window of −0.25–1.2 V *vs.* Ag/AgCl for 10 cycles and the scan rate was 50 mV s^{-1}. The fullerene layer was used on the surface of GCE and SPCE by the drop casting method. The modified SPCE was employed to determine dopamine in a linear range of 0.35–133.35μM. The limit of detection was calculated to be 0.056 μM [88].

Pd NPs have been utilised successfully in the fabrication of biosensors, for example. The electro-deposited Pd NPs and glucose oxidize enzyme on CNT film [89] and the MWCNTs decorated with Pd NPs [90] were employed to fabricate an efficient glucose biosensor.

2.6.6 Hybrids of Au-Pd NPs

Au NPs can be hybridised with other metal NPs in forms of alloys or core-shell structures. These bimetallic combinations demonstrated improved catalytic, electronic and optical features compared with monometals. In addition, the electrochemical properties of the bimetals are promoted significantly due to their synergic effect and improved catalytic activity (for example: the rate of charge transport multiplied) [91, 92].

Hybrids of Au-Pd NPs have been synthesised and applied in a wide range of sensing areas. Various synthesis methods have been employed in the preparation of bimetals such as chemical reduction and electrochemical reduction. The chemical reduction synthesis method can be conducted in a one-step (one batch) or two-step procedure.

Au-Pd NPs in the form of a core shell, where the Au is covered with a shell of Pd, were synthesised by applying the chemical reduction method. Firstly, the ethylene glycol as a reductant was added to the stirring aqueous solution of $AuCl_3$ and carbon black as a conductive and low-cost support in the ultrasonic bath for 4 h, stirred constantly for 24h in 120 °C and dried in an oven. Then the mixture of Au NPs/carbon black and ethylene glycol was added to the acidified solution of $PdCl_2$ and the reduction procedure was continued as in the first step. The dispersed solution of Au-Pd NPs/carbon black and dihexadecylphosphate was dropped on the surface of GCE. The modified GCE was successfully applied to detect a low concentration of hydrazine (as a water pollutant) in lake water samples (LOD: 0.23 μmol L^{-1}) [93].

Au-Pd nanoalloys can be dispersed into the graphene support in the form of nitrogen and sulphur functionalised to result in an effective modifier for GCE, which was employed in the determination of dopamine. Au-Pd nanoalloys were synthesised using the chemical reduction method. H_2PdCl_4 and $HAuCl_4$ were applied to synthesised Pd and Au nanostructures using an ascorbic acid solution as a reducing factor in the presence of cetyltrimethylammonium chloride (for H_2PdCl_4), and cetyltrimethylammonium bromide (for $HAuCl_4$) in two separate batches. Then, the prepared Pd and Au nanostructures were mixed with each other rapidly for 20 min, and the mixture was kept undistributed for 24 h to achieve Au-Pd nanoalloys [91].

Au-Pd NPs can be synthesised and electro-deposited simultaneously on the surface of GCE by applying the CV method from an acidified solution of $HAuCl_4{:}3H_2O$ and $PdCl_2$ (the potential window was −0.2–1.2 V *vs.* SCE, sweep rate was 0.05 V s^{-1}, 10 cycles). However, the presence of a reduced graphene layer on the GCE surface as a support for Au-Pd NPs played an effective role in the Au-Pd NPs/graphene/GCE electrocatalytic performance. So, a layer of reduced graphene was deposited on the GCE by the drop casting method, then Au-Pd NPs were electrochemically deposited on the reduced graphene support to fabricate a modified electrode for detecting caffeic acid in the concentration range of 0.03–938.97 mM and the limit of detection was calculated to be 6 nM (reported in 2017) [94]. A similar method was applied to fabricate Au-Pd NPs by Shahrokhian *et al.* They employed MWCNT as a support for the electro-deposition of Au-Pd NPs on a GCE surface. The electrochemical deposition of the Pd–Au NPs was conducted for 5 s at a constant potential of −0.2 V (*vs.* Ag/AgCl) in 0.5 M H_2SO_4 aqueous solution containing 0.5 mM gold (III) chloride and 1 mM $PdCl_2$.

In one step, Au-Pd NPs/reduced graphene oxide was synthesised and electro-deposited on the surface of GCE by Kumar *et al.* A fast, simple and environmentally-friendly method was conducted using the CV method in the potential range −800–1500 mV in the suspension of graphene oxide, $HAuCl_4$ and $PdCl_2$. This modified electrode was successfully employed to detect low concentrations of lomefloxacin (LOD: 81 nM) and amoxicillin (LOD: 9 M) [95].

A composite of Au-Pd NPs/reduced graphene oxide can be fabricated in one pot by the chemical reduction method. In this method, $HAuCl_4$, Pd $(OAc)_2$ and ascorbic acid were added to the well-dispersed suspension of graphene oxide and trisodium citrate dehydrate (as a preservative) and refluxed in an oil bath to reduce completely. The prepared nanocomposite was dropped on the GCE surface to fabricate a CME, which was applied in the determination of sunset yellow with a limit of detection of 1.5 nM [96].

2.6.7 Titanium dioxide nanostructures

Titanium dioxide (TiO_2) nanostructures as a semi-conductor have attracted much interest in terms of investigation and application in various fields of technology including photo-catalysts, electro-analysis, gas sensors, solar cells, water treatment and sensors. The photo-catalytic performance of TiO_2, which was counted as an important discovery, was introduced by Kenichi Honda and Akira Fujishima in 1972. The high versatility of TiO_2 is rooted in its interesting properties including chemical stability, low cost, non-toxicity and environmental friendliness [97, 98]. Regarding the application of TiO_2 nanostructures in the fabrication of CMEs, various preparation techniques (such as hydrothermal, CVD, sol-gel and direct oxidation methods) and modifying methods (such as coating, doping, coupling and capping) have been developed to provide TiO_2 nanostructures with higher catalytic activity, enhanced surface area and more stability (in the form of TiO_2 film) [99-103].

The modified CPE with TiO_2 NPs demonstrated advantages including an amplified charge transport rate, higher chemical stability and lower background current compared to unmodified CPE, solid graphite and noble metal electrodes [13]. Among various synthesis techniques, the sol-gel method has been applied widely in the fabrication of modified CPEs with TiO_2 NPs. In this method, a definite volume of $TiCl_4$ was dropped

into the solution of ethanol or methanol and a suitable surfactant (while the solution was being stirred). The prepared solution was gelatinised (24 h) to make a sol-gel solution, which changed to dry-gel after vaporising the solvent. TiO_2 NPs powder was formed after calcination of the dry-gel, then TiO_2 NPs powder, graphite powder and mineral oil were mixed with each other (with suitable ratios). The homogenised paste was applied to fabricate the modified CPE. TiO_2 NPs enhanced the electrochemical performance of the modified CPE effectively by increasing the surface area and sensitivity. The fabricated CME was successfully employed in the determination of different analytes including clozapine [104], p-cresol [105] and Cd (II) [106] and buzepide methiodide [107]. The modified CPE with TiO_2 NPs and ionic liquid was employed to detect low concentration of benserazide [108].

TiO_2 NPs can be synthesised on the surface of GCE by the electro-deposition method. In this method the GCE was immersed in the voltammetric solution of Ti $(SO_4)_2$, KCl, H_2O_2 under a constant potential of −0.1 V for 30 min [109, 110]. TiO_2 nanostructures could be efficiently employed in preparation of biosensors. For example; TiO_2 nanostructures could be utilised as a support for immobilising haemoglobin and providing a composite of TiO_2/haemoglobin, which greatly increased the rate of charge transport of haemoglobin. The nanocomposite of TiO_2/haemoglobin was employed to modify the surface of GCE and prepare a biosensor with promoted electrocatalytic activity for hydrogen peroxide [111].

Modification with carbon-based nano-materials such as CNTs [112], graphene [113] and activated carbon [114] increased the catalytic activity of TiO_2 nanostructures effectively. In addition, the modified carbon-based electrodes with TiO_2 nanostructures were fabricated inexpensively and demonstrated broader potential windows, more stability and sensitivity in sensing target samples [112]. Carbon-based materials especially graphene and MWCNT were known as a promising support for TiO_2 NPs, which could increase the catalytic behaviour of TiO_2 significantly due to their impressive electronic features and improved surface area. In addition, graphene layers could made pathways with lower charge transport resistance among the graphene/TiO_2 nanocomposite for better charge transport. Nanocomposites of graphene/TiO_2 or MWCNT/TiO_2 were prepared by mixing powders of graphene or MWCNT and TiO_2 NPs under ultrasonication. Then, they were used to modify the GCE surface by the drop casting method. The modified GCE was successfully used to determine catechol, hydroquinone [113] and diazinon [109].

Another effective way of enhancing the catalytic activity of TiO_2 NPs, especially their photocatalytic activity, is carbonisation which is conducted easily by heating TiO_2 at an optimised temperature (150 to 400˚C) in ethanol gas atmosphere, prepared by bubbling pure argon through ethanol liquid [115, 116]. The carbon-modified TiO_2 obtained demonstrated developed surface area and improved adsorption capacity for adsorbing organic and inorganic materials, which is useful in the fabrication of CMEs for detecting environmental contaminates.

2.6.8 **Conducting polymers (CPs)**

CPs have attracted much interest in recent years. CPs demonstrate the impressive characteristics of metals (high conductivity) and polymers (plasticity and simple

preparation) [1]. The significant discovery of CPs as a good alternative for metals was made by Alan Heeger, Alan Mac Diarmid and Hideki Shirakawa. The electrical conductivity of CPs is strongly related to the electronic structure of their polymeric backbone (electron hopping between delocalised π electrons), which is not comparable to the conductivity of metal. However, high conductivity is gained by the addition of a suitable ion as the "dopant". The significant chemical and physical properties of CPs such as switching reversibly between the positively charged (conducting) and neutral (insulating) states, rapid exchange of the doping ion, good stability and high conductance make CPs a unique material in a wide range of fields such as solar cells, light-emitting diodes, sensors, lasers, super capacitors, and memory devices [1, 117]. The CPs family has been applied to modify the surface or body of carbon-based electrodes. Members of the CPs family include polyacetylene, polypyrrole, polyaniline, and polythiophene [118].

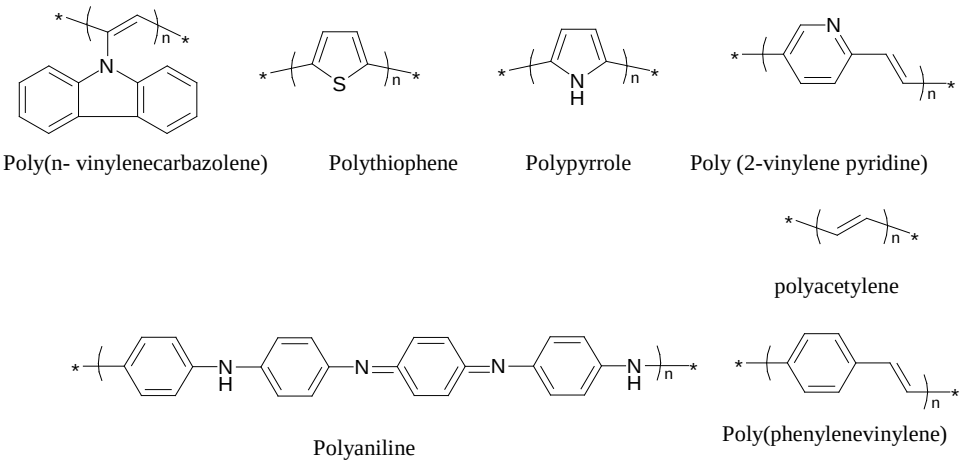

Figure 2.4: Conducting polymers family.

Polyaniline (PANI) is one of the most interesting CPs due to its switchable conductivity states versus the pH of the medium. Regarding oxidation state, PANI appears in different forms such as a fully oxidised pernigraniline base, a half-oxidised emeraldine base and a fully reduced leucoemeraldine base. The emeraldine form of PANI demonstrates high conductivity and stability compared to other forms [119]. PANI can be simply and inexpensively prepared and applied to the modification of carbon-based electrodes. For example, in one step PANI can be constructed and modified on the surface of carbon-based electrodes using an electrochemical method, or it can be synthesised chemically and then used for the modification of the body of the CPEs. PANI performs well in the enhancement of charge transport kinetics.

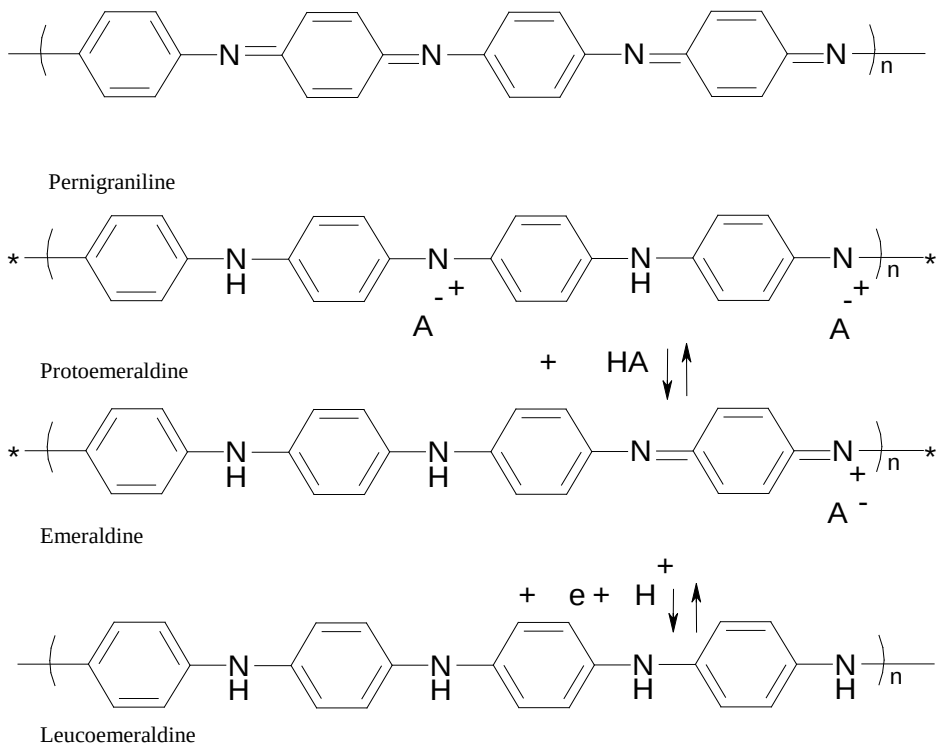

Figure 2.5: Different oxidation states of PANI.

In addition, the ionic and electronic conductivity, chemical stability and electrocatalytic properties of the electrodes modified with CPs could be improved by doping the materials with metal NPs [120]. Metal NPs can be dispersed into the CPs successfully due to the synergistic effect between metal NPs and CPs [120]. Physical adsorption is one of the most common and effective methods of embedding metal NPs into CPs due to its easy operation and low cost. For example, gold NPs have been used widely due to their good electrical properties, high surface area and high electrocatalytic activity [7, 77]. It was reported that the presence of the thiol or nitrogen groups at the monomer structure can improve the adsorption of gold NPs on the matrix of polymer [59, 121].

Table 2.1: Some electroanalytical application of the CMEs

Working electrode	Modifier type	Analyte	LOD (M)	Dynamic range (M)	Reference
GCE	Pd NPs/1Gr	Dopamine AA	N/A	10×10^{-6}–1200×10^{-6} 20×10^{-6}–6500×10^{-6}	[122]
GCE	Pd NPs/Gr/WCNTs	Glucose	1×10^{-6}	Up to 19.5×10^{-3}	[123]
GCE	Pd NPs/[2]ErGO	Dopamine	0.233×10^{-6}	1×10^{-6}–150×10^{-6}	[124]
GCE	[3]PDDA/Gr Pd NPs	Triclosan	3.5×10^{-9}	9.0×10^{-9}–20.0×10^{-6}	[125]
GCE	Pd NPs/rGO/MWCNTs	Hydrazine	0.15×10^{-6}	1.0×10^{-6}–1100×10^{-6}	[126]
GCE	Pd NPs/rGO	Desipramine	1.04×10^{-9}	0.3×10^{-6}–2.5×10^{-6}	[127]
GCE	Au NPs-Pd NPs-ErGO	Lomefloxacin Amoxicillin	81×10^{-9} 9×10^{-6}	4×10^{-6}–500×10^{-6} 30×10^{-6}–350×10^{-6}	[128]
GCE	Pd NPs/porous aromatic framework	Vanillin	2×10^{-10}	10×10^{-10}–820×10^{-10}	[129]

GCE	Pd NPs/porous activated carbon	Cd^{2+} Pb^{2+} Cu^{2+} Hg^{2+}	41×10^{-9} 50×10^{-9} 66×10^{-9} 54×10^{-9}	0.5×10^{-6}–5.5×10^{-6} 0.5×10^{-6}–8.9×10^{-6} 0.5×10^{-6}–5.0×10^{-6} 0.24×10^{-6}–7.5×10^{-6}	[130]
GCE	Pd NPs	m-nitrophenol	N/A	0.20×10^{-3}–5.00×10^{-3}	[131]
GCE	[4]WO_3 NPs/CNTs	Paracetamol	5.54×10^{-11}	1.0×10^{-9}–2.0×10^{-7}	[132]
GCE	MWCNTs/[5]CTS–Cu	Paracetamol	0.024×10^{-6}	0.1×10^{-6}–200×10^{-6}	[133]
CPE	Pt/CNTs/[6]ILCPE	Sudan I	0.003×10^{-6}	0.008×10^{-6}–600×10^{-6}	[134]
CPE	MWCNTs/[7]CILE	Norepinephrine	0.09×10^{-6}	0.3×10^{-6}–30.0×10^{-6} 30.0×10^{-6}–450.0×10^{-6}	[135]
CPE	[8]EF/NiO/MWCNTs	Glutathione Acetaminophen	0.006×10^{-6} 0.5×10^{-6}	0.01×10^{-6}– 200×10^{-6} 0.8×10^{-6}–600×10^{-6}	[136]
CNTPE	Triton X 100	Acetaminophen Aspirin Caffeine	2.58×10^{-8} 8.47×10^{-8} 8.83×10^{-8}	2.91×10^{-7}–6.27×10^{-5}	[137]

CNTPE	[9]2PHC	Epinephrine	9.4×10^{-9}	5×10^{-8}–5.5×10^{-4}	[138]
GCE	[10]MIPs/Au NPs	Bisphenol	1.1×10^{-9}	1.5×10^{-8}– 5.5×10^{-5}	[139]
CPE	Au NPs/MWCNTs	Thiocyanate	5×10^{-9}	0.01×10^{-6}–200.0×10^{-6}	[58]
CPE	Au NPs-[11]MPS	Catechol Hydroquinone	1.2×10^{-6} 1.1×10^{-6}	10.0×10^{-6}–1.0×10^{-3} 30.0×10^{-6}–1.0×10^{-3}	[140]
CPE	GC microparticles/Au NPs/[12]XOD	Xanthine Hypoxanthine	N/A	5.00×10^{-7}–1.00×10^{-5} 5.00×10^{-6}–1.50×10^{-4}	[141]
GCE	Au NPs/MWCPE	Ceftazidime	1.0×10^{-9}	0.05×10^{-6}–50×10^{-6}	[4]
CPE	Au NPs	Eugenol	2.0×10^{-6}	5×10^{-6}–250×10^{-6}	[75]
CFME	Au NPs	Arsenic	0.0120×10^{-9}	0.064×10^{-9}–0.8×10^{-9}	[142]
CPE	Cu–YHA-TETA[13]	Nitrite ions	1.46×10^{-6}	0–1.38×10^{-2}	[143]
CPE	Cu–YHA-EDA[14]	Nitrite ions	2.17×10^{-6}	0–1.38×10^{-2}	[143]

Au	Mercapto-terminated binuclear Cu(II) complex	Dopamine	0.08×10^{-6}	0.2×10^{-6}– 30×10^{-6}	[144]
GCE	Tetraphenyl-porphyrin Co(II)	Oxygen consumption in biological samples	N/A	N/A	[145]
CME	Ni salen complexes	Amines	10×10^{-6}	N/A	[146]
GCE	Ni- and Co-phthalocyanine complexes	Nitric oxide	N/A	N/A	[147]
CPE	Cobalt(II)-Schiff base complex and magnetite nanospheres	Nitrite ion	1.5×10^{-2}	0.2×10^{-6}_30.0×10^{-6}	[148]
CPE	Cobalt(II)-4-methylsalophen	Cysteine AA	$<1.0\times10^{-6}$	1×10^{-4}–5×10^{-7} 1×10^{-4}–1×10^{-6}	[149]
CPE	Cobalt-5-nitrolsalophen	Captopril	1.1×10^{-6}	4.0×10^{-6}–1.1×10^{-4}	[38]
CPE	Cobalt salophen	AA UA	8.0×10^{-9} 8.0×10^{-9}	5.0×10^{-4}–1.0×10^{-8} 1.0×10^{-3}–1.0×10^{-8}	[37]
CPE	Co NPs	Chlorpromazine	0.6×10^{-9}	0.002×10^{-6}–1.0×10^{-6}	[150]

GCE	MWCNT/Co NPs	Thioridazine	5.0×10^{-8}	5.0×10^{-7}–1.0×10^{-4}	[151]
GCE	MWCNT/Co NPs	Paracetamol Dopamine	1.0×10^{-9} 1.5×10^{-8}	5.2×10^{-9}–4.5×10^{-7} 5.0×10^{-8}–3.0×10^{-6}	[132]
GCE	CoO NPs/MWCNTs	Warfarin	3.3×10^{-9}	8.0×10^{-9}–50.0×10^{-6} 50.0×10^{-6}–$800.\times10^{-6}$	[152]
CPE	Flower-like cobalt	Chlorpheniramine	8.0×10^{-8}	1.0×10^{-7}–1.0×10^{-5}	[153]
GCE	Co NPs/G	Cysteine	0.89×10^{-3}	1.1×10^{-3}–12.3×10^{-3}	[154]
^{15}Si NWE	Co NPs	AA	2.0×10^{-7}	3.0×10^{-7}–1.0×10^{-4}	[155]
CPE	Co NPs	AA	N/V	N/V	[156]
CPE	CTS/MWCNT/Co NPs	Daclatasvir	8.82×10^{-10}	1.0×10^{-12}–12×10^{-6}	[157]
CPE	Co NPs	Sulphite	0.4×10^{-5}	1.0×10^{-5}–5.9×10^{-5} 2×10^{-5} –8×10^{-3}	[158]

GCE	MWCNTs/poly (4,5-dihydro-1,3-thiazol-2-ylsulfanyl-3-methyl-1,2-benzenediol)/Au	Hydrazine	0.6×10^{-6}	2.0×10^{-6} –350.0×10^{-6}	[59]
GCE	MWCNTs/ (4-amino-3hydroxynaphthalene sulfonic acid)	Histamine	7.62×10^{-8}	1.0×10^{-7}–1.0×10^{-4}	[159]
GCE	Poly(4vinylpyridin) /MWCNTs	Aspirin Caffeine	4.42×10^{-9} 1.19×10^{-9}	0.04×10^{-6}–350×10^{-6} 2.0×10^{-6} –200×10^{-6}	[160]
CPE	PANI	Amoxicillin	7.3×10^{-10}	N/A	[161]
GCE	PANI/tungsten oxide	Phenanthrene	0.123×10^{-10}	1.0×10^{-10}–6.0×10^{-10}	[162]
GCE	PANI/MnO_2	Guanine Adenine Thymine Cytosine	N/A	N/A	[163]
GCE	PANI/paratoluene sulfonic acid	Au^{+}	0.4×10^{-9}	0.6×10^{-9}–1×10^{-6}	[164]
GCE	G/PANI	Aminophenol	6.5×10^{-8}	0.2×10^{-6}–20×10^{-6} 20×10^{-6}–100×10^{-6}	[165]

[1]Gr: reduced graphene
[2]ErGO: Electrochemically reduced graphene oxide
[3]PDDA: Poly (diallyldimethylammonium chloride) functionalised

[4]WO_3: Tungsten oxide NPs
[5] CTS: Chitosan
[6]IL IL: Ionic liquid
[7]CILE: Carbon ionic liquid electrode
[8]EF: Ethynylferrocene
[9]2PHC: 2-(4-oxo-3-phenyl-3,4-dihydro-quinazolinyl)-N′-phenyl hydrazine carbthioamide
[10]MIP: Molecularly imprinted polymer
[11]MPS: Mesoporous silica
[12] XOD: Xanthine oxidase enzyme
[13]Cu–YHA-EDA: Copper complexes formed with Algerian humic acid modified with ethylenediamine
[14]Cu–YHA-TETA: Copper complexes formed with Algerian humic acid modified with triethylenetetramine
[15]NWE: nanowire electrode

2.7 Electrochemical characterisation methods

Cyclic voltammetry and electrochemical impedance spectroscopy methods have been applied to evaluate the effects of the modification on the performance of the modified electrode. These techniques are very useful for investigating the thermodynamics and kinetics of the electron transport process on the electrode surface. In addition, the efficiency of the electron mediators is elucidated using these electrochemical methods.

2.7.1 Cyclic voltammetry (CV)

The CV method has been applied widely as a high-performance technique to study the electrochemical performance of the modified electrode since its presentation by Randies in 1938. In addition, the reversibility of a reaction, the mechanism of the reaction, the redox potential, the redox current of the electroactive species and the effect of the modification on the electron transfer rate can be studied by this method [1].

The basic voltammogram of variation of current versus potential is demonstrated in Figure 2.6. At the initial potential (E_i), only the reduced species (R) are present in the bulk solution (because $E_i<E_{redox}$ for conversion of R into O). In region A, by increasing the potential towards the standard potential of the cell half reaction, anodic peak current ($I_{p,a}$) starts to ascend (almost exponentially this is controlled by the electrode kinetic) and, with electrons being transferred between the electrode and R which converts into O, the established concentration gradients of R and O lead to diffusion transport of R to the surface and O from the surface. In region B, the concentration of R descends greatly, as E_{redox} is positive enough to oxidise any R on the electrode surface to O which leads to a decrease in $I_{p,a}$ as it becomes transport limited. Before region C, the concentration of O is at maximum and the concentration of R is at minimum. During region C, the direction of the potential inverses and O species starts to reduce to the R species, which causes a cathodic peak current ($I_{p,c}$) (region D). By continuance in the CV sweeping, the O species decreases and current almost returns to zero [166]. The Nernst equation (for fast electrode kinetics) has a fundamental role in most of the electrochemical reactions, which demonstrates the relationship between concentrations of the oxidised species to reduced species and the potential of the electrode, respecting the Equation 2.1 [1, 2].

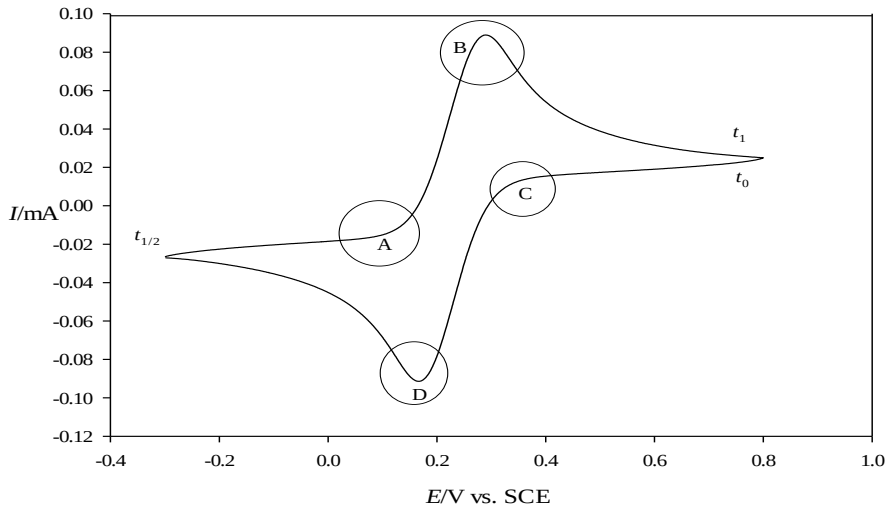

Figure 2.6: Typical CV for a reversible redox process $O + ne^- \rightleftharpoons R$.

$$\mathbf{O + ne^- \rightleftharpoons R}$$

$$E = E^{\circ\prime} + \mathrm{RT/nF}\ln(C_\mathrm{O}/\mathrm{C_R}) \tag{2.1}$$

Here E is the potential of cell (evaluated when current is zero), $E^{\circ'}$ is the formal reduction potential, R is the gas constant (8.314 J K^{-1} mol^{-1}) and T is the temperature (K), n is the number of moles of electron involved in the redox reaction, F is Faraday's constant (96485 C mol^{-1}), C_o is the concentration of O and C_R is the concentration R in the bulk solution.

The Randles-Ševčík equation is employed to evaluate the peak current (I_p) in a reversible system [10].

$$I_p = 0.4463nFA\,(\frac{nF}{RT})^{1/2}\,D^{1/2}\,C_v\,v^{1/2} \tag{2.2}$$

Regarding the Equation 2.2, n is the number of moles of electron involved in the redox reaction, F is Faraday's constant (96485 C mol^{-1}) , A is the electrode surface area (cm^2), R is the gas constant (8.314 J K^{-1} mol^{-1}) and T is the temperature (K), D is the diffusion coefficient (cm^2 s^{-1}), C is the concentration of the analyte in bulk solution (mole cm^{-3}), and v is the scan rate (V s^{-1}).

In an ideal reversible system (both chemically and electrochemically reversible), I_{pa}/I_{pc} equals unity, the peak potential separation and the formal potential are calculated in the Equations 2.3 and 2.4 [10].

$$\Delta E_p = (E_{pa} - E_{pc}) = 57/n \text{ mV} \quad (2.3)$$

$$E_f^\circ = (E_{pa} + E_{pc})/2 \quad (2.4)$$

In irreversible systems, the peak current is evaluated by Equation 2.5 (at 298 K). The peak current is related to the value of α, which is the transfer coefficient. Comparison with the reversible systems; the peak current value is smaller [10].

$$I_p = (2.99 \times 10^5) n(\alpha n_a)^{1/2} A C D^{1/2} v^{1/2} \quad (2.5)$$

$$E_p = E_f^\circ - \frac{RT}{\alpha nF}\left[0.78 + \ln\frac{D^{1/2}}{K^\circ} + 0.5\ln\left(\frac{\alpha nF v}{RT}\right)\right] \quad (2.6)$$

Regarding the Equation 2.6, E_P occurs at potentials higher than the formal potential with the over-potential related to rate constant (k^o) and the transfer coefficient (α) [10]. In the reversible system, scanning the potential in the negative direction makes the electrode a stronger reductant, whereas scanning the potential in the positive direction makes it a better oxidant. In the case of irreversible electrode reaction, the electron transfer kinetics are not sufficient to keep the Nernstian equation balanced. In a totally irreversible reaction, reverse peak is absent in reverse sweep. The change of the electrode reaction behaviour from reversible to irreversible at higher sweep rates can be seen in the plot of I_p *vs.* $v^{\frac{1}{2}}$ [167, 168].

2.7.2 Electrochemical impedance spectroscopy (EIS)

EIS is an informative method in electrochemistry that provides valuable information about the interfacial properties of the modified electrodes (especially biosensors) such as double-layer capacitance, charge transfer resistance, uncompensated resistance, diffusion coefficients, kinetic parameters, the effect of the number of layers of modifier, surface roughness and the porosity of a surface-modified electrode. So EIS is used to study any process that affects the conductivity of a system. In summary, impedance (*Z*) refers to the frequency-dependant resistance (the opposition force to electrical current (*I*) and is evaluated in Ohms (Ω) in an AC system. EIS is run in a reversible redox system such as $Fe(CN)_6^{3-}/Fe(CN)_6^{4-}$ or $Ru(NH_3)_6^{3+}$ to investigate the effects of the modification of a bare electrode on the interfacial electron transfer rate. EIS measurements are performed by applying small sinusoidal AC potential through the electrochemical cell at a set frequency to measure current. The responses are recorded and the impedance is computed at each frequency. This process is repeated for a wide range of frequencies (for example 10 kHz to 0.01 Hz) to obtain the real (*Z*') and imaginary (*Z*'') impedance value and draw its plot (Nyquist or a Bode plot) for analysis [169]. The study of the Nyquist diagram is informative in gaining a clear understanding of the electron transport mechanism. For example, in Figure 2.7 the Nyquist curve

consists of two regions, a semi-circular region that is dependent on the electron transport resistance (R_{et}), and the linear region which is associated with the diffusion phenomenon. The modification process is performed to change the electron transport kinetic and R_{et} at the electrode surface. By comparison with the Nyquist diagrams of the modified electrode with an unmodified electrode, the influence of modification on the electron transport kinetic becomes obvious.

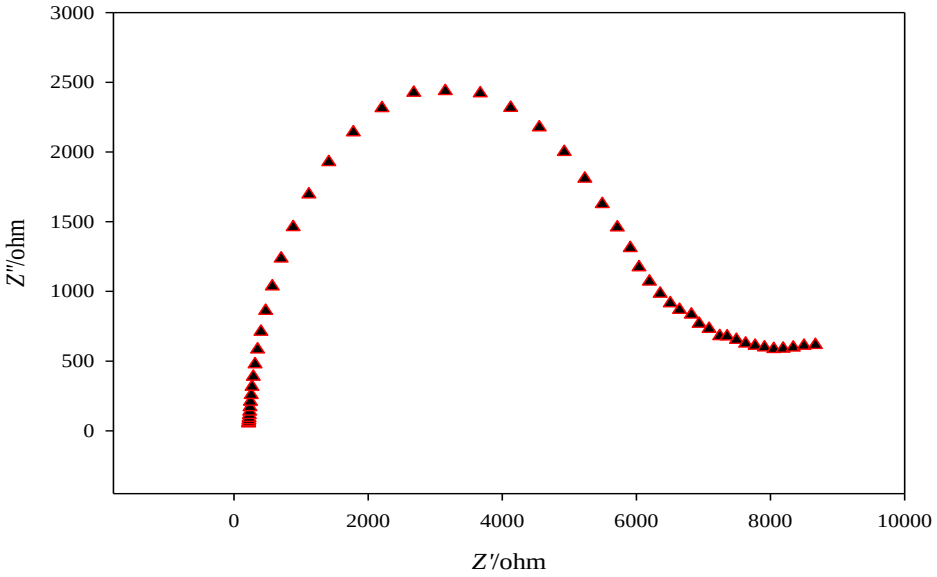

2.7: Nyquist diagram for a reversible redox system at GCE.

A Bode plot shows the variation of the absolute impedance and the phase shift (φ) versus the frequency. Modelling of the impedance results in an electrically equivalent circuit is an efficient way to gain valuable information from the displayed plots. The three important members of an electrical circle are capacitors (C), resistors (R) and inductors (L), which must be associated physically with the electrochemical cell. Other elements of equivalent circuit are the constant phase element (CPE), where the phase shift (φ) is independent of frequency and the Warburg element (ZW), which is employed to show the diffusion layer of the system [170].

(A) (B)

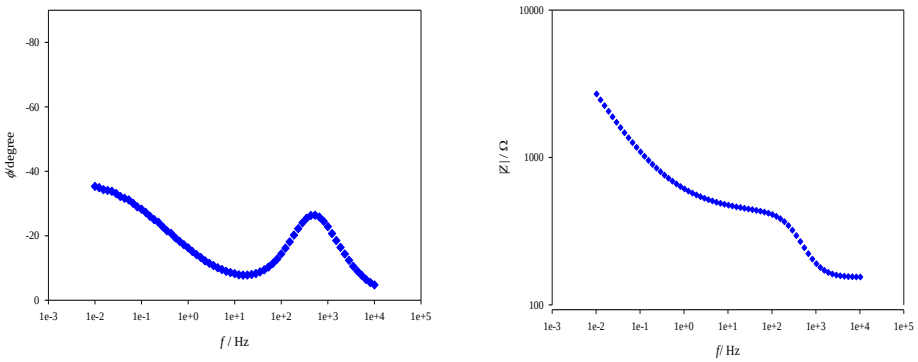

2.8: Bode plots for a reversible redox system at GCE.

3 Objectives of the work

The aim of this study was focused on the fabrication of novel, non-toxic, low-cost and high-performance modified carbon-based electrodes. Various modifiers including KolliphorEL, Au/Pd/MWCNT nanocomposite, Pd NPs and carbon-modified titanium dioxide nanocomposite (CMTN) were synthesised and employed to fabricate a new electrochemical electrode, then the electrochemical behaviour of the modified electrodes was studied by CV and EIS. Another aim of this investigation was focused on the study of the efficiency of the modified electrodes in sensing the target medicament.

The main aims of papers (I-IV) are given as follows:

1. Synthesising suitable modifiers (papers II-IV).
2. Characterising the modifiers using various techniques such as XPS, SEM, FTIR and XRD (papers II, IV).
3. Modifying carbon-based electrodes with suitable modifiers (papers I-IV).
4. Investigating the voltammetric behaviour of modified carbon-based electrodes and comparing with unmodified working electrodes by CV and EIS methods (papers I-IV).
5. Studying the performance of the modified electrode compared with an unmodified electrode in the absence and presence of the target analyte (papers I-IV).
6. Investigating the effect of pH and potential sweep rate on the response of the modified electrodes by CV to study the optimum conditions, and analysing the mechanism of the electrocatalytic process on the surface of the modified electrodes (papers I-IV).
7. Determining dynamic linear ranges and the detection limit of the target analyte by applying DPV (papers II-IV).

4 Experimental work

4.1 Chemical reagents

- KolliphorEL; Cremophor EL (CAS number 61791-12-6; MW ca. 2450 g mol-1) was purchased from Aldrich (I)
- MWCNT (purity of 95%, outer diameter: 10 – 20 nm, inner diameter: 5 – 10 nm and tube length: 0.5 – 200 nm) was purchased from Nanostructured & Amorphous Materials (Houston, TX, USA) (II)
- $HAuCl_4$ (purity of 99%) was obtained from Sigma Aldrich (II)
- $PdCl_2$ (purity of 99%) was purchased from sigma-Aldrich (III)
- TiO_2 nano-powder (purity ≥99.5, average size:25 nm) was purchased from sigma-Aldrich (IV)
- Ferrocenedimethanol (98%), ferrocene acetic acid (98%), ferrocene acetonitrile were obtained from Aldrich, n-butyl ferrocene (oil, 98%) and N,N' dimethylaminomethylferrocene (oil, 98%) were purchased from Alfa Aesar and TCI Europe (I)
- Timolol maleate was purchased from U. S. Pharmacopeia (II)
- Terazosin was supplied by Arya pharmaceutical company (Tehran, Iran) (III)
- Methylene blue was obtained from Merck (IV)

4.2 Instrumentation

- An Ivium 104 (model B08084) (I) and an Autolab potentiostat/galvanostat (PGSTAT12) (II, III and IV)
- A conventional three-electrode system was used with a working electrode (CPE or GCE), a saturated calomel reference electrode as reference electrode and platinum wire as the counter electrode
- A digital pH/mV/Ion meter
- Ultrasonic bath
- SEM (Hitachi S-4800 Ultra-High Resolution) (II, III and IV) and EDS (S4800) (III)
- A Thermo Scientific K-Alpha XPS spectrometer (I)
- X-ray diffractometer (Panalytical X'PERT PRO) (IV)
- FTIR spectrophotometer (Bruker Optics, Germany) (IV)
- Zetasizer Nano ZS (ZEN3500, Malvern) (IV)
- A Micromeritics ASAP2010 (IV)

4.3 Characterisation

Voltammetric investigations (CV and EIS) were conducted with a conventional three-electrode system using an Ivium 104 (model B08084) (I) and an Autolab potentiostat/galvanostat (PGSTAT12) (II, III and IV). A saturated calomel reference electrode (SCE), a working electrode (CPE and GCE) and a platinum auxiliary electrode were utilised. The modified electrode surface morphology was studied by SEM (II, III and IV). EDS was employed to study the elements of Au/Pd/MWCNT nanocomposite (II). The attachment of KolliphorEL monolayer on the GCE surface was

investigated with XPS (I). The surface charge of CMTN and its variation with pH were investigated using Zetasizer Nano ZS (IV). The textural properties and surface area of CMTN were investigated using N_2 adsorption/desorption isotherms with a Micromeritics ASAP2010 (IV). The FTIR method was used to study the surface functional groups of CMTN (IV). The XRD technique investigated the crystalline phase of TiO_2 NPs and CMTN (IV). The characterisation was undertaken under ambient temperature and pressure conditions.

4.4 Working electrode preparation

CPE: The CPE was constructed from a Teflon tube-shaped body (3.0 mm diameter) with a copper wire in its back to make an electrical contact. The Teflon tube was filled with a homogenised carbon paste made from graphite powder and paraffin oil (75:25, w/w). The surface of CPE was polished on the weighting paper to obtain a mirror-like surface and rinsed with doubly-distilled or deionised water (II, III).

GCE: The surface of GCE (3.0 mm diameter) was polished with alumina powder (smaller than 0.05 µm) on a polishing cloth to obtain a shiny (mirror-like) surface, then the GCE was rinsed with deionised water and dried with nitrogen gas before use (I, IV).

(A) (B)

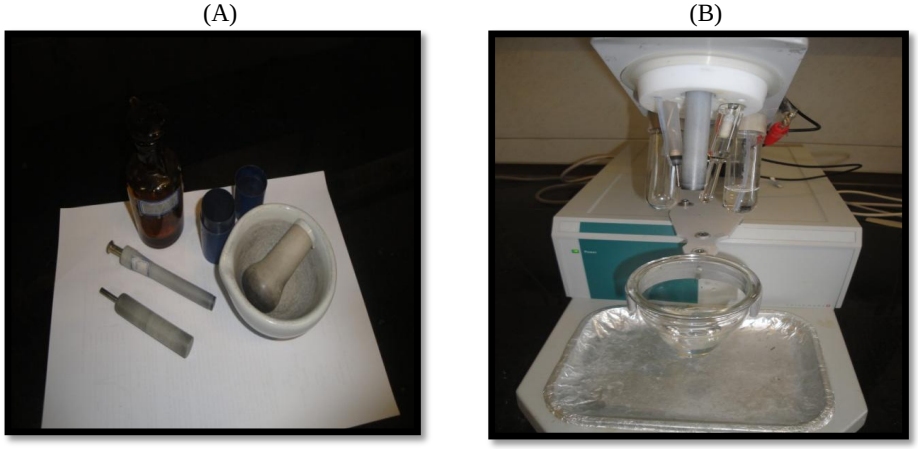

Figure 4.1: (A) Preparation of CPE (II, III) and (B) A conventional three-electrode system in Metrohm Computrace voltammetric analyser model 797VA.

4.4.1 KolliphorEL monolayer grafted electrode (I)

Before surface modification of GCE, the surface of GCE should be cleaned by polishing with alumina paste, rinsing with deionised water and using a CV in aqueous solution of $K_3Fe(CN)_6$ (5 mM, from Aldrich), $K_4Fe(CN)_6$ (5 mM, from Fisons) and KNO_3 (0.1 M, from Sigma-Aldrich), which have significant effect on wiping any history effect from GCE surface.

The KolliphorEL was grafted onto the surface of GCE (d= 3mm) using a fixed anodic potential of +1.6 V for 1200 s in a $LiClO_4$ (20 mM, as a supporting electrolyte, from

Sigma-Aldrich) and KolliphorEL solution. Then, the surface of modified GCE was rinsed with deionised water to remove any residual KolliphorEL and dried with nitrogen gas (I).

4.4.2 Carbon paste/Au/Pd/MWCNTs nanocomposite electrode (II)

Chemical reduction method was used to synthesis Au/Pd/MWCNTs nanocomposite. The preparation of Au/Pd/MWCNTs nanocomposite is explained in detailed in paper (II). The matrix modification of CPE was conducted by blending the graphite powder, paraffin oil and modifier powder (Au/Pd/MWCNT nanocomposite (75:25:5, w/w). The surface of modified CPE was polished on the weighting paper to obtain a mirror-like surface and rinsed with doubly-distilled water (II).

4.4.3 Pd NPs/CPE (III)

The surface of polished CPE was covered with Pd NPs by running CV scanning from a potential of +1.20 V to −0.250 V ten times in deaerated solution of $PdCl_2$ (1.0 mM) and sulphuric acid (0.5 M). Then, the surface of modified CPE was rinsed with deionised water and dried (III).

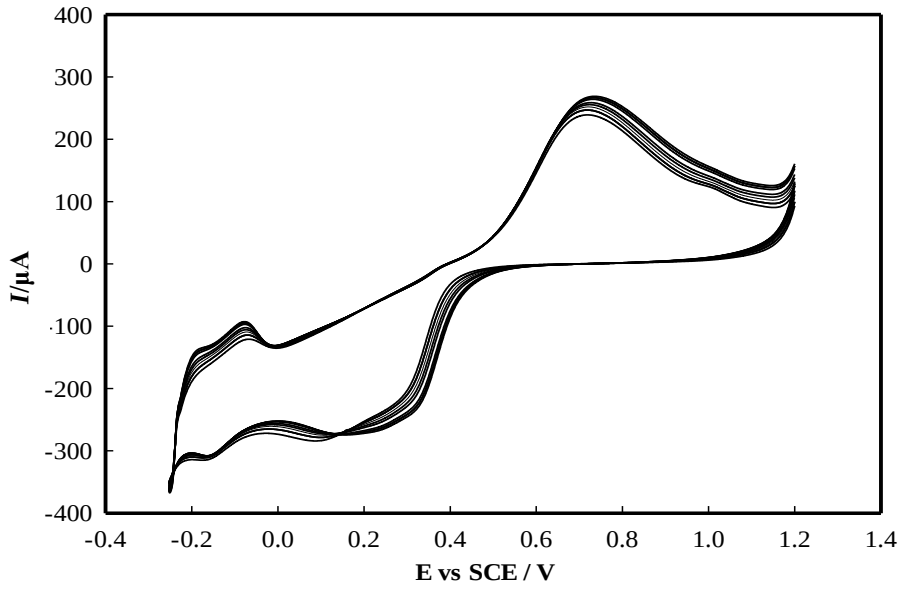

Figure 4.2: Repeated CVs for electro-deposition of Pd NPs on the surface of CPE (III).

4.4.4 CMTN/GCE (IV)

The synthesised CMTN (the preparation of CMTN is explained in detailed in paper (IV) [45] was dispersed in solution of acetonitrile (1:1, w/v ratio) under ultrasonic agitation for 30 min. Then, a droplet of CMTN solution (5.0μL) was employed on the surface of GCE and allowed to evaporate to appear as a black layer on the GCE surface (IV).

4.5 Pharmaceutical preparation procedure

A known value of the pharmaceutical sample (tablet) was powdered and diluted with appropriate buffer solution in optimum pH. Then, the mixture including pharmaceutical sample and buffer solution is stirred for 30 min and was ultrasonicated for 15 min. The prepared solution was filtered and was used to prepare pharmaceutical sample solution (II, III).

4.6 Standard addition method

The standard addition technique is known as a reliable calibration approach to study the applicability of the modified electrode in determination of target analyt in real samples and the effect of matrix. In this regard, the same value of real sample was added to various amounts of standard solutions in a concentration range (under the optimum conditions). In next step, the prepared samples were analysed by using appropriate voltammetric method and the obtained data were used to draw calibration plot (peak current *vs*. analyt concentration), and to evaluate recovery (II, III and IV).

5 Results and discussion

5.1 Interfacial electron-shuttling processes across KolliphorEL monolayer grafted electrodes (I)

Electrochemical modification of electrode surface is an attractive route for electroanalytical applications [171]. Various methods have been reported to graft various organic molecules [172, 173] such as diazonium salts [168], amines [174] (for example ethylene diamine), aliphatic primary alcohols and poly (ethylene glycol) (or PEG) derivatives [173, 175] onto the carbon electrode surfaces [167, 168].

Here, an electrochemical attachment method adapted from Maeda *et al.* was employed for the anodic grafting of KolliphorEL onto the surface of GCE. The KolliphorEL consisted of poly(ethylene glycol) which was terminated with hydroxyl groups and could attach to the carbon surfaces [176]. The experimental conditions of the anodic electrochemical grafting method such as the anodic potential and time were optimised to prepare monolayer coverage of KolliphorEL on the GCE surface. The presence of the KolliphorEL monolayer on the GCE surface was studied and confirmed using the XPS method (I). CV and EIS methods were employed to investigate the performance of modified GCE compared to the bare GCE at $Fe(CN)_6^{3-/4-}$ solution as a redox probe. The CV response signal at the bare GCE was quasi-reversible. However, the signal decreased significantly at the surface of the modified electrode due to the role of the KolliphorEL monolayer in the collapse of the interfacial charge transport in the $Fe(CN)_6^{3-/4-}$ redox system. The EIS method successfully demonstrated the effect of GCE surface modification on the collapse of the interfacial charge transport (I).

$$Fe(CN)^{3-}{}_6 + e^- \underset{\leftarrow}{\rightarrow} Fe(CN)^{4-}{}_6 \qquad (5.1)$$

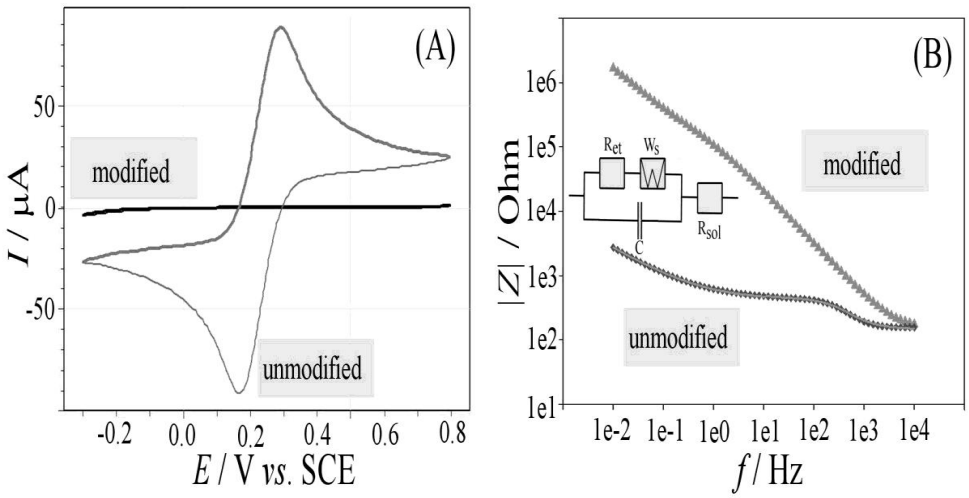

Figure 5.1: (A) CVs and (B) EIS data of modified and unmodified GCE into the solution of 5 mM $Fe(CN)_6^{3-}$, 5 mM $Fe(CN)_6^{4-}$, and 0.1 M KNO_3 (I).

A hydrophobic zone on the surface of the modified GCE was constructed from the triglyceride groups of KolliphorEL. This hydrophobic zone provided an opportunity for hydrophobic reagents to travel along the KolliphorEL layer, to attach to the modified GCE surface and to improve interfacial charge transfer (I).

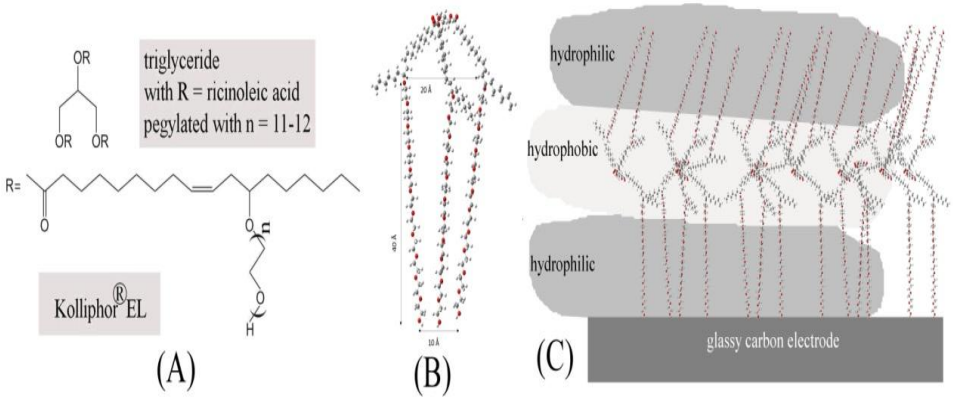

Figure 5.2: (A) KolliphorEL main component molecular structure and (B) 3D rendering (GaussView 5.0) (d: 3-5 nm approximately). (C) The resultant hydrophobic area from triglyceride group of a KolliphorEL (I).

The ferrocene (Fc) family as a hydrophobic electron mediator could act as a shuttle for the transport of electrons through the KolliphorEL layer, so the presence of low values of Fc derivatives could unlock the interfacial charge transport very well and restore the redox signal partially or entirely (I).

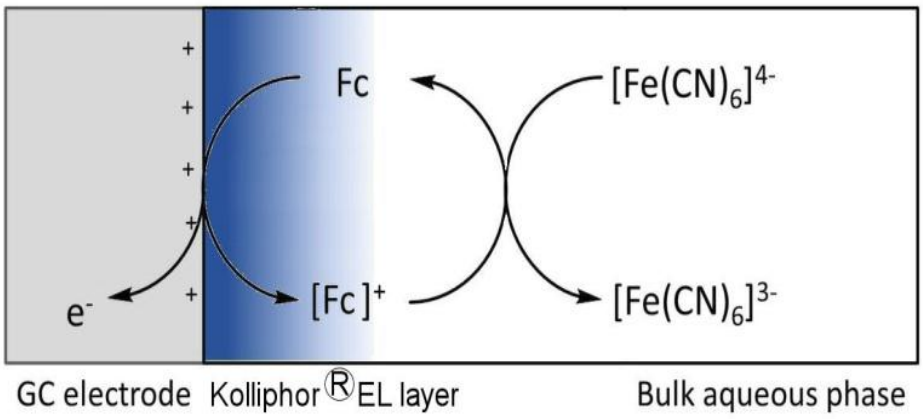

Figure 5.3: Schematic electron shuttling mechanism of Fc for the $Fe(CN)_6^{3-/4-}$ redox system (I).

The electron shuttling performance of five members of Fc family was studied and compared with each other. The efficiencies of Fc derivatives in the electron transportation through the KolliphorEL monolayer were compared with each other using CV and EIS results. The reversible potential (E_0) of $Fe(CN)_6^{3-/4-}$ was located at +0.19 V. This value shifted to the positive potentials for Fc derivatives that made Fc

derivatives better electron mediators in improving the oxidation process of $Fe(CN)_6^{3-/4-}$ compared to the reduction process. In addition, the scale of the $I_{p,a}$ was connected to the peak separation (ΔE_p^a). A broader gap between peaks demonstrated a slower charge transport rate, which could follow the reduction in charge shuttling and anodic signal. Other factors effective on Fc electron shuttling efficiency were correlated with the aggregating or linking ability to the modified GCE surface and with holding a desirable electrostatic charge with respect to $Fe(CN)_6^{3-/4-}$. Among the Fc derivatives, ferrocene-acetic acid and ferrocene-acetonitrile demonstrated less electron shuttling efficiency with respect to their less positive E_0^a and wider ΔE_p^a, and dimethylaminomethyl ferrocene showed high performance compared to others with sub-micromolar LOD. The investigated Fc derivatives are listed in Table 5.1the most efficient Fc was at the top (II).

Table 5.1: Summary of the results obtained by CV of the modified GCE in the solution of 5 mM $Fe(CN)_6^{3-}$, 5 mM $Fe(CN)_6^{4-}$, 0.1 M KNO_3 in the presence of 50 µM Fc sample (I).

	E^0 / V *vs.* SCE	ΔE_p / V
Dimethylamino-methyl-ferrocene	0.27	0.10
n-butyl-ferrocene	0.22	0.04
Ferrocene-dimethanol	0.28	0.11
Ferrocene-acetonitrile	0.21	0.22
Ferrocene-acetic acid	0.20	0.22

The obtained quantitative data of the EIS study were collected in Table 5.2. Some parameters such as solution resistance (R_{sol}) and apparent capacitance (CPE_T) were unchanged, approximately the same as the bare GCE capacitance of the double layer. The electron transfer resistance (R_{et}) variation did not follow an obvious pattern with respect to Fc concentration or Fc structure. The apparent diffusion layer thickness (δ_{app}) was connected to the Warburg element W_T. The value of δ_{app} could be calculated by following equation (I).

$$\delta_{app} = (W_T \times D)^{1/2} \tag{5.2}$$

The approximate value of diffusion coefficient (D) was noted to be 0.6×10^{-9} m^2s^{-1} [177]. The calculated value of δ_{app} for Fc derivatives could be employed as a factor for

evaluating and comparing Fc derivatives with respect to their electron shuttling ability. The low value of δ_{app} correlated to more effective electron shuttling along the KolliphorEL film (assuming low concentration of Fc and constant concentration of $Fe(CN)^{4-}_6$). The EIS results were in agreement with the CV results. Dimethylaminomethyl ferrocene was found to be the best electron shuttle on the surface of the modified GCE with the lowest value of δ_{app} (I).

Table 5.2: Summary of the results obtained by the CV and EIS study of the modified GCE in the solution of 5 mM $Fe(CN)_6^{3-}$, 5 mM $Fe(CN)_6^{4-}$, 0.1 M KNO_3 in the presence of Fc (I).

	Fc /µM	R_{sol} /Ω	R_{et} /Ω	W_R /kΩ	W_T /s	CPE_T /µF	CPE_P	δ_{app}/µm
Dimethylamino-methyl-ferrocene	1	135	6180	123	2.82	4.01	0.795	41
	10	138	3092	335	19.0	2.69	0.838	107
n-butyl-ferrocene	1	130	6557	139	8.14	1.82	0.789	70
	10	127	1117	127	222	3.94	0.743	365
Ferrocene-dimethanol	1	127	9177	524	38.9	2.84	0.796	153
	10	134	5073	268	5.16	2.78	0.798	56
Ferrocene-acetonitrile	1	137	2958	690	82.5	2.39	0.816	222
	10	150	5332	635	67.3	2.30	0.835	201
Ferrocene-acetic acid	1	123	7815	1720	393	2.32	0.843	486
	10	132	6063	89	11.8	2.58	0.832	84

5.2 Carbon paste electrode with Au/Pd/MWCNT nanocomposite for nanomolar determination of Timolol (II)

Timolol maleate (TM) is the first β-blocker medicine with high applicably in the treatment of various heart-related diseases [178]. Determining and monitoring the TM values in its pharmaceutical products is essential to keeping the TM effective dosage. In this study, the fabrication of a new modified CPE was considered for investigating TM concentrations. Metal NPs have played a significant role in the development of modified carbon-based electrodes. Metal NPs can act as electron mediators to increase the rate of charge transport in electrochemical processes. The utilisation of a high conducting substrate for establishing homogenised distribution of the metal NPs is useful in the process of modifier preparation and can improve the electrocatalytic performance of metal NPs and the conductivity of the employed modifier effectively [179, 180]. Here, Au NPs and Pd NPs were synthesised, dispersed and embedded into the MWCNT matrix to prepare a nanocomposite of Au/Pd/MWCNT, then the body of the CPE was modified with Au/Pd/MWCNT nanocomposite. The existence of Au NPs, Pd NPs and MWCNT was successfully demonstrated with SEM and EDS (Figure 5.4).

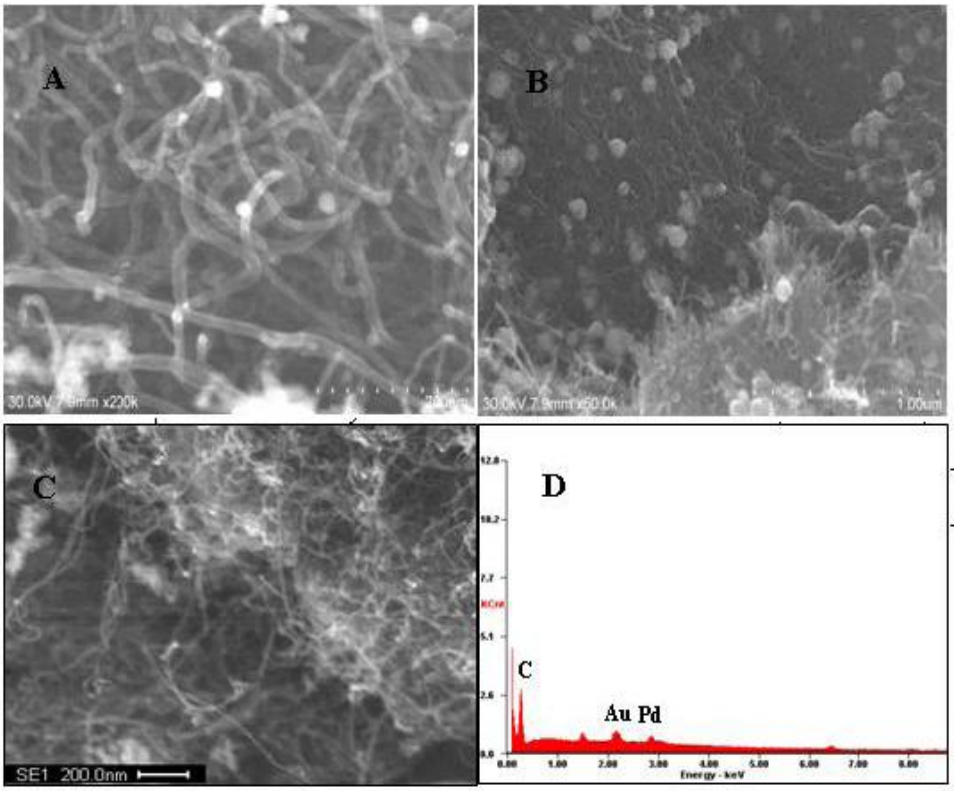

Figure 5.4: The SEM images of (A) the Au/MWCNT nanocomposite, (B) Pd/MWCNT nanocomposite, (C) Au/Pd/MWCNT nanocomposite and (D) corresponding EDS diagram showing peaks for Au/Pd NPs attached to a MWCNT matrix (II).

The utility of the modified CPE with Au/Pd/MWCNT nanocomposite was tested in the detection of TM using the CV method. Regarding CV investigation, the performance of the unmodified CPE and modified CPE was studied in the presence of a 1.0×10^{-3} M TM solution. The signal peak of the modified CPE was higher than the unmodified signal, which demonstrated the high efficiency of Au/Pd/MWCNT nanocomposite in enhancing the kinetic of the electron transport. Figure 5.5 demonstrated and compared well the resultant CVs of unmodified CPE, modified CPE with MWCNT, modified CPE with Pd NPs/MWCNT and modified CPE with Au/Pd/MWCNT in the presence of TM. The signal obtained at Au/Pd/MWCNT/CPE was well defined and much higher than the signal gained at MWCNT/CPE and Pd/MWCNT/CPE, which revealed that the MWCNT acted well as a conductive support for promoting the electrocatalytic performance of Au/Pd NPs, and the combination of Au/Pd/MWCNT in CPE was successful in detecting TM.

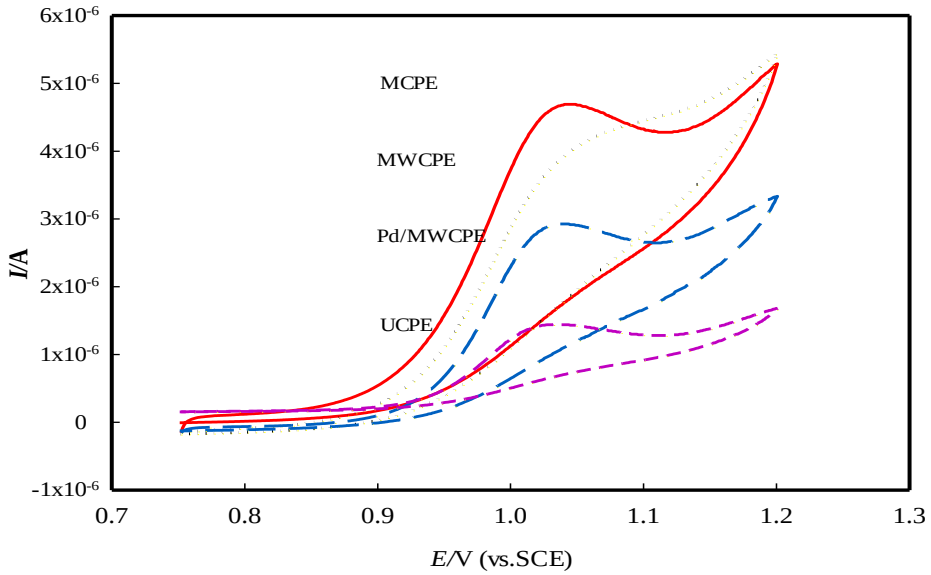

Figure 5.5: CVs in the presence of TM (1 mM, pH 2.0) at unmodified CPE (UCPE) (short-dashed line), at Pd NPs/MWCNT/CPE (long-dashed line) and MWCNT/CPE (dotted line) and Au/Pd/MWCNT/CPE (solid line) (v was 100 mVs^{-1}) (II).

In order to obtain a well-defined response peak, various parameters such as solution pH, rate of scanning, and the amount of employed Au/Pd/MWCNT nanocomposite in matrix of CPE were investigated and optimised. The best signal was gained at pH 2.0, so all the voltammetric measurements were conducted at pH 2.0. The pH dependency of the TM oxidation response peak is shown in Figure 5.6.

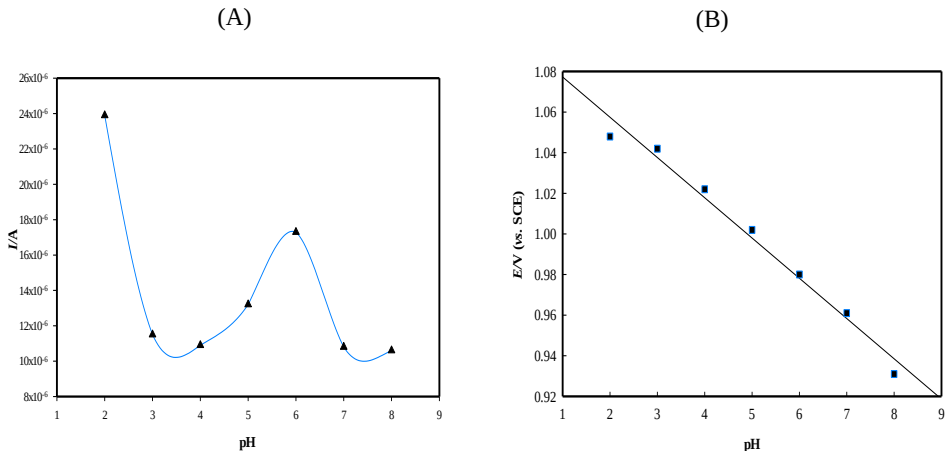

Figure 5.6: (A) Effect of variation of pHs *vs.* I_{pa} (B) Variation of E_{pa} *vs.* pHs (v was 100 mVs^{-1}) (II).

The mechanism of the electron transport on the surface of the modified CPE with Au/Pd/MWCNT nanocomposite was evaluated by studying the plot of the TM oxidation peak current variation with the square root of *v*. The observed linear relationship suggested a diffusion-controlled mechanism. The obtained slope from the log–log I-*v* plot was 0.43, which was in agreement with the expected slope 0.5 for a diffusion-controlled mechanism [10]. The number of electrons that participated in the rate-determining level was calculated to be one by drawing a Tafel plot.

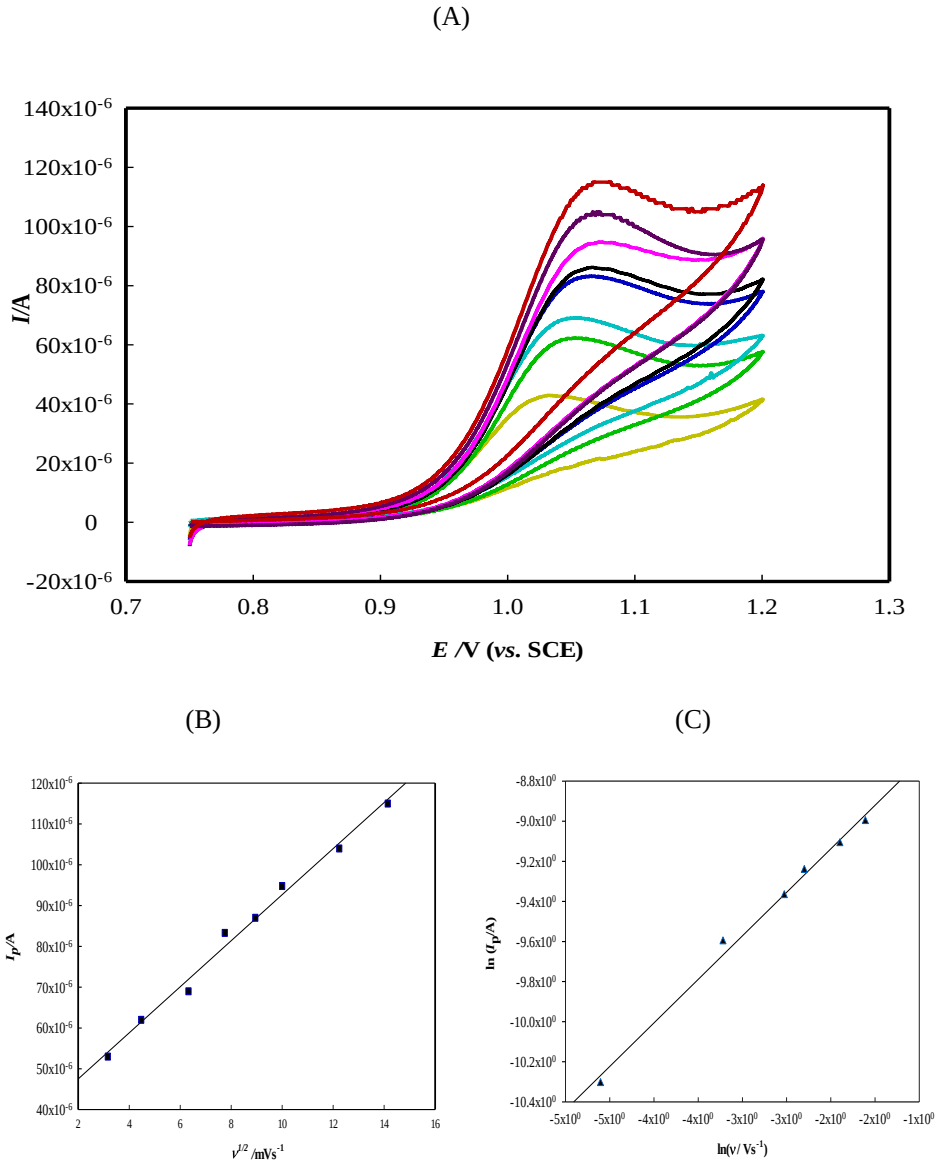

Figure 5.7: (A) Dependence of the CV response at Au/Pd/MWCNT/CPE on ν in 1.0 mM TM in pH 2.0 B-R buffer. Scan rates from bottom to top: 10, 20, 40, 60, 80, 100, 150, 200 mV s^{-1} (B) variation of I_{pa} *vs.* $\nu^{1/2}$(C) Dependence of Ln I_{pa} versus Ln ν.

DPV was selected to determine low concentration of TM due to its high sensitivity. A low detection limit of 5.8×10^{-11} M was evaluated and two dynamic linear ranges were observed (1.0×10^{-5}–1.0×10^{-3} M and 5.0×10^{-9}–8.0×10^{-7} M). The applicability of the modified CPE with Au/Pd/MWCNT nanocomposite was examined in the detection of the pharmaceutical sample of TM. A recovery of 98.83% was estimated using the standard addition method. In addition, the repeatability of the obtained results and the

reproducibility and stability of the modified CPE with Au/Pd/MWCNT nanocomposite were tested successfully in the detection of TM.

$$I_{pa} / A = 11.3 \times 10^{-6} + (0.0172 C / M) \qquad (R^2=0.994) \qquad (5.3)$$

$$I_{pa} / A = 2.83 \times 10^{-7} + (7.896 C / M) \qquad (R^2=0.998) \qquad (5.4)$$

(A) (B)

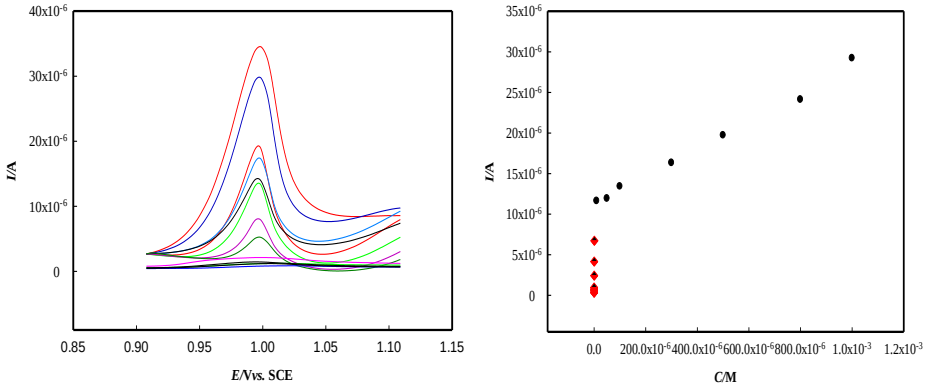

Figure 5.8: (A) DPVs of TM oxidation (1.0×10^{-3}–5.0×10^{-9} M), on the surface of Au/Pd/MWCNT/CPE (B) Variation of I_{pa} *vs.* TM concentration (1.0×10^{-3}–5.0×10^{-9} M) (ν was 100 mV s^{-1}) (II).

The proposed CME compared with previously employed working electrodes, demonstrated remarkable advantages such as good limit of detection in a wider linear concentration range for the detection of TM. In previously reported methods, the employed working electrodes were mostly mercury-based electrodes. The proposed CME employed CPE for modification, which involved interesting advantages such as inert nature, environmental friendliness, low cost, high compatibility, ease of preparation, and renewal and modification with various modifiers compared to mercury-based electrodes, which demonstrated high toxicity. The modified CPE with Au/Pd/MWNT demonstrated great electrochemical performance, high reproducibility and good stability (14 days).

Table 5.3: Previously reported working electrodes employed for determination of TM (II).

Method	Electrode	DLR (M)	LOD (M)	Reference
CCV- FI	Au microelectrode	1.0×10^{-10}–1.0×10^{-8}	1.0×10^{-11}	[181]
AdSV-SWP	HMDE	1.0×10^{-9}–1.2×10^{-8} 1.2×10^{-8}–1.0×10^{-7}	6.6×10^{-10}	[182]
SWP	HMDE	4.0×10^{-8}–3.0×10^{-6}	2.5×10^{-8}	[182]
AdSV-SWP	HMDE	1.0×10^{-7}–1.5×10^{-6}	1.26×10^{-8}	[183]
DPV	SMDE	1.0×10^{-6}–5.0×10^{-6}	2.5×10^{-6}	[184]
DPV	Fe_3O_4@GO-GC	2.0×10^{-7}–3.4×10^{-4}	2.0×10^{-8}	[185]
DPV	Au/Pd/MWNT-CPE	1.0×10^{-3}–1.0×10^{-5} 1.0×10^{-7}–8.0×10^{-9}	1.0×10^{-9}	(II)

5.3 Palladium nanoparticles in electrochemical sensing of trace terazosin in human serum and pharmaceutical preparations (III)

CPE surface modification methods have been found to be useful as well as the body modification method in the fabrication of efficient modified CPE. The electro-depositing of metal NPs on the surface of CPE using CV is a reliable method among surface modification methods. Pd NPs film was electro-deposited on the surface of the CPE. The Pd NPs coverage on the CPE surface was successfully observed using SEM.

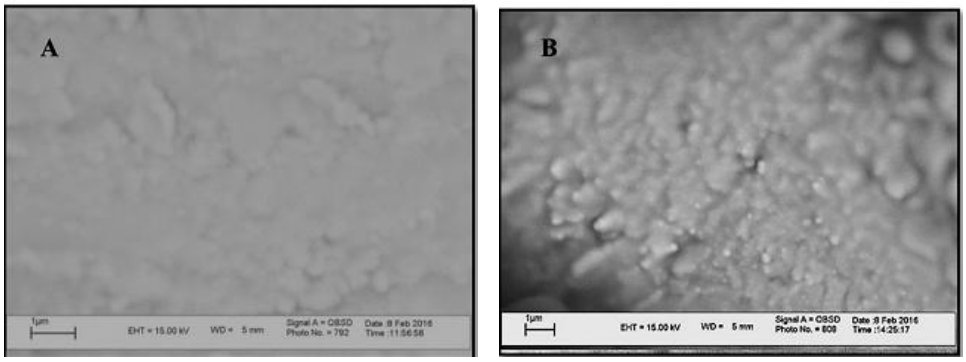

Figure 5.9: SEM image of (A) bare CPE and (B) Pd NPs/CPE (III).

The effective thickness of the Pd NPs film on the CPE surface was investigated and optimised using CV and EIS methods. The thickness enhancement of Pd NPs layer was connected to the number of CV scans. The CV signal growth was observable in Figure 5.10. The EIS method was applied efficiently to study the effect of Pd NPs thickness on the charge transport process. It was observed that the rate of charge transport on the modified CPE surface increased by increasing the number of CV scans to 10, but continued CV sweeping improved the electron transfer resistance, which was attributed to the unfavourable event of Pd NPs aggregation. The charge transport resistance decreased significantly on the surface of CPE modified with Pd NPs compared to bare CPE, which demonstrated well the effect of Pd NPs on improving the rate of charge transport (Figure 5.11). Regarding the number of Pd NPs deposition cycles 5, 10 and 20 on the surface of CPE, the surface areas were calculated using the Randles-Ševčík equation, and were estimated to be 2.88, 7.20, 4.32 cm^2. These results were in agreement with the CV and EIS results, so ten cycles of electro-deposition of Pd NPs on the CPE surface were selected for the experiments.

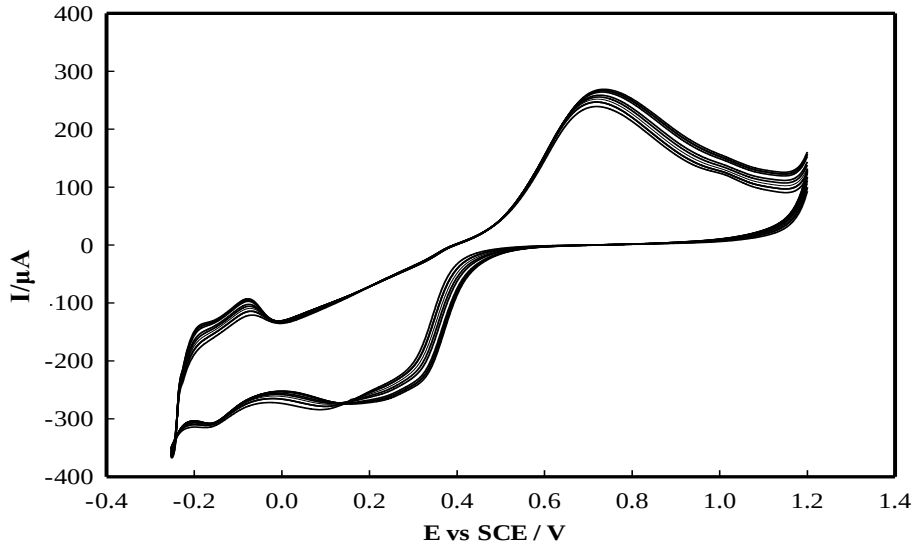

Figure 5.10: CVs of electro-deposited Pd NPs on CPE from 0.5 M H_2SO_4 and 1.0 mM K_2PdCl_4 in potential range of +1.2 to −0.25 V (*v* was 100 mV s^{-1}) (III).

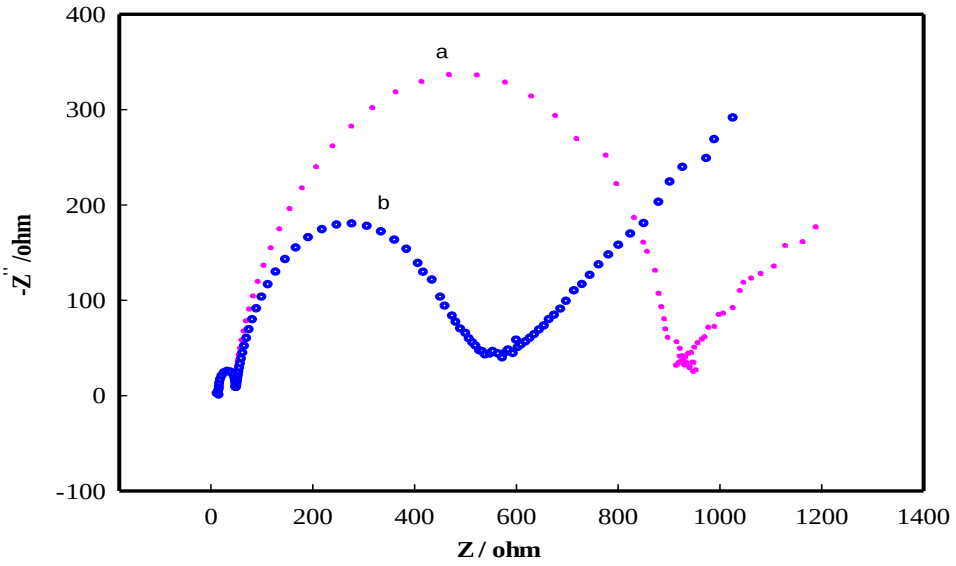

Figure 5.11: Nyquist plot for (a) bare CPE (b) Pd NPs/CPE in a solution of 5 mM $Fe(CN)_6^{3-}$, 5 mM $Fe(CN)_6^{4-}$, and 0.1 M KCl (the formal potential was 0.2 V and the frequency range was from 0.1 Hz to 10,000 Hz) (III).

The utility of the surface-modified CPE with Pd NPs film was examined in the detection of terazosin (TR). TR is an effective medicine prescribed for the treatment of urinary retention disorder in benign prostatic hyperplasia [186, 187] (Figure 5.12). The surface-modified CPE with Pd NPs film determined a well-defined anodic signal for oxidation of TR, which was much higher than the signal obtained from bare CPE (Figure 5.13). The electrochemical performance of the modified CPE was greatly enhanced due to modification with Pd NPs, which obviously increased the surface area and rate of charge transport on the surface of the modified CPE.

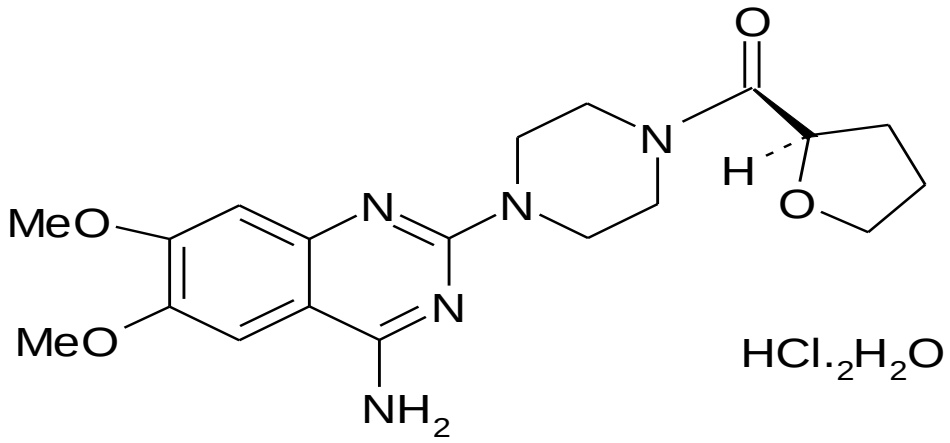

Figure 5.12: Chemical structure of TR (III).

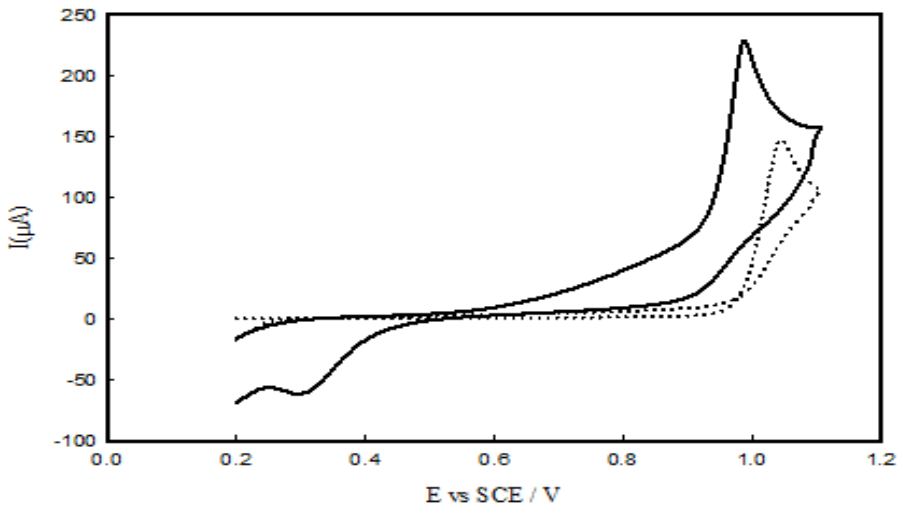

Figure 5.13: CVs of 1.0 mM TR on bare CPE (dashed line) and Pd NPs/CPE (solid line) surface, under optimised conditions (ν was 100 mV s^{-1}) (III).

Investigation of the effects of pH and ν on response peak current in the presence of TR was a useful way to optimise the experiment conditions and efficient determination of TR concentrations. The best-defined and sharpest response peak was observed at pH 2.0, so further experiments were conducted at pH 2.0. The movement of the anodic potential to less positive potentials displayed the role of H^+ in the charge transport mechanism and the pH dependency of I_{pa} to E_{pa} (Figure 5.14) (III).

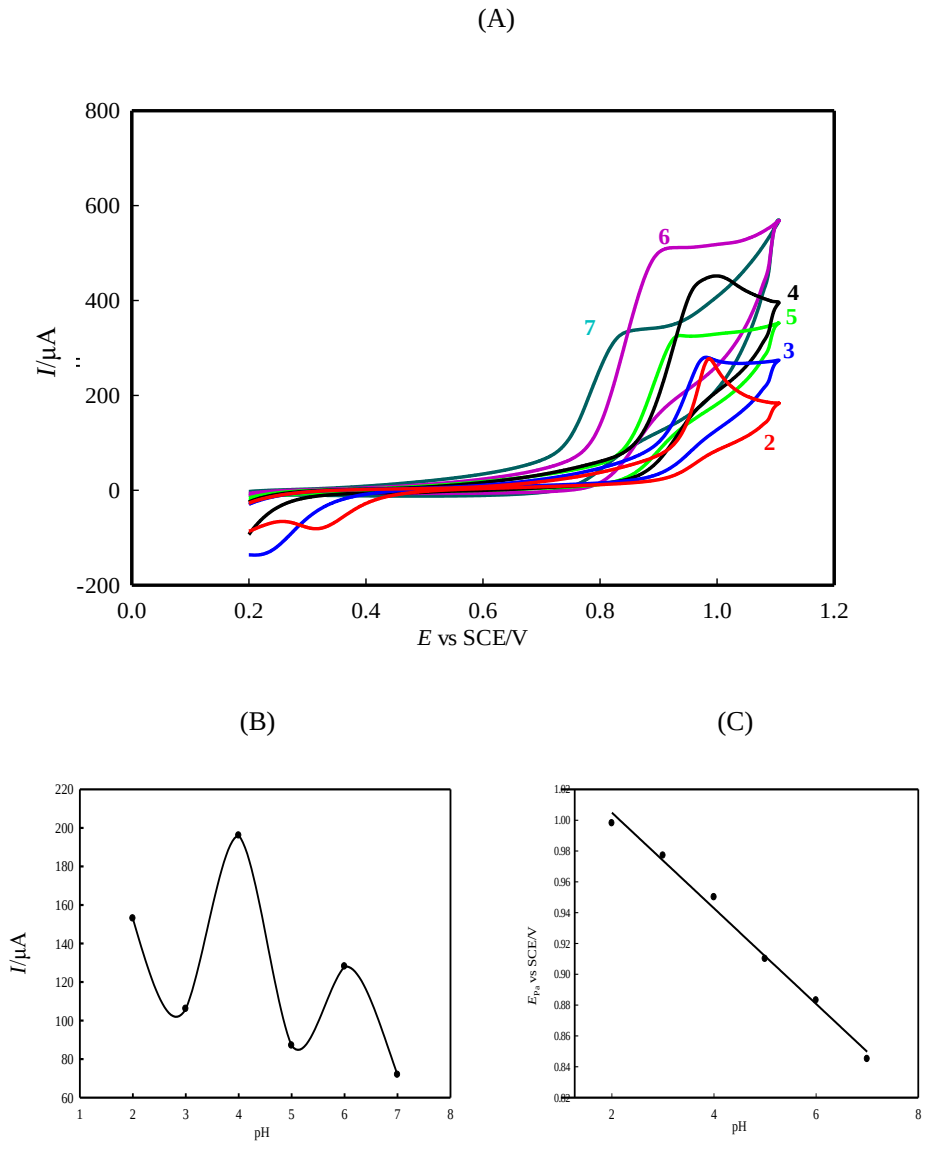

Figure 5.14: (A) The CVs of 1.0 mM TR oxidation on the surface of CPE modified with Pd NPs/CPE at different pHs. ν was 100 mV s^{-1}. (B) The pH dependency of I_{pa} and (C) E_{pa}.

The resultant data from the investigation of the variation of $I_{p,a}$ of TR with the square root of ν showed a linear relationship that demonstrated the diffusion-controlled mechanism in TR oxidation on the surface of the modified CPE with Pd NPs film (Figure 5.15) (III).

(A) (B)

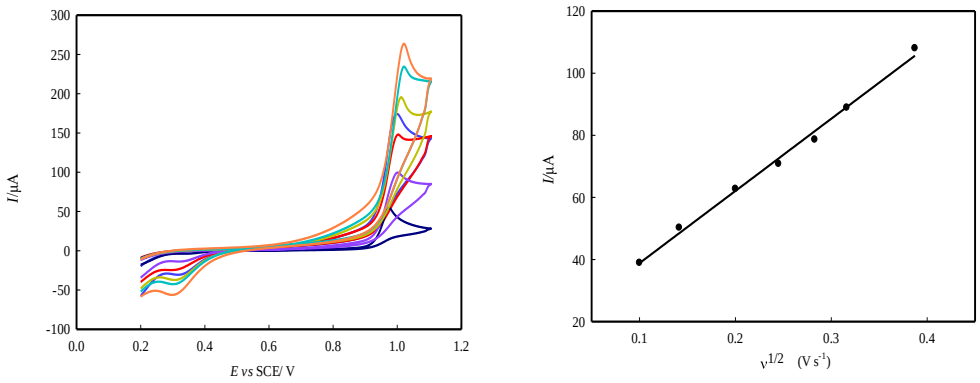

Figure 5.15: (A) CVs of 1.0 mM TR at Pd NPs/CPE in various ν: 10, 20, 40, 60, 80, 100, 150, and 200 mV/s. (B) Variation of I_{pa} *vs.* $\nu^{1/2}$.

The modified CPE with Pd NPs film was employed to investigate the low concentrations of TR by DPV method in optimised conditions. The $I_{p,a}$ ascended with increasing TR concentration. A wide dynamic linear range of 1.0×10^{-8}–1.0×10^{-3}M with an excellent limit of detection of 1.9×10^{-9} M was estimated in the detection of TR (Figure 5.16) (III).

$$I_p / \mu A = 4.436 + (0.154C) \qquad (R^2 = 0.9971,\ C \text{ is in M}) \qquad (5.5)$$

The efficiency of the modified CPE with Pd NPs film was evaluated in the detection of a TR pharmaceutical sample and synthetic serum sample using the standard addition method successfully with a recovery of 98.24%. In addition, the selectivity of the modified CPE with Pd NPs film towards TR was studied in the presence of common prescribed medicines such as tamsulocin and ciprofloxacin and other possible compounds including ascorbic acid, dopamine and uric acid, and the obtained signal displayed a difference of less than 5%. The repeatability and reproducibility were investigated successfully. The results demonstrated the high performance of the modified CPE with Pd NPs film for the sub-micromolar determination of TR.

(A) (B)

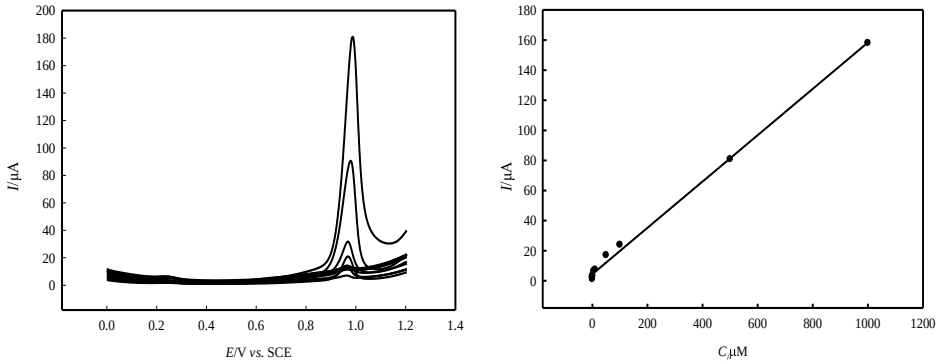

Figure 5.16: (A) DPVs of TR oxidation at surface-modified CPE with Pd NPs. (B) Plot of I_{pa} *vs.* TR concentration (down to up: 1.0×10^{-8}M, 5.0×10^{-8}M, 1.0×10^{-7}M, 5.0×10^{-7}M, 1.0×10^{-6}M, 5.0×10^{-6}M, 1.0×10^{-5}M, 5.0×10^{-5}M, 1.0×10^{-4} M, 5.0×10^{-4} M and 1.0×10^{-3} M), (50 mV pulse amplitude and 5 mV step potential were employed) (III).

The proposed modified CPE is compared with previously employed working electrodes in Table 5.4. The surface-modified CPE with a Pd NPs layer demonstrated wider dynamic linear range, good limit of detection, good repeatability and reproducibility.

Table 5.4: Previous employed working electrodes in the determination of TR(III).

Electrode	Modifier	DLR (M)	LOD (M)	Method	Reference
Hanging mercury drop	-	1.0×10^{-5}– 1.0×10^{-8}	1.5×10^{-11}	SWV	[188]
CPE	Gold NPs	5.4×10^{-5}– 8.0×10^{-9}	1.2×10^{-10}	CV	[189]
Ion selective electrode	-	1.0×10^{-2}–1.0×10^{-5}	7.9×10^{-6}	Potentiometry	[190]
GCE	Presence of Surfactant	2.4×10^{-6}–4.0×10^{-8}	4.5×10^{-9}	DPV	[191]

CPE	ZnO/rGO	1.0×10^{-5}–1.0×10^{-8}	2.0×10^{-9}	CV	[192]
CPE	Pd NPs	1.0×10^{-3}–1.0×10^{-8}	1.9×10^{-9}	DPV	(III)

5.4 Pre-adsorbed methylene blue at carbon-modified TiO_2 electrode: application for lead sensing in water (IV)

Methylene blue (MB) is a cationic organic dye. Wastewater containing MB released into the aquatic environment contaminates the local ecosystem and has a harmful impact on the health of human beings. In addition, MB is a pharmaceutical product prescribed for the treatment of methemoglobinemia, cyanide poisoning and Alzheimer's disease [193]. The prescribed dosage varies according to the age and general health of the patient, so design of a new, high-performance, mercury-free voltammetric method can be useful in the determination of MB.

Here, CMTN were successfully synthesised with the ethanol carbonisation method. CMTN was employed to modify the GCE surface. The synthesised CMTN was characterised successfully using various methods such as SEM, XRD, FTIR and voltammetric. The textural properties and surface area of CMTN were investigated using N_2 adsorption/desorption isotherms, which showed the obvious enhancement of the total surface area of CMTN compared to TiO_2. The appearance of a new peak corresponding to the methyl group in the range of 2,850–3,000 cm^{-1} demonstrated the carbon modification of TiO_2 NPs well by the FTIR method. The XRD technique investigated the crystalline phase of TiO_2 NPs and CMTN and confirmed no change in their crystalline phase of TiO_2 NPs after carbon modification (Figure 5.17).

The surface charge of CMTN and its variation with pH were investigated using zeta potential (*ZP*). Investigation of the effect of pH on *ZP* better explained the adsorption of CMTN on the GCE surface. Previous studies showed that the pH at the point of zero charge (pH_{PZC}) of CMTN (calculated to be 6.53) defined the surface charge of CMTN. In this regard, the adsorbent surface gained a negative charge at a pH more than pH_{PZC}, while the surface charge is positive at a pH less than pH_{PZC} [116]. So, a negative charge was predicted for CMTN at pHs higher than a pH_{PZC} of 6.53, which could interact with positive MB electrostatically (Figure 5.17).

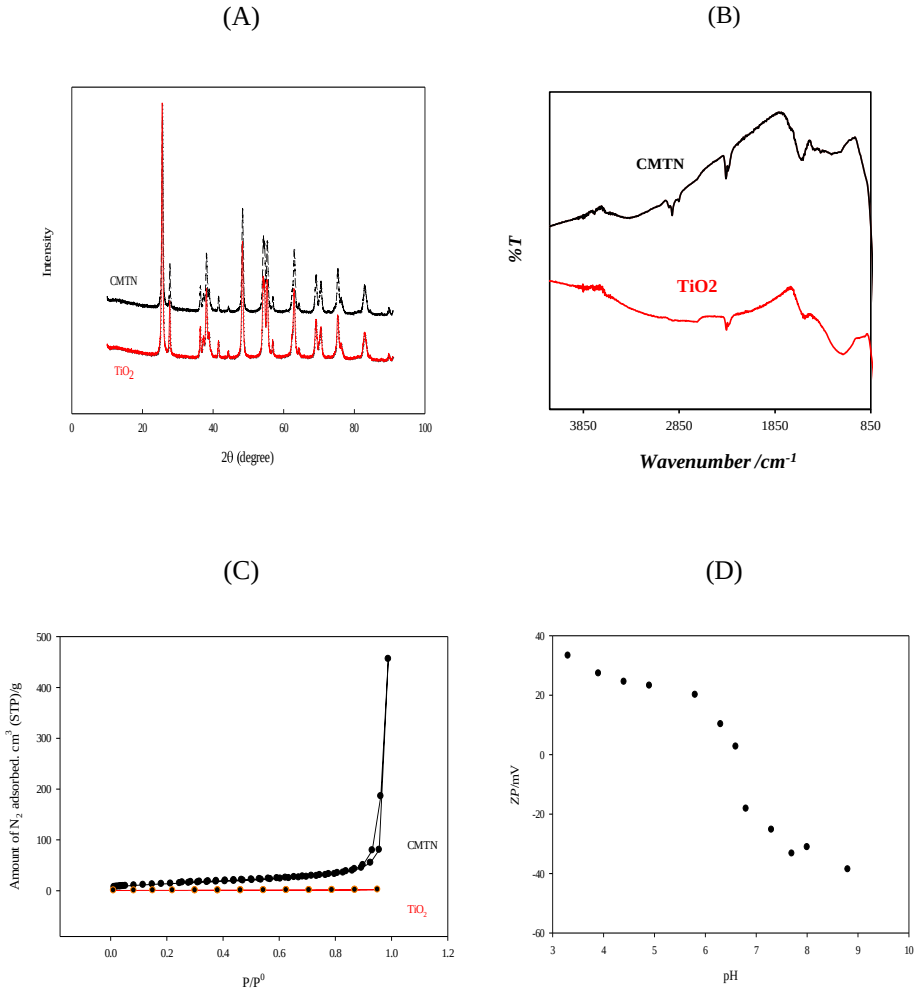

Figure 5.17: (A) XRD patterns of CMTN and TiO_2 precursor. (B) FTIR spectra of CMTN and TiO_2 precursor. (C) Nitrogen adsorption/desorption isotherms of CMTN and TiO_2 precursor. (D) ZP *vs.* pH for CMTN (IV).

The SEM method approximately estimated the size range of CMTN 30-50 nm radiuses. In addition, the SEM study demonstrated well the establishment of a rough coverage on the GCE surface compared with bare GCE (IV) (Figure 5.18). The porous structure of CMTN extended the surface area on the GCE/CMTN, which led to better and improved sensing performance.

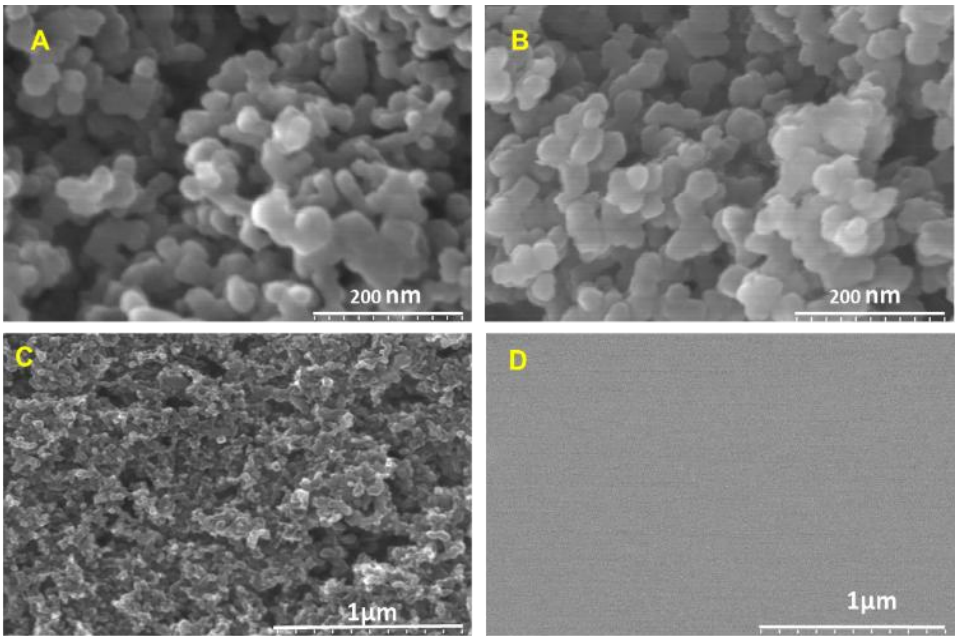

Figure 5.18: SEM images of (A) TiO_2, (B) CMTN, (C) GCE/CMTN and (D) GCE (IV).

EIS was applied as an effective technique to study the surface of GCE/CMTN. EIS measurements were conducted in an aqueous solution containing 5.0 mM $Fe(CN)_6^{4-}$, 5.0 mM $Fe(CN)_6^{3-}$ and 0.1 M KNO_3 at bare GCE (a) and GCE/CMTN (b) (Figure 5.19). The Nyquist plot showed a semi-circular part in the high-frequency zone corresponding to the electron transfer kinetic resistance (R_{ct}) of the electrochemical reaction, and a linear part in the lower frequency zone demonstrated the diffusion-controlled electrode process. The R_{ct} value on the bare GCE (1050 Ω) was much higher than the measured R_{ct} on the surface of GCE/CMTN (333.4 Ω), indicating that modification of GCE with CMTN had a significant effect on decreasing electron transfer resistance and increasing electron transfer rate on the surface of GCE/CMTN (IV).

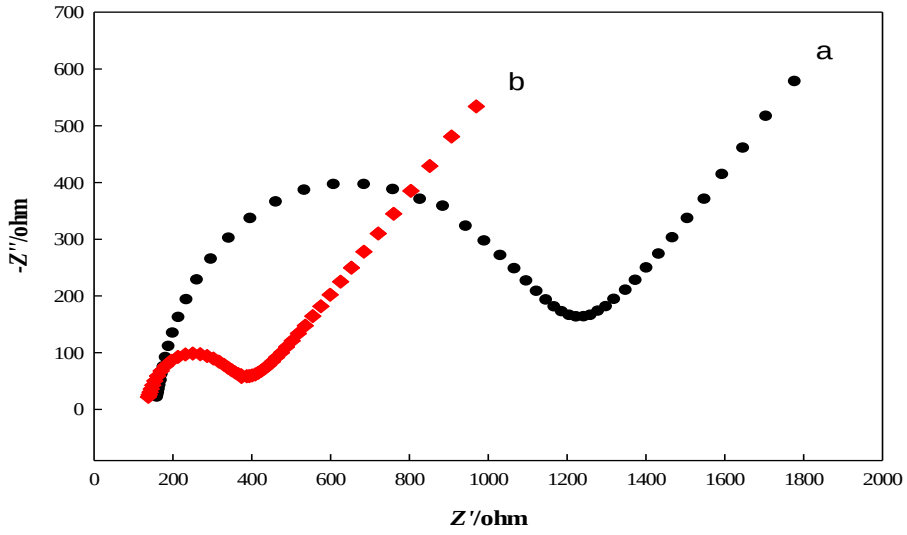

Figure 5.19: Nyquist diagram (–Z″ versus Z′) for the EIS measurements in 5.0 mM $Fe(CN)_6^{4-}$, 5.0 mM $Fe(CN)_6^{3-}$ and 0.1 M KNO_3 at the formal potential 0.2 V *vs.* SCE (a) bare GCE, (b) GCE/CMTN. Potential: 0.2 V *vs.* SCE, frequency range: 1 Hz–10,000 Hz (IV).

5.4.1 CMTN/GCE for MB sensing (IV)

The applicability of GCE/CMTN was investigated in terms of determining MB using CV. The observed signal at GCE/CMTN (solid line) was much higher than the signal obtained from bare GCE (dotted line) under similar experimental conditions. It can be concluded that CMTN performed well as a modifier for improving the efficiency of GCE. In addition, the investigated voltammetric signal for the pre-adsorbed MB was much better than the obtained voltammetric signal of MB in solution (dashed-line).

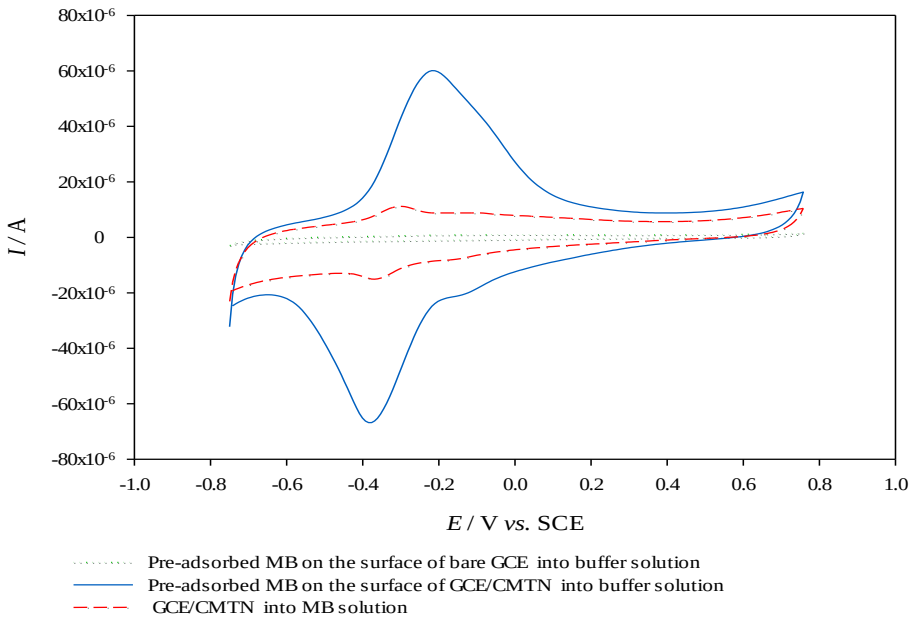

Figure 5.20: CVs of 0.1 mM solution of MB in buffer solution pH 7.0 at GCE/CMTN (short-dashed line). The working electrode was immersed for 4 min in MB solution and then rinsed and moved into phosphate buffer solution pH 7.0 for CV measurement at GCE/CMTN (solid line) and at bare GCE (dotted line). *v* was 100 mVs^{-1} (IV).

The influence of various parameters such as time, pH and stirring rate on the peak current of MB was investigated to optimise the best conditions of MB pre-adsorption on the surface of CMTN. The best signal was obtained at 1,000 rpm after 4 min. The maximum $I_{p,a}$ was obtained at pH 7.0 which was in agreement with *ZP* results. The cationic MB was extracted efficiently on the surface GCE/CMTN due to strong electrostatic interaction between cationic MB and the negative surface of the CMTN at pHs higher than pH_{PZC} of 6.53 (IV).

The effect of pH on the voltammetric signal was investigated and the best signal was obtained at pH 7.0. The decrease in the CV's peak current and the appearance of peak shoulder at pHs lower than pH 7.0 resulted from the weaker electrostatic interactions of MB and CMTN (regarding CMTN *ZP*). MB molecules were lost from the GCE/CMTN surface and leaked into the voltammetric solution at lower pHs, which decreased the stability and efficiency of the pre-adsorbed MB on the surface of GCE/CMTN [194], so the voltammetric measurements were conducted at pH 7.0 for better results.

The study of the pH dependency of $E_{p,a}$ and $E_{p,c}$ indicated a negative shift by increasing the pH of buffer solutions that demonstrated H^+ participation in charge transport. According the resultant slope –0.0584, the equal number of protons and electrons were expected to participate in the MB oxidation/reduction mechanism (Figure 5.22) (IV) [195].

$$E_{p,a}/V=-0.0584\ (\pm0.002)\ pH + 0.223(\pm0.012) \qquad (R^2= 0.993) \qquad (5.6)$$

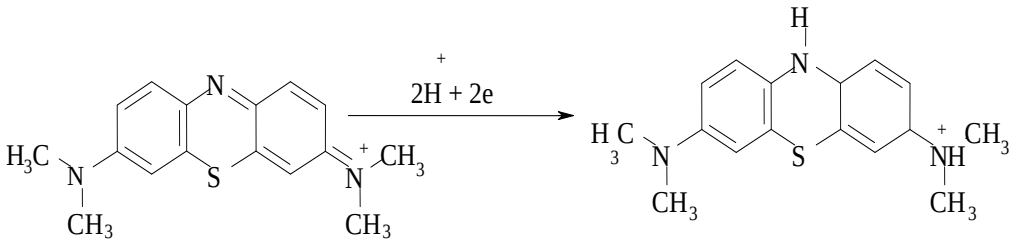

MB (Oxidized) MB (Reduced)

Figure 5.21: Electrochemical reaction of MB (IV).

(A) (B)

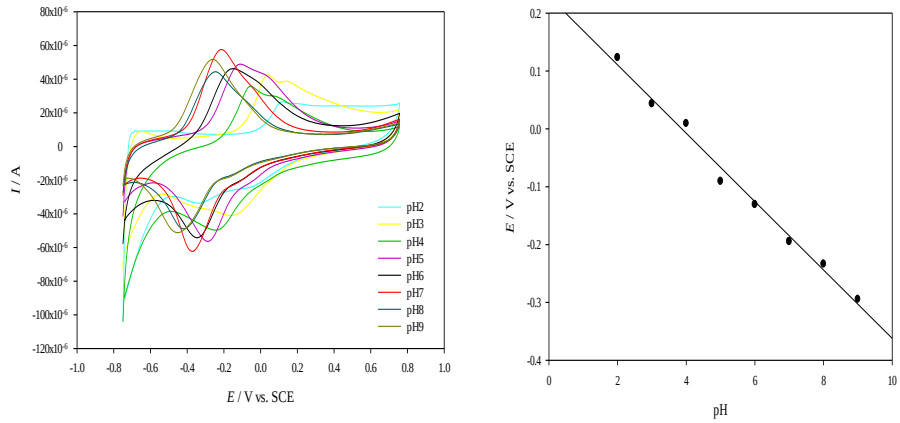

Figure 5.22: (A) variation of $I_{p,a}$ *vs.* various pHs. (B) Variation of $E_{p,a}$ *vs.* various pHs. GCE/CMTN immersed in a solution of 1×10^{-4} M MB pH 7.0 then rinsed and moved to phosphate buffer solutions pH 2.0, 3.0, 6.0, 7.0, 8.0, 9.0 and acetate buffer solutions pH 4.0 and 5.0 for CV measurement, ν was 100 mV s^{-1} (IV).

The effect of ν on the peak current at GCE/CMTN was investigated to study the charge transport mechanism. The relationship between $I_{p,a}$ and $I_{p,c}$ and ν variation was observed to be linear, which suggested an adsorption-controlled mechanism (Figure 5.23B) (IV).

$$I_{p,a} / A = -5.89\times10^{-6} + (4.0\times10^{-4}\nu/(Vs^{-1})) \qquad (R^2 = 0.988) \qquad (5.7)$$

$$I_{p,c} / A = -8.34\times10^{-6} - (4.39\times10^{-4}\nu/(Vs^{-1})) \qquad (R^2= 0.989) \qquad (5.8)$$

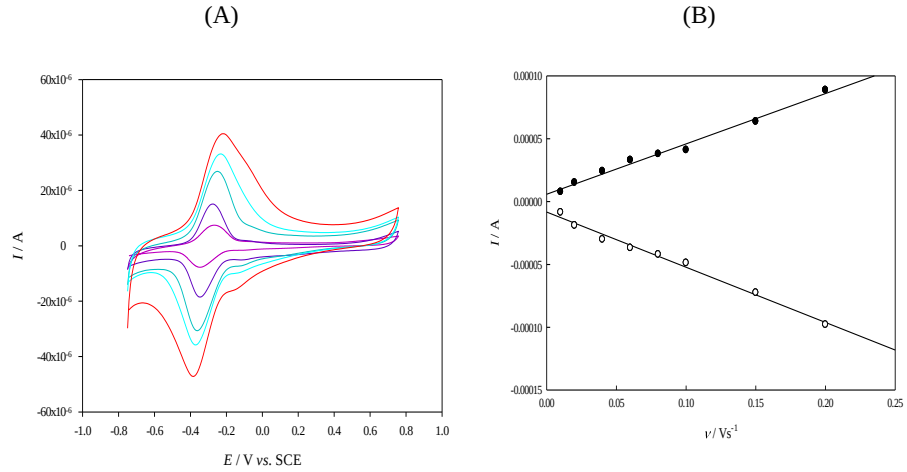

Figure 5.23: (A) CVs of pre-adsorbed MB in various *v*. (B) Plot of $I_{p,a}$ and $I_{p,c}$ *vs.* different *v* (10, 20, 40, 60, 80, 100, 150 and 200 mV s^{-1}) at GCE/CMTN. (GCE/CMTN. immersed for 4 min in 1×10^{-4} M MB pH 7.0 solution for pre-adsorption then rinsed and moved in phosphate buffer solution pH 7.0 for voltammetric analysis).

DPV was employed to investigate the anodic signal versus the variation of MB concentration. The recorded current showed a linear enhancement by increasing the MB concentration in the range of 1.0×10^{-8}–1.0×10^{-5} M with a slope of 0.407 A/M and a correlation coefficient (R^2) of 0.993. The detection limit for MB determination was evaluated to be 3×10^{-9} M (IV).

$$I_{p,a}/\mathrm{A} = 1.76 \times 10^{-6} + (0.407\ C) \qquad (R^2 = 0.993,\ \mathrm{C\ is\ in\ M}) \qquad (5.9)$$

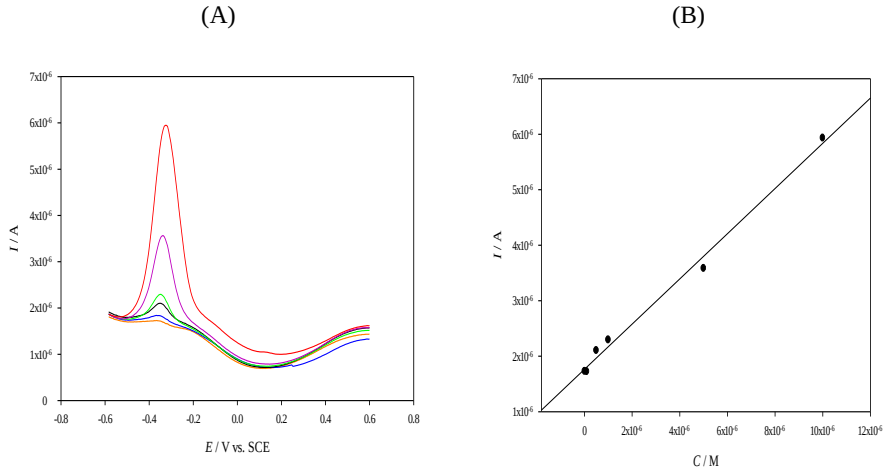

Figure 5.24: (A) In DPVs of pre-adsorption measurements, GCE/CMTN immersed for 4 min in the solution of various concentrations of MB (1×10^{-5}, 5×10^{-6}, 1×10^{-6}, $5\times10^{-}7$, 1×10^{-7} and 1×10^{-8} M), phosphate buffer pH 7.0 then rinsed and moved in clean phosphate buffer solution pH 7.0 for voltammetric analysis, v was 100 mV s^{-1}. (B) Calibration curve under optimum conditions for MB in the range of 1.0×10^{-5}–1.0×10^{-8} M.

Regarding MB determination, a small number of analytical techniques were employed including ultraviolet-visible spectroscopy [196, 197], liquid chromatography tandem mass spectrometry [198], capillary electrophoresis [199], surfaces-enhanced Raman spectroscopy [200] and electrochemical methods [201-203]. Electrochemical methods showed more advantages such as high sensitivity, low cost, simple operation and fast response in comparison with other analytical methods. Table 5.5 compared the performance of previously reported electrochemical techniques by the proposed method. Regarding the results obtained, GCE/CMTN could determine low concentrations of MB in the wider dynamic linear range and had a better limit of detection.

Table 5.5: Previous reported electrochemical electrodes in the detection of MB (IV).

Electrode	Modifier	DLR (M)	LOD (M)	Method	Reference
Gold Electrode	–	0.2×10^{-6}–10.0×10^{-6}	–	CV	[202]
CPE	Thiol functionalised-clay	1.0×10^{-6}–14.0×10^{-6}	4.0×10^{-6}	CV	[203]
CPE	Ibuprofen coated Au NPs	1.0×10^{-8}–1.1×10^{-6}	3.9×10^{-9}	DPV	[201]
GCE	CMTN	1.0×10^{-8}–1.0×10^{-5}	3.0×10^{-9}	DPV	(IV)

5.4.2 Sensing of lead using pre-adsorbed MB on the surface of CMTN/GCE (MB/CMTN/GCE) (IV)

Lead (Pb(II)) as a hazardous industrial pollutant has been a concern for decades due to its severe damage to the human immune, nervous, reproductive and gastrointestinal systems and the environment [204, 205], so fabrication of an efficient, simple and mercury-free CME has become a prime target for sensing development, which could determine these water pollutants with high sensitivity. MB as an electron mediator has been applied successfully in the modification of carbon-based electrodes. The application of nano-material support such as graphene [206] MWCNTs [207] and titanate nanotubes [194] enhanced the stability of the MB layer on the surface CMEs, the catalytic activity of MB and the rate of charge transport between electrode surface and target analytes such as lead and cadmium [208, 209], folic acid [206], maltol [210], uric acid and dopamine [207, 211]. Here, CMTN was applied as a conducting support to stabilise MB on the GCE surface and bring about better electrocatalytic activity. The strong electrostatic interaction of cationic MB on the negative surface of the CMTN (regarding CMTN *ZP*) improved MB adsorption and smoothed the charge transport between the GCE/CMTN surface and Pb(II).

In addition to MB catalytic activity at MB/GCE/CMTN, MB could coordinate with Pb(II) by its lone pare of nitrogen and adsorb Pb(II) from the solution. The reaction mechanism for Pb(II) on the surface of MB/GCE/CMTN can be explained as follows:

(Pb^{2+}) solution + (Modifier) surface $\longrightarrow$ $(Pb^{2+}$ –Modifier) adsorption (the extraction stage)

$(Pb^{2+}$ –Modifier) adsorption+ 2e $\longrightarrow$ (Pb –Modifier) adsorption (the reduction stage)

(Pb –Modifier) adsorption $\longrightarrow$ (Pb^{2+}) solution+ (Modifier) surface+ 2e (the stripping stage)

The MB/CMTN/GCE was examined in the detection of Pb(II). A new anodic signal was recorded for Pb(II) at a potential of –653 mV *vs.* SCE ($I_{p,a}$= 3.20 µA) which was higher than the signal ($I_{p,a=}$ 2.72 µA) obtained at CMTN/GCE and MB/GCE. Regarding these results, MB on the surface of CMTN/GCE played a major role in enhancing the rate of electron transport on the surface of CMTN/GCE (Figure 5.25), which may be related to the supramolecular interaction between CMNT and the phenothiazine ring in MB through π–π interactions.

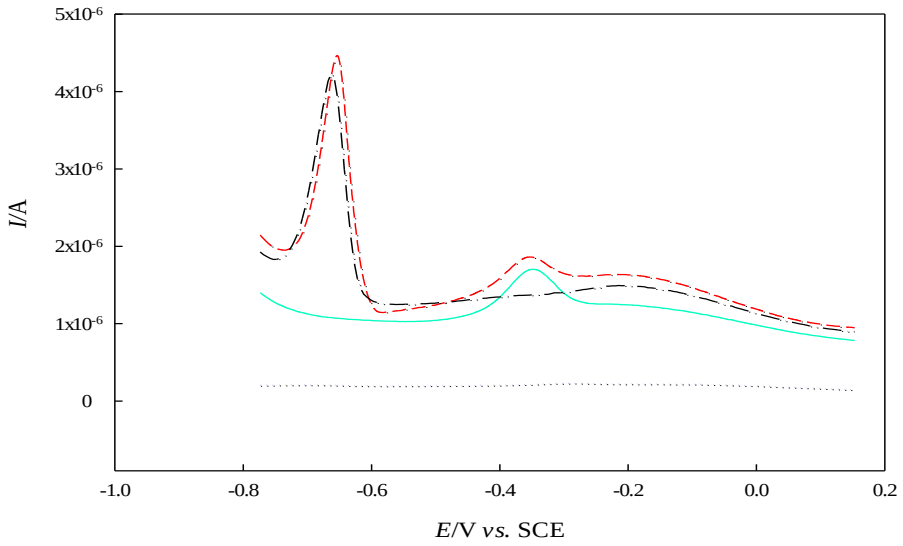

Figure 5.25: DPVs of pre-adsorbed 1×10^{-6} M MB on the surface of CMTN/GCE with Pb(II) adsorption step (solid line) and without Pb(II) adsorption step (dashed line) and DPV of pre-adsorbed MB on the surface of bare GCE with Pb(II) adsorption step (dotted line) and DPV of pre-adsorbed 1×10^{-4} M Pb(II) on the surface of CMTN/GCE (without MB adsorption step)(dashed-dotted line). The working electrode was immersed for 4 min in the solution of 1×10^{-6} M MB pH 7.0 for pre-adsorption then rinsed and immersed for 4 min in the solution of 1×10^{-4} M Pb(II) acetate buffer pH 5.0 for adsorption then rinsed and transferred to phosphate buffer solution pH 7.0 for analysis under optimum conditions. v was 100 mV s^{-1} (IV).

The influence of various parameters such as time, pH, stirring rate and MB concentration on the peak current of Pb(II) were optimised for the extraction step and determination of Pb(II). The best $I_{p,a}$ was gained for 1.0 µM MB at 1,000 rpm after 4 min and the best signal was gained at pH 5.0. At higher pHs, Pb(II) precipitated in the form of $Pb(OH)_2$ and the peak current decreased (IV), so further studies were conducted under optimised conditions.

The effect of v variation on the $I_{p,a}$ at MB/CMTN/GCE in a buffered solution of pH 7.0 was investigated and a linear relationship was observed in the range of 10–200 mV s^{-1} (V). The equations for $I_{p,a}$ and $I_{p,c}$ versus v were:

$$I_{p,a} / A = 0.49\times10^{-6} + 0.464\times10^{-4}\nu/(Vs^{-1}) \qquad (R^2 = 0.99) \qquad (5.10)$$

$$I_{p,c} / A = -0.23\times10^{-7} - (0.587\times10^{-4}\nu/(Vs^{-1}) \qquad (R^2 = 0.99) \qquad (5.11)$$

(A) (B)

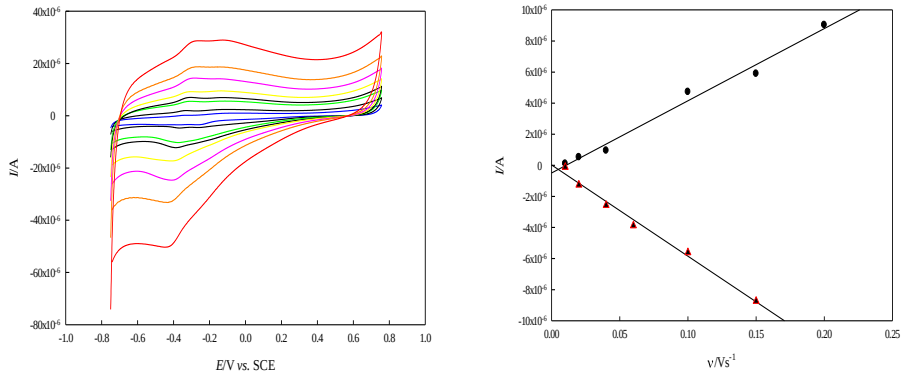

Figure 5.26: (A) CVs of pre-adsorbed MB on the surface of CMTN/GCE with Pb(II) adsorption step in various *v* (10, 20, 40, 60, 100, 150 and 200 mV s^{-1}). (B) Plot of $I_{p,a}$ and $I_{p,c}$ versus different *v* (CMTN/GCE was immersed for 4 min in the solution of 1×10^{-6} M MB pH 7.0 for pre-adsorption then rinsed and immersed for 4 min in the solution of 1×10^{-4} M Pb(II) acetate buffer pH 5.0 for adsorption then rinsed and transferred to phosphate buffer solution pH 7.0 for analysis) (IV).

DPV measurements were performed by immersing MB/CMTN/GCE in a solution of various concentrations of Pb(II) under optimum conditions (Figure 5.27A). The linear calibration curve was observed for Pb(II) in the range of 5×10^{-4} to 1×10^{-7} M and the limit of detection was estimated to be 3×10^{-8} M (for S/N=3) (IV).

$$I / A = 1.73\times10^{-6} + 2.97\times10^{-3}C \qquad (R^2 = 0.994, \text{ C is in M}) \qquad (5.12)$$

The performance of MB/CMTN/GCE in detecting of Pb(II) in water samples was studied by applying a standard addition method under optimised conditions. A recovery of 102% was evaluated for the local tap water sample and a recovery of 101% for the local lake water sample (Pankalampi, Mikkeli, Finland). In addition, the effect of coexisting ions on the signal of Pb(II) showed no interference for ions Ni^{2+}, Co^{2+}, a 1,000-fold excess of Zn^{2+}, a 100-fold excess of Cr^{2+}, a twofold excess of Cu^{2+}, Mg^{2+} and a one-fold excess of Cd^{2+} (IV).

Regarding determination of Pb(II), previously modified carbon-based electrodes are compared with each other in Table 5.6. MB/CMTN/GCE demonstrated wide dynamic linear range and good limit of detection in comparison to other reported CMEs. In addition, MB/CMTN/GCE covered other required factors for the fabrication of high-performance CME, including high sensitivity, low cost and environmental friendliness.

(A) (B)

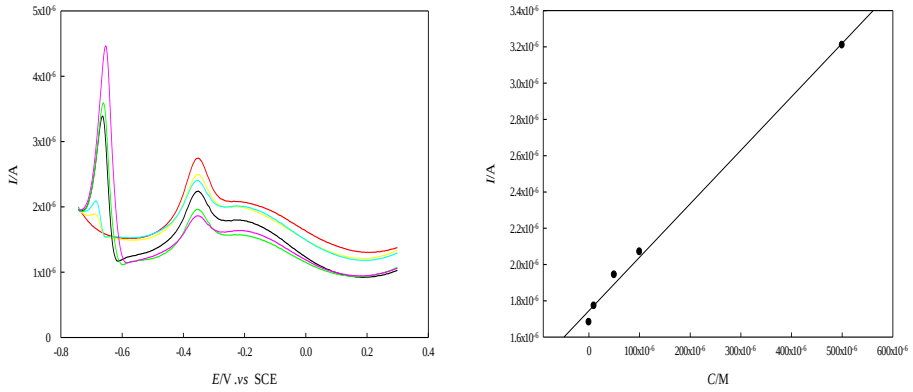

Figure 5.27: (A) In DPVs of pre-adsorption measurements, CMTN/GCE was immersed for 4 min in a solution of 1×10^{-6} M MB pH 7.0 for pre-adsorption then rinsed and immersed for 4 min in a solution of various concentration of Pb(II) (5×10^{-4},1×10^{-4}, 5×10^{-5}, 1×10^{-5}, 5×10^{-6}, 1×10^{-6} and 1×10^{-7} M), acetate buffer pH 5.0 then rinsed and transferred into a clean phosphate buffer solution pH 7.0 for DPV analysis. *v* was 100 mV s^{-1}. (B) Calibration curve under optimum conditions for Pb(II) in range of 5×10^{-4} to 1×10^{-7} M (IV).

Table 5.6: Previously employed CME in the detection of Pb(II) (IV).

Electrode	Modifier	DLR (M)	LOD (M)	Method	Reference
GCE	PANI/MMT[1]	0.004×10^{-6}–0.1×10^{-6}	0.001×10^{-6}	DPASV[2]	[212]
GCE	Band Fe_3O_4/rGO[3]	0.4×10^{-6}–1.5×10^{-6}	0.169×10^{-6}	SWASV	[213]
CPE	TPP[4]	0.3×10^{-6}–20.0×10^{-6}	0.084×10^{-6}	DPASV	[214]
GCE	$MnFe_2O_4$ NC[5]	0.2×10^{-6}–1.1×10^{-6}	0.054×10^{-6}	SWASV	[215]
GC spheres	2-Hyroxy benzoic acid diazonium tetrafluroborate	1.0×10^{-6}–10.0×10^{-6}	0.18×10^{-6}	DPASV	[216]
GCE	5-Br-PADAP[6]/MWCNT	4.34×10^{-9}–5.5×10^{-7}	4.8×10^{-10}	DPASV	[217]

CPE	α- and β-cyclodextrins	1×10^{-5}–1×10^{-3}	–	DPASV	[218]
CPE	periodic mesoporous organosilica	9.6×10^{-9}–4.8×10^{-7}	2.4×10^{-9}	SWASV	[219]
GCE	siloxane-crown ether polyamide copolymer	9.6×10^{-8}–3.3×10^{-6}	1.69×10^{-8}	DPASV	[220]
GCE	MB/CMTN	1×10^{-7}–5.0×10^{-4}	3.0×10^{-8}	DPV	(IV)

[1] Na^{+}–montmorillonites/polyaniline nanocomposite
[2] Differential pulse anodic stripping voltammetry, SWASV: square-wave anodic voltammetry
[3] Band Fe_3O_4 decorated reduced graphene oxide, TPP: Kaolinite clay modified with tripolyphosphate
[4] Kaolinite clay modified with tripolyphosphate
[5] $MnFe_2O_4$ nanocrystal clusters
[6] 2-(5-bromo-2-pyridylazo)-5-diethylaminophenol

6 Conclusion and future work

In this research, new high-performance, low-cost and environmentally-friendly modified electrodes such as KolliphorEL/GCE, Pd NPs/CPE, Au/Pd/MWCNT/CPE, CMTN/GCE and MB/CMTN/GCE were fabricated successfully.

Modification methods favourably changed the rate of charge transport on the surface of these modified electrodes. The electrochemical performances of these new modified carbon-based electrodes were investigated using EIS and CV methods and the obtained results were compared with the results of unmodified electrodes. The utility of these new modified electrodes was examined in the detection of pharmaceutical and biological compounds such as TM, TR, MB, hydrophobic compounds and environmental contaminants such as Pb(II). In addition, their applicability in the detection of various analytes in real samples such as synthetic serum, pharmaceutical preparations and lake water was tested. The repeatability of the obtained results and the reproducibility and stability of these modified carbon-based electrodes were investigated successfully.

Here, the finding of this research is briefly summarised.

The surface of GCE was modified with KolliphorEL monolayer. The interfacial charge transport investigation at KolliphorEL/GCE in a $Fe(CN)_6^{3-/4-}$ solution as a redox probe demonstrated a blocked electron transfer that could be opened in the presence of Fc derivatives. Fc derivatives performed well as electron shuttles through the KolliphorEL monolayer. This electron shuttling system was introduced for the first time. The electron shuttling ability of Fc derivatives was variable regarding their hydrophobicity nature, linking ability to a KolliphorEL/GCE surface and whether they held a desirable electrostatic charge with regard to $Fe(CN)_6^{3-/4-}$. In the Fc family, low values of butylferrocene and dimethylaminomethyl-ferrocene were more active. Further investigation should be conducted to study stability of the modified electrode. In future, this electron shuttling system could be investigated for sensing trace amounts of other redox-active molecules including medicine, bio-markers, environmental contaminants, which could be acted as a signal amplifier in redox processes. Study of other hydrophobic mediators will be useful in further studies. In addition, this electrochemical surface modification method was conducted fast and simply, which could be interesting to use for anodic grafting of other PEGylated molecules (I).

The decorated MWCNTs with Au/Pd NPs was employed to modify the body of CPE. Au/Pd/MWCNTs/CPE performed well in the determination of low concentrations of TM with high repeatability. Au/Pd/MWCNT/CPE showed a mercury-free electrode with high sensitivity, fast response and with a renewable surface that was employed to determine TM in its pharmaceutical sample. Surface modification of GCE or CPE with a droplet of Au/Pd/MWCNTs or electrochemical synthesis and attachment of Au/Pd/MWCNT may be interesting to study and developed in future. Application of graphene instead of MWCNTs will be interesting to form Au/Pd/graphene nanocomposite and use in modification of GCE or CPE in further studies (II).

The surface of CPE was modified with Pd NPs simply, quickly by using CV. Pd NPs/CPE demonstrated promising results in the determination of TR such as good repeatability and sensitivity, low limit of detection and rapid response. All these advantages make it desirable to apply Pd NPs/CPE in the pharmaceutical and clinical industries. This simple and reliable electrochemical modification method could be improved for attachment of other metal NPs or bimetals in further studies (III).

CMTN was synthesised with a simple and low-cost method (ethanol carbonisation) and employed to modify the surface of GCE. The advantages of CMTN/GCE compared to bare GCE were successfully investigated by SEM, EIS and CV. CMTN/GCE showed high performance in the detection of sub-micromolar MB in a wide linear range. Furthermore, the pre-adsorbed MB on the surface of CMTN/GCE acted effectively in the determination of low values of Pb(II). MB/CMTN/GCE suggested a low-cost, simple and fast way of detecting Pb(II) in the presence of other coexisting ions. Further studies should be conducted to evaluate the applicability of CMTN/GCE for detecting other biomarkers and pollutants. The use of CMTN as an adsorbent in wastewater treatment could be investigated in future research (IV).

7 References

1. Wang, J., *Analytical Electrochemistry*. Wiley-VCH, ed. S. edition. 2000: Wiley-VCH
2. Švancara, I., *et al*., *Carbon Paste Electrodes in Modern Electroanalysis.* Critical Reviews in Analytical Chemistry, 2001. **31**(4): p. 311-345.
3. Huang, J., *et al*., *Simultaneous electrochemical determination of dopamine, uric acid and ascorbic acid using palladium nanoparticle-loaded carbon nanofibers modified electrode.* Biosensors and Bioelectronics, 2008. **24**(4): p. 632-637.
4. Shahrokhian, S., R. Salimian, and S. Rastgar, *Pd–Au nanoparticle decorated carbon nanotube as a sensing layer on the surface of glassy carbon electrode for electrochemical determination of ceftazidime.* Materials Science and Engineering: C, 2014. **34**: p. 318-325.
5. Shaidarova, L.G., *et al.*, *Electrooxidation of oxalic acid at a carbon-paste electrode with deposited palladium nanoparticles.* Journal of Analytical Chemistry, 2006. **61**(4): p. 375-381.
6. Mukdasai, S., *et al.*, *Electrodeposition of palladium nanoparticles on porous graphitized carbon monolith modified carbon paste electrode for simultaneous enhanced determination of ascorbic acid and uric acid.* Sensors and Actuators B: Chemical, 2015. **218**: p. 280-288.
7. Afkhami, A., F. Soltani-Felehgari, and T. Madrakian, *Gold nanoparticles modified carbon paste electrode as an efficient electrochemical sensor for rapid and sensitive determination of cefixime in urine and pharmaceutical samples.* Electrochimica Acta, 2013. **103**: p. 125-133.
8. Farahi, A., *et al.*, *Electrochemical determination of paraquat in citric fruit based on electrodeposition of silver particles onto carbon paste electrode.* Journal of Food and Drug Analysis, 2015. **23**(3): p. 463-471.
9. Peter Kissinger, W.R.H., *Laboratory Techniques in Electroanalytical Chemistry*. CRC Press, ed. Second Edition. 1996 CRC Press.
10. Bard A.J., F.L.R., *Electrochemical Methods-Fundamentals and Applications*. 2nd ed. John Wiley & Sons, New York, ed. N.Y. John Wiley & Sons. 2001: John Wiley & Sons, New York.
11. Stradiotto, N.R., H. Yamanaka, and M.V.B. Zanoni, *Electrochemical sensors: a powerful tool in analytical chemistry.* Journal of the Brazilian Chemical Society, 2003. **14**: p. 159-173.
12. Valentini, F., *et al.*, *Carbon Nanotube Purification: Preparation and Characterization of Carbon Nanotube Paste Electrodes.* Analytical Chemistry, 2003. **75**(20): p. 5413-5421.
13. Kalcher, K., *et al.*, *Sensors based on carbon paste in electrochemical analysis: a review with particular emphasis on the period 1990–1993.* Electroanalysis, 1995. **7**(1): p. 5-22.
14. McCreery, R.L., *Advanced carbon electrode materials for molecular electrochemistry.* Chem. Rev, 2008. **108**(7): p. 2646-2687.
15. Švancara, I., *et al.*, *Carbon Paste Electrodes in Facts, Numbers, and Notes: A Review on the Occasion of the 50-Years Jubilee of Carbon Paste in Electrochemistry and Electroanalysis.* Electroanalysis, 2009. **21**(1): p. 7-28.

16. Sanghavi, B.J., *et al.*, *Nanomaterial-based electrochemical sensing of neurological drugs and neurotransmitters.* Microchimica Acta, 2015. **182**(1): p. 1-41.
17. Yuan, B., *et al.*, *Glassy carbon electrode modified with 7, 7, 8, 8-tetracyanoquinodimethane and graphene oxide triggered a synergistic effect: Low-potential amperometric detection of reduced glutathione.* Biosensors and Bioelectronics, 2017. **96**: p. 1-7.
18. Nasir, T., *et al.*, *Electrografting of 3-aminopropyltriethoxysilane on a glassy carbon electrode for the improved adhesion of vertically oriented mesoporous silica thin films.* Langmuir, 2016. **32**(17): p. 4323-4332.
19. Sun, Y., K. Wu, and S. Hu, *Fabrication of a Multi-wall Carbon Nanotubes Modified Glassy Carbon Electrode and its Catalytic Effect on the Oxidation of Estradiol, Estrone and Estriol.* Microchimica Acta, 2003. **142**(1): p. 49-53.
20. Angus, J.C., Y.V. Pleskov, and S.C. Eaton, *Chapter 3 Electrochemistry of diamond*, in *Semiconductors and Semimetals*, C.E. Nebel and J. Ristein, Editors. 2004, Elsevier. p. 97-119.
21. Ivandini, T.A. and Y. Einaga, *Diamond Electrochemistry*, in *Reference Module in Chemistry, Molecular Sciences and Chemical Engineering*. 2017, Elsevier.
22. Lawrence, N.S., *et al.*, *Electroanalytical applications of boron-doped diamond microelectrode arrays.* Talanta, 2006. **69**(4): p. 829-834.
23. Sanghavi, B.J., *et al.*, *Nanomaterial-based electrochemical sensing of neurological drugs and neurotransmitters.* Microchimica Acta, 2015. **182**(1-2): p. 1-41.
24. Hart, J.P. and S.A. Wring, *Recent developments in the design and application of screen-printed electrochemical sensors for biomedical, environmental and industrial analyses.* TrAC Trends in Analytical Chemistry, 1997. **16**(2): p. 89-103.
25. Hart, J.P., *et al.*, *Sensors/biosensors, based on screen-printing technology for biomedical applications.* 2003.
26. Cowell, D.C., *et al.*, *Screen-printed disposable biosensors for environmental pollution monitoring.* Biomonitors and Biomarkers as Indicators of Environmental Change 2, 2001: p. 157-174.
27. Zhang, W., *et al.*, *Recent development of carbon electrode materials and their bioanalytical and environmental applications.* Chemical Society Reviews, 2016. **45**(3): p. 715-752.
28. Rodriguez, N.M., A. Chambers, and R.T.K. Baker, *Catalytic Engineering of Carbon Nanostructures.* Langmuir, 1995. **11**(10): p. 3862-3866.
29. Zestos, A.G., *et al.*, *Epoxy insulated carbon fiber and carbon nanotube fiber microelectrodes.* Sensors and Actuators B: Chemical, 2013. **182**: p. 652-658.
30. Zoski, C.G., *Ultramicroelectrodes: Design, Fabrication, and Characterization.* Electroanalysis, 2002. **14**(15-16): p. 1041-1051.
31. Tuzhi, P., *et al.*, *Constant Potential Pretreatment of Carbon Fiber Electrodes for In Vivo Electrochemistry.* Analytical Letters, 1991. **24**(6): p. 935-945.
32. Wang, J., *Modified electrodes for electrochemical sensors.* Electroanalysis, 1991. **3**(4-5): p. 255-259.
33. Yang, D., *et al.*, *Anodic stripping voltammetric determination of traces of Pb(II) and Cd(II) using a glassy carbon electrode modified with bismuth nanoparticles.* Microchimica Acta, 2014. **181**(11): p. 1199-1206.

34. Jain, R. and S. Sharma, *Glassy carbon electrode modified with multi-walled carbon nanotubes sensor for the quantification of antihistamine drug pheniramine in solubilized systems.* Journal of Pharmaceutical Analysis, 2012. **2**(1): p. 56-61.
35. Wang, Z., *et al.*, *A Selective Voltammetric Method for Detecting Dopamine at Quercetin Modified Electrode Incorporating Graphene.* Electroanalysis, 2011. **23**(10): p. 2463-2471.
36. Salimi, A., R. Hallaj, and S. Soltanian, *Immobilization of hemoglobin on electrodeposited cobalt-oxide nanoparticles: Direct voltammetry and electrocatalytic activity.* Biophysical chemistry, 2007. **130**(3): p. 122-131.
37. Amiri, M., *et al.*, *Simultaneous voltammetric determination of uric acid and ascorbic acid using carbon paste/cobalt Schiff base composite electrode.* Journal of Solid State Electrochemistry, 2012. **16**(6): p. 2187-2195.
38. Shahrokhian, S., M. Karimi, and H. Khajehsharifi, *Carbon-paste electrode modified with cobalt-5-nitrolsalophen as a sensitive voltammetric sensor for detection of captopril.* Sensors and Actuators B: Chemical, 2005. **109**(2): p. 278-284.
39. Arvand, M., M. Vaziri, and M. Vejdani, *Electrochemical study of atenolol at a carbon paste electrode modified with mordenite type zeolite.* Materials Science and Engineering: C, 2010. **30**(5): p. 709-714.
40. Balint, R., N.J. Cassidy, and S.H. Cartmell, *Conductive polymers: towards a smart biomaterial for tissue engineering.* Acta biomaterialia, 2014. **10**(6): p. 2341-2353.
41. Gorton, L., *Carbon paste electrodes modified with enzymes, tissues, and cells.* Electroanalysis, 1995. **7**(1): p. 23-45.
42. W. Sun, Q.J., M. Xi, K. Jiao, *Determination of 3, 4-dihydroxybenzoic acid by electrocatalytic oxidation at an ionic liquid modified electrode.* Microchim. Act, 2009. **166**: p. 343-348.
43. Geim, A.K. and K.S. Novoselov, *The rise of graphene.* Nature materials, 2007. **6**(3): p. 183-191.
44. Uslu, B. and S.A. Ozkan, *Electroanalytical application of carbon based electrodes to the pharmaceuticals.* Analytical Letters, 2007. **40**(5): p. 817-853.
45. Yadav, B. and R. Kumar, *Structure, properties and applications of fullerenes.* International Journal of Nanotechnology and Applications, 2008. **2**(1): p. 15-24.
46. Kharlamov, A., M. Bondarenko, and N. Kirillova, *New method for synthesis of fullerenes and fullerene hydrides from benzene.* Russian Journal of Applied Chemistry, 2012. **85**(2): p. 233-238.
47. Ikeda, T., T. Kamo, and M. Danno, *New synthesis method of fullerenes using microwave-induced naphthalene-nitrogen plasma at atmospheric pressure.* Applied physics letters, 1995. **67**(7): p. 900-902.
48. Bakry, R., *et al.*, *Medicinal applications of fullerenes.* International journal of nanomedicine, 2007. **2**(4): p. 639.
49. Sutradhar, S. and A. Patnaik, *A new fullerene-C60 – Nanogold composite for non-enzymatic glucose sensing.* Sensors and Actuators B: Chemical, 2017. **241**(Supplement C): p. 681-689.
50. Demirbakan, B. and M.K. Sezgintürk, *A novel immunosensor based on fullerene C60 for electrochemical analysis of heat shock protein 70.* Journal of Electroanalytical Chemistry, 2016. **783**(Supplement C): p. 201-207.

51. Hovancová, J., *et al.*, *Nanomaterial-based electrochemical sensors for detection of glucose and insulin.* Journal of Solid State Electrochemistry, 2017. **21**(8): p. 2147-2166.
52. Li, Z., *et al.*, *Electrodeposition of palladium nanoparticles on fullerene modified glassy carbon electrode for methane sensing.* Electrochimica Acta, 2012. **76**: p. 288-291.
53. Shenderova, O.A., V.V. Zhirnov, and D.W. Brenner, *Carbon Nanostructures.* Critical Reviews in Solid State and Materials Sciences, 2002. **27**(3-4): p. 227-356.
54. Barsan, M.M., M.E. Ghica, and C.M. Brett, *Electrochemical sensors and biosensors based on redox polymer/carbon nanotube modified electrodes: A review.* Analytica Chimica Acta, 2015. **881**: p. 1-23.
55. Trojanowicz, M., *Analytical applications of carbon nanotubes: a review.* TrAC Trends in Analytical Chemistry, 2006. **25**(5): p. 480-489.
56. Rajarao, R., *et al.*, *GreenApproach to Decorate Multi-walled Carbon Nanotubes by Metal/Metal Oxide Nanoparticles.* Procedia Materials Science, 2014. **5**: p. 69-75.
57. Zhang, W., *et al.*, *Fabrication of carbon nanotube-nickel nanoparticle hybrid paste electrodes for electrochemical sensing of carbohydrates.* Sensors and Actuators B: Chemical, 2014. **192**: p. 459-466.
58. Afkhami, A., F. Soltani-Felehgari, and T. Madrakian, *Highly sensitive and selective determination of thiocyanate using gold nanoparticles surface decorated multi-walled carbon nanotubes modified carbon paste electrode.* Sensors and Actuators B: Chemical, 2014. **196**: p. 467-474.
59. Fakhari, A.R., *et al.*, *Fabrication of novel redox-active poly (4, 5-dihydro-1, 3-thiazol-2-ylsulfanyl-3-methyl-1, 2-benzenediol)-gold nanoparticles film on MWCNTs modified electrode: Application as the electrochemical sensor for the determination of hydrazine.* Sensors and Actuators B: Chemical, 2015. **213**: p. 82-91.
60. Rashid, M.H., *et al.*, *Synthesis of spongy gold nanocrystals with pronounced catalytic activities.* Langmuir, 2006. **22**(17): p. 7141-7143.
61. Arvand, M. and M. Dehsaraei, *A simple and efficient electrochemical sensor for folic acid determination in human blood plasma based on gold nanoparticles–modified carbon paste electrode.* Materials Science and Engineering: C, 2013. **33**(6): p. 3474-3480.
62. Woźnica, E., *et al.*, *Dithizone modified gold nanoparticles films for potentiometric sensing.* Analytical chemistry, 2012. **84**(10): p. 4437-4442.
63. Song, Y.-S., G. Muthuraman, and J.-M. Zen, *Trace analysis of hydrogen sulfide by monitoring As (III) at a poly (L-lactide) stabilized gold nanoparticles modified electrode.* Electrochemistry communications, 2006. **8**(8): p. 1369-1374.
64. Hrapovic, S., *et al.*, *Metallic nanoparticle− carbon nanotube composites for electrochemical determination of explosive nitroaromatic compounds.* Analytical chemistry, 2006. **78**(15): p. 5504-5512.
65. Shan, C., *et al.*, *Graphene/Au NPs/chitosan nanocomposites film for glucose biosensing.* Biosensors and bioelectronics, 2010. **25**(5): p. 1070-1074.
66. Rassaei, L., *et al.*, *Binding site control in a layer-by-layer deposited chitosan–carbon nanoparticle film electrode.* New Journal of Chemistry, 2008. **32**(7): p. 1253-1258.

67. Florea, A., *et al., Label free MUC1 aptasensors based on electrodeposition of gold nanoparticles on screen printed electrodes.* Electrochemistry Communications, 2013. **33**: p. 127-130.
68. Brugnerotto, P., *et al., Gold Nanoparticles Stabilized in β-Cyclodextrin and Decorated with Laccase Applied in the Construction of a Biosensor for Rutin.* Electroanalysis, 2017. **29**(4): p. 1031-1037.
69. German, N., *et al., Glucose biosensor based on glucose oxidase and gold nanoparticles of different sizes covered by polypyrrole layer.* Colloids and Surfaces A: Physicochemical and Engineering Aspects, 2012. **413**: p. 224-230.
70. German, N., A. Ramanavicius, and A. Ramanaviciene, *Amperometric Glucose Biosensor Based on Electrochemically Deposited Gold Nanoparticles Covered by Polypyrrole.* Electroanalysis, 2017. **29**(5): p. 1267-1277.
71. Karim-Nezhad, G. and Z. Khorablou, *Selective analysis of epinephrine in the presence of uric acid by using an amplified electrochemical sensor employing a gold nanoparticle decorated cysteic acid film.* Analytical Methods, 2017. **9**(45): p. 6394-6402.
72. Taei, M., *et al., Simultaneous electrochemical sensing of cysteine, uric acid and tyrosine using a novel Au-nanoparticles/poly-Trypan Blue modified glassy carbon electrode.* Journal of Electroanalytical Chemistry, 2017. **789**: p. 140-147.
73. Taei, M., *et al., Simultaneous determination of cysteine, uric acid and tyrosine using Au-nanoparticles/poly (E)-4-(p-tolyldiazenyl) benzene-1, 2, 3-triol film modified glassy carbon electrode.* Materials Science and Engineering: C, 2016. **59**: p. 120-128.
74. Taei, M. and G. Ramazani, *Simultaneous determination of norepinephrine, acetaminophen and tyrosine by differential pulse voltammetry using Au-nanoparticles/poly (2-amino-2-hydroxymethyl-propane-1, 3-diol) film modified glassy carbon electrode.* Colloids and Surfaces B: Biointerfaces, 2014. **123**: p. 23-32.
75. Afzali, D., *et al., Gold nanoparticles modified carbon paste electrode for differential pulse voltammetric determination of eugenol.* Materials Science and Engineering: C, 2014. **43**: p. 97-101.
76. Gholivand, M.B. and M.H. Parvin, *Voltammetric study of acetazolamide and its determination in human serum and urine using carbon paste electrode modified by gold nanoparticle.* Journal of electroanalytical chemistry, 2011. **660**(1): p. 163-168.
77. German, N., *et al., Glucose biosensor based on graphite electrodes modified with glucose oxidase and colloidal gold nanoparticles.* Microchimica Acta, 2010. **168**(3-4): p. 221-229.
78. Pham, X.-H., *et al., Electrochemical detection of nitrite using urchin-like palladium nanostructures on carbon nanotube thin film electrodes.* Sensors and Actuators B: Chemical, 2014. **193**: p. 815-822.
79. De Bonis, A., *et al., First application of homogeneous Pd nanoparticles prepared by pulsed laser ablation in liquid to a Suzuki-type reaction.* Catalysis Communications, 2017. **100**: p. 164-168.
80. Sharada, S., *et al., Synthesis of palladium nanoparticles using continuous flow microreactor.* Colloids and Surfaces A: Physicochemical and Engineering Aspects, 2016. **498**(Supplement C): p. 297-304.
81. Jensen, K.F., *Microreaction engineering—is small better?* Chemical Engineering Science, 2001. **56**(2): p. 293-303.

82. Renard, D., *et al.*, *Electrocatalytic properties of in situ-generated palladium nanoparticle assemblies towards oxidation of multi-carbon alcohols and polyalcohols.* Colloids and Surfaces A: Physicochemical and Engineering Aspects, 2014. **463**(Supplement C): p. 44-54.
83. Alexander, C. and K. Bandyopadhyay, *Two dimensional palladium nanoparticle assemblies as electrochemical dopamine sensors.* Inorganica Chimica Acta, 2017. **468**(Supplement C): p. 171-176.
84. Thiagarajan, S., R.-F. Yang, and S.-M. Chen, *Palladium nanoparticles modified electrode for the selective detection of catecholamine neurotransmitters in presence of ascorbic acid.* Bioelectrochemistry, 2009. **75**(2): p. 163-169.
85. Salama, N.N., *et al.*, *A novel methionine/palladium nanoparticle modified carbon paste electrode for simultaneous determination of three antiparkinson drugs.* RSC Advances, 2015. **5**(19): p. 14187-14195.
86. Absalan, G., *et al.*, *Efficient electrocatalytic oxidation and determination of isoniazid on carbon ionic liquid electrode modified with electrodeposited palladium nanoparticles.* Journal of Electroanalytical Chemistry, 2016. **761**: p. 1-7.
87. Li, Z., *et al.*, *Electrodeposition of palladium nanoparticles on fullerene modified glassy carbon electrode for methane sensing.* Electrochimica Acta, 2012. **76**(Supplement C): p. 288-291.
88. Palanisamy, S., *et al.*, *Palladium nanoparticles decorated on activated fullerene modified screen printed carbon electrode for enhanced electrochemical sensing of dopamine.* Journal of Colloid and Interface Science, 2015. **448**(Supplement C): p. 251-256.
89. Lim, S.H., *et al.*, *A glucose biosensor based on electrodeposition of palladium nanoparticles and glucose oxidase onto Nafion-solubilized carbon nanotube electrode.* Biosensors and Bioelectronics, 2005. **20**(11): p. 2341-2346.
90. Singh, B., *et al.*, *Palladium nanoparticles decorated electrostatically functionalized MWCNTs as a non enzymatic glucose sensor.* Sensors and Actuators A: Physical, 2014. **220**: p. 126-133.
91. Li, R., *et al.*, *Synthesis of palladium@ gold nanoalloys/nitrogen and sulphur-functionalized multiple graphene aerogel for electrochemical detection of dopamine.* Analytica Chimica Acta, 2017. **954**: p. 43-51.
92. López-Suárez, F.E., *et al.*, *Pt–Sn/C catalysts prepared by sodium borohydride reduction for alcohol oxidation in fuel cells: Effect of the precursor addition order.* Journal of Power Sources, 2014. **268**: p. 225-232.
93. Deroco, P.B., *et al.*, *Carbon black supported Au–Pd core-shell nanoparticles within a dihexadecylphosphate film for the development of hydrazine electrochemical sensor.* Sensors and Actuators B: Chemical, 2018. **256**: p. 535-542.
94. Thangavelu, K., *et al.*, *Nanomolar electrochemical detection of caffeic acid in fortified wine samples based on gold/palladium nanoparticles decorated graphene flakes.* Journal of Colloid and Interface Science, 2017. **501**: p. 77-85.
95. Kumar, N. and R.N. Goyal, *Gold-palladium nanoparticles aided electrochemically reduced graphene oxide sensor for the simultaneous estimation of lomefloxacin and amoxicillin.* Sensors and Actuators B: Chemical, 2017. **243**: p. 658-668.

96. Wang, J., *et al.*, *Highly sensitive electrochemical determination of sunset yellow based on the ultrafine Au-Pd and reduced graphene oxide nanocomposites.* Journal of Colloid and Interface Science, 2016. **481**: p. 229-235.
97. Bubacz, K., B. Tryba, and A.W. Morawski, *The role of adsorption in decomposition of dyes on TiO_2 and N-modified TiO_2 photocatalysts under UV and visible light irradiations.* Materials Research Bulletin, 2012. **47**(11): p. 3697-3703.
98. Di Paola, A., *et al.*, *Photocatalytic activity of nanocrystalline TiO_2 (brookite, rutile and brookite-based) powders prepared by thermohydrolysis of $TiCl_4$ in aqueous chloride solutions.* Colloids and Surfaces A: Physicochemical and Engineering Aspects, 2008. **317**(1): p. 366-376.
99. Zhang, X., *et al.*, *A novel CdS/S-TiO_2 nanotubes photocatalyst with high visible light activity (vol 66, pg 417, 2009).* Separation and Purification Technology, 2009. **68**(3): p. 433-433.
100. Graetzel, M. and R.F. Howe, *Electron paramagnetic resonance studies of doped titanium dioxide colloids.* Journal of Physical Chemistry, 1990. **94**(6): p. 2566-2572.
101. Mills, A. and S. Le Hunte, *An overview of semiconductor photocatalysis.* Journal of Photochemistry and Photobiology A: Chemistry, 1997. **108**(1): p. 1-35.
102. Jafari, S., *et al.*, *A comparative study for the removal of methylene blue dye by N and S modified TiO_2 adsorbents.* Journal of Molecular Liquids, 2015. **207**: p. 90-98.
103. Jafari, S., *et al.*, *The role of adsorption in the photocatalytic decomposition of Orange II on carbon-modified TiO_2.* Journal of Molecular Liquids, 2016. **220**: p. 504-512.
104. Mashhadizadeh, M.H. and E. Afshar, *Electrochemical investigation of clozapine at TiO_2 nanoparticles modified carbon paste electrode and simultaneous adsorptive voltammetric determination of two antipsychotic drugs.* Electrochimica Acta, 2013. **87**(Supplement C): p. 816-823.
105. Zhang, S., *Electrochemical determination of p-cresol using mesoporous TiO_2-modified carbon paste electrode.* Russian Journal of Electrochemistry, 2011. **47**(11): p. 1257-1261.
106. Ramezani, S., M. Ghobadi, and B.N. Bideh, *Voltammetric monitoring of Cd (II) by nano-TiO_2 modified carbon paste electrode sensitized using 1,2-bis-[o-aminophenyl thio] ethane as a new ion receptor.* Sensors and Actuators B: Chemical, 2014. **192**(Supplement C): p. 648-657.
107. Kalanur, S.S., J. Seetharamappa, and S.N. Prashanth, *Voltammetric sensor for buzepide methiodide determination based on TiO_2 nanoparticle-modified carbon paste electrode.* Colloids and Surfaces B: Biointerfaces, 2010. **78**(2): p. 217-221.
108. Ensafi, A.A., *et al.*, *Application of ionic liquid–TiO_2 nanoparticle modified carbon paste electrode for the voltammetric determination of benserazide in biological samples.* Materials Science and Engineering: C, 2013. **33**(2): p. 831-835.
109. Ghodsi, J. and A.A. Rafati, *A voltammetric sensor for diazinon pesticide based on electrode modified with TiO_2 nanoparticles covered multi walled carbon nanotube nanocomposite.* Journal of Electroanalytical Chemistry, 2017. **807**(Supplement C): p. 1-9.

110. Jiang, L.-C. and W.-D. Zhang, *Electrodeposition of TiO_2 Nanoparticles on Multiwalled Carbon Nanotube Arrays for Hydrogen Peroxide Sensing.* Electroanalysis, 2009. **21**(8): p. 988-993.
111. Song, M., *et al.*, *Direct electrochemistry and electrocatalysis of hemoglobin–TiO_2 whisker film modified glassy carbon electrode.* Electroanalysis, 2010. **22**(6): p. 668-672.
112. Mao, A., *et al.*, *Determination of mercury using a glassy carbon electrode modified with nano TiO_2 and multi-walled carbon nanotubes composites dispersed in a novel cationic surfactant.* Journal of Electroanalytical Chemistry, 2015. **751**: p. 23-29.
113. Zhang, Y., *et al.*, *Simultaneous electrochemical determination of catechol and hydroquinone based on graphene–TiO_2 nanocomposite modified glassy carbon electrode.* Sensors and Actuators B: Chemical, 2014. **204**: p. 102-108.
114. Hayat, A., *et al.*, *An electrochemical sensor based on TiO_2/activated carbon nanocomposite modified screen printed electrode and its performance for phenolic compounds detection in water samples.* International Journal of Environmental Analytical Chemistry, 2016. **96**(3): p. 237-246.
115. Janus, M., *et al.*, *Carbon-modified TiO_2 photocatalyst by ethanol carbonisation.* Applied Catalysis B: Environmental, 2006. **63**(3): p. 272-276.
116. Jafari, S., *et al.*, *The influence of carbonization temperature on the modification of TiO_2 in the removal of methyl orange from aqueous solution by adsorption.* Desalination and Water Treatment, 2016. **57**(40): p. 18825-18835.
117. Ates, M., *Review study of electrochemical impedance spectroscopy and equivalent electrical circuits of conducting polymers on carbon surfaces.* Progress in Organic Coatings, 2011. **71**(1): p. 1-10.
118. Simões, F.R., L.H. Mattoso, and C.M. Vaz, *Modified carbon paste-polyaniline electrodes for the electrochemical determination of the herbicide 2, 4-D.* Sensor Letters, 2004. **2**(3-1): p. 221-225.
119. Kumar, D. and R. Sharma, *Advances in conductive polymers.* European polymer journal, 1998. **34**(8): p. 1053-1060.
120. Xi, L., *et al.*, *Electrochemical analysis of ascorbic acid using copper nanoparticles/polyaniline modified glassy carbon electrode.* Journal of Electroanalytical Chemistry, 2010. **650**(1): p. 127-134.
121. Zhang, Z. and M. Wan, *Nanostructures of polyaniline composites containing nano-magnet.* Synthetic Metals, 2003. **132**(2): p. 205-212.
122. Kumar, M.A., *et al.*, *Ultra-selective dopamine detection in an excess of ascorbic acid and uric acid using pristine palladium nanoparticles decorated graphene modified glassy carbon electrode.* Journal of The Electrochemical Society, 2015. **162**(9): p. H651-H660.
123. Nayak, P., S.P. Nair, and S. Ramaprabhu, *Enzyme-less and low-potential sensing of glucose using a glassy carbon electrode modified with palladium nanoparticles deposited on graphene-wrapped carbon nanotubes.* Microchimica Acta, 2016. **183**(3): p. 1055-1062.
124. Palanisamy, S., S. Ku, and S.-M. Chen, *Dopamine sensor based on a glassy carbon electrode modified with a reduced graphene oxide and palladium nanoparticles composite.* Microchimica Acta, 2013. **180**(11-12): p. 1037-1042.
125. Wu, T., *et al.*, *Electrochemical sensor for sensitive detection of triclosan based on graphene/palladium nanoparticles hybrids.* Talanta, 2017. **164**: p. 556-562.

126. Hu, J., *et al., Synthesis of palladium nanoparticle modified reduced graphene oxide and multi-walled carbon nanotube hybrid structures for electrochemical applications.* Applied Surface Science, 2017. **396**: p. 523-529.
127. Cincotto, F.H., *et al., Electrochemical sensor based on reduced graphene oxide modified with palladium nanoparticles for determination of desipramine in urine samples.* Sensors and Actuators B: Chemical, 2017. **239**: p. 488-493.
128. Kumar, N., Rosy, and R.N. Goyal, *Gold-palladium nanoparticles aided electrochemically reduced graphene oxide sensor for the simultaneous estimation of lomefloxacin and amoxicillin.* Sensors and Actuators B: Chemical, 2017. **243**: p. 658-668.
129. Vilian, A.T.E., *et al., Fabrication of Palladium Nanoparticles on Porous Aromatic Frameworks as a Sensing Platform to Detect Vanillin.* ACS Applied Materials & Interfaces, 2016. **8**(20): p. 12740-12747.
130. Veerakumar, P., *et al., Palladium Nanoparticle Incorporated Porous Activated Carbon: Electrochemical Detection of Toxic Metal Ions.* ACS Applied Materials & Interfaces, 2016. **8**(2): p. 1319-1326.
131. Shi, Q. and G. Diao, *The electrocatalytical reduction of m-nitrophenol on palladium nanoparticles modified glassy carbon electrodes.* Electrochimica Acta, 2011. **58**: p. 399-405.
132. Kutluay, A. and M. Aslanoglu, *An electrochemical sensor prepared by sonochemical one-pot synthesis of multi-walled carbon nanotube-supported cobalt nanoparticles for the simultaneous determination of paracetamol and dopamine.* Analytica Chimica Acta, 2014. **839**: p. 59-66.
133. Mao, A., *et al., Fabrication of electrochemical sensor for paracetamol based on multi-walled carbon nanotubes and chitosan–copper complex by self-assembly technique.* Talanta, 2015. **144**: p. 252-257.
134. Elyasi, M., M.A. Khalilzadeh, and H. Karimi-Maleh, *High sensitive voltammetric sensor based on Pt/CNTs nanocomposite modified ionic liquid carbon paste electrode for determination of Sudan I in food samples.* Food chemistry, 2013. **141**(4): p. 4311-4317.
135. Salmanpour, S., *et al., Voltammetric determination of norepinephrine in the presence of acetaminophen using a novel ionic liquid/multiwall carbon nanotubes paste electrode.* Materials Science and Engineering: C, 2012. **32**(7): p. 1912-1918.
136. Shahmiri, M.R., *et al., Ethynylferrocene–NiO/MWCNT nanocomposite modified carbon paste electrode as a novel voltammetric sensor for simultaneous determination of glutathione and acetaminophen.* Sensors and Actuators B: Chemical, 2013. **177**: p. 70-77.
137. Sanghavi, B.J. and A.K. Srivastava, *Simultaneous voltammetric determination of acetaminophen, aspirin and caffeine using an in situ surfactant-modified multiwalled carbon nanotube paste electrode.* Electrochimica Acta, 2010. **55**(28): p. 8638-8648.
138. Beitollahi, H., H. Karimi-Maleh, and H. Khabazzadeh, *Nanomolar and Selective Determination of Epinephrine in the Presence of Norepinephrine Using Carbon Paste Electrode Modified with Carbon Nanotubes and Novel 2-(4-Oxo-3-phenyl-3,4-dihydro-quinazolinyl)-N′-phenyl-hydrazinecarbothioamide.* Analytical Chemistry, 2008. **80**(24): p. 9848-9851.
139. Zhao, W.-R., *et al., A novel electrochemical sensor based on gold nanoparticles and molecularly imprinted polymer with binary functional monomers for*

sensitive detection of bisphenol A. Journal of Electroanalytical Chemistry, 2017. **786**: p. 102-111.

140. Tashkhourian, J., *et al., Simultaneous determination of hydroquinone and catechol at gold nanoparticles mesoporous silica modified carbon paste electrode.* Journal of Hazardous Materials, 2016. **318**: p. 117-124.
141. Çubukçu, M., S. Timur, and Ü. Anik, *Examination of performance of glassy carbon paste electrode modified with gold nanoparticle and xanthine oxidase for xanthine and hypoxanthine detection.* Talanta, 2007. **74**(3): p. 434-439.
142. Carrera, P., *et al., Electrochemical determination of arsenic in natural waters using carbon fiber ultra-microelectrodes modified with gold nanoparticles.* Talanta, 2017. **166**: p. 198-206.
143. C. Ait Ramdane-Terbouche, A.T., S. Djebbar, D. Hauchard, *Electrochemical sensors using modified electrodes based on copper complexes formed with Algerian humic acid modified with ethylenediamine or triethylenetetramine for determination of nitrite in water* Talanta,, 2014. **119**.
144. Jiang, G., *et al., Application of a mercapto-terminated binuclear Cu (II) complex modified Au electrode to improve the sensitivity and selectivity for dopamine detection.* Sensors and Actuators B: Chemical, 2015. **209**: p. 122-130.
145. Saravia, L., *et al., Development of a tetraphenylporphyrin cobalt (II) modified glassy carbon electrode to monitor oxygen consumption in biological samples.* Journal of Electroanalytical Chemistry, 2016. **775**: p. 72-76.
146. Vereshchagin, A.A., *et al., Interaction of amines with electrodes modified by polymeric complexes of Ni with salen-type ligands.* Electrochimica Acta, 2016. **211**: p. 726-734.
147. Oni, J., *et al., Metallophthalocyanine-modified glassy carbon electrodes: effects of film formation conditions on electrocatalytic activity towards the oxidation of nitric oxide.* Sensors and Actuators B: Chemical, 2005. **105**(2): p. 208-213.
148. Parsaei, M., Z. Asadi, and S. Khodadoust, *A sensitive electrochemical sensor for rapid and selective determination of nitrite ion in water samples using modified carbon paste electrode with a newly synthesized cobalt (II)-Schiff base complex and magnetite nanospheres.* Sensors and Actuators B: Chemical, 2015. **220**: p. 1131-1138.
149. Shahrokhian, S. and M. Karimi, *Voltammetric studies of a cobalt (II)-4-methylsalophen modified carbon-paste electrode and its application for the simultaneous determination of cysteine and ascorbic acid.* Electrochimica acta, 2004. **50**(1): p. 77-84.
150. Parvin, M.H., *et al., Carbon paste electrode modified with cobalt nanoparticles and its application to the electrocatalytic determination of chlorpromazine.* Journal of Electroanalytical Chemistry, 2012. **683**: p. 31-36.
151. Shahrokhian, S., *et al., Multi-walled carbon nanotubes with immobilised cobalt nanoparticle for modification of glassy carbon electrode: application to sensitive voltammetric determination of thioridazine.* Biosensors and Bioelectronics, 2009. **24**(11): p. 3235-3241.
152. Gholivand, M.B. and M. Solgi, *Sensitive warfarin sensor based on cobalt oxide nanoparticles electrodeposited at multi-walled carbon nanotubes modified glassy carbon electrode (CoxOyNPs/MWCNTs/GCE).* Electrochimica Acta, 2017. **246**: p. 689-698.

153. Amiri, M., *et al., Cobalt flower-like nanostructure as modifier for electrocatalytic determination of chloropheniramine.* Industrial & Engineering Chemistry Research, 2012. **51**(44): p. 14384-14389.
154. Song, Y., *et al., Electrochemical and electrocatalytic properties of cobalt nanoparticles deposited on graphene modified glassy carbon electrode: Application to some amino acids detection.* Electrochimica Acta, 2011. **58**: p. 757-763.
155. Zhao, L., *et al., Electro-oxidation of Ascorbic Acid by Cobalt Core–Shell Nanoparticles on a H-Terminated Si(100) and by Nanostructured Cobalt-Coated Si Nanowire Electrodes.* ACS Applied Materials & Interfaces, 2013. **5**(7): p. 2410-2416.
156. Siadat, S.R., *Green Synthesized Cobalt Nano Particles for using as a Good Candidate for Sensing Organic Compounds.* Journal of Electrochemical Science and Technology, 2015. **6**(4): p. 111-115.
157. Azab, S.M. and A.M. Fekry, *Electrochemical design of a new nanosensor based on cobalt nanoparticles, chitosan and MWCNT for the determination of daclatasvir: a hepatitis C antiviral drug.* RSC Advances, 2017. **7**(2): p. 1118-1126.
158. Devaramani, S. and P. Malingappa, *Synthesis and characterization of cobalt nitroprusside nano particles: Application to sulfite sensing in food and water samples.* Electrochimica Acta, 2012. **85**: p. 579-587.
159. Geto, A., M. Tessema, and S. Admassie, *Determination of histamine in fish muscle at multi-walled carbon nanotubes coated conducting polymer modified glassy carbon electrode.* Synthetic Metals, 2014. **191**: p. 135-140.
160. Ghadimi, H., *et al., Electrochemical determination of aspirin and caffeine at MWCNTs-poly-4-vinylpyridine composite modified electrode.* Journal of the Taiwan Institute of Chemical Engineers, 2016. **65**: p. 101-109.
161. Kumari, M.M., S.A. Aromal, and D. Philip, *Synthesis of monodispersed palladium nanoparticles using tannic acid and its optical non-linearity.* Spectrochimica Acta Part A: Molecular and Biomolecular Spectroscopy, 2013. **103**: p. 130-133.
162. Tovide, O., *et al., Graphenated polyaniline-doped tungsten oxide nanocomposite sensor for real time determination of phenanthrene.* Electrochimica Acta, 2014. **128**: p. 138-148.
163. Prathap, M.A., R. Srivastava, and B. Satpati, *Simultaneous detection of guanine, adenine, thymine, and cytosine at polyaniline/MnO_2 modified electrode.* Electrochimica Acta, 2013. **114**: p. 285-295.
164. Liu, Q., *et al., Polyaniline Langmuir–Blodgett film modified glassy carbon electrode as a voltammetric sensor for determination of Ag+ ions.* Electrochimica Acta, 2010. **55**(5): p. 1795-1800.
165. Fan, Y., *et al., Graphene–polyaniline composite film modified electrode for voltammetric determination of 4-aminophenol.* Sensors and Actuators B: Chemical, 2011. **157**(2): p. 669-674.
166. C.M.A.Brett, A.M.O.Brett., *Electrochemistry: Principles Methods and Applications*. Oxford University Press Eds. 1993: Oxford University Press Eds.
167. Chow, E. and J.J. Gooding, *Peptide modified electrodes as electrochemical metal ion sensors.* Electroanalysis, 2006. **18**(15): p. 1437-1448.
168. Qiu, S.Y.G., S.; Lin, Z.Y.; Chen, G.N. , *Advances in Click Chemistry.* Prog. Chem, 2011. **23**: p. 637-648.

169. Macdonald, E.B.a.J.R., *Impedance Spectroscopy - Theory, Experiment, and Applications*. Wiley-Interscience 2005: Wiley-Interscience
170. Orazem, M.E. and B. Tribollet, *Electrochemical impedance spectroscopy*. Vol. 48. 2011: John Wiley & Sons.
171. Mandler, D. and S. Kraus-Ophir, *Self-assembled monolayers (SAMs) for electrochemical sensing.* Journal of Solid State Electrochemistry, 2011. **15**(7-8): p. 1535.
172. Bélanger, D. and J. Pinson, *Electrografting: a powerful method for surface modification.* Chemical Society Reviews, 2011. **40**(7): p. 3995-4048.
173. Maeda, H., *et al.*, *Anodization of glassy carbon electrodes in oligomers of ethylene glycol and their monomethyl ethers as a tool for the elimination of protein adsorption.* Analytical sciences, 1997. **13**(5): p. 721-727.
174. Abiman, P., *et al.*, *Contrasting pK_a of Protonated Bis (3-aminopropyl)-Terminated Polyethylene Glycol "Jeffamine" and the Associated Thermodynamic Parameters in Solution and Covalently Attached to Graphite Surfaces.* Chemistry–A European Journal, 2007. **13**(34): p. 9663-9667.
175. Maeda, H., *et al.*, *Effective method for the covalent introduction of the 2-(2-carboxymethoxyethoxy) ethoxy group on a glassy carbon electrode by anodization in triethylene glycol.* Analytical sciences, 1999. **15**(6): p. 531-536.
176. Maeda, H., *et al.*, *Direct covalent modification of glassy carbon surfaces with 1-alkanols by electrochemical oxidation.* Chemical and pharmaceutical bulletin, 1994. **42**(9): p. 1870-1873.
177. French, R.W., A.M. Collins, and F. Marken, *Growth and application of paired gold electrode junctions: evidence for nitrosonium phosphate during nitric oxide oxidation.* Electroanalysis, 2008. **20**(22): p. 2403-2409.
178. Marley, A. and D. Connolly, *Determination of (R)-timolol in (S)-timolol maleate active pharmaceutical ingredient: Validation of a new supercritical fluid chromatography method with an established normal phase liquid chromatography method.* Journal of Chromatography A, 2014. **1325**: p. 213-220.
179. Shahrokhian, S. and S. Rastgar, *Construction of an electrochemical sensor based on the electrodeposition of Au-Pt nanoparticles mixtures on multi-walled carbon nanotubes film for voltammetric determination of cefotaxime.* Analyst, 2012. **137**(11): p. 2706-15.
180. Rassaei, L., *et al.*, *Nanoparticles in electrochemical sensors for environmental monitoring.* TrAC Trends in Analytical Chemistry, 2011. **30**(11): p. 1704-1715.
181. Norouzi, P., *et al.*, *Novel method for fast determination of ultra trace amounts of timolol maleate by continuous cyclic voltammetry at Au microelectrode in flowing injection systems.* Sensors and Actuators B: Chemical, 2005. **110**(2): p. 239-245.
182. Arranz, A., *et al.*, *Electroanalytical study and square wave voltammetric techniques for the determination of β-blocker timolol at the mercury electrode.* Analytica Chimica Acta, 1999. **389**(1): p. 225-232.
183. Al-Ghamdi, A.F., *Stripping voltammetric determination of timolol drug in pharmaceuticals and biological fluids.* American Journal of Analytical Chemistry, 2011. **2**(02): p. 174.
184. Türkdemir, M., *et al.*, *Voltammetric determination of timolol maleate: a β-adrenergic blocking agent.* Journal of Analytical Chemistry, 2001. **56**(11): p. 1047-1050.

185. Hasanzadeh, M., *et al.*, *Determination of diltiazem in the presence of timolol in human serum samples using a nanoFe_3O_4@ GO modified glassy carbon electrode.* RSC Advances, 2014. **4**(93): p. 51734-51744.
186. Shrivastava, A. and V.B. Gupta, *Various treatment options for benign prostatic hyperplasia: A current update.* Journal of mid-life health, 2012. **3**(1): p. 10.
187. Shin, I.S., *et al.*, *Inhibitory effect of Yukmijihwang-tang, a traditional herbal formula against testosterone-induced benign prostatic hyperplasia in rats.* BMC complementary and alternative medicine, 2012. **12**(1): p. 48.
188. Ghoneim, M., *et al.*, *A validated stripping voltammetric procedure for quantification of the anti-hypertensive and benign prostatic hyperplasia drug terazosin in tablets and human serum.* Talanta, 2004. **64**(3): p. 703-710.
189. Atta, N.F., A. Galal, and S.M. Azab, *Gold nanoparticles modified electrode for the determination of an antihypertensive drug.* Electroanalysis, 2012. **24**(6): p. 1431-1440.
190. Hosseini, M., E. Nasli-Esfahani, and P. Norouzi, *Terazosin potentiometric sensor for quantitative analysis of terazosin hydrochloride in pharmaceutical formulation based on computational study.* Int. J. Electrochem. Sci, 2010. **5**: p. 200-214.
191. Atta, N.F., *et al.*, *Effect of surfactants on the voltammetric response and determination of an antihypertensive drug.* Talanta, 2007. **72**(4): p. 1438-1445.
192. Madrakian, T., *et al.*, *ZnO/rGO nanocomposite/carbon paste electrode for determination of terazosin in human serum samples.* RSC Advances, 2016. **6**(4): p. 2552-2558.
193. Oz, M., *et al.*, *Cellular and molecular actions of methylene blue in the nervous system.* Medicinal research reviews, 2011. **31**(1): p. 93-117.
194. Xiao, M., *et al.*, *Electrochemical study of methylene blue/titanate nanotubes nanocomposite and its layer-by-layer assembly multilayer films.* Journal of Solid State Electrochemistry, 2008. **12**(9): p. 1159-1166.
195. Korshoj, L.E., A.J. Zaitouna, and R.Y. Lai, *Methylene blue-mediated electrocatalytic detection of hexavalent chromium.* Analytical Chemistry, 2015. **87**(5): p. 2560-2564.
196. Bélaz-David, N., *et al.*, *Spectrophotometric determination of methylene blue in biological fluids after ion-pair extraction and evidence of its adsorption on plastic polymers.* European Journal of Pharmaceutical Sciences, 1997. **5**(6): p. 335-345.
197. Wagner, J.G., *A modern view of pharmacokinetics.* Journal of Pharmacokinetics and Biopharmaceutics, 1973. **1**(5): p. 363-401.
198. Xu, J.Z., *et al.*, *Determination of methylene blue residues in aquatic products by liquid chromatography-tandem mass spectrometry.* Journal of Separation science, 2009. **32**(23-24): p. 4193-4199.
199. Borwitzky, H., W.E. Haefeli, and J. Burhenne, *Analysis of methylene blue in human urine by capillary electrophoresis.* Journal of Chromatography B, 2005. **826**(1): p. 244-251.
200. de Araujo Nicolai, S.H., *et al.*, *Electrochemical and spectroelectrochemical (SERS) studies of the reduction of methylene blue on a silver electrode.* Journal of Electroanalytical Chemistry, 2002. **527**(1): p. 103-111.
201. Hassan, S.S., *et al.*, *Ultra-trace level electrochemical sensor for methylene blue dye based on nafion stabilized ibuprofen derived gold nanoparticles.* Sensors and Actuators B: Chemical, 2015. **208**: p. 320-326.

202. Li, J., *et al.*, *Adsorptive and stripping behavior of methylene blue at gold electrodes in the presence of cationic gemini surfactants.* Electrochimica Acta, 2005. **51**(2): p. 297-303.
203. Tonlé, I.K., *et al.*, *Sorption of methylene blue on an organoclay bearing thiol groups and application to electrochemical sensing of the dye.* Talanta, 2008. **74**(4): p. 489-497.
204. Tüzen, M., *Determination of heavy metals in soil, mushroom and plant samples by atomic absorption spectrometry.* Microchemical Journal, 2003. **74**(3): p. 289-297.
205. Deng, J.-H., *et al.*, *Simultaneous removal of Cd (II) and ionic dyes from aqueous solution using magnetic graphene oxide nanocomposite as an adsorbent.* Chemical Engineering Journal, 2013. **226**: p. 189-200.
206. Zhang, D., *et al.*, *Voltammetric determination of folic acid using adsorption of methylene blue onto electrodeposited of reduced graphene oxide film modified glassy carbon electrode.* Electroanalysis, 2016. **28**(2): p. 312-319.
207. Yang, S., *et al.*, *Simultaneous voltammetric detection of dopamine and uric acid in the presence of high concentration of ascorbic acid using multi-walled carbon nanotubes with methylene blue composite film-modified electrode.* Journal of Solid State Electrochemistry, 2011. **15**(9): p. 1909-1918.
208. Xiao, Y., Rowe, A.A. and Plaxco, K.W. *Electrochemical Detection of Parts-Per-Billion Lead via an Electrode-Bound DNAzyme Assembly.* Journal of the American Chemical Society, 2007. **129**(2): p. 262-263.
209. Chao, M. and Ma, X. *Simultaneous electrocatalytic determination of lead and cadmium ions employing a poly (methylene blue)/graphene modified glassy carbon electrode.* Russian Journal of Electrochemistry, 2015. **51**(1): p. 39-48.
210. Ma, X. and Chao, M. *Rapid voltammetric determination of maltol in some foods and beverages using a poly (methylene blue)/graphene-modified glassy carbon electrode.* Journal of Solid State Electrochemistry, 2014. **18**(3): p. 621-628.
211. Liu, C., *et al.*, *Electrocatalytic Oxidation of Dopamine at a Nanocuprous Oxide-Methylene Blue Composite Glassy Carbon Electrode.* Electroanalysis, 2006. **18**(5): p. 478-484.
212. Sun, Y., *et al.*, *Controlled synthesis various shapes Fe_3O_4 decorated reduced graphene oxide applied in the electrochemical detection.* Journal of Alloys and Compounds, 2015. **638**: p. 182-187.
213. Gómez, Y., *et al.*, *Characterization of a carbon paste electrode modified with tripolyphosphate-modified kaolinite clay for the detection of lead.* Talanta, 2011. **85**(3): p. 1357-1363.
214. Wang, Y., *et al.*, *Metal–organic framework modified carbon paste electrode for lead sensor.* Sensors and Actuators B: Chemical, 2013. **177**: p. 1161-1166.
215. Han, X.-J., *et al.*, *Mesoporous $MnFe_2O_4$ nanocrystal clusters for electrochemistry detection of lead by stripping voltammetry.* Journal of Electroanalytical Chemistry, 2015. **755**: p. 203-209.
216. Raghu, G.K., Sampath, S. and Pandurangappa, M. *Chemically functionalized glassy carbon spheres: a new covalent bulk modified composite electrode for the simultaneous determination of lead and cadmium.* Journal of Solid State Electrochemistry, 2012. **16**(5): p. 1953-1963.
217. Salmanipour, A. and M.A. Taher, *An electrochemical sensor for stripping analysis of Pb (II) based on multiwalled carbon nanotube functionalized with 5-*

Br-PADAP. Journal of Solid State Electrochemistry, 2011. **15**(11-12): p. 2695-2702.

218. Morales, G.R., Silva, T.R. and Galicia, L. *Carbon paste electrodes electrochemically modified with cyclodextrins.* Journal of Solid State Electrochemistry, 2003. **7**(6): p. 355-360.
219. Morante-Zarcero, S., Pérez-Quintanilla, D. and Sierra, I. *A disposable electrochemical sensor based on bifunctional periodic mesoporous organosilica for the determination of lead in drinking waters.* Journal of Solid State Electrochemistry, 2015. **19**(7): p. 2117-2127.
220. Simionca, I.M., *et al.*, *Siloxane-Crown Ether Polyamide Based Electrode for Electrochemical Determination of Lead (II) in Aqueous Solution.* Electroanalysis, 2012. **24**(10): p. 1995-2004.

Publication I

Nekoueian, K., Hotchen, CE., Amiri, M., Sillanpää, M., Nelson, GW. Foord, JS., Holdway, P., Buchard, A., Parker, SC., Marken, F.

Interfacial electron-shuttling processes across KolliphorEL monolayer grafted electrodes

Reprinted with permission from
Applied Materials & Interfaces
Vol. 7 pp.15458-15465, 2015
© 2015 American Chemical Society

ACS APPLIED MATERIALS & INTERFACES

Research Article

www.acsami.org

Interfacial Electron-Shuttling Processes across KolliphorEL Monolayer Grafted Electrodes

Khadijeh Nekoueian,[†,‡,§] Christopher E. Hotchen,[†] Mandana Amiri,[‡] Mika Sillanpää,[§] Geoffrey W. Nelson,[∥] John S. Foord,[⊥] Philip Holdway,[#] Antoine Buchard,[†] Stephen C. Parker,[†] and Frank Marken*[,†]

[†]Department of Chemistry, University of Bath, Bath BA2 7AY, United Kingdom

[‡]Department of Chemistry, University of Mohaghegh Ardabili, Ardabil 56199-11367, Iran

[§]Laboratory of Green Chemistry, School of Engineering Science, Lappeenranta University of Technology, Sammonkatu 12, FI-50130 Mikkeli, Finland

[∥]Imperial College London, Department of Materials, Royal School of Mines, Exhibition Road, London SW7 2AZ, United Kingdom

[⊥]Chemistry Research Laboratories, Oxford University, South Parks Road, Oxford OX1 3TA, United Kingdom

[#]Department of Materials, Oxford University, Begbroke Science Park, Begbroke Hill, Oxford OX5 1PF, United Kingdom

ABSTRACT: Covalently grafted KolliphorEL (a poly(ethylene glycol)-based transporter molecule for hydrophobic water-insoluble drugs; MW, ca. 2486; diameter, ca. 3 nm) at the surface of a glassy-carbon electrode strongly affects the rate of electron transfer for aqueous redox systems such as $Fe(CN)_6^{3-/4-}$. XPS data confirm monolayer grafting after electrochemical anodization in pure KolliphorEL. On the basis of voltammetry and impedance measurements, the charge transfer process for the $Fe(CN)_6^{3-/4-}$ probe molecule is completely blocked after KolliphorEL grafting and in the absence of a "guest". However, in the presence of low concentrations of suitable ferrocene derivatives as guests, mediated electron transfer across the monolayer via a shuttle mechanism is observed. The resulting amplification of the ferrocene electroanalytical signal is investigated systematically and compared for five ferrocene derivatives. The low-concentration electron shuttle efficiency decreases in the following sequence: (dimethylaminomethyl)ferrocene > *n*-butyl ferrocene > ferrocene dimethanol > ferroceneacetonitrile > ferroceneacetic acid.

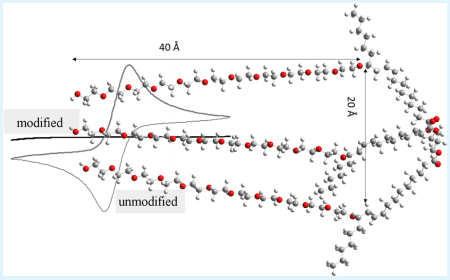

KEYWORDS: *Cremophor, PEGylation, amplification, voltammetry, tunneling, sensor*

1. INTRODUCTION

Surface-modified electrodes are widely used in sensors[1] and in film electrodes.[2−4] Covalent grafting of a monolayer onto carbon electrode surfaces can be achieved by diazonium methods,[5,6] "click" chemistry,[7] amide chemical attachment,[8] or many other similar processes.[9] Electrochemical surface modification offers the advantage (over chemical processes) of potential control and optimization to achieve well-defined monolayer coverage. A wide range of often radical-based intermediates are known to attach spontaneously to carbon electrode surfaces.[10,11] We have recently adapted a methodology introduced by Maeda and co-workers[12,13] to attach poly(ethylene glycol) (PEG) derivatives to glassy-carbon and boron-doped diamond electrode surfaces.[14] An anodic treatment was developed to allow monolayer attachment of PEGs with a resulting structure-dependent retardation of the rate of heterogeneous electron transfer. In this study, a PEGylated castor oil derivative, KolliphorEL (CAS no. 61791-12-6; MW, ca. 2486 g mol^{-1}; Figure 1) is selected to demonstrate this anodic grafting process for a more complex molecule.

For PEGylated molecules such as KolliphorEL, the hydroxyl end groups are sensitive to oxidation with radical intermediates likely to bind to the carbon electrode surface.[15] As a PEGylated castor oil derivative, KolliphorEL (Figure 1) is often employed as medicinal additive or drug carrier reagent[16] to allow water-insoluble drug molecules to be solubilized and carried to the location of action. On the basis of this use, it could introduce interesting new properties (with a hydrophobic layer, Figure 1C) to the modified carbon electrode surface. Similarly, PEGylation is widely used to impose hydrophilic character to surfaces, particles, and molecules.[17] In this study, the KolliphorEL surface layer is employed as (i) a barrier to electron transfer and (ii) a host film to allow hydrophobic

Received: April 27, 2015
Accepted: June 24, 2015
Published: June 24, 2015

ACS Publications © 2015 American Chemical Society

DOI: 10.1021/acsami.5b03654
ACS Appl. Mater. Interfaces 2015, 7, 15458−15465

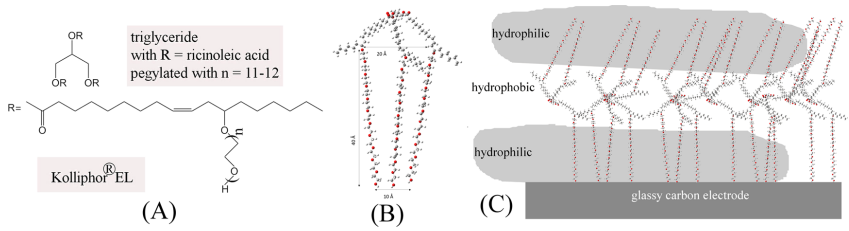

Figure 1. (A) Molecular structure of the main component in KolliphorEL and (B) 3D rendering (GaussView 5.0) showing the approximate diameter of 3−5 nm. (C) Schematic drawing of a KolliphorEL monolayer with a hydrophobic region resulting from the triglyceride.

reagents to bind and enhance or amplify interfacial electron transfer.

Amplification of electroanalytical signals is often desirable and possible, for example, (i) by direct feedback in generator-collector electrode devices[18] and (ii) in catalytic processes where an enzyme[19] or nanoparticle catalyst[20] is employed to enhance the analytical response. Here, amplification is achieved simply on the basis of a difference in the rate of heterogeneous electron transfer for two redox systems. Figure 2 shows a

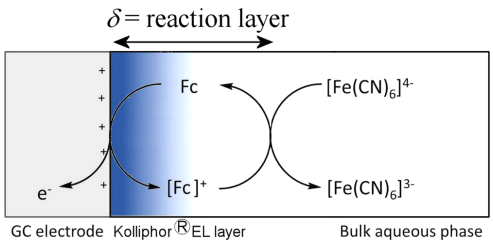

Figure 2. Schematic drawing of the amplification mechanism for the low-concentration ferrocene (Fc) redox process in the presence of the suppressed $Fe(CN)_6^{3-/4-}$ electron transfer.

schematic drawing of the electrode surface with a layer of KolliphorEL immobilized. The direct electron transfer to the $Fe(CN)_6^{3-/4-}$ redox system is suppressed, but the presence of a shuttle molecule such as ferrocene (Fc) can be employed to restore electron transfer. Very low concentrations of ferrocene can therefore be detected as relatively large amplified currents.

Here, the Maeda method is employed to produce a KolliphorEL monolayer on a glassy-carbon electrode surface. It is shown that this results in a dramatic decrease in the rate of heterogeneous electron transfer for aqueous $Fe(CN)_6^{3-/4-}$. Ferrocene derivatives are then compared with respect to their shuttle ability for electrons to pass through the KolliphorEL layer. A quantitative study reveals the structural parameters that govern the shuttle process. Future applications are envisaged in the amplification (or modulation) of other types of electron-transfer processes, e.g., in analytical drug or explosives detection applications.

2. EXPERIMENTAL SECTION

2.1. Chemical Reagents. KolliphorEL (CAS number 61791-12-6; MW ca. 2450 g mol^{-1}; previously also known as Cremophor EL; Aldrich) is a PEGylated castor oil derivative (Figure 1). Lithium perchlorate ($LiClO_4$, Sigma-Aldrich, ≥ 95%, ACS reagent grade) was used as background electrolyte in neat KolliphorEL solutions. Ferrocene dimethanol ($Fc(MeOH)_2$, Aldrich, 98%), ferroceneacetic acid (FcAcOH, Aldrich, 98%), ferroceneacetonitrile (FcMeCN, Aldrich), *n*-butyl ferrocene (BuFc, Alfa Aesar, 98%, oil), *N*,*N*′-(dimethylaminomethyl)ferrocene ($MeFcNMe_2$, TCI Europe, oil), potassium ferrocyanide(II) ($K_4Fe(CN)_6$, Fisons, 98%), and potassium ferricyanide(III) ($K_3Fe(CN)_6$, Aldrich, 99+ %) were used as redox species in aqueous solutions containing 0.1 M potassium nitrate (KNO_3, Sigma-Aldrich, ≥ 99.0%) as background electrolyte.

2.2. Instrumentation. All electrochemical measurements were carried out using an Ivium Compactstat 104 Model B08084 (Ivium Technologies NL). A step potential of 1 mV was used in cyclic voltammetry experiments. Electrochemical impedance spectroscopy (EIS) was carried out at open-circuit potential (OCP) = 0.19 V versus SCE in a 0.1 M KNO_3 solution containing 5 mM $Fe(CN)_6^{3-}$ and 5 mM $Fe(CN)_6^{4-}$, with an amplitude of 10 mV. The frequency was varied from 10 kHz to 0.01 Hz. Equivalent circuit data fitting was carried out using ZView software.

X-ray photoelectron spectroscopy (XPS) experiments were carried out using a Thermo K Alpha (Thermo Scientific) spectrometer (operating at ∼10^{-8}−10^{-9} Torr), a 180° double-focusing hemispherical analyzer running in constant-analyzer energy (CAE) mode with a 128-channel detector. A monochromated Al Kα radiation source (1486.7 eV) was used. Peak fitting was carried out with XPS Peak Fit (v. 4.1) software using Shirley background subtraction. Peaks were referenced to the adventitious carbon C 1s peak (284.6 eV), and peak areas were normalized to the photoelectron cross section of the F 1s photoelectron signal using atomic sensitivity factors.[21]

2.3. Procedure for KolliphorEL Grafting. KolliphorEL is a viscous liquid and can be employed directly as a solvent in electrochemical experiments after addition of suitable electrolyte. Here, a solution of 20 mM $LiClO_4$ in KolliphorEL is employed for the electrode modification process. A 3 mm diameter glassy-carbon electrode is placed into this solution with +1.6 V versus SCE applied for 20 min (optimized previously).[14] The electrode is then rinsed with water and dried. The extent of surface modification is apparent from XPS data for two independently prepared samples K1 and K2 (Figure 3).

Survey spectra show photoelectron signals from contaminant-free surfaces containing C and O (Figure 3A). The C 1s photoelectron signals show evidence for a PEG-like interface. The C 1s spectra associated with KolliphorEL samples K1 and K2 are shown in Figure 3B. The spectra could be fitted (section 2) into four chemical environments: adventitious carbon and hydrocarbon (284.6 eV), ether (C−O, ∼286.1 eV), carbonyl (C═O, ∼287.1 eV), and carboxyl (C═O(OH), ∼288.1 eV).[22] The O 1s photoelectron signal in Figure 3C was curve-fitted using the model established by Schlapak et al.[23] as follows: hydroxyl (−OH, ∼531 eV), ether (C−O, ∼532.2 eV), and water (H_2O, ∼533.5 eV). The above spectra are consistent with PEG-like surface chemistry, with contribution from C−O from repeated poly(ethylene glycol) units dominating the observed photoelectron signal. The presence of hydroxyl and water O 1s signals suggests that trace water is present within the interface, which is to be expected because water binds strongly to PEG. XPS data are summarized in Table 1. Variation between samples K1 and K2 suggest some position dependence and/or sample-to-sample variability. Key changes in comparison to the bare glassy-carbon surface are (i) an increase in O

DOI: 10.1021/acsami.5b03654
ACS Appl. Mater. Interfaces 2015, 7, 15458−15465

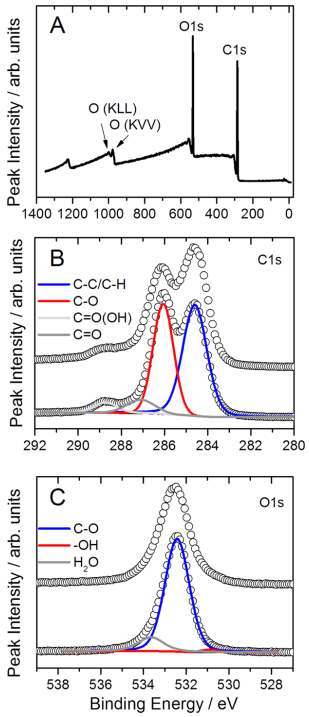

Figure 3. (A) Representative survey XPS spectra of KolliphorEL modification of glassy carbon. XPS core level spectra of modified substrate (B) C 1s and (C) O 1s. Representative curve fits (section 2) are shown for C 1s and O 1s and for two independently investigated samples (dotted lines K1, bottom, and K2, above; Table 1).

1s/C 1s ratio, mainly caused by C−O, (ii) an increase in C 1s for C−O, and (iii) an increase in O 1s for C−O.

3. RESULTS AND DISCUSSION

3.1. KolliphorEL Grafting Affects Heterogeneous Electron-Transfer Kinetics. KolliphorEL is medicinal formulation additive and a transporter molecule for drugs and poorly water-soluble materials.[16] It is employed here when grafted as a monolayer directly onto glassy-carbon electrode surfaces. Although only monolayer deposition occurs, a dramatic effect of this surface modification is detected in heterogeneous electron transfer for the $Fe(CN)_6^{3-/4-}$ redox system (eq 1).

$$Fe(CN)_6^{3-} + e^- \rightleftarrows Fe(CN)_6^{4-} \quad (1)$$

This redox system is often employed to probe surface-modification effects,[24] and here it is shown to be highly sensitive to KolliphorEL grafts. Figure 4A displays cyclic voltammetry data first for the unmodified glassy-carbon electrode and then for the KolliphorEL-modified electrode. The heterogeneous electron transfer to $Fe(CN)_6^{3-/4-}$ is almost completely suppressed within the potential range investigated here. The approximate diameter of the KolliphorEL molecules is 1 nm (Figure 1), which appears to be sufficient to essentially switch off heterogeneous electron transfer. A gentle polish is sufficient to reverse the effect.

The experiment was repeated with impedance analysis to explore the effect in the time domain. Figure 4B shows impedance data for unmodified and modified electrodes. For the unmodified electrode, a conventional Randles circuit model (inset in Figure 4B) was employed giving R_{sol} = 154 Ω, R_{et} = 266 Ω, C = 1.8 μF, W_P = 0.5, W_T = 107, and W_R = 6310 Ω. (The line of best fit overlays data in Figure 4B.) For the KolliphorEL-modified electrode, the impedance response is associated mainly with capacitive charging (Figure 4B), with R_{sol} and C values similar to those for the unmodified electrode. However, a good fit was not possible. This is believed to be due to low-frequency data revealing additional complexity, which could be due to some remaining porosity in the grafted layer and associated with some electron transfer at frequencies below 1 Hz. In summary, the KolliphorEL grafting strongly suppresses electron transfer to $Fe(CN)_6^{3-/4-}$, and it is now possible to introduce guest molecules to explore shuttle effects and changes in electron transfer.

3.2. KolliphorEL Grafting Affecting Heterogeneous Electron-Transfer Kinetics: Ferrocene Mediators. In contrast to the dramatic change in the rate of heterogeneous electron transfer observed for hydrophilic $Fe(CN)_6^{3-/4-}$, the rates of electron transfer for many more hydrophobic ferrocene derivatives are potentially less sensitive to surface modification. This is consistent with the less hydrated and more hydrophobic ferrocene derivatives penetrating into the KolliphorEL film and effectively operating as electron shuttles between the electrode surface and the solution redox species (such as $Fe(CN)_6^{3-/4-}$). The shuttle efficiency is investigated for five different ferrocene derivatives.

Ferrocene dimethanol (Figure 5) is modestly water-soluble and employed here as an electron shuttle at 0, 5, 10, and 50 μM concentrations to lower the electron-transfer impedance between the electrode and $Fe(CN)_6^{3-/4-}$. The voltammetric signal at the KolliphorEL-modified glassy carbon increases from no signal to 42 μA peak current (Figure 5A), which is close to the diffusion-limited value for the $Fe(CN)_6^{3-/4-}$ species (compare to Figure 4A). The underlying voltammetric signal for the ferrocene dimethanol itself remains insignificant on this

Table 1. XPS Ratios and Surface Composition for Two Independently Investigated Samples with KolliphorEL monolayer (K1 and K2) and a Bare Glassy-Carbon (GC) Substrate[a]

		C 1s composition (%)				O 1s composition (%)		
sample	O 1s/C 1s	C−C	C−O	C═O	C═O(OH)	OH	H_2O	C−O
K1	2.94	39.1	50.2	6.4	4.3	1.3	12.6	86.1
K2	3.12	54.7	33.8	4.8	6.7	5.3	12.8	81.9
GC	1.29	66	11	11	8	12	33	55

[a]Peak integration methods based on literature models for C 1s[17] and O 1s[18] were employed.

DOI: 10.1021/acsami.5b03654
ACS Appl. Mater. Interfaces 2015, 7, 15458−15465

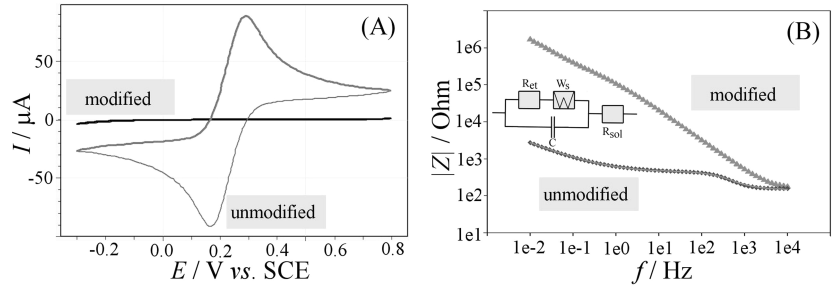

Figure 4. (A) Cyclic voltammograms (scan rate = 50 mV s^{-1}) for a 3 mm glassy-carbon electrode immersed in aqueous 5 mM $Fe(CN)_6^{3-}$, 5 mM $Fe(CN)_6^{4-}$, and 0.1 M KNO_3 before and after KolliphorEL grafting. (B) Impedance data for the same system at the equilibrium potential.

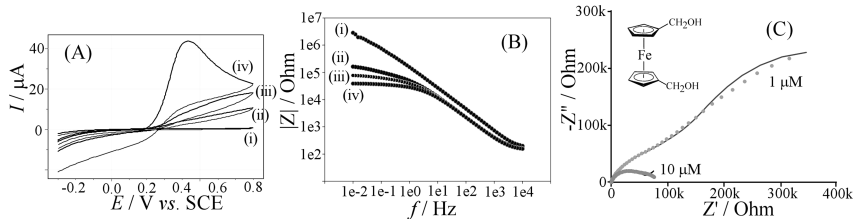

Figure 5. (A) Cyclic voltammograms (scan rate = 50 mV s^{-1}) for a 3 mm glassy-carbon electrode immersed in aqueous 5 mM $Fe(CN)_6^{3-}$, 5 mM $Fe(CN)_6^{4-}$, and 0.1 M KNO_3 with addition of (i) 0, (ii) 5, (iii) 10, and (iv) 50 μM ferrocene dimethanol. (B) Impedance data for this system at equilibrium potential. (C) Nyquist plot with simulation model data (line) and experimental data (dots) for 1 and 10 μM ferrocene dimethanol.

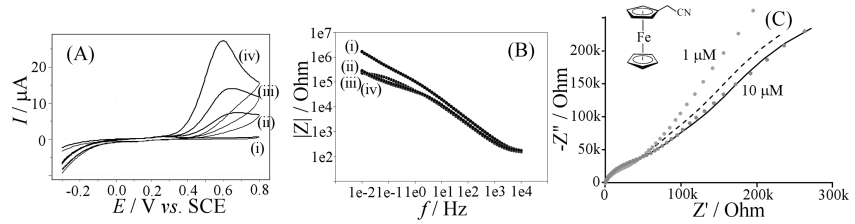

Figure 6. (A) Cyclic voltammograms (scan rate = 50 mV s^{-1}) for a 3 mm glassy-carbon electrode immersed in aqueous 5 mM $Fe(CN)_6^{3-}$, 5 mM $Fe(CN)_6^{4-}$, and 0.1 M KNO_3 with addition of (i) 0, (ii) 5, (iii) 10, and (iv) 50 μM ferroceneacetonitrile. (B) Impedance data for this system at equilibrium potential. (C) Nyquist plot with simulation model data (dashed and solid lines) and experimental data (dots) for 1 and 10 μM ferroceneacetonitrile.

scale and is not detected in this experiment. Only the amplified net current for the $Fe(CN)_6^{3-/4-}$ redox system is detected.

The electron shuttle effect is also seen in the impedance data (Figure 5B), where a significant change in the lower-frequency range (below 10 Hz) is consistent with the flow of Faradaic current catalyzed by the ferrocene dimethanol mediator. Figure 5C shows two sets of experimental impedance data (dots) with simulation data (line), which will be discussed below.

When employing ferroceneacetonitrile as the electron shuttle (Figure 6A), a similar change in the cyclic voltammetry peak current is observed. However, the peak currents for oxidation (Figure 6A) appear lower compared to data in Figure 5A, with less cathodic current observed on the reverse scan. Table 2 summarizes some data for voltammetric features (and impedance data, vide infra) observed for the different ferrocene derivatives in experiments at KolliphorEL-modified glassy-carbon electrodes. The reversible potential for $Fe(CN)_6^{4-/3-}$ here is 0.19 V versus SCE, and it can be seen that for all ferrocene derivatives a higher E_0 (consistent with less driving force for reduction) makes the amplification process asymmetric with less driving force for the cathodic signal. The magnitude of the anodic peak signal is also likely to be correlated to the peak-to-peak separation ΔE_p (indicative of slower electron transfer kinetics; Table 2). Therefore, the lower mediated oxidation peaks for ferroceneacetonitrile (Figure 6) and for ferroceneacetic acid (Figure 7), compared to other ferrocene derivatives, are likely to be linked here primarily to the slower kinetics of electron transfer (consistent with a wider peak-to-peak separation) limiting the electron shuttle rate.

Next, ferroceneacetic acid is employed as the electron shuttle (Figure 7), and similar trends are observed. However, the suppression of the oxidation peaks is more pronounced. On the basis of data in Table 2, very similar behavior for ferroceneacetonitrile and ferroceneacetic acid could be predicted, but

DOI: 10.1021/acsami.5b03654
ACS Appl. Mater. Interfaces 2015, 7, 15458−15465

Table 2. Summary of Data from Voltammetry and Impedance Spectroscopy[a]

	E_0 (V vs SCE)[b]	ΔE_p (V)[b]	[Fc] (μM)	R_{sol} (Ω)	R_{et} (Ω)	W_R (kΩ)[c]	W_T (s)[c]	CPE_T (μF)	CPE_P	δ_{app} (μm)
ferrocenedimethanol	0.28	0.11	1	127	9177	524	38.9	2.84	0.796	153
			10	134	5073	268	5.16	2.78	0.798	56
ferroceneacetonitrile	0.21	0.22	1	137	2958	690	82.5	2.39	0.816	222
			10	150	5332	635	67.3	2.30	0.835	201
ferroceneacetic acid	0.20	0.22	1	123	7815	1720	393	2.32	0.843	486
			10	132	6063	89	11.8	2.58	0.832	84
(dimethylaminomethyl)ferrocene	0.27	0.10	1	135	6180	123	2.82	4.01	0.795	41
			10	138	3092	335	19.0	2.69	0.838	107
n-butyl ferrocene	0.22	0.04	1	130	6557	139	8.14	1.82	0.789	70
			10	127	1117	127	222	3.94	0.743	365

[a]Solution with 50 μM ferrocene derivative, 5 mM $Fe(CN)_6^{3-}$ and 5 mM $Fe(CN)_6^{4-}$, in 0.1 M KNO_3 (scan rate = 50 mV s^{-1}). Impedance data relate to a Randles circuit (see text) with $W_P = 0.5$ and $\delta_{app} = (W_T \times D)^{1/2}$, with $D = 0.6 \times 10^{-9}$ m^2 s^{-1} as an approximate value[25] used for all ferrocene derivatives. [b]Obtained from cyclic voltammograms of 50 μM solution of ferrocene derivative in 0.1 M KNO_3 at a KolliphorEL-modified glassy-carbon electrode. Note that signals in particular for ferroceneacetonitrile, (dimethylaminomethyl)ferrocene, and *n*-butyl ferrocene are complicated by the interaction with the electrode surface [c]A short Warburg element was selected to reflect the electron transfer to $Fe(CN)_6^{3-/4-}$

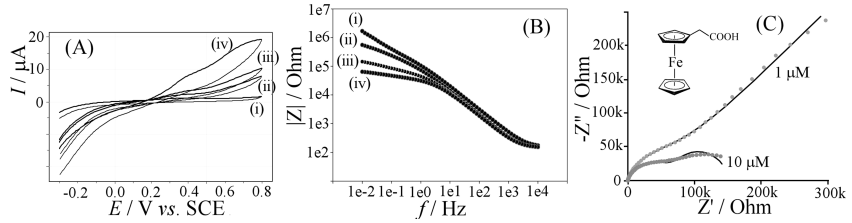

Figure 7. (A) Cyclic voltammograms (scan rate = 50 mV s^{-1}) for a 3 mm glassy-carbon electrode immersed in aqueous 5 mM $Fe(CN)_6^{3-}$, 5 mM $Fe(CN)_6^{4-}$, and 0.1 M KNO_3 with addition of (i) 0, (ii) 5, (iii) 10, and (iv) 50 μM ferroceneacetic acid. (B) Impedance data for this system at equilibrium potential. (C) Nyquist plot with simulation model data (line) and experimental data (dots) for 1 and 10 μM ferroceneacetic acid.

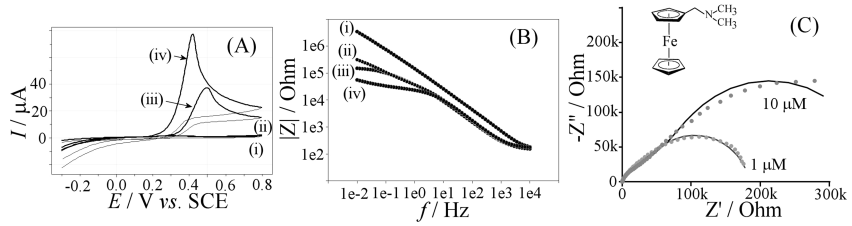

Figure 8. (A) Cyclic voltammograms (scan rate = 50 mV s^{-1}) for a 3 mm glassy-carbon electrode immersed in aqueous 5 mM $Fe(CN)_6^{3-}$, 5 mM $Fe(CN)_6^{4-}$, and 0.1 M KNO_3 with addition of (i) 0, (ii) 5, (iii) 10, and (iv) 50 μM (dimethylaminomethyl)ferrocene. (B) Impedance data for this system at equilibrium potential. (C) Nyquist plot with simulation model data (line) and experimental data (dots) for 1 and 10 μM dimethylamino-methyl-ferrocene.

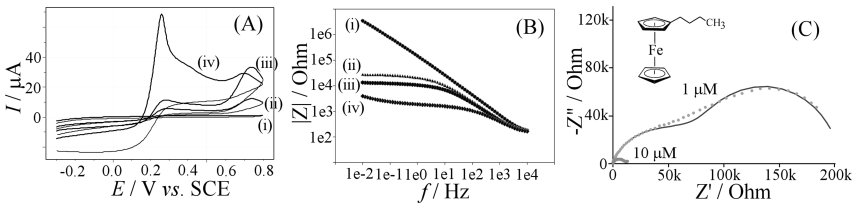

Figure 9. (A) Cyclic voltammograms (scan rate = 50 mV s^{-1}) for a 3 mm glassy-carbon electrode immersed in aqueous 5 mM $Fe(CN)_6^{3-}$, 5 mM $Fe(CN)_6^{4-}$, and 0.1 M KNO_3 with addition of (i) 0, (ii) 5, (iii) 10, and (iv) 50 μM butyl ferrocene. (B) Impedance data for this system at equilibrium potential. (C) Nyquist plot with simulation model data (line) and experimental data (dots) for 1 and 10 μM butyl ferrocene.

DOI: 10.1021/acsami.5b03654
ACS Appl. Mater. Interfaces 2015, 7, 15458−15465

additional electrostatic repulsion (at neutral pH) of the negatively charged ferrocene-acetate and the $Fe(CN)_6^{3-/4-}$ redox system is likely to limit further the electron shuttle efficiency. The impedance at the equilibrium potential shows very similar features compared to the data for ferrocene-acetonitrile, with somewhat lower impedance for higher ferrocene mediator concentration.

The (dimethylaminomethyl)ferrocene electron shuttle (Figure 8) is positively charged in neutral aqueous solution with possible implication on reactivity. Voltammetric responses shown in in Figure 8A are consistent with redox mediator activity but with an additional shift in the response and a high peak current at 50 μM (dimethylaminomethyl)ferrocene concentration. Voltammetric data in Table 2 suggest that (dimethylaminomethyl)ferrocene should be similar in reactivity when compared to ferrocene dimethanol; therefore, the additional anodic current (and the unusually sharp peak shape) may be associated with additional complexity, e.g., favorable interaction with the modified surface or between cationic (dimethylaminomethyl)ferrocene and $Fe(CN)_6^{3-/4-}$ at the electrode surface.

Finally, butyl ferrocene is employed as electron shuttle (Figure 9), and similar trends are observed. The solubility of butyl ferrocene in the aqueous phase is low, and at 50 μM nominal concentration, additional anodic activity is clearly seen in Figure 9A (a sharp peak), caused by aggregation at the electrode surface. It is likely that at lower butyl ferrocene concentration accumulation of the more lipophilic redox probe into the KolliphorEL film occurs to further aid the electron shuttle process.

On the basis of the qualitative comparison of electron shuttle efficiency, it appears likely that improved mediator effects are linked to (i) ferrocene derivatives with higher rate of electron transfer across the KolliphorEL layer and (ii) ferrocene derivatives with the ability to bind or aggregate at the KolliphorEL surface. A more detailed investigation of the underlying mechanism is presented next.

3.3. KolliphorEL Grafting Affecting Heterogeneous Electron-Transfer Kinetics: Mechanism. The equivalent circuit describing the electron shuttle mechanism reasonably closely is shown in Figure 10. The solution resistance R_{sol} and

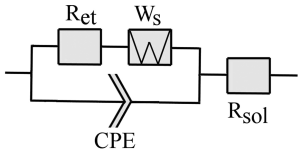

Figure 10. Schematic drawing of the equivalent circuit associated with the modified electrode in contact to the solution.

the resistance for heterogeneous electron transfer to the ferrocene derivative R_{et} are complemented with a "short" Warburg impedance to represent, at least at first approximation, the $Fe(CN)_6^{3-/4-}$ redox system feeding electrons into the layer, and a constant phase element (CPE) is employed to cope with nonideal capacitive behavior (caused by pores and heterogeneity at the surface). The short Warburg impedance is acceptable as a description of the mechanism here as long as the concentration of $Fe(CN)_6^{3-/4-}$ is not perturbed, thereby resulting in additional diffusion contributions. This condition is valid only for low ferrocene concentrations, and it seems to give reliable results only for (dimethylaminomethyl)ferrocene and butyl ferrocene (vide infra).

Data summarized in Table 2 describe the results from quantitative impedance data fitting (Figures 5C−9C). It can be observed that the R_{sol} value changes insignificantly, and capacitance C also remains similar to the value observed for the bare glassy-carbon electrode. R_{et} appears to be in the kilo-ohm range, without a clear trend attributable to the structure of ferrocene derivatives. An interesting parameter is W_T, which for the short Warburg element, is linked to the apparent diffusion layer thickness $\delta_{app} = (W_T \times D)^{1/2}$ (with $D = 0.6 \times 10^{-9}$ m^2 s^{-1} here estimated for the ferrocene derivatives[20]). When inspecting the apparent diffusion layer thickness δ_{app}, it is obvious that all values from 41 to 486 μm are considerably greater than the thickness of the KolliphorEL film grafted onto the electrode. Therefore, diffusion of ferrocene and ferricenium may occur well within the solution phase (Figure 2). Some of the δ_{app} values are considerable, which suggests that another type of physical process (such as slow bimolecular electron transfer or an additional heterogeneous electron transfer) could be hidden within the data. It is also interesting that although the first three ferrocene derivatives show a decrease in δ_{app} with higher mediator concentration (dimethylaminomethyl)-ferrocene and butyl ferrocene show an increase in δ_{app} with ferrocene concentration. The increase is expected when considering a stronger perturbation of the $Fe(CN)_6^{3-/4-}$ concentration; however, the decrease again suggests another type of physical process underlying the overall process. These trends are also observed in the corresponding data for 5 and 50 μM ferrocene mediator (not shown).

For the three more-soluble ferrocenes (ferrocene dimethanol > ferroceneacetonitrile > ferroceneacetic acid), a clear trend of lower δ_{app} for more efficient electron shuttling is seen (see for comparison voltammetry data). The most effective electron shuttle here appears to be (dimethylaminomethyl)ferrocene with the smallest diffusion length δ = 41 μm at 1 μM concentration. It is likely that this is linked to some binding of the electron shuttle to the KolliphorEL film and an indication that in future for this type of ferrocene even lower mediator concentrations are effective.

Finally, the effect of the $Fe(CN)_6^{3-/4-}$ redox system in the aqueous phase is assessed. Figure 11A shows data for a KolliphorEL-modified electrode immersed in solutions of 5, 10, 20, and 50 mM each of $Fe(CN)_6^{3-}$ and $Fe(CN)_6^{4-}$. The increase in the rate of electron transfer provides evidence for the first-order nature of the heterogeneous electron transfer. Impedance data in Figure 11B further demonstrate this effect. Finally, in the presence of 50 μM butyl ferrocene electron shuttle, an increase in the current response and change in peak shape are seen (Figure 11C), consistent with the voltammetric responses at high mediator concentration being (i) first-order in $Fe(CN)_6^{3-/4-}$ and (ii) now in part $Fe(CN)_6^{3-/4-}$ diffusion-controlled.

4. CONCLUSIONS

KolliphorEL has been shown to form monolayer films on glassy carbon when an anodic grafting protocol is applied. Given the ability of KolliphorEL to carry guest species, it is shown here for the first time that guest ferrocene derivatives can be employed to transport electrons across the KolliphorEL monolayer. For a range of ferrocene electron shuttle systems, a comparison and kinetics analysis were conducted and shuttle efficiencies evaluated. For all systems, the anodic process

DOI: 10.1021/acsami.5b03654
ACS Appl. Mater. Interfaces 2015, 7, 15458−15465

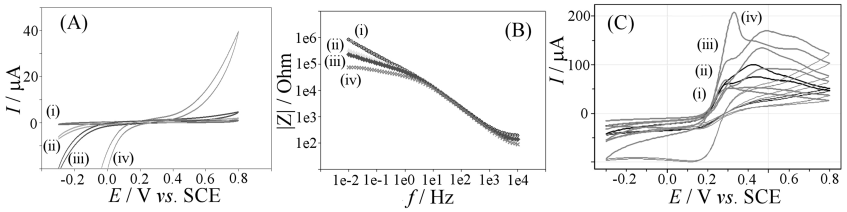

Figure 11. (A) Cyclic voltammograms (scan rate = 50 mV s^{-1}) for a 3 mm glassy-carbon electrode immersed in aqueous (i) 5, (ii) 10, (iii) 20, and (iv) 50 mM $Fe(CN)_6^{3-}$ and $Fe(CN)_6^{4-}$ in 0.1 M KNO_3. (B) Impedance data for the same system at equilibrium potential. (C) Cyclic voltammograms in the presence of 50 μM butyl ferrocene and with varying $Fe(CN)_6^{3-/4-}$ concentration.

appears to be considerably faster compared to the cathodic process (causing apparent irreversibility), in line with ferrocenes generally being oxidized at more positive potentials compared to $Fe(CN)_6^{3-/4-}$. The key parameters affecting the electron shuttle effect are (i) binding or aggregation ability predominantly on the basis of hydrophobicity and (ii) ability to penetrate the KolliphorEL film with faster heterogeneous electron transfer. At low concentration especially, butylferrocene and (dimethylaminomethyl)ferrocene are highly effective.

In future, a wider range of electron shuttle systems could be evaluated in particular with the aim of detecting very low concentrations of redox-active molecules (drugs, biomarkers, pollutants, etc.). It will be interesting to explore lower concentrations and more hydrophobic mediator systems.

AUTHOR INFORMATION

Corresponding Author

*E-mail: f.marken@bath.ac.uk.

Notes

The authors declare no competing financial interest.

ACKNOWLEDGMENTS

C.E.H. thanks the University of Bath for a Ph.D. scholarship. K.N. thanks LUT for financial support.

REFERENCES

(1) Mandler, D.; Kraus-Ophir, S. Self-assembled Monolayers (SAMs) for Electrochemical Sensing. *J. Solid State Electrochem.* **2011**, *15* (7−8), 1535−1558.

(2) Liu, J. Q.; Liu, Z.; Barrow, C. J.; Yang, W. R. Molecularly Engineered Graphene Surfaces for Sensing Applications: A review. *Anal. Chim. Acta* **2015**, *859*, 1−19.

(3) Ates, M.; Sarac, A. S. Conducting Polymer Coated Carbon Surfaces and Biosensor Applications. *Prog. Org. Coat.* **2009**, *66* (4), 337−358.

(4) Murray, R. W. Chemically Modified Electrodes. *Acc. Chem. Res.* **1980**, *13* (5), 135−141.

(5) Gooding, J. J. Advances in Interfacial Design Sensors: Aryl Diazonium Salts for Electrochemical Biosensors and for Modifying Carbon and Metal Electrodes. *Electroanalysis* **2008**, *20* (6), 573−582.

(6) Allongue, P.; Delamar, M.; Desbat, B.; Fagebaume, O.; Hitmi, R.; Pinson, J.; Saveant, J. M. Covalent Modification of Carbon Surfaces by Aryl Radicals Generated from the Electrochemical Reduction of Diazonium Salts. *J. Am. Chem. Soc.* **1997**, *119* (1), 201−207.

(7) Decreau, R. A.; Collman, J. P.; Hosseini, A. Electrochemical Applications. How Click Chemistry Brought Biomimetic Models to the Next Level: Electrocatalysis under Controlled Rate of Electron Transfer. *Chem. Soc. Rev.* **2010**, *39* (4), 1291−1301.

(8) Abiman, P.; Wildgoose, G. G.; Crossley, A.; Jones, J. H.; Compton, R. G. Contrasting pKa of Protonated Bis(3-aminopropyl)-terminated Polyethylene Glycol "Jeffamine" and the Associated Thermodynamic Parameters in Solution and Covalently Attached to Graphite Surfaces. *Chem. - Eur. J.* **2007**, *13* (34), 9663−9667.

(9) Chow, E.; Gooding, J. J. Peptide Modified Electrodes as Electrochemical Metal Ion Sensors. *Electroanalysis* **2006**, *18* (15), 1437−1448.

(10) Belanger, D.; Pinson, J. Electrografting: a Powerful Method for Surface Modification. *Chem. Soc. Rev.* **2011**, *40* (7), 3995−4048.

(11) Maeda, H.; Saka-iri, Y.; Ogasawara, T.; Huang, C. Z.; Yamauchi, Y.; Ohmori, H. Anodization in Oligo(ethylene glycol) as an Initial Derivatization Tool for Preparing glassy-carbon electrodes Covalently Modified with Amino Compounds: Effective Access to a 2,2,6,6-Tetramethylpiperidinyl-1- oxyl (TEMPO)-Modified glassy-carbon electrode. *Chem. Pharm. Bull.* **2001**, *49* (10), 1349−1351.

(12) Maeda, H.; Itami, M.; Katayama, K.; Yamauchi, Y.; Ohmori, H. Anodization of glassy-carbon electrodes in Oligomers of Ethylene Glycol And their Monomethyl Ethers as a Tool for the Elimination of Protein Adsorption. *Anal. Sci.* **1997**, *13* (5), 721−727.

(13) Maeda, H.; Kitano, T.; Huang, C. Z.; Katayama, K.; Yamauchi, Y.; Ohmori, H. Effective Method for the Covalent Introduction of the 2-(2- Carboxymethoxyethoxy)ethoxy Group on a glassy-carbon electrode by Anodization in Triethylene Glycol. *Anal. Sci.* **1999**, *15* (6), 531−536.

(14) Hotchen, C. E.; Maybury, I. J.; Nelson, G. W.; Foord, J. S.; Holdway, P.; Marken, F. Amplified Electron Transfer at Poly-Ethylene-Glycol (PEG) Grafted Electrodes. *Phys. Chem. Chem. Phys.* **2015**, *17*, 11260−11268.

(15) Maeda, H.; Yamauchi, Y.; Hosoe, M.; Li, T. X.; Yamaguchi, E.; Kasamatsu, M.; Ohmori, H. Direct Covalent Modification of Glassy Carbon Surfaces with 1-Alkanols by Electrochemical Oxidation. *Chem. Pharm. Bull.* **1994**, *42* (9), 1870−1873.

(16) Gelderblom, H.; Verweij, J.; Nooter, K.; Sparreboom, A. Chremophor EL: the Drawbacks and Advantages of Vehicle Selection for Drug Formulation. *Eur. J. Cancer* **2001**, *37* (13), 1590−1598.

(17) Ishihara, H. Current Status and Prospects of Polyethyleneglycol-Modified Medicines. *Biol. Pharm. Bull.* **2013**, *36* (6), 883−888.

(18) Barnes, E. O.; Lewis, G. E. M.; Dale, S. E. C.; Marken, F.; Compton, R. G. Generator-Collector Double Electrode Systems: A review. *Analyst* **2012**, *137* (5), 1068−1081.

(19) Wang, X. Y.; Pang, G. C. Amplification Systems of Weak Interaction Biosensors: Applications and Prospects. *Sens. Rev.* **2015**, *35* (1), 30−42.

(20) Si, Y. M.; Sun, Z. Z.; Zhang, N.; Qi, W.; Li, S. Y.; Chen, L. J.; Wang, H. Ultrasensitive Electroanalysis of Low-Level Free microRNAs in Blood by Maximum Signal Amplification of Catalytic Silver Deposition using Alkaline Phosphatase-Incorporated Gold Nanoclusters. *Anal. Chem.* **2014**, *86* (20), 10406−10414.

(21) (a) Wagner, C. D.; Davis, L. E.; Zeller, M. V.; Taylor, J. A.; Raymond, R. M.; Gale, L. H. *Surf. Interface Anal.* **1981**, *3*, 211. (b) Wagner, C. D. Appendix 6. In *Practical Surface Analysis*, 2nd ed.; Briggs, D., Seah, M. P., Eds.; J. Wiley and Sons: New York, 1990; Vol. *1*.

(22) Ferro, S.; Dal Colle, M.; De Battisti, A. Chemical Surface Characterization of Electrochemically and Thermally Oxidized Boron-Doped Diamond Film Electrodes. *Carbon* **2005**, *43* (6), 1191−1203.

DOI: 10.1021/acsami.5b03654
ACS Appl. Mater. Interfaces 2015, 7, 15458−15465

(23) Schlapak, R.; Caruana, D.; Armitage, D.; Howorka, S. Semipermeable Poly(ethyleneglycol) Films: the Relationship Between Permeability and Molecular Structure of Polymer Chains. *Soft Matter* **2009**, *5*, 4104−4112.
(24) Xiong, L. H. J.; Batchelor-McAuley, C.; Ward, K. R.; Downing, C.; Hartshorne, R. S.; Lawrence, N. S.; Compton, R. G. Voltammetry at Graphite Electrodes: The Oxidation of Hexacyanoferrate (II) (Ferrocyanide) does not Exhibit Pure Outer-Sphere Electron Transfer Kinetics and is Sensitive to Pre- Exposure of the Electrode to Organic Solvents. *J. Electroanal. Chem.* **2011**, *661* (1), 144−149.
(25) French, R. W.; Collins, A. M.; Marken, F. Growth and Application of Paired Gold Electrode Junctions: Evidence for Nitrosonium Phosphate During Nitric Oxide Oxidation. *Electroanalysis* **2008**, *20* (22), 2403−2409.

DOI: 10.1021/acsami.5b03654
ACS Appl. Mater. Interfaces 2015, 7, 15458−15465

Publication II

Nekoueian, K., Amiri, M., Sillanpää, M.

Carbon paste electrode with Au/Pd/MWCNT nanocomposite for nanomolar determination of Timolol

Reprinted with permission from
International Journal of Electrochemical Science
Vol. 12, PP.1612-1624, 2017
© 2017 ESG

Int. J. Electrochem. Sci., 12 **(2017)** 1612 – 1624, doi: 10.20064/2017.02.56

International Journal of
ELECTROCHEMICAL
SCIENCE
www.electrochemsci.org

Carbon Paste Electrode with Au/Pd/MWCNT Nanocomposite for Nanomolar Determination of Timolol

Khadijeh Nekoueian[1,*], *Mandana Amiri*[2], *Mika Sillanpää*[1]

[1] Laboratory of Green Chemistry, Faculty of Technology, Lappeenranta University of Technology, Sammonkatu 12, FI-50130 Mikkeli, Finland
[2] Department of Chemistry, University of Mohaghegh Ardabili, Ardabil, Iran
[*]E-mail: kh.nekoueian@gmail.com

Received: 25 October 2016 / *Accepted:* 22 December 2016 / *Published:* 30 December 2016

Fabrication of Au/Pd/MWCNT nanocomposite was performed by using chemical method. The nanocomposite was characterized by scanning electron microscopy (SEM), energy-dispersive X-Ray spectroscopy (EDS) and electrochemical methods. Palladium and gold nanoparticles were dispersed in multi-walled carbon nanotubes (MWCNT). The Au/Pd/MWCNT nanocomposite was applied as a modifier in carbon paste electrode for electro-oxidation of timolol. This modified electrode displayed high efficiency for sub-micromolar determination of timolol maleate. The effect of pH of the buffered solutions and potential sweep rate on the response of the electrode for the oxidation of timolol were investigated. Differential pulse voltammetry was used for quantitative determination. Dynamic linear ranges were obtained in the two ranges of 1.0×10^{-5} - 1.0×10^{-3} M and 5.0×10^{-9}- 8.0×10^{-7} M and the detection limit was estimated to be 5.8×10^{-11} M. The practical utility of this modified electrode was investigated by detecting timolol maleate in pharmaceutical sample (eye drop) and synthetic serum.

Keywords: Timolol maleate, Pd nanoparticles, Au nanoparticles, Multi-walled carbon nanotubes, Voltammetric sensor

1. INTRODUCTION

Timolol maleate (TM), (S)-1-[(1, 1-dimethyl) amino]-3[4-(-morpholinyl9-1, 2, 5-thiadiazol-3-yl) oxy]-2-propanol is a non-specific beta-adrenergic blocking drug which applied to treat high blood pressure, angina (heart pain), heart attacks and migraine headaches [1]. TM (scheme. 1, TM) was the first β-blocker that has been used as an antglaucoma agent. Investigating TM concentrations in ophthalmologic solutions, tablets and urine is an important issue which required sensitive methods. In recent literature, various analytical techniques have been applied for detection of TM such as liquid

chromatography [3, 4], high performance liquid chromatography [5], high performance thin layer chromatography [6], and spectroscopic methods [7-10]. However, most of these methods are time consuming, reagent consuming, expensive and need skillful operators. Compare to these techniques, electrochemical methods are cheaper, simpler and faster [11-14]. A few electrochemical methods for determination of TM have been reported [2, 11- 14] which most of them are based on reduction of TM. Unfortunately, some of these methods used the toxic and expensive mercury electrodes for TM detection [12, 13]. Carbon paste electrodes (CPEs) have been applied as an adaptable working electrode. Easy modifiability of CPEs, which improve electrode efficiently, made them efficient working electrodes for detecting various analytes [15].

Carbon nanotubes (CNTs), due to their outstanding mechanical, electrical, chemical properties, thermal stability and high aspect ratio have been applied in sensors [16, 17]. The CNTs material have other benefits over supporting material such as having more defined crystalline structure with high conductivity, eliminating potential poisoning effects to electrocatalysts due to containing little impurities and having three dimensional structure thus favoring the flow of reactant and preparing a large reaction zone when applied into electrodes [18]. Multi-walled carbon nanotubes (MWCNT) can be used as highly conducting support dispersion of metal nanoparticles due to their large surface area and morphology [19, 20]. In addition, MWCNT can be applied to improve electron transfer reactions. The decoration of MWCNTs with metal NPs has been introduced in new fields of possible applications especially as modifier in CPEs [18-22].

Metal nanoparticles (NPs) have been attracted lots of interest due to their unique physical, optical, electronic, catalytic and magnetic properties [13, 14, 23, 24]. NPs improve the redox process significantly, which is the reason of their vast applications at sensors and biosensors [23, 24]. Among the metal NPs, gold and palladium NPs have been applied widely in various field of technology [24-32].

AuNPs have a vast application in the field of electronics, catalysis and biosensors and due to their large aspect ratio; biocompatibility and high electrical conductivity have been widely employed as modifiers [24, 25]. On the other hand, palladium is an important noble metal NP due to its better stability and well understood physicochemical properties [26] and it has been applied widely in catalytic applications including hydrogenations [27, 28] oxidations [29, 30] and electrochemical reactions [31, 32]. Gold and palladium NPs mixture shows an interestingly high activity toward useful chemical reaction [33-37]. Catalytic activity of metal NPs can be significantly affected by the applied substrate [38-42].

In this work, Au/Pd/MWCNT nanocomposite has been prepared and characterized. By profiting from excellent electrocatalytic properties of combination of MWCNT and Au/Pd NPs, an efficient modifier was prepared to fabricate a modified CPE to detect and study electrocatalytic oxidation of TM in real samples.

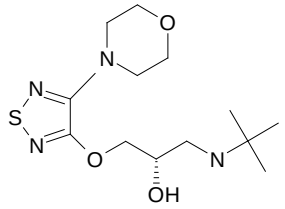

Scheme 1. The structure of TM.

2. EXPERIMENTAL

2.1 Chemicals and reagents

Multi-walled carbon nanotube synthesized by catalytic chemical vapor deposition (CVD, purity N 95%) with outer diameter (o.d.) of 10 – 20 nm, inner diameter (i.d.) of 5 –10 nm and tube length of 0.5 –200 nm was obtained from Nanostructured & Amorphous Materials (Houston, TX, USA), H_2PdCl_4 and $HAuCl_4$, were purchased from Sigma Aldrich, timolol (purity >99.5%) was provided from U.S. Pharmacopeial Convention (USP). All other chemical were analytical reagent grade from Merck. All aqueous solutions were prepared with doubly distilled deionized water. Britton–Robinson (B–R) (0.04 M) buffer solutions of pH 2.0–9.0 (CH_3COOH + H_3BO_3 + H_3PO_4) were used as the supporting electrolyte. The pH was adjusted using 0.2 M NaOH. Voltammetric experiments were carried out in the buffered solutions, which were deoxygenated by purging the pure nitrogen. Deionized and ultra-pure water were taken from a Millipore water purification system.

2.2 Apparatus

All Voltammetric experiments were performed using potentiostate/galvanostate Autolab model PGSTAT12/30/302. A conventional three-electrode system was used for all electrochemical experiments with a CPE as working electrode, a KCl-saturated calomel reference electrode (SCE) and a platinum wire as the counter electrode. A digital pH/mV/Ion meter (Inolab WTW series) was employed for preparing buffer solutions. The scanning electron microscope (SEM) images were obtained applying Hitachi S-4800 Ultra-High Resolution coupled with energy dispersive X-ray spectroscopy (EDS) (S4800).

2.3 Procedure I: Multi-walled carbon nanotube materials pretreatment

Different purification methods have been applied to remove the probable amorphous carbons and metallic impurities, and to improve the electron transfer properties and allow further functionalization [43]. According to one of the suggested methods in literature, 500 mg of the prepared

MWCNT was heated in an oven at 400 °C in nitrogen atmosphere for 2 h. To eliminate metal oxide catalysts, the heated processed amount MWCNT was dispersed in 50 mL of 6.0 M HCl for 2 h under ultrasonic agitation and under the nitrogen atmosphere then filtered on a Watman 42 filter paper and washed with doubled distilled water until the pH of the solution became neutral; and finally, dried [44].

2.4 Procedure II: Preparation of Au/Pd/MWCNT nanocomposite

Pd/MWCNT nanocomposite and Au/Pd/MWCNT nanocomposite were synthesized chemically with a same way by using literature methods [47, 48]. 20 mg of treated MWCNT was dispersed in 20 mL ethanol/water (1:1, v/v ratio) in a beaker to form a uniform suspension for 5 min. Then the suspension was mixed with 10 mL of 5.0×10^{-3} M of H_2PdCl_4 and 5.0×10^{-3} M of $HAuCl_4$,and stirred for 12 h. A fresh 50 mg $NaBH_4$ in 10 mL deaerated ultra-pure water was added drop wise into the solution under vigorous stirring. After stirring for 2 h a black solid was centrifuged and washed with ultra-pure water several times and dried in oven at 60 ˚C for 6 h.

2.5 Procedure III: Preparation unmodified of modified carbon paste electrodes

After optimization of the ratio of graphite powder to binder, unmodified carbon paste electrode UCPE was prepared by thoroughly hand mixing the graphite powder and paraffin oil in a ratio 75:25 (w/w) in an agate mortar, using a pestle and then homogenized by dissolving in dichloromethane. The mixture was stirred until all the solvent evaporated. A portion of the resulting homogeneous paste was packed into the cave of the Teflon tube (ca. 2.5 mm i.d.). A copper wire was fixed to a graphite rod and inserted into the Teflon tube served to establish electrical contact with the external circuit.

The multi-walled carbon nanotubes modified carbon paste electrode (MWCPE) was prepared by mixing 75% (w/w) MWCNTs and graphite powder (MWCNT: graphite powder 5:95 %) with 25% (w/w) paraffin oil. The modified composite was then air dried for 24 h and used in the same way as the UCPE.

The modified carbon paste electrode with Pd/MWCNT and Au/MWCNT nanocomposite (Pd/MWCPE and Au/MWCPE) was prepared in the same manner by mixing 75% (w/w) Pd/MWCNT nanocomposite and graphite powder (Pd/MWCNT: graphite powder 5:95 %) with 25% (w/w) paraffin oil. The modified composite was then air dried for 24 h and used in the same way as the UCPE.

The modified carbon paste electrode with Au/Pd/MWCNT nanocomposite (MCPE) was prepared in the same manner by mixing 75% (w/w) Au/Pd/MWCNT nanocomposite and graphite powder (Au/Pd/MWCNT: graphite powder 5:95 %) with 25% (w/w) paraffin oil. The modified composite was then air dried for 24 h and used in the same way as the UCPE. The amount of Au/Pd/MWCNT nanocomposite (in different percentages of 3%, 5%, 10%, and 15%) was optimized.

3. RESULTS AND DISCUSSION

3.1. Characterization of the MCPE

3.1.1 SEM study of Au/Pd/MWCNT nanocomposite

The SEM images of the Au/MWCNT nanocomposite, Pd/MWCNT nanocomposite, Au/Pd/MWCNT nanocomposite are illustrated in Fig. 1. MWCNTs are decorated with Au NPs with an average diameter of 18 nm (Fig 1A) and with Pd NPs with an average diameter of 45 nm (Fig. 1 B). The nanoparticles are well dispersed and embedded throughout the MWCNT matrix. Fig. 1C shows the morphology of Au/Pd/MWCNT nanocomposite. The presence of Au/PdNPs and MWCNT in the nanocomposite has been demonstrated in EDS results in (Fig. 1 D). The interconnected Au/Pd/MWCNT network may establish electrical conduction pathways throughout the whole composite, which is responsible for the electrical conductivity and electrochemical sensing [44].

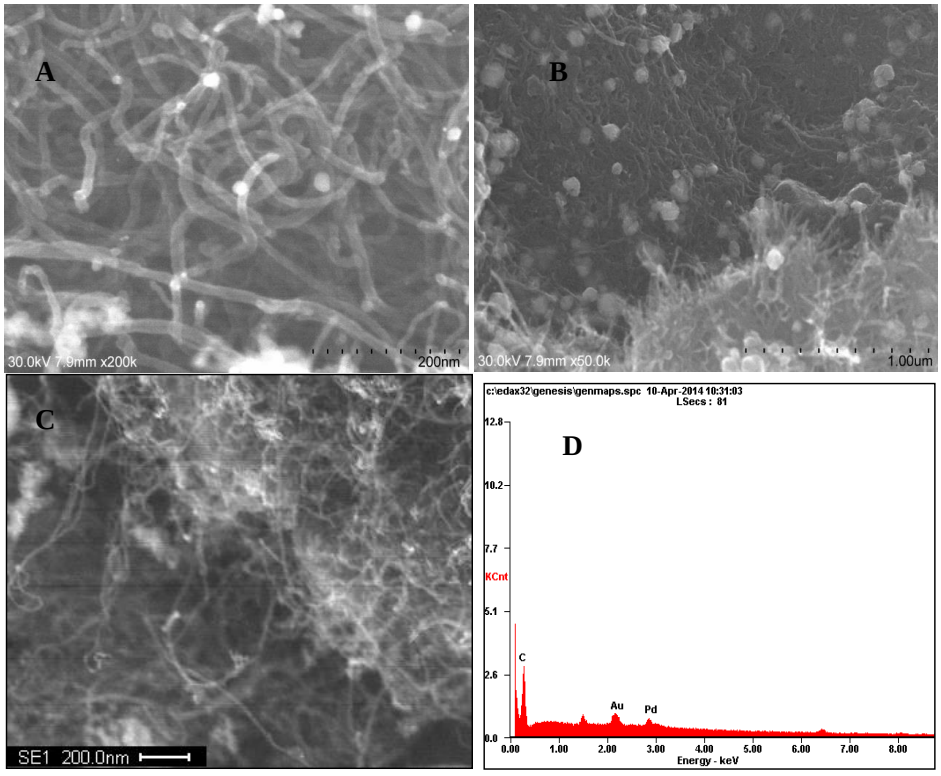

Figure 1. The SEM images of (A) the Au/ MWCNT nanocomposite, (B) Pd/ MWCNT nanocomposite, (C) Au/Pd/MWCNT nanocomposite and (D) corresponding EDS diagram showing peaks for Au/Pd NPs attached to MWCNT.

3.2 Electrocatalytic oxidation study of TM

Fig. 2 shows cyclic voltammograms of UCPE (dashed line) and MCPE (solid line) which were recorded in presence of 1.0×10^{-3} M of TM in B-R buffer solution of pH 2.0 (cyclic voltammograms for MWCPE, Au/MWCPE and Pd/MCPE have not been show to avoid complexity). At the UCPE, the electro-oxidation of TM occurs at approximately 1.038 V with peak current 14.81×10^{-6} A. By modification of CPE with MWCNT, Pd/MWCNT and Au/MWCPE the electro-oxidation of TM occurs at approximately 1.042, 1.040 and 1.040 V with peak current 22.1, 21.7 and 23.5 μA. Electro-oxidation of TM at the surface of MCPE presents an anodic wave with peak current 47.6 μA in a potential near 1.03 V (See Fig. 2) .The obtained results reveals the considerable impact of decoration of MWCNT with Au/PdNPs at promoting of peak current of TM electrooxidation which is due to the effective role of MWCNT as a conductive substrate to present high dispersion of NPs to improve effective surface area. As it can be seen, the peak current increases when PdNPs and Au NPs both exist in MWCNT matrix. It can be concluded, the presence of both NPs with each other shows synergic effect for electro-oxidation of TM.

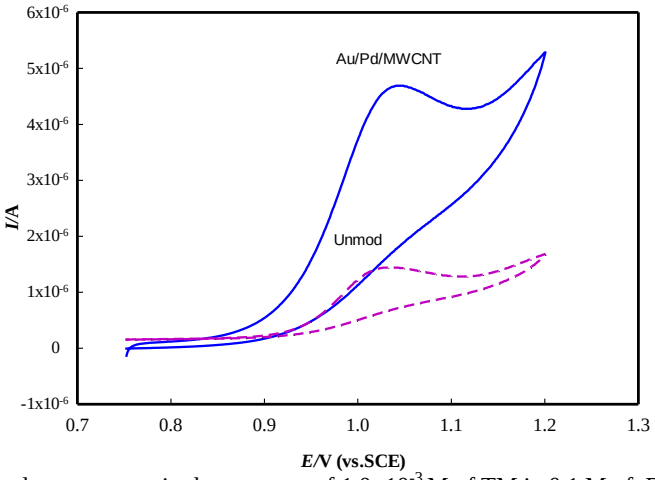

Figure 2. Cyclic voltammograms in the presence of 1.0×10^{-3} M of TM in 0.1 M of B-R buffer solution of pH 2.0 at the surface of UCPE (dashed line), and MCPE (solid line) and scan rate was 0.10 V s^{-1}.

3.2.1. The effect of pH on voltammetric response of TM

The effect of pH on the oxidation of TM was investigated by recording cyclic voltammograms for 1.0×10^{-3} M of TM in the pH range between 2.0 and 8.0at the surface of MCPE (See Fig. 3A). Finding the optimum pH for achieving higher response is important. The peak current decreased with the increasing pH to 3.0 dramatically and then it increased with increasing pH up to 6.0 and finally, the peak current decreased again.The maximum peak current value was observed at pH 2.0 so it was

selected for studying TM in this work (Fig. 3B). As can be seen in Fig. 3C, the anodic peak shifted to less positive values with the increase of pH which shows the pH dependency of oxidation potential of TM. This behavior of TM is in agreement with literature [14].

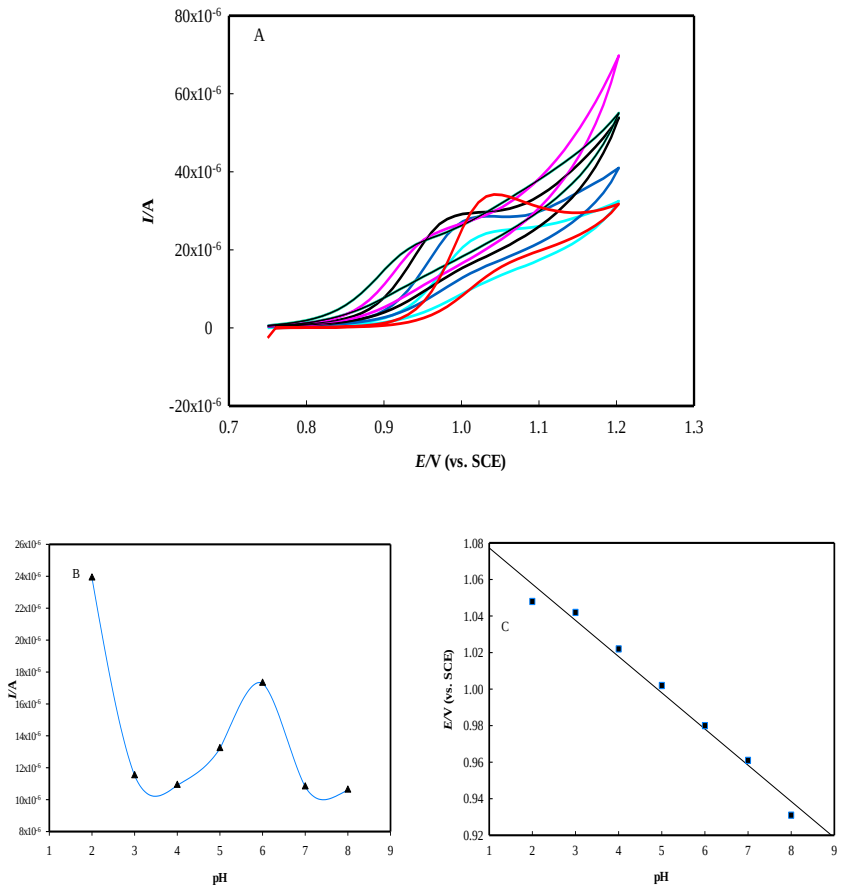

Figure 3. (A) Cyclic voltammograms of TM at the surface of MCPE in B-R buffer solutions pHs 2.0, 3.0, 4.0, 5.0, 6.0, 7.0 and 8.0. Scan rate was 0.10 V s^{-1}. (B) pH dependency of oxidation peak current of TM (C) pH dependency of oxidation potential of TM.

3.2.2 The effect of scan rate

The effect of scan rate on the peak current of TM was studied. Fig.4A exhibits the cyclic voltammograms of MCPE in 1.0×10^{-3} M of TM (pH 2.0 B-R buffer solution) at various scan rates in

the range of 0.01-0.20 Vs^{-1}. The results showed that the peak current (I_{pa}) varied linearly with the square root of scan rate ($v^{1/2}$) (Fig.4B) which suggesting that the electrooxidation of TM on the surface of MCPE followed a diffusion controlled mechanism in the studied range of potential sweep rates. The linear regression equation was obtained as following equation:

$$I_{pa}/A=0.0002\ \upsilon^{1/2}/(V\ s^{-1})^{1/2}+4.0\times10^{-5} \qquad (R^2=0.991) \qquad (1)$$

In addition, the dependence of ln I_p on ln υ is linear and obtained as ln I_p/A = 0.433 ln υ (Vs^{-1}) - 8.27; R^2=0.993 (Fig. 4C). Its slope is 0.433, which confirmed the diffusion control of the electron transfer process. A slope close to 0.5 is expected for a diffusion-controlled process [45].

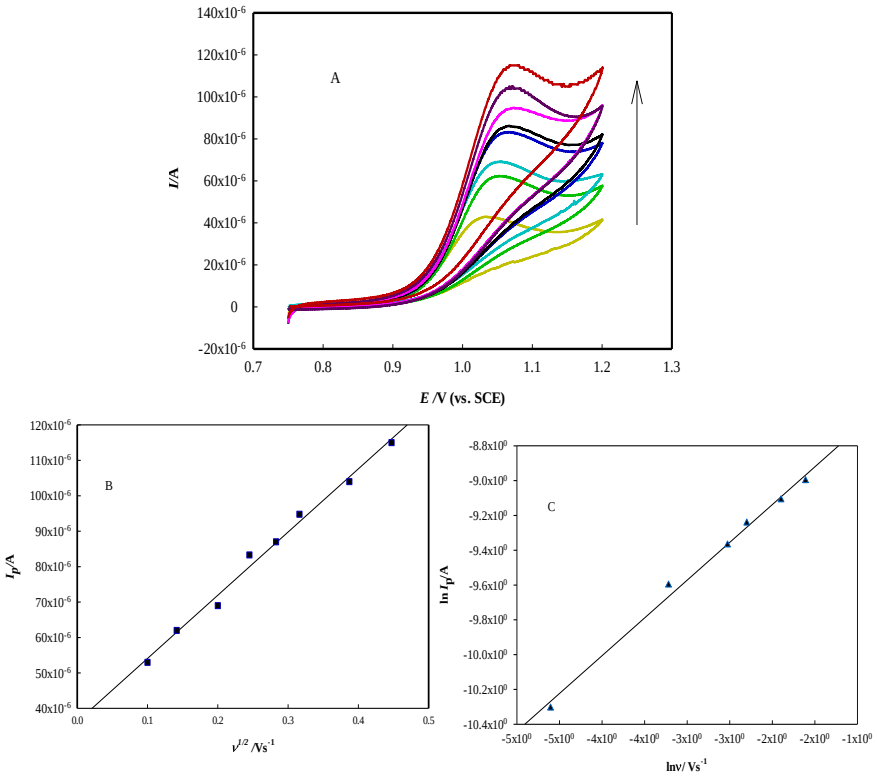

Figure 4. (A) Cyclic voltammograms of 1.0×10^{-3} M of TM at the surface of MCPE at different scan rates (down to top: 0.01, 0.02, 0.04, 0.06, 0.08, 0.10, 0.15 and 0.20 Vs^{-1}) in 0.1 M of B-R buffer solution of pH 2.0. (B) Variation of the electrocatalytic peak current with the square root of scan rate. (C) Variation of the electrocatalytic peak current with the neperian logarithm of scan rate of TM.

The Tafel plot and its corresponding slop were used to obtain the information on the rate determining step. Tafel plot was drawn using the data of rising part of current-voltage curve recorded at a scan rate of 0.2 Vs^{-1} (Fig 5). The slop of Tafel plot is equal to n (1-α) F/2.3RT [45]. In this

condition, the number of electron involved in the rate determining step can be calculated from the slop of Tafel plot which was obtained 9.19 Vdecade-^{1} (inset of Fig. 5) .The value of αn_a was obtained 0.54 indicating one electron transfer to be rate limiting (assuming α=0.5) in the electrocatalytic oxidation of TM.

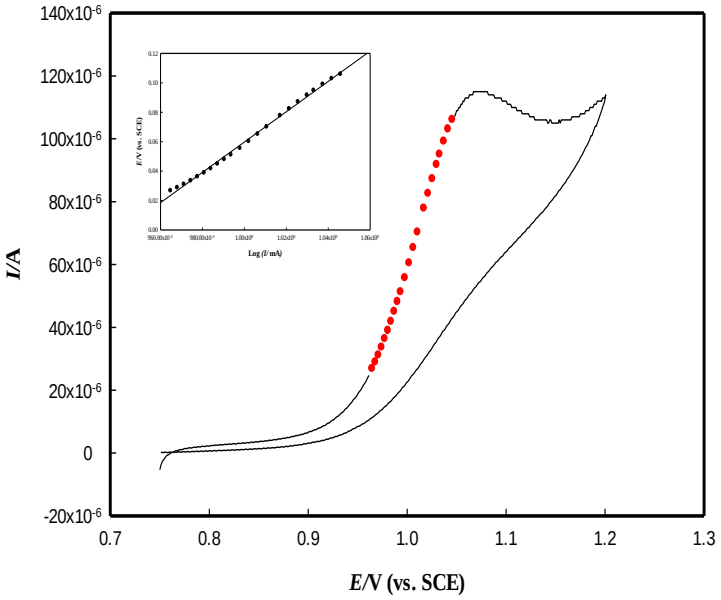

Figure 5. Tafel plot derived from rising part of voltammogram recorded at scan rate 0.20 Vs^{-1}in the presence of 1.0×10^{-3} M of TM in 0.1 M of B-R buffer solution of pH 2.0 at the surface of MCPE.

3.2.3 Analytical Results I.: Test Samples

Differential pulse voltammetry (DPV) was applied as a sensitive and reliable method with low limit of detection for measuring trace values of TM in 0.1 M of B-R buffer solution (pH 2.0). Figure 6A shows differential pulse voltammograms of various concentration of TM in the concentration range of 5.0×10^{-9} -1.0×10^{-3} M. The peak current of TM oxidation was increased by increasing the concentration. Two dynamic linear ranges were obtained in concentrations of 1.0×10^{-5} -1.0×10^{-3} M (Eq. 2, Fig 6B) and 5.0×10^{-9}-8.0×10^{-7} M (Eq. 3, Fig. 6C) and the detection limit was calculated to be 5.8×10^{-11} M. The following equations were obtained for the plot of peak current versus the TM concentrations:

I_{pa}/A = 11.3 ×10^{-6} + 0.0172 C_{TM} / M (R^2=0.994) (2)

I_{pa}/A = 2.83 ×10^{-7} + 7.896 C_{TM} / M (R^2=0.998) (3)

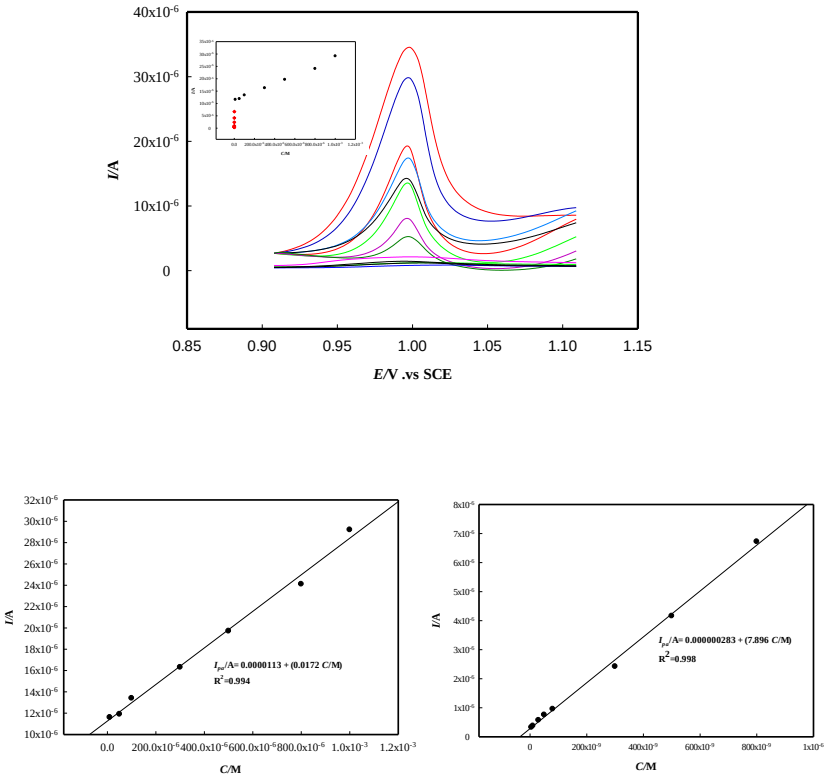

Figure 6. (A) Differential pulse voltammograms of MCPE in B-R buffer solution pH 2.0 containing different concentration of TM, from outer to inner correspond to 1.0×10^{-3}, 8.0×10^{-4}, 5.0×10^{-4}, 3.0×10^{-4}, 1.0×10^{-4}, 5.0×10^{-5}, 1.0×10^{-5}, 8.0×10^{-7}, 5.0×10^{-7}, 3.0×10^{-7}, 8.0×10^{-8}, 5.0×10^{-8}, 3.0×10^{-8}, 1.0×10^{-8}, 5.0×10^{-9} M (B) Variation of the electrocatalytic peak current with the TM concentration in two linear ranges of 1.0×10^{-3} -1.0×10^{-5} M and 8.0×10^{-7} -5.0×10^{-9} M (scan rate 0.10 Vs^{-1}; pulse amplitude 50 mV; step potential 5 mV; Modulation time = 25 mV).

Table 1 compares most electrochemical methods, which were previously used for the determination of TM. In the most of the cases, TM was measured by using adsorptive stripping voltammetry (ACSV) methods. In the presented work, CPE is used instead of mercury electrode which is toxic. In addition, CPE has many advantages compare with mercury electrode such as good reproducibility, stability, easy renewal and good compatibility with different modifiers such as metal NPs with high surface area and electrocatalytic properties have been used to improve the properties of CPE. Compared to other methods, the wider dynamic linear range and noticeable limit of detection were obtained at current work.

Table 1.Comparison of some electrochemical methods that previously used for the determination of TM

Method	**Electrode**	**DLR (M)**	**LOD (M)**	**Reference**
CCV- FI	Au microelectrode	1.0×10^{-10} -1.0×10^{-8}	1.0×10^{-11}	[2]
AdSV-SWP	HMDE	1.0×10^{-9} -1.2×10^{-8} and 1.2×10^{-8} -1.0×10^{-7}	6.6×10^{-10}	[12]
SWP	HMDE	4.0×10^{-8} -3.0×10^{-6}	2.5×10^{-8}	[12]
AdSV-SWP	HMDE	1.0×10^{-7}-1.5×10^{-6}	1.26×10^{-9}	[13]
DPV	SMDE	1.0×10^{-6}-5.0×10^{-6}	2.5×10^{-6}	[11]
DPV	nanoFe3O4 @GO-GC	2.0×10^{-7}-3.4×10^{-4}	2.0×10^{-8}	[14]
DPV	**Au/Pd/MWNT-CPE**	**1.0×10^{-3} -1.0×10^{-5} and 8.0×10^{-7} - 5.0×10^{-9}**	**5.8×10^{-11}**	**This work**

3.2.4 Analytical Results II: Real Samples

A standard addition method was applied for the determination of TM in the commercially available pharmaceutical sample (eye drop, containing 5.0 mg of TM in 1.0 ml) by using the DPV method. The content of drop samples was diluted with B-R buffer solution of pH 2.0 to prepare an aliquot equal to 1.26×10^{-3} M. The slope of the calibration curve, which is obtained by the spiked standard solutions of TM in the range of 1.0×10^{-3} to 1.0×10^{-5} M, was 0.0175 A/ M with a correlation coefficient of R^2=0.990. According to standard addition plot and comparing two slops of standards and spiked drug samples, a recovery of 98.83% was obtained which indicates the efficiency of the modified electrode for the determination of TM in presence of the matrix of drug sample. Recovery test of TM was carried out by spiking of TM in synthetic serum. The serum sample was spiked with different amount of TM. Recovery has been found to be 104.6 %.

3.3 Reproducibility of sensor preparation

The reproducibility of electrode (by preparing four electrodes with the same method at different days and measuring their peak current) was investigated in the presence of 1.0×10^{-5} M of TM in B-R buffer solution pH 2.0 and potential scan rate 0.01 V s^{-1}. The relative standard deviation based on the average of five measurements per MCPE was 2.95%. The repeatability of the peak current of MCPE

was evaluated with repeating voltammetric measurement ten times with the same MCPE in a 1.0×10^{-5} M of TM solution. The relative standard deviation based on ten measurements was 2.15%.

The electrode response has retained 91.3% of its initial peak current after remaining the MCPE at room conditions for two weeks. These results show good reproducibility and repeatability and long-term stability of the modified electrode in these experiments.

4. CONCLUSION

In this work, the modified CPE with MWCNT which was decorated with Au/Pd NPs applied for preparing a sensitive electrode for detecting submicromolar concentration of TM. The electrooxidation of TM was studied using presented modified electrode for the first time. Satisfactory results of MCPE for determination of TM in pharmaceutical sample, good repeatability and accuracy of results reveal the potential of this presented sensor. In addition, this sensor can be prepared easily and it is stable for a long period.

ACKNOWLEDGEMENTS
K.N. thanks LUT for financial support.

References

1. A. Marley, D. *J*. Connolly, *Chromatogr*. A., 1325 (2014) 213– 220.
2. P. Norouzi, M. R. Ganjali, A. Sepehri, M. Ghorbani, *Sens. Actuators. B*., 110 (2005) 239–245.
3. R. D. Marini, P. Chiap, B. Boulanger, W. Dewe, P. Hubert, *J. Sep. Sci***.,** 26 (**2003**) 809–817.
4. R. D. Marini, N. Matthijs, Y. Vander -Heyden, J. Smeyers-Verbeke, P. Dehouck, J. Hoogmartens, P. Silvestre, A. Ceccato, Ph. Goedert, J. Saevels, C. Herbots, G. Caliaro, R. Herr´aez Hern´andez, J. Verd´u-Andr`es, P. Camp´ıns-falc´o , W. Van de Wauwh, J. De Beer, B. Boulanger, P. Chiap, J. Crommenj, Ph. Hubert, *Anal. Chim. Acta*., 546 (2005) 182–192.
5. F. Nasira, Iqbal, Z.; A. Khan, L. Ahmad, Y. Shah, A. Z. Khan, J. A. Khan, S. *J*. Khan, *Chromatogr. B.*, 879 (2011) 3434–3443.
6. S. P. Kulkarni, P. D. Amin, *J. Pharm. Biomed. Anal*., 23 (2000) 983–987.
7. M. C. F. Ferraro, P. M. Castellano, T. S. Kaufman, *J. Pharm. Biomed.* Anal., 34 (2004) 305–314.
8. N. Erk, *J. Pharm. Biomed. Anal*., 28 (2002) 391–397.
9. L. I. Bebawy, *J. Pharm. Biomed. Anal*., 27 (2002) 737–746.
10. M. Hanna, C.A. Lau-Cam, *J. Pharm. Biomed. Anal*., 13 (1995) 1313-1319.
11. M. H. Türkdemir, G. Erdögdu, T. Aydemir, A. A. Karagözler, A. E. Karagözler, *J. Anal. Chem*., 56 (2001) 1196-1200.
12. A. Arranz, I. Dolara, S. F. de Betono, J. M. Moreda, A. Cid, J. F. Arranz, *Anal. Chim. Acta.*, 389 (1999) 225-232.
13. A.F. Al-Ghamdi, Am. *J. Anal. Chem*., 2 (2011) 174-181.
14. M. Hasanzadeh, M. H. Pournaghi-Azar, N. Shadjou, A. Jouyban, *RSC Adv*., 4 (2014) 51734-51744.
15. I. Svancara, K. Vytras, K. Kalcher, A. Walcarius, *J*. Wang, *Electroanal*., 21 (2009) 7 – 28.
16. Y. Zheng,, L. Ye, L.Yan, Y. Gao, *Int. J. Electrochem. Sci.*, 9 (2014) 238-248.
17. A. Afkhami, T. Madrakian, A. Shirzadmehr, M. Tabatabaee, H. Bagheri, *Sens. Actuator B-Chem.*, 174 (2012) 237-244.
18. R. Andrews, D. Jacques, D. Qian, T. Rantell, *Acc. Chem. Res*., 35 (2002) 1008–1017.

19. J. Wang, G. Yin, H. Liu, R. Li, R. L. Flemming, X. Sun, *J. Power Sources*, 194 (2009) 668–673.
20. G. G. Wildgoose, C. E. Banks, R. G Compton, *Small*, 2(2006) 182–193.
21. H. Beitollahi, A. Mohadesi, S. Khalilzadeh Mahani, H. Karimi-Maleh, A. Akbari, *Turkish Journal of Chemistry*, 36 (2012) 526-536.
22. S. Shahrokhian, M. Ghalkhani, M. Adeli, M. K. Amini, *Biosens. Bioelectron.*, 24 (2009) 3235-3241.
23. S. Shahrokhian, S. Rastgar, *Analyst*, 137 (2012) 2706-15.
24. L. Rassaei, F. Marken, M. Sillanpää, M. Amiri, C. M. Cirtiu, M. Sillanpää, *Trends Anal. Chem*., 30 (2011) 1704–1715.
25. C. Zhou, S. Li, W. Zhu, H. Pang, H. Ma, *Electrochim. Acta*, 113 (2013) 454– 463
26. Y. W. Lee, M. J. Kim, Z. H. Kim, S. W. Han, *J. Am. Chem. Soc*., 131 (2009) 17036–17037
27. D. Ferrer, A. Torres-Castro, X. Gao, S. Sepulveda-Guzma, U. Ortiz-Mendez, M. Jose-Yacama, *Nano Lett*., 7 (2007) 1701–1705.
28. R. Harpeness, A. Gedanken, *Langmuir*., 20, (2004) 3431–3434.
29. L. Kuai, X. Yu, S. Z. Wang, Y. Sang, B. Y. Geng, *Langmuir*, 28 (2012) 7168–7173.
30. J. W. Hong, D. Kim, Lee, Y. W. Kim, M. Kang, S. W. Han, *Angew. Chem*.,123 (2011) 9038–9042.
31. A.M. Prasad, A. N. Santhosh, *Appl. Nanosci*., 2 (2012) 457-466.
32. E. Baldrich, R. Gomez, G. Gabriel, F. X. Munoz, *Biosens. Bioelectron*., 26 (2011) 1876–1882.
33. J. Qu, Y. Shen, X. Qu, S. Dong, *Chem. Commun*., 1 (2004) 34–35.
34. Z. Hai, N. E. Kolli, J. Chen, H. Remita, *New J. Chem*., 38 (2014) 5279–5286
35. Ü.Yilmaz, H. Kucukbay, S. Turktekin Celikesir, M.Akkurt, O. Buyukgungor, *Turkish Journal of Chemistry*, 37(2013) 721-733.
36. T. Madrakian, E. Haghshenas, Afghani, *Sens. Actuator B-Chem.*, 193 (2014) 451– 460.
37. S. Shahrokhian, R. Salimian, S. Rastgar, *Mater. Sci. Eng. C.*, 34 (2014) 318–325.
38. P. C. Pandey, A. K. Pandey, D. S. Chauhan, *Electrochim. Acta*, 17(2012) 23–31.
39. J. B. Xu, T. S. Zhao, Y. S. Li, W. W. Yang, *Int. J. Hydrogen Energy*, 35, (2010) 9693-9700.
40. J. Nelayah, N. T. Nguyen, D. Alloyeau, G. Y. Wang, C. Ricolleau, *Nanoscale*, 6 (2014)10423-10430.
41. A. Felten, J. Ghijsen, J. J. Pireaux, W. Drube, R. L. Johnson, D. Liang, M. Hecq, G. Van-Tendeloo, C. Bittencourt, *Micron*, 40 (2009) 74–79.
42. L. Jiang, L. Gao, *Carbon*, 41 (2003) 2923–2929.
43. N. S. Lee, D. S. Chung, I. T. Han, J. H. Kang, Y. S. Choi, H. Y. Kim, S. H. Park, Y. W. Jin, W.K. Yi, M. J. Yun, J. E. Jung, C. J. Lee, J. H. You, S. H. Jo, C. G. Lee, J. M. Kim, *Diamond Relat. Mater*., 10 (2001) 265–270.
44. X. M. Liu, Z. Huang, D. S. W. Oh, B. Zhang, P. C. Ma, M. M. F. Yuen, J. K. Kim, *Compos. Sci. Technol.*, 72 (2012) 121-144.
45. A. J. Bard, L. R. Faulkner, Electrochemical methods: fundamentals and applications; 2nd ed, Wiley: New York, 2001.

© 2017 The Authors. Published by ESG (www.electrochemsci.org). This article is an open access article distributed under the terms and conditions of the Creative Commons Attribution license (http://creativecommons.org/licenses/by/4.0/).

Publication III

Sefid-sefidehkhan[1], Y., Nekoueian[1], K., Amiri, M., Sillanpää, M., Eskandari, H.

Palladium nanoparticles in electrochemical sensing of trace terazosin in human serum and pharmaceutical preparations

Reprinted with permission from
Materials Science and Engineering
Vol. 75 pp. 368–374
© 2017 Elsevier B.V.

Materials Science and Engineering C 75 (2017) 368–374

Contents lists available at ScienceDirect

Materials Science and Engineering C

journal homepage: www.elsevier.com/locate/msec

Palladium nanoparticles in electrochemical sensing of trace terazosin in human serum and pharmaceutical preparations

Yasaman Sefid-sefidehkhan [a,1], Khadijeh Nekoueian [b,1], Mandana Amiri [a,*], Mika Sillanpaa [b], Habibollah Eskandari [a]

[a] Department of Chemistry, University of Mohaghegh Ardabili, Ardabil, Iran
[b] Laboratory of Green Chemistry, Faculty of Technology, Lappeenranta University of Technology, Sammonkatu 12, FI-50130 Mikkeli, Finland

ARTICLE INFO

Article history:
Received 2 July 2016
Received in revised form 23 November 2016
Accepted 14 February 2017
Available online 16 February 2017

Keywords:
Terazosin
Voltammetric sensor
Electrodeposition
Pd nanoparticles

ABSTRACT

In this approach, palladium nanoparticle film was simply fabricated on the surface of carbon paste electrode by electrochemical deposition method. The film was characterized using scanning electron microscopy, electrochemical impedance spectroscopy and cyclic voltammetry. The prepared electrode exhibited an excellent electrocatalytic activity toward detection of trace amounts of terazosin, which is an antihypertensive drug. Under the optimum experimental conditions, a linear range of 1.0×10^{-8}–1.0×10^{-3} mol L^{-1} with a detection limit of 1.9×10^{-9} mol L^{-1} was obtained for determination of terazosin using differential pulse voltammetry as a sensitive method. The efficiency of palladium nanoparticle film on the surface of carbon paste electrode successfully proved for determination of terazosin in pharmaceutical sample and human serum sample with promising recovery results. The effect of some foreign species has been studied.

© 2017 Elsevier B.V. All rights reserved.

1. Introduction

Terazosin (TR), RS-1-(4-amino-6,7-dimethoxy-2-quinazolinyl)-4-[(tetra-hydro-2-furanyl)carbonyl]- piperazine monohydrochloride (Scheme 1), is in a group of drugs called alpha-adrenergic blockers with a long lasting effect. TR is used to treat hypertension (high blood pressure), and to improve urination in men with benign prostatic hyperplasia (enlarged prostate) by relaxing the smooth muscles of the arteries, the prostate, and the bladder neck [1,2]. Applying an accurate, sensitive and reliable analytical method is essential to monitor the amount of TR in treated patients to adjust drug level and avoid toxic concentration of the medicine [1–3]. Several analytical techniques have been applied for the quantitative measurement of TR in pharmaceuticals or biological fluids such as spectrofluorimetry and spectrophotometry [4–10], direct high-performance liquid chromatography [11–13], mass spectrometry [14], potentiometry [15–17] and voltammetry [18,19].

In recent years, nanostructures have been employed to modify the electrochemical sensors significantly. Among the nanostructures, metal nanoparticles (NPs) have attracted tremendous interest due to their especial electronic, optical, magnetic, catalytic properties, promoting the redox processes and large specific surface area [20]. Palladium (Pd) is the most active noble metal which has interesting properties such as high heterogeneous catalysis and electrocatalysis activity, versatility, non-toxicity and relatively low cost [21]. Its application in the field of analytical electrochemistry is considerable. The Pd/single-wall carbon nanotubes thin film electrode showed strong electrocatalytic activity to produce a low detection limit for nitrite determination [21], electrochemical co-deposition of Pd and glucose oxidase enzymes on to nafion-solubilized carbon nanotube film applied as a glucose biosensor [22], palladium nanoparticles (PdNPs) decorated electrostatically functionalized multi-walled carbon nanotubes acted as a non-enzymatic glucose sensor [23]. In another report, PdNPs modified electrodes used for the selective detection and determination of catecholamines in presence of ascorbic acid [24]. Also, PdNPs loaded on carbon modified TiO_2 nanobelts applied for enhanced methanol electrooxidation [25]. The PdNPs-fullerene modified glassy carbon electrode was applied for methane sensing [26], electrodeposited PdNPs on a glassy carbon electrode can efficiently catalyze the reduction of m-nitrophenol [27], simultaneous electrochemical determination of dopamine, uric acid and ascorbic acid was offered by using Pd NPs-loaded carbon nanofibers modified electrode [28]. A simple, novel and reproducible method for the separation and simultaneous determination of entacapone, levodopa and carbidopa was achieved based on applying a methionine/PdNPs modified carbon paste electrode [29]. Recently, PdNPs deposited on porous graphitized carbon monolith modified carbon paste electrode for simultaneous determination of ascorbic acid and uric acid [30].

Over the past five decades, carbon paste has become one of the most popular electrode materials used for the laboratory preparation of various electrodes, sensors, and detectors. Such a position is undoubtedly the result of optimal constellation of physicochemical and

* Corresponding author.
E-mail address: mandanaamiri@uma.ac.ir (M. Amiri).
[1] Y. S and K. N. are first authors because they have the equal participation in this work.

http://dx.doi.org/10.1016/j.msec.2017.02.061
0928-4931/© 2017 Elsevier B.V. All rights reserved.

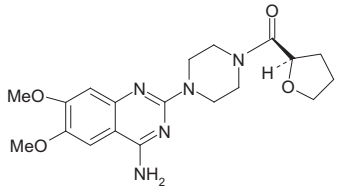

Scheme 1. Chemical structure of TR.

electrochemical properties of this carbon-like substrate, which soon obtained a high reputation among both theoretical and practical electrochemists, as well as elsewhere, beyond the boundary of electrochemical sciences [31]. Nowadays, the testing and seeking of the proper usage for modifier materials is one of the most significant trends in the electrochemistry with modified carbon pastes. The new forms of carbon (i.e., nanotubes, nanofibres, and fullerenes [32– 34]), nanoparticle materials and composites (e.g., nano-gold [35]), nano-sized electrocatalysts (Co (II)-phthalocyanine [36]), or magnetic core-shells [37], molecular wires/nanowires [38] and inorganic/organic hybrid materials (e.g., supramolecular helical chains [39]) have been applied as modifiers in carbon paste, recently.

Considering the essential need of monitoring TR trace amounts and high electrocatalytic ability of PdNPs, the PdNPs were electrochemically deposited at the surface of carbon paste electrode (CPE) using cyclic voltammetry. The electrode was characterized by using various methods. Finally, the fabricated electrode was employed as a sensitive sensor for determination of TR in pharmaceutical and clinical samples by using differential pulse voltammetry (DPV).

2. Experimental

2.1. Materials

Palladium (II) chloride ($PdCl_2$) was purchased from sigma-Aldrich, USA. TR reference was kindly provided by Arya pharmaceutical company (Tehran, Iran). Stock solutions of TR were freshly prepared in an appropriate buffer solution at the desired pH and protected from light during investigation. All reagents were purchased from Merck and were of analytical reagent grade. All aqueous solutions were prepared with doubly distilled deionized water.

2.2. Instruments

Voltammetric experiments and the electrodeposition of PdNPs were performed by using a Metrohm Computrace voltammetric analyzer model 797VA. A conventional three-electrode system was applied with a CPE (unmodified or modified) as working electrode, a KCl-saturated Calomel reference electrode and a Pt wire as the counter electrode. A digital pH/mV/Ion meter was used for preparation of the buffer solutions, which were used as the supporting electrolyte in the voltammetric experiments. The scanning electron microscope (SEM) images were obtained applying Hitachi S-4800 Ultra-High Resolution.

2.3. Modified electrode preparation

By mixing graphite powder with appropriate amount of mineral oil (Nujol) by using a mortar and pestle (75:25, w/w), the unmodified carbon paste electrode (UCPE) was prepared. A small portion of the composite mixture was packed into the end of a Teflon tube (about 3.0 mm i.d.). Electrical contact was made by forcing a copper pin down into the Teflon and into the back of the composite [40]. After fabrication UCPE, the surface of the electrode was polished and smoothed with clean paper and then at a plane glass surface to produce a flat surface and rinsed thoroughly with deionized water. The modified electrode (PdNPs/CPE) was obtained by cyclic voltammetric scanning from 1.20 to −0.250 V (vs. SCE) in a deaerated solution of 0.5 M H_2SO_4 containing 1.0 mM $PdCl_2$ at a scan rate of 100 mV s^{-1} for 10 cycles at the surface of UCPE. Then, the modified electrode was rinsed with doubly distilled deionized water, dried carefully and was finally applied for electrochemical studies [24]. The modified electrode was generated in each experiment with the same procedure.

3. Results and discussion

3.1. Characterization of PdNPs/CPE

3.1.1. Cyclic voltammetric studies

Fig. 1 shows the cyclic voltammograms (CV) of PdNPs during electrodeposition. The CVs show the characteristic current features of Pd reduction (at 0.29 V), Pd oxide formation (at 0.71 V) and hydrogen adsorption and desorption (0.1 to −0.1 V) process. On scanning the potential in negative direction, PdNPs are deposited on the electrode surface and the peak at −0.14 V shows the reduction process of protons to hydrogen, which are adsorbed by Pd. This reduction peak confirms the hydrogen adsorption process on the Pd surface. During the positive potential scanning process, the peak at −0.08 V appeared due to the oxidation of hydrogen atoms. In the next step, the deposited PdNPs are further oxidized to Pd^{2+} to form a Pd oxide layer (at 0.71 V) on the electrode surface. The formed Pd oxides are reduced on the negative scans, leading back to PdNPs with hydrogen adsorption process. During this repetitive cycling process, all the peaks are found growing which confirms the PdNPs deposition process on the UCPE. The expected reduction process of the $PdCl_4^{2-}$ complex to Pd is as follows [24];

$$PdCl_4^{2-} + 2e^- \rightarrow Pd + 4Cl^-$$

Fig.2 exhibits voltammetric behavior of UCPE (dotted line) and PdNPs/CPE (solid line) in phosphate buffer solution (0.1 M, pH 2.0). As can be seen, there is no voltammetric peak for UCPE in the buffer solution. However, a cathodic peak potential appears at 0.29 mV correspond to the Pd^{2+} reduction when PdNPs/CPE was immersed in the buffer solution. It can be resulted that PdNPs at the surface of CPE can be reduced. It proved the formation of PdNPs at the surface of CPE.

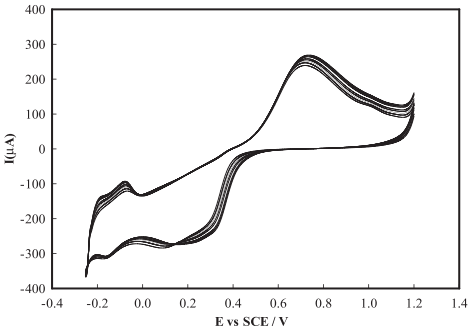

Fig. 1. Repeated CVs of electrodeposited PdNPs on CPE from 0.5 M H_2SO_4 containing K_2PdCl_4 (1×10^{-3} M) and potential scan between 1.2 and −0.25 V for 10 cycles (Scan rate of 100 mV s^{-1}).

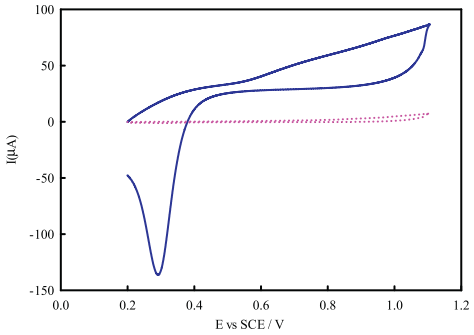

Fig. 2. SEM image of (A) UCPE and (B) PdNPs/CPE.

3.1.2. Morphological characterization of surface

To study the surface morphology of the modified carbon paste electrode, SEM has been utilized. Scanning electron micrographs (see Fig. 3A and B) show the surface of UCPE and PdNPs/CPE. As can be seen PdNPs have been formed at the surface of CPE. The estimated size of nanoparticles is 80–120 nm.

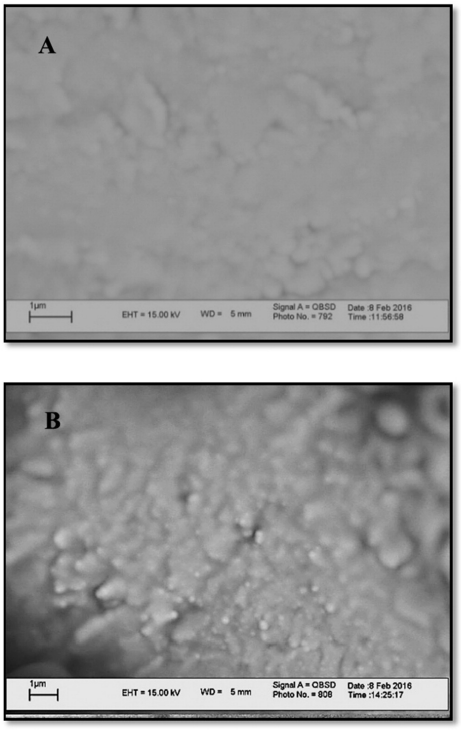

Fig. 3. CVs of PdNPs/CPE (solid line) and UCPE (dotted line) in phosphate buffer pH 2.0, the scan rate was 100 mV s^{-1}.

3.1.3. Electrochemical impedance spectroscopic study

Electrochemical impedance spectroscopy (EIS) was employed to investigate the impedance changes of the electrode surface, after the modification step with 5, 10, 20 cycles of PdNPs deposition. The Nyquist plots of the EIS of UCPE, CPE/PdNPs (5 cycles), CPE/PdNPs (10 cycles), and CPE/PdNPs (20 cycles), in 5.0 mM $K_4Fe(CN)_6/K_3Fe(CN)_6$ (1:1) containing 0.1 M KCl were obtained. Fig. 4a and b shows the Nyquist plots of $K_3Fe(CN)_6/K_4Fe(CN)_6$ at the UCPE and PdNPs/CPE (10 cycles). In these studies, high frequency zone, which appears as a nearly semicircle plot, can be ascribed to the kinetic limitations (R_{ct}) of the electrochemical reaction. On the other hand, the linear behavior of Z' versus Z'' in a low frequency region shows a diffusion-controlled electrode process in PdNPs/CPE. As can be seen in Fig. 4a, a semicircle with a very large diameter is observed at UCPE. However, the diameter of the semicircle is significantly reduced with PdNPs/CPE (See Fig. 4b), which suggests that the surface of the modified electrode exhibits lower electron transfer resistance (greatly increases the electron transfer rate). However, the diameter of the semicircle is decreased with the deposition of PdNPs at the surface of electrode from 5 to 10 cycles of deposition step. But with increasing the number of cycles to 20, the diameter increased. The R_{ct} values of the CPE/PdNPs (5 cycles), CPE/PdNPs (10 cycles), CPE/PdNPs (20 cycles) were calculated 519, 417 and 498 Ω, respectively. The results show with increasing the number of cycles to 20, charge transfer resistance increased which can be related to aggregation of PdNPs [41].

3.2. Electrochemical study of TR on the PdNPs/CPE, UCPE

The electrochemical behavior of 1.0 mM TR in 0.1 M phosphate buffer solution at pH 2.0 at the surface of bare CPE and PdNPs/CPE was studied by using CV (See Fig. 5). The electro-oxidation of TR on the surface of CPE was recorded, an oxidation peak appeared at 1.04 V with peak current of 72.2 μA. However, at the surface of PdNPs/CPE an enhanced peak current (121 μA) at a lower positive potential 0.98 V appeared. This accretion in the oxidation peak current of TR on the surface of PdNPs/CPE is attributed to the crucial role of PdNPs in development of specific surface area and increasing electron transfer rate on the surface of the modified electrode.

3.2.1. The effect of number of scanning cycles on the PdNPs electrodeposition and TR response

PdNPs were synthesized on the CPE surface by cyclic voltammetry method. The number of CV cycles was varied (5, 10 and 20 cycles) to prepare the CPE/PdNPs. Then, cyclic voltammetry experiments have been performed in solution of $K_4Fe(CN)_6$ 1 mM as probe in various

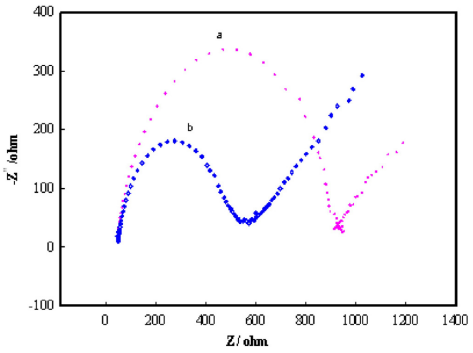

Fig. 4. Nyquist plot for (a) UCPE (b) PdNPs/CPE in KCl 0.1 M containing 5 mM [$K_3Fe(CN)_6$/$K_4Fe(CN)_6$]. at the formal Potential: 0.2 V, Frequency range: 0.1 Hz–10,000 Hz.

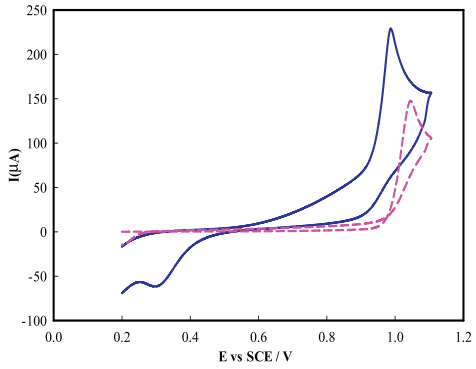

Fig. 5. CVs of 1.0 mM TR in 0.1 M phosphate buffer solution at pH 2.0 on the surface of CPE (dashed line) and PdNPs/CPE (solid line). The scan rate was 100 mV s^{-1}.

scan rates. The Randle-Sevick equation was applied to estimate the surface areas with different deposition cycles which leads to different amount of PdNPs. The surface areas were calculated 2.88, 7.20, 4.32 cm^2 for 5, 10 and 20 cycles of Pd deposition, respectively. Nevertheless the amount of Pd at the surface increased with increasing the number of cycles from 10 to 20 but the surface area decreased. It could be related to aggregation of Pd at the surface of electrode causes decreasing surface area [41]. These results confirm what obtained in Section 3.1.3.

The electrochemical response of 1 mM TR in 0.1 M phosphate buffer solution at pH 2.0 was investigated at the surface of CPE/PdNPs with various deposition cycles. The obtained results reveal that the maximum oxidation peak current was obtained in 10 scanning cycles. With increasing number of cycles from 5 to 10, the amount of PdNPs increased at the surface of electrode but after 10 cycles, it may the PdNPs will be aggregate at the surface of CPE when the number of deposition cycles increased. The aggregation cause to decrease surface area and then the oxidation peak current of TR would descend. The 10 cycles has been selected for further studies.

3.2.2. Effect of pH on the electrochemical response of TR

The impact of pH on the cyclic voltammetric responses of 1.0 mM TR was investigated in 0.1 M phosphate buffer solutions with different pHs (2, 3, 6 and 7), as well as 0.1 M acetate buffer solutions with pHs equal to 4 and 5 (Fig. 6a). The study of pH dependency of the oxidation peak potential indicated a negative shift for the anodic peak potential ($E_{p,a}$)with increasing pH of the buffer solution (See Fig. 6c). This electrochemical behavior suggested that protonation/deprotonation is taking part in the charge transfer process. The linear correlation between the anodic oxidation peak potential and pH is given by Eq. (1).

$$E_{p,a} = -0.031pH + 1.067 \qquad \left(R^2 = 0.993\right) \qquad (1)$$

It can be concluded the number of transferred electrons are two fold of protons.

The maximum oxidation current signal was obtained in pH 4.0 and the minimum in 7.0. Because the sharpest oxidation current signal with well-known shape was appeared at pH 2.0 (See Fig. 6b), the electrochemical measurements were examined at phosphate buffer solution with pH 2.0 in further studies.

3.2.3. Effect of potential scan rate

The cyclic voltammograms were recorded for 1.0 mM TR on the surface of the PdNPs/CPE in 0.1 M phosphate buffer solution with pH 2.0, at

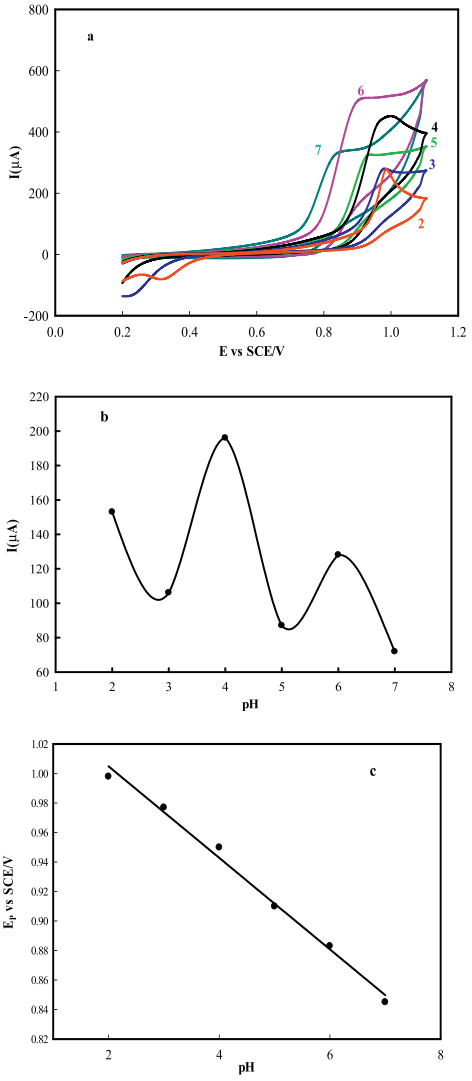

Fig. 6. (a) Cyclic voltammograms of 1.0 mM TR at PdNPs/CPE in various pHs (2,3, 4, 5, 6 and 7). The scan rate was 100 mV s^{-1}. (b) Plot of variation of anodic peak current and (c) anodic peak potential vs. pH.

different potential sweep rates (20 to 150 mV s^{-1}) (Fig. 7a). The oxidation peak current shows a linear relation to the square root of the scan rate (υ), with the following linear equation (Fig. 7b):

$$I_{pa}(\mu A) = 235.5\upsilon^{1/2}\left(Vs^{-1}\right)^{1/2} + 15.59 \qquad \left(R^2 = 0.994\right) \qquad (2)$$

The result indicated that the oxidation of TR on the surface of the PdNPs/CPE was followed by a diffusion-controlled mechanism.

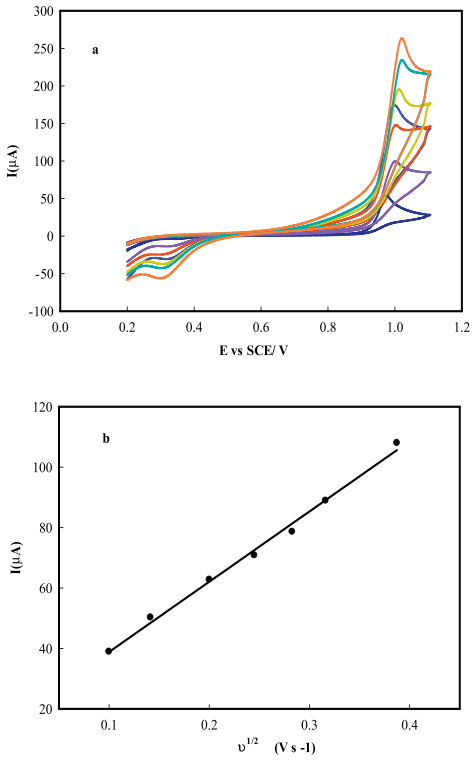

Fig. 7. (a) CVs of 1.0 mM TR in 0.1 M phosphate buffer solution with pH 2.0 on at PdNPs/CPE in various υ: 10, 20, 40, 60, 80, 100, 150, and 200 mV s^{-1}. (b) Oxidation peak current vs. υ.

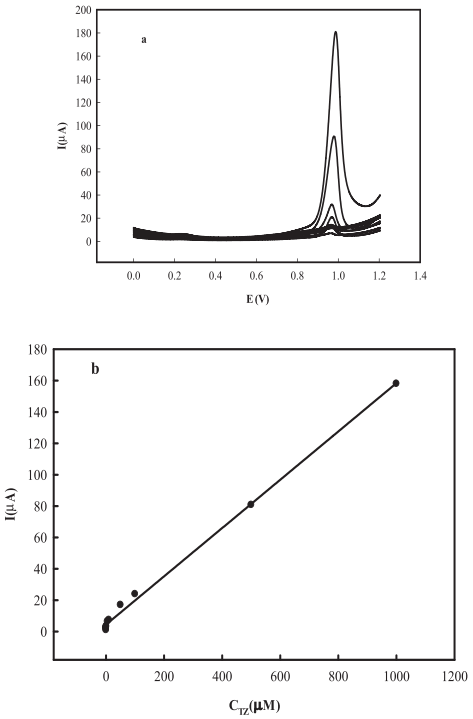

Fig. 8. (a) DPVs for the oxidation of TR in phosphate buffer solution 0.1 M. At pH 2.0 with the PdNPs/CPE (down to up:1.0×10^{-8} M, 5.0×10^{-8} M, 1.0×10^{-7} M, 5.0×10^{-7} M, 1.0×10^{-6} M, 5.0×10^{-6} M,1.0×10^{-5} M, 5.0×10^{-5} M, 1.0×10^{-4} M, 5.0×10^{-4} M and 1.0×10^{-3} M), (b) calibration curve.

3.3. Analytical measurements

3.3.1. Calibration curves

DPV was selected for as a highly sensitive and rapid electrochemical method for the determination of trace amounts of TR. DPV measurements were performed in 0.1 M phosphate buffer solution with pH 2.0 as supporting electrolyte (Fig. 8a). The calibration curve of peak current versus concentration of TR has been shown in Fig. 8b. It demonstrates a dynamic linear range of 1.0×10^{-8}–1.0×10^{-3} M with a slope of 0.153 A/M and a correlation coefficient (R^2) of 0.997. The detection limit for determination TR was obtained as 1.9×10^{-9} M (for S/N = 3) by using the optimum conditions.

$$I_p/\mu A = 4.4362 + (0.1539C) \qquad \left(R^2 = 0.9971, C \text{ is in } \mu M\right) \qquad (3)$$

Table 1 compares some of the electrochemical methods, which have been used to determine of TR with presented work. As can be seen, the presented method shows wider linear range and good detection limit.

The repeatability of the modified electrode was investigated for two concentration levels (high and low) of TR at pH 2.0 for five measurements. The relative standard deviations were 3.4% for 1.0×10^{-4} M and 7.4% for 5.0×10^{-7} M. In addition, the reproducibility of the electrode was examined; the RSD% for five electrodes was obtained which was less than 5.4%. The results elucidated a high efficiency of PdNPs/CPE for determination of TR.

3.3.2. Effects of foreign species

The influence of various species such as biological compounds (ascorbic acid, dopamine, uric acid) and pharmaceuticals, which recommended usually with TR (tamsulocin and ciprofloxacin) on the determination of TR was studied under the optimum conditions. The variations of signal in presence of all above compounds were less than 5%. It can be concluded that the PdNPs/CPE shows efficient capability to determination of TR in presence of foreign species.

3.3.3. Determination of TR in human serum

For investigating the applicability of the proposed route in the real sample analysis, PdNPs/CPE was used to determine TR in human serum. The standard addition method was applied and the recoveries in spiking of TR to human serum were monitored. The slope of the calibration curve, which was obtained with the spiked standard solutions of TR in the range of 1.0×10^{-8}–1.0×10^{-3} M, was 0.1512 μA/μM with a correlation coefficient of (R^2) 0.973. Compared with the calibration curve, 0.1539 μA/μM, a recovery of 98.24% was obtained. It reveals that this method is appropriate for accurate determination of TR in real and complex human serum samples. DPV and calibration curve have been shown in Supplementary data (S1).

Table 1
Comparison of some electrochemical methods which used for the determination of terazosin.

Electrode	Modifier	DLR (M)	LOD (M)	Method	Reference
Ion selective electrode	–	1.0×10^{-5}–1.0×10^{-2}	7.9×10^{-6}	Potentiometry	[17]
CPE	Gold NPs	5.4×10^{-9}–8.0×10^{-5}	1.2×10^{-10}	CV	[18]
Glassy carbon electrode	Surfactant	2.4×10^{-8}–4.0×10^{-6}	4.5×10^{-9}	DPV	[42]
Hanging mercury drop	–	1.0×10^{-8}–1.0×10^{-5}	1.5×10^{-11}	SWV	[19]
CPE	ZnO/rGO nanocomposite	1.0×10^{-8}–1.0×10^{-5}	2.0×10^{-9}	CV	[43]
CPE	PdNPs	1.0×10^{-8}–1.0×10^{-3}	1.9×10^{-9}	DPV	This work

3.3.4. Determination of TR in pharmaceutical preparation

A standard addition method was applied to investigate the applicability of PdNPs/CPE for the determination of the TR in a commercial tablet as a real sample. Three tablets samples of a TR sample (with labeled values of 2 mg TR per tablet) were powdered and an aliquot equal to 1×10^{-6} M of TR was prepared in 0.1 M phosphate buffer solution of pH 2.0. Then, a defined amount of the tablet sample was spiked with various concentrations of TR standard solution in the range of 1×10^{-8} to 1×10^{-3} M, diluted with 0.1 M phosphate buffer solution with pH 2.0 and mixed well. The slope of the calibration curve was obtained as 0.1525 μA/μM with a correlation coefficient of (R^2) 0.9916. By comparing the two slops of the standard and spiked drug sample, a recovery of 99.09% was calculated, that proved the tablet matrix did not make any considerable interference on the electrochemical determination of TR in presented method. DPV and calibration have been shown in Supplementary data (S2).

4. Conclusions

A new and reliable electrochemical sensor for determination of trace amounts of TR was presented in this study. Simple and inexpensive fabricated PdNPs/CPE demonstrated promising results for determination of TR such as good repeatability and sensitivity, low limit of detection and rapid response. All these advantages make it desirable to apply PdNPs/CPE in pharmaceutical and clinical industry.

Acknowledgements

M. A. and Y. S. gratefully acknowledge the support of this work by University of Mohaghegh Ardabili research council, (grant no. 534) Ardabil, Iran. K.N. thanks Lappeenranta University of Technology for financial support.

Appendix A. Supplementary data

Supplementary data to this article can be found online at http://dx.doi.org/10.1016/j.msec.2017.02.061.

References

[1] A. Shrivastava, V.B. Gupta, Various treatment options for benign prostatic hyperplasia: a current update, J. Midlife Health 3 (2012) 10–19.
[2] I.S. Shin, M.Y. Lee, H.K. Ha, C.S. Seo, H.K. Shin, Inhibitory effect of Yukmijihwangtang, a traditional herbal formula against testosterone-induced benign prostatic hyperplasia in rats, BMC Complement. Altern. Med. 12 (2012) 1472–6882.
[3] A. Shrivastava, Various analytical methods for the determination of terazosin in different matrices, World J. Anal. Chem. 1 (2013) 80–86.
[4] M. Zeeb, M. Sadeghi, Sensitive determination of terazosin in pharmaceutical formulations and biological samples by ionic-liquid microextraction prior to spectrofluorimetry, Int. J. Anal. Chem. 2012 (2012) 1–7.
[5] C.V.N. Prasad, A. Gautham, V. Bhardwaj, P. Praimoo, Quantitative determination of terazosin HCl in tablet preparation by fluorimetry, Indian J. Pharm. Sci. 60 (1998) 167–169.
[6] C.J. Jiang, M.X. Gao, J.X. He, Study of the interaction between terazosin and serum albumin synchronous fluorescence determination of terazosin, Anal. Chim. Acta 452 (2002) 185–189.
[7] C.C. Wang, M.O. Luconi, A.N. Masi, L. Fernandez, Determination of terazosin by cloud point extraction-fluorimetric combined methodology, Talanta 72 (2007) 1779–1785.
[8] N.A. Mohamed, S. Ahmed, S.A. El Zohny, A specific high-performance thin-layer chromatography with fluorescence detection for the determination of some α_1-blockers, J. Liq. Chromatogr. Relat. Technol. 38 (2015) 271–282.
[9] V. Sankar, S. Raghuraman, V. Sivanand, V. Ravichandran, Spectrophotometric method for the estimation of terazosin in tablets, Indian J. Pharm. Sci. 61 (2000) 463–464.
[10] H.H. Abdine, F.A. El-Yazbi, S.M. Blaih, R.A. Shaalan, Spectrophotometric and spectrofluorimetric methods for the determination of terazosin in dosage forms, Spectrosc. Lett.: Int. J. Rapid Commun. 31 (1998) 969–980.
[11] R. Ferretti, B. Gallinella, F.L. Torre, L. Zanitti, L. Turchetto, A. Mosca, R. Cirilli, Direct high-performance liquid chromatography enantioseparation of terazosin on an immobilised polysaccharide-based chiral stationary phase under polar organic and reversed-phase conditions, J. Chromatogr. A 1216 (2009) 5385–5390.
[12] J. Wang, Q. Li, L. Yang, Y. Zhang, J. Yu, X. Zhao, J. Zheng, Y. Zhang, X. Zheng, Binding interactions between prazosin and α-1Aadrenoceptor: investigation on the thermodynamic behaviors and the binding mechanism by high performance affinity chromatography, Anal. Methods 7 (2015) 3340–3346.
[13] V. Srivatsan, A.K. Dasgupta, P. Kale, R. Verma, P. Joshi, D.i Soni, M. Patel, G. Soni, J. Patel, H. Mod, Determination of mycophenolic acid in human plasma by high-performance liquid chromatography, J. Chromatogr. A 1031 (2004) 259–264.
[14] M.A. Zayed, M.A. Fahmey, M. El-Desawy, Y.S. Farrag, Structure characterization of terazosin drug using mass spectrometry and thermal analyses techniques in comparison with semi-empirical molecular orbital (MO) calculations, J. Therm. Anal. Calorim. 120 (2015) 1061–1069.
[15] K.G. Kumar, S. John, R. Poduval, Pearl Augustine, The electrochemical determination of terazosin in pure form and in dosage forms, Chin. Pharm. J. 1 (2005) 29–36.
[16] A.M. Badawey, A.E.B. Abd El-Aleem, N.T. Lamie, Membrane sensors for the selective determination of terazosin hydrochloride dihydrate in presence of its degradation product, Int. J. Comp. Pharm. 2 (2011) 1–5.
[17] M.R. Ganjali, F. Faridbod, B. Larijani, S. Riahi, M. Hosseini, E. Nasli-Esfahani, Terazosin potentiometric sensor for quantitative analysis of terazosin hydrochloride in pharmaceutical formulation based on computational study, Int. J. Electrochem. Sci. 5 (2010) 200–214.
[18] N.F. Atta, A. Galal, S.M. Azab, Gold nanoparticles modified electrode for the determination of an antihypertensive drug, Electroanalysis 24 (2012) 1431–1440.
[19] M.M. Ghoneim, M.A. El Ries, E. Hammam, A.M. Beltagi, A validated stripping voltammetric procedure for quantification of the anti-hypertensive and benign prostatic hyperplasia drug terazosin in tablets and human serum, Talanta 64 (2004) 703–710.
[20] S. Shahrokhian, R. Salimian, S. Rastgar, Pd–Au nanoparticle decorated carbon nanotube as a sensing layer on the surface of glassy carbon electrode for electrochemical determination of ceftazidime, Mater. Sci. Eng. C 34 (2014) 318–325.
[21] X.H. Pham, C.A. Li, K.N. Han, B.C. Huynh-Nguyen, T.H. Le, E. Ko, J.H. Kim, G.H. Seong, Electrochemical detection of nitrite using urchin-like palladium nanostructures on carbon nanotube thin film electrodes, Sensors Actuators B 193 (2014) 815–822.
[22] S.H. Lim, J. Weia, J. Lin, Q. Li, J.K. You, A glucose biosensor based on electrodeposition of palladium nanoparticles and glucose oxidase onto nafion-solubilized carbon nanotube electrode, Biosens. Bioelectron. 20 (2005) 2341–2346.
[23] B. Singh, N. Bhardwaj, V.K. Jain, V. Bhatia, Palladium nanoparticles decorated electrostatically functionalized MWCNTs as a non-enzymatic glucose sensor, Sensors Actuators A 220 (2014) 126–133.
[24] S. Thiagarajan, R.F. Yang, S.M. Chen, Palladium nanoparticles modified electrode for the selective detection of catecholamine neurotransmitters in presence of ascorbic acid, Bioelectrochemistry 75 (2009) 163–169.
[25] R. Liang, A. Hu, J. Persic, Y.N. Zhou, Palladium nanoparticles loaded on carbon modified TiO2 nanobelts for enhanced methanol electrooxidation, Nano-Micro Lett. 5 (2013) 202–212.
[26] Zh. Li, J. Zhang, Y. Zhou, S. Shuang, C. Dong, M.M.F. Choi, Electrodeposition of palladium nanoparticles on fullerene modified glassy carbon electrode for methane sensing, Electrochim. Acta 76 (2012) 288–291.
[27] H. Li, L. Han, J. Cooper-White, I. Kim, Palladium nanoparticles decorated carbon nanotubes: facile synthesis and their applications as highly efficient catalysts for the reduction of 4-nitrophenol, Green Chem. 14 (2012) 586–591.
[28] J. Huang, Y. Liua, H. Hou, T. You, Simultaneous electrochemical determination of dopamine, uric acid and ascorbic acid using palladium nanoparticle-loaded carbon nanofibers modified electrode, Biosens. Bioelectron. 24 (2008) 632–637.
[29] N.N. Salama, S.M. Azab, M.A. Mohamed, A.M. Fekry, A novel methionine/palladium nanoparticle modified carbon paste electrode for simultaneous determination of three antiparkinson drugs, RSC Adv. 5 (2015) 14187–14195.
[30] S. Mukdasai, U. Crowley, M. Pravda, X. He, E.P. Nesterenko, P.N. Nesterenko, B. Paull, S. Srijaranai, J.D. Glennon, E. Moore, Electrodeposition of palladium nanoparticles on porous graphitized carbon monolith modified carbon paste electrode for simultaneous enhanced determination of ascorbic acid and uric acid, Sensors Actuators B Chem. 218 (2015) 280–288.

[31] I. Svancara, K. Vytras, K. Kalcher, A. Walcarius, J. Wang, Carbon paste electrodes in facts, numbers, and notes: a review on the occasion of the 50-years jubilee of carbon paste in electrochemistry and electroanalysis, Electroanalysis 21 (2009) 7–28.
[32] G.A. Rivas, M.D. Rubianes, M.L. Pedano, N.F. Ferreyra, G.L. Luque, M.C. Rodriguez, S.A. Miscoria, Carbon nanotubes paste electrodes: a new alternative for the development of electrochemical sensors, Electroanalysis 19 (2007) 823–831.
[33] G. Shul, M.A. Murphy, G.D. Wilcox, F. Marken, M. Opallo, Effects of carbon nanofiber composites on electrode processes involving liquid vertical bar liquid ion transfer, J. Solid State Electrochem. 9 (2005) 874–881.
[34] A. Miranda Hernandez, M.E. Rincon, I. Gonzalez, Characterization of carbon–fullerene–silicone oil composite paste electrodes, Carbon 43 (2005) 1961–1967.
[35] D. Afzali, S. Zarei, F. Fathirad, A. Mostafavi, Gold nanoparticles modified carbon paste electrode for differential pulse voltammetric determination of eugenol, Mater. Sci. Eng. C 43 (2014) 97–101.
[36] R. Nascimento, T.M.G. Selva, W.F. Ribeiro, M.F. Belian, L. Angnes, V.B. Nascimento, Flow-injection electrochemical determination of citric acid using a cobalt(II)–phthalocyanine modified carbon paste electrode, Talanta 105 (2013) 354–359.
[37] M.H. Mashhadizadeh, H. Jeilanpour, Voltammetric investigation of Ketotifen using carbon paste electrode modified by magnetic core-shell Fe_3O_4@TMSPT nanoparticles, Anal. Bioanal. Electrochem. 6 (2014) 308–320.
[38] L. Liu, J. Song, Voltammetric determination of mefenamic acid at lanthanum hydroxide nanowires modified carbon paste electrodes, Anal. Biochem. 354 (2006) 22–27.
[39] Z. Han, Y. Zhao, J. Peng, Q. Liu, E. Wang, Inorganic/organic hybrid polyoxometalate containing supramolecular helical chains: Preparation, characterization and application in chemically bulk-modified electrode, Electrochim. Acta 51 (2005) 218–224.
[40] M. Amiri, A. Bezaatpour, Z. Pakdel, Kh. Nekoueian, Simultaneous voltammetric determination of uric acid and ascorbic acid using carbon paste/cobalt Schiff base composite electrode, Solid State Electron. 16 (2012) 2187–2195.
[41] T. Hezard, K. Fajerwerg, D. Evrard, V. Collière, P. Behra, P. Gros, Gold nanoparticles electrodeposited on glassy carbon using cyclic voltammetry: application to Hg(II) trace analysis, J. Electroanal. Chem. 664 (2012) 46–52.
[42] N.F. Atta, S.A. Darwish, S.E. Khalil, A. Galal, Effect of surfactants on the voltammetric response and determination of an antihypertensive drug, Talanta 72 (2007) 1438–1445.
[43] T. Madrakian, H. Ghasemi, A. Afkhami, Esmaeel Haghshenas, ZnO/rGO nanocomposite/carbon paste electrode for determination of terazosin in human serum samples, RSC Adv. 6 (2016) 2552–2558.

Publication IV

Nekoueian, K., Jafari, S., Amiri, M., Sillanpää, M.
Pre-adsorbed Methylene Blue at carbon-modified TiO_2 electrode: application for lead sensing in water

Reprinted with permission from
IEEE Sensors Journal
Vol.18 pp. 9477-9485, 2018
© 2018 IEEE

Pre-Adsorbed Methylene Blue at Carbon-Modified TiO_2 Electrode: Application for Lead Sensing in Water

Khadijeh Nekoueian, Shila Jafari, Mandana Amiri, and Mika Sillanpää

***Abstract*— Carbon modified titanium dioxide nanostructured (CMTN) was successfully fabricated by ethanol carbonization method and applied to modify the surface of glassy carbon electrode. This modified electrode was employed in the extraction and the electrochemical determination of methylene blue. The considerable increment in the voltammetric signal for pre-adsorbed methylene blue compared with those for solution, demonstrated a strong tendency of methylene blue to CMTN which was rooted in porous structure of CMTN and the electrostatic interaction between cationic methylene blue with negative surface of the CMTN. By applying differential pulse voltammetry, a calibration curve is obtained for methylene blue in the range of 1.0×10^{-8} to 1.0×10^{-5} M and the limit of detection was evaluated to be 3.0×10^{-9} M. In addition, the pre-adsorbed methylene blue on the surface of the modified electrode performed well in the determination of the trace amounts of lead in the real samples such as lake and tap water. Dynamic linear range for lead was investigated in the range of 1.0×10^{-7} to 5.0×10^{-4} M and the limit of detection was calculated to be 3.0×10^{-8} M.**

***Index Terms*— Lead, titanium compounds, nanocomposite, amperometric sensors, chemical analysis.**

Manuscript received February 24, 2018; revised September 12, 2018; accepted September 17, 2018. Date of publication September 20, 2018; date of current version November 13, 2018. The associate editor coordinating the review of this paper and approving it for publication was Prof. Venkat R. Bhethanabotla. *(Corresponding authors: Khadijeh Nekoueian; Mandana Amiri.)*

K. Nekoueian and S. Jafari are with the Laboratory of Green Chemistry, Faculty of Technology, Lappeenranta University of Technology, 50130 Lappeenranta, Finland (e-mail: kh.nekoueian@gmail.com).

M. Amiri is with the Department of Chemistry, University of Mohaghegh Ardabili, Ardabil 5619911367, Iran (e-mail: mandanaamiri@yahoo.com).

M. Sillanpää is with the Department of Civil and Environmental Engineering, Florida International University, Miami, FL 33174 USA (e-mail: mika.sillanpaa@lut.fi).

This paper has supplementary downloadable multimedia material available at http://ieeexplore.ieee.org provided by the authors. The Supplementary Material includes materials and Instruments Sections: S1. (A) Nitrogen adsorption/desorption isotherms of CMTN and TiO_2 precursor, (B) ZP vs. pH for CMTN. S2. The optimization of various parameters such as A) time, B) pH and C) stirring rate on adsorption of MB and response peak by CMTN/GCE. S3. Investigation of optimum conditions for extraction and detection of Pb(II) as (A) time, (B) agitation rate and (C) MB concentration. S4. (A) Cyclic voltammograms of 1×10^{-4} M Pb(II) at GCE/CMTN/MB in various υ(10, 20, 4, 60, 80, 100, 150 and 200 mV s^{-1}). (B) Plot of the anodic and cathodic peak currents versus different υ(GCE/CMTNwas immersed for 4 min in the solution of 1×10^{-6} M MB pH 7.0 for pre-adsorption then rinsed and immersed for 4 min in the solution of 1×10^{-4} M Pb(II) acetate buffer pH 5.0 for adsorption then rinsed and transferred to phosphate buffer solution pH 7.0 for analysis. S5. (A) DPVs of various concentration of Pb(II) (5×10^{-4}, 1×10^{-4}, 5×10^{-5}, 1×10^{-5}, 1×10^{-6} and 1×10^{-7} M) on the surface of GCE/CMTN/MB. υ was 100 mV s^{-1}. (B) Calibration curve under optimum conditions for Pb(II) in the concentration range of 5×10^{-4} to 1×10^{-7} M. S6. Investigation of interference effect. This material is 718 KB in size.

Digital Object Identifier 10.1109/JSEN.2018.2871437

I. Introduction

THE demand for environmental monitoring has encouraged researchers to investigate efficient methods to detect trace and ultra-trace amounts of organic and inorganic pollutants in water samples such as waste water, ground water and surface waters [1]. Among water pollutants, dyes and heavy metal ions have been concerned extensively due to their neglecting will cause severe damage on nature as well as human health and hygiene [2].

Among industrial dyes, methylene blue (MB) as a cationic organic dye is commonly applied in textile industry [1]. The released MB-containing wastewaters into aquatic environment causes harmful impacts on humans such as increasing heart rate, vomiting, shock, Heinz body formation, cyanosis, jaundice, quadriplegia and tissue necrosis [1]. On the other hand, MB demonstrates an effective role in various areas of medicine, biology and chemistry. As a biological stain [3], as a redox mediator for facilitating the process of the electron transfer in electrocatalytic and biological systems [4], [5], as a bio-label for electrochemical marking due to its well-defined redox peaks [6] and MB has been utilized in fabrication of electrochemical sensors due to its interesting electrocatalytic and adsorption properties [5]–[7]. A few analytical methods have been reported for determination of MB using techniques such as ultraviolet-visible spectroscopy [8], [9], liquid chromatography tandem mass spectrometry [10], capillary electrophoresis [11] and surfaces-enhanced Raman spectroscopy [12]. MB has been determined by voltammetric methods using nafion stabilized ibuprofen derived gold nanoparticles electrode [13], gold electrode [14] and thiol functionalized clay modified carbon paste electrode [15].

Among the different hazardous environmental contaminates, monitoring of heavy metals especially lead (Pb(II)) in water resources has been considered remarkably due to the high affinity of Pb(II) to accumulate in environmental matrices and living organism which has severe influence on immune, nervous, reproductive and gastrointestinal systems [16]. Various sensitive techniques have been improved for monitoring of Pb(II), such as; atomic absorption spectroscopy (AAS) [17], flame atomic absorption spectroscopy (FAAS) [18], inductively coupled plasma mass spectroscopy (ICP-MS) [19] and inductively couple plasma optical emission spectroscopy (ICP-OES) [20]. However, these techniques are mostly concerned as expensive methods, which are time consuming,

1558-1748 © 2018 IEEE. Personal use is permitted, but republication/redistribution requires IEEE permission.
See http://www.ieee.org/publications_standards/publications/rights/index.html for more information.

solvent consuming and need expert operators. On the other hand, the electrochemical methods are ecofriendly, easy to use, portable and fast response. Advantages of electrochemical methods to other methods have motivated researchers to employ them to detect trace amounts of Pb(II) in effluents and drinking water samples. Various working electrodes has been used to determine Pb(II) including mercury-based electrodes [21]–[24], chemically modified glassy carbon electrodes [25], [26], modified carbon paste electrodes [27], [28], bismuth film electrodes [29], [30] and modified gold electrodes [31]. It is of importance to detect metals and dyes simultaneously due to their potential coexistence. Beyond that coexist metals and dyes in industrial wastewater and synergistic environmental is hazardous and has an important ecological impact on ecosystems due to their strong toxicity, environmental persistence, and bioaccumulation that why is needed to consider detection of both contaminants [32]. One suggested approach is to fabricate an efficient working electrode with high sensitivity, simplicity and environmentally friendly characteristics to detect both of these contaminants in water samples.

Titanium dioxide (TiO_2) is an active semiconductor material in chemical reactions. Numerous advantages of TiO_2 is rooted from its chemically stable, inexpensive, availability, biocompatibility, active in reactions and nontoxic nature [33], [34] which leading to high potential in various applications, such as; antibacterial coating [35], paper industry [36], gas filtration [37], water treatment [38], solar cell [39] and electroanalysis as an electrode modifier [40].

Modification of TiO_2 with various materials is an efficient way to enhance the performance of TiO_2. Among different modifiers, carbon structures such as graphen [41] and carbon nanotubes [42] have been reported as effective materials to achieve excellent electrochemical catalytic performance [43] and to promote the capacity of TiO_2 for dye adsorption [44]. The idea of modifying porous structure of TiO_2 with carbon for ascending surface area of TiO_2 and adsorption capacity encouraged us to synthesis inexpensive and practical CMTN just by simple and low cost method of ethanol carbonization and to employ CMTN in electrochemistry.

Here, we applied the synthesized CMTN to modify the surface of glassy carbon electrode (GCE) for fabricating GCE/CMTN to detect trace amount cationic MB by using voltammetric methods. The applicability of GCE/CMTN was investigated toward determination of MB by cyclic voltammetric method. MB has been known as an efficient modifier in fabrication of various chemically modified carbon-based electrodes due to its remarkable electrocatalytic behavior, which provide a smooth and fast charge transfer between electrode surface and target analyst. Surface of carbon-based electrodes can be modified with MB solely or its combination with conducting nano-materials support such as graphene [45] and multi walled carbon nanotubes [46] and other porous nano structures such as titanate nanotubes [47]. These conducting nano materials immobilized MB on the electrode surface efficiently and improved the electrochemical performance of MB modified electrodes, MB layer stability and MB catalytic activity. For example; high molecular interaction of graphene and MB causing better adsorption and quick charge transport among them, which increased the efficiently of the modified electrode in the detection of lead [48]. In addition, MB in DNAzyme-gold electrode played an effective role in electron transport in presence of lead ion [49].

MB as a strong electron mediator was applied successfully in determination of various analyts such as lead and cadmium [48], [49], folic acid [45], maltol [50], uric acid and dopamine [46], [51].

The porous structure of CMTN with high-specific surface area resulting higher electrostatic interaction of cationic MB with negative surface of the CMTN and fast charge transport, which made CMTN, an ideal support for immobilizing MB and improving its catalytic activity. The MB modified GCE/CMTN was prepared and its application in the determination of Pb(II) investigated successfully. To the best of our knowledge, no study involving GCE/CMTN for determining MB and Pb(II) has been reported.

II. Experimental

A. Chemicals

They are in detail in Supplementary data.

B. Apparatus

They are in detail in Supplementary data.

C. Procedure I: Synthesis CMTN

The CMTN was fabricated by adapting the method reported by Jafari *et al.* [44]. In this method, 1.0 g of TiO_2 was heated up to the 200 °C for 40 min in a porcelain boat with a pipe furnace under the ethanol gas atmosphere and was kept at that temperature for 1 h. The applied ethanol vapor was provided by bubbling pure argon through ethanol at room temperature.

D. Procedure II: Preparation of GCE/CMTN

The GCE was polished with wet alumina paste with particle diameter of 0.3 μm and then with 0.05 μm followed by rinsing thoroughly with ultra-pure water and dried with nitrogen gas. A stable suspension of CMTN containing 1.0 mg/ml in acetonitrile using 30 min ultrasonic agitation was prepared. 5.0 μL of this suspension was casted on the pretreated GCE surface and dried in the air to evaporate solvent. The obtained modified GCE was characterized by SEM and EIS techniques.

E. Procedure III: Extraction of MB From Aqueous Media Onto the Surface of GCE/CMTN

The adsorption of MB was performed onto the surface of GCE/CMTN in 25 mL phosphate buffer solution pH 7.0 with appropriate amount of MB. The volume of adsorption solution was kept constant in all experiments. Regarding the adsorption time, the stirrer was turned off and GCE/CMTN was removed from the adsorption cell, rinsed with ultra-pure water and moved into the voltammetric cell containing phosphate buffer solution pH 7.0.

The oxidation potentials of target analyts were studied by CV and DPV methods. Regarding oxidation potentials of MB (−345 mV vs. SCE) and Pb(II) (−345 mV vs. SCE), the potential window of −0.75V – +0.75V was the best choice to demonstrate well defined CVs or DPVs.

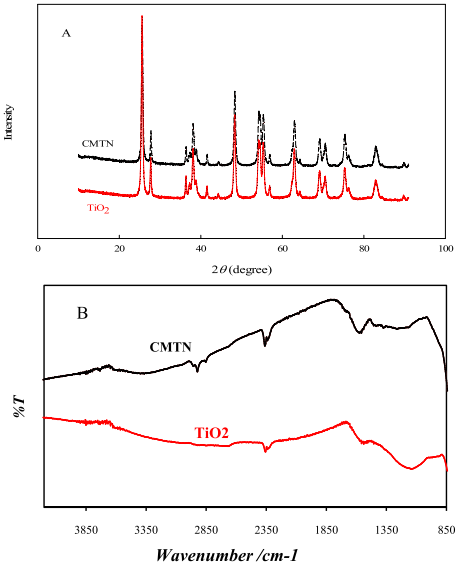

Fig. 1. (A) XRD patterns of CMTN and TiO2 precursor, (B) FTIR spectra of CMTN and TiO2 precursor.

So, voltammograms were recorded in the potential range of −0.75 to +0.75 V vs. SCE. All the measurements were performed in optimized conditions.

F. Procedure IV: Extraction of Pb(II) From Aqueous Media Onto the Surface of Pre-Adsorbed MBGCE/CMTN

The GCE/CMTN was placed into the 1×10^{-6} M MB in phosphate buffer solution pH 7.0 and stirred for 4 min. The GCE/CMTN was removed from the MB solution and rinsed with ultra-pure water. Then, the GCE/CMTN with pre-adsorbed MB on its surface was placed into the appropriate amount of Pb(II) in acetate buffer solution pH 5.0 and agitated for 4 min. Then, GCE/CMTN was transferred from the adsorption cell to the voltammetric cell containing phosphate buffer solution pH 7.0 and the voltammograms were recorded in the potential range of −0.75 to +0.75 V vs. SCE.

III. Results and Discussion

A. CMTN Characterization

Crystalline phases of TiO_2 precursor and CMTN were studied by XRD technique. It is obvious that modification with carbon didn't effect on crystalline phase and no phase transition happened (Figure 1A). The FTIR spectra of the TiO_2 precursor and CMTN are shown in Figure 1B. Appearing of a new peak related to methyl group in the range of 2850–3000 cm^{-1} confirms existence of carbon in CMTN. N_2 adsorption/desorption isotherms were applied to evaluate textural properties and surface area of CMTN, the obtained results confirmed that the total surface area of CMTN was enhanced compared with TiO_2 precursor (Supplementary data S1A).

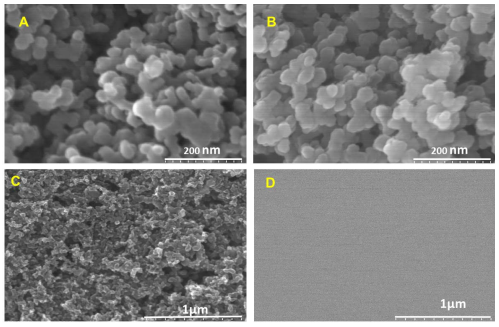

Fig. 2. SEM images of (A) TiO2, (B) CMTN, (C) GCE/CMTN and (D) GCE.

TABLE I
TEXTURAL PROPERTIES OF TiO_2 AND CMTN

Adsorbent	S_{BET} (m^2/g)	V_{total} $_{0.95}$ (cm^3/g)	$V_{mikro\ DR}$ (cm^3/g)	V_{mezo} (cm^3/g)
TiO_2	44.000	0.016	0.016	0.004
CMTN	51.250	0.712	0.032	0.680

Zeta potential (*ZP*) was investigated to characterize the surface charge of CMTN and its variation with pH. Studying the influence of pH on *ZP* reveals the role of pH in adsorption step better. The pH at the point of zero charge (pH_{PZC}) for CMTN was evaluated to be at pH 6.53 (Supplementary data S1B). The adsorbent surface possessed a negative charge at pH more than pH_{PZC}, while the surface charge is positive at pH less than pH_{PZC} [44]. It can be predicted, there is a highly strong electrostatic interaction between MB that is positive and negative surface of the CMTN, resulting in maximum adsorption efficiency in pHs higher than pH_{PZC} of 6.53.

The surface morphology of the TiO_2 precursor, CMTN and GCE/CMTN were investigated by SEM. The SEM image of the CMTN powder (Figure 2B) demonstrated a nano-sized porous structure as well as TiO_2 precursor (Figure 2A). The particles size of TiO_2 precursor and CMTN are about 3050 nm radiuses. Figure 2C and Figure 2D demonstrated SEM images of GCE/CMTN and bare GCE, the deposition of CMTN suspension on the surface of GCE established a rough surface with porous structure to develop the surface area and the adsorption capacity of GCE/CMTN for higher sensing performance in voltammetric studies.

B. Voltammetric Studies of MB on the Surface of GCE/CMTN

The performance of GCE/CMTN in detection of MB was investigated by using cyclic voltammtry. This experiment was performed by immersing GCE/CMTN into MB solution for 4 min and then rinsed and moved into phosphate buffer solution pH 7.0 for cyclic voltammetry measurement (Figure 3). The observed enhancement of signal at GCE/CMTN (solid line) compare to the signal at bare GCE (dash-dotted line) under the similar experiment conditions can be related to the ability of CMTN to adsorb MB because of more porosity and surface area. It can be concluded that CMTN performed well as a modifier for improving the efficiency of GCE.

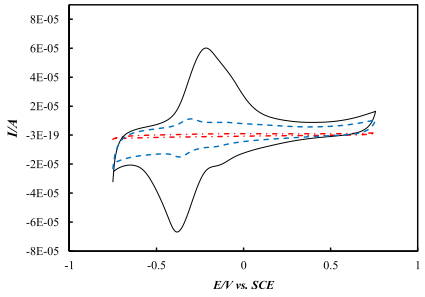

Fig. 3. Cyclic voltammograms of 0.1 mM MB in buffer solution pH 7.0 on the surface of GCE/CMTN (solid line) and bare GCE (dotted line). Scan rate was 100 mV s^{-1}.

In addition, the voltammetric signal for the pre-adsorbed MB was much higher than the voltammetric signal of MB in solution (dashed-line) that shows MB can be adsorb at the surface of GCE/MCTN effectively.

C. The Optimization of Pre-Adsorption of MB on the Surface of GCE/CMTN

The influence of various parameters such as time, pH and stirring rate on the peak current of MB were investigated and optimized to achieve the best conditions to determine MB (Supplementary S2). Effect of different adsorption times 2, 4, 6, 10, 15 min were studied and the maximum peak current was obtained at 4 min. The adsorption process was developed by increasing time and after 4 min all binding site were occupied by MB. Thus, the adsorption time of 4 min was employed for further measurements. The effect of pH on adsorption efficiency as an effective parameter was studied in the range of pH 2.0-9.0. The best pH for adsorption was achieved in 0.1 M phosphate buffer solution pH 7.0. Regarding *ZP* investigation in pH 7.0, the surface charge of CMTN was evaluated to be negative. Therefore, there was a highly strong electrostatic interaction between MB that is positive and negative surface of the CMTN, resulting easier moving of MB to the surface of the GCE/CMTN in pHs higher than pH_{PZC} of 6.53. Agitation demonstrated a definite impact on mass transfer process and extraction. So, effect of agitation rates of 250, 500, 750 and 1000 rpm were studied and the best signal was obtained for 1000 rpm.

D. Voltammetric Results of MB on the Surface of GCE/CMTN

The impact of pH on the cyclic voltammetric responses of pre-adsorbed MB on the surface of GCE/CMTN was investigated in different buffer solutions pHs 2.0-9.0 in voltammetric cell (Figure 4). The best well-defined signal was obtained at pH 7.0. The smaller anodic and cathodic peak currents and appearance of peak shoulder in lower pHs were attributed to the weaker electrostatic interactions of MB and CMTN (regarding CMTN *ZP*). When the pH of solution decreased the surface charge of GCE/CMTN changed and MB molecules lost on GCE/CMTN surface and leaked into the voltammetric

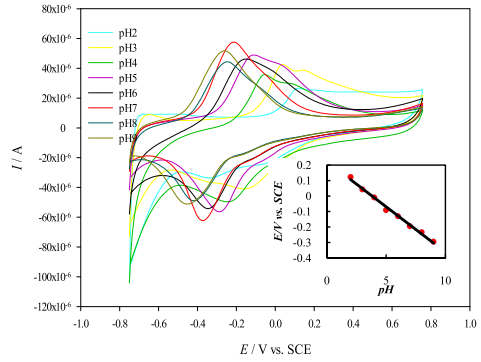

Fig. 4. Variation of anodic peak current vs. various pHs, Inset: variation of anodic peak potential vs. various pHs. GCE/CMTN immersed into the solution of 1×10^{-4}M MB pH 7.0 then rinsed and moved to phosphate buffer solutions pH 2.0, 3.0, 6.0, 7.0, 8.0, 9.0 and acetate buffer solutions pH 4.0 and 5.0 for cyclic voltammetry measurement, Scan rate was 100 mV s^{-1}.

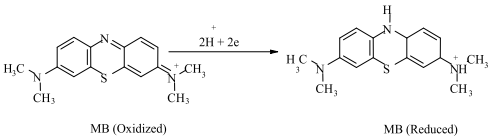

Scheme 1. Proposed mechanism for MB oxidation.

solution, which effected on the stability of adsorbed MB on the GCE/CMTN, the electrocatalytic activity and efficiently of the modified electrode significantly [47]. This study demonstrated well the pH dependency performance of the pre-adsorbed MB on the GCE/CMTN. So, further voltammetric measurements were examined in phosphate buffer solution pH 7.0 to gain best response.

Study of pH dependency of the oxidation/reduction peak potential indicated a negative shift by increasing the pH of buffer solutions. This behavior demonstrated that H^+ performs in both sides of MB correspond to Scheme 1. Regarding the resulted slope from Equation 1, participation of two protons and two electrons were expected for MB oxidation/reduction mechanism (Figure 4 Inset) [5].

$$E_{p,a}/\mathrm{V} = -0.0584(\pm0.002)\ \mathrm{pH} + 0.223(\pm0.012) \quad (R^2 = 0.993) \qquad (1)$$

Figure 5 demonstrated the effect of various scan rates (υ) on the peak current of pre-adsorbed MB on the surface of GCE/CMTN in phosphate buffer solution pH 7.0. The cathodic and anodic peak currents were linearly associated to υ that suggested an adsorption-controlled mechanism for MB oxidation/reduction on the surface of GCE/CMTN (Figure 5 inset). The following equations were obtained for anodic and cathodic peak currents versus υ.

$$I_{\mathrm{p,a}}/\mu\mathrm{A} = 5.89(\pm1.83) + (400(\pm17.88)\upsilon/(\mathrm{Vs}^{-1})), \quad (R^2 = 0.988) \qquad (2)$$

$$I_{\mathrm{p,c}}/\mu\mathrm{A} = -8.34(\pm1.91) - (439(\pm18.66)\upsilon/(\mathrm{Vs}^{-1})), \quad (R^2 = 0.989) \qquad (3)$$

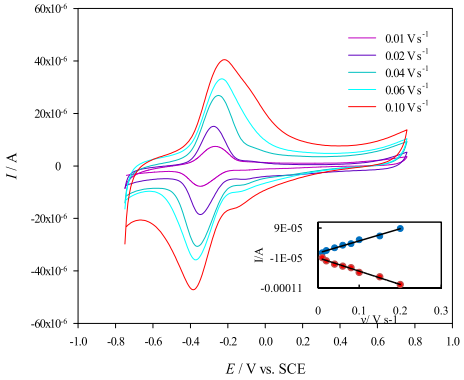

Fig. 5. Cyclic voltammograms of pre-adsorbed MB in various υ (10, 20, 40, 60, 80 and 100 mVs-1) Inset: Plot of the anodic and cathodic peak currents vs. different υ at GCE/CMTN. (GCE/CMTN. immersed for 4 min in 1×10^{-4} M MB pH 7.0 solution for pre-adsorption then rinsed and moved in phosphate buffer solution pH 7.0 for voltammetric analysis).

E. Analytical Measurements of MB

The performance of the GCE/CMTN toward various concentration of MB during the adsorption step was investigated by employing differential pulse voltammetry (DPV) as a sensitive electrochemical method under the optimum conditions. DPV measurements were performed in 0.1 M phosphate buffer solution of pH 7.0 as a supporting electrolyte (Figure 6A). By increasing of MB concentration, the peak current enhanced linearly. The peak current was proportional to the MB concentration in range of 1.0×10^{-8}–1.0×10^{-5} M with slop of 0.407 μA/μM and a correlation coefficient (R^2) of 0.993. The detection limit for MB determination was evaluated 3×10^{-9} M (Figure 6B). The obtained results were compared with some previous electrochemical methods in MB detection. The presented GCE/CMTN determined MB in the wider dynamic linear range with better limit of detection (Table 2).

$$I/\mu\text{A} = 1.76(\pm 0.08) + (0.407(\pm 0.017)\text{C}), \quad (\text{R}^2 = 0.993, \text{C is in } \mu\text{M}) \qquad (4)$$

F. Extraction and Voltammetric Studies of Pb(II) With Pre-Adsorbed MB on the Surface of GCE/CMTN

The efficiency of GCE/CMTN in extraction and detection of Pb(II) in presence and absent of pre-adsorbed MB on the surface of GCE/CMTN was studied by using voltammetric method in clean phosphate buffer solution pH 7.0. MB can act as an efficient electron mediator and shows excellent electrocatalytic activities in many electrochemical reactions [45], [46], [48]. The lone pare of nitrogen on methylene blue can coordinate with Pb^{2+} and extract it from solution, in addition, there is electrocatalytic effect of MB as an electron mediator. It also can be seen from Fig. 7 that the oxidation peak current corresponding to the two species at the MB/CMNT/GCE almost increase paring to the responses

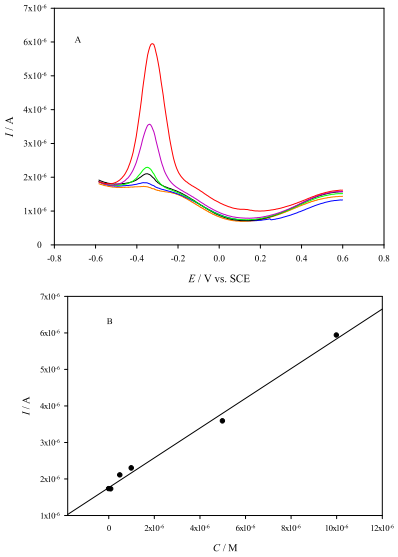

Fig. 6. (A) In DPVs of pre-adsorption measurements, GCE/CMTN immersed for 4 min in the solution of various concentration of MB (1×10^{-5}, 5×10^{-6}, 1×10^{-6}, 5×10^{-7}, 1×10^{-7} and 1×10^{-8} M), phosphate buffer pH 7.0 then rinsed and moved in clean phosphate buffer solution pH 7.0 for voltammetric analysis, υ was 100 mV s^{-1} (B) Calibration curve under optimum conditions for MB in range of 1.0×10^{-5}–1.0×10^{-8} M.

TABLE II
COMPARISON ELECTROCHEMICAL METHODS THAT PREVIOUSLY APPLIED FOR THE DETERMINATION OF MB

Electrode	Modifier	DLR (M)	LOD (M)	Method	Reference
Gold Electrode	–	0.2×10^{-6}-10.0×10^{-6}	–	CV[a]	[14]
CPE [b]	Thiol functionalized-clay	1.0×10^{-6}_ 14.0×10^{-6}	4.0×10^{-6}	CV	[15]
CPE	Ibuprofen coated gold	1.0×10^{-8}_-1.1×10^{-6}	3.9×10^{-9}	DPV[c]	[13]
GCE[d]	nanoparticles CMTN	1.0×10^{-8} -1.0×10^{-5}	3.0×10^{-9}	DPV	This work

[a]Cyclic voltammetry
[b]Carbon paste electrode
[c] Differential pulse voltammetry
[d] Glassy carbon electrode

at the CMNT/GCE and the MB/GCE, showing better catalytic effect. This may be attributed to the supramolecular interaction between CMNT and the phenothiazine ring in methylene blue through π–π interactions, resulting strong adsorption and fast electron transfer rate between them. The synergized effect of

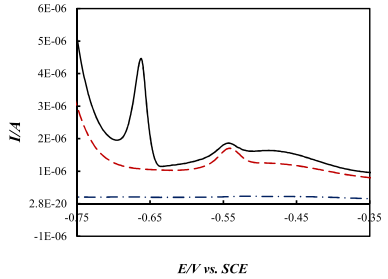

Fig. 7. DPVs of pre-adsorbed 1×10^{-6}M MB on the surface of GCE/CMTN with Pb(II) adsorption step (solid line) and without Pb(II) adsorption step (dashed line) and DPV of pre-adsorbed MB on the surface of bare GCE with Pb(II) adsorption step (dash-dotted line). The working electrode was immersed for 4 min in the solution of 1×10^{-6}M MB pH 7.0 for pre-adsorption then rinsed and immersed for 4 min in the solution of 1×10^{-4}M Pb(II) acetate buffer pH 5.0 for adsorption then rinsed and transferred in phosphate buffer solution pH 7.0 for analysis under optimum conditions. υ was 100 mV s^{-1}.

MB and CMNT makes the catalysis and the electron transfer much more efficient. The reaction mechanism of Pb^{2+} at the electrode surface can be described as shown in Scheme:

(Pb^{2+}) solution + (Modifier) surface ⟶ (Pb^{2+}-Modifier) adsorption (the extraction stage)
(Pb^{2+}–Modifier) adsorption+ 2e⟶(Pb –Modifier) adsorption (the reduction stage)
(Pb –Modifier) adsorption⟶(Pb^{2+}) solution+ (Modifier) surface + 2e (the stripping stage).

The experiment was performed by immersing working electrode for 4 min into MB solution for adsorption of MB then the pre-adsorbed MB on the surface of GCE/CMTN rinsed and immersed for 4 min into the solution of Pb(II) with pH 5.0 for extraction of Pb(II) then rinsed and transferred into clean phosphate buffer solution pH 7.0 for voltammetric analysis at bare GCE (dotted line) and at GCE/CMTN (solid line) under optimum conditions. The appearance of sharp and well-defined peaks at GCE/CMTN indicated high performance of GCE/CMTN compared to bare GCE in detection of Pb(II) and MB significantly.

Voltammograms of pre-adsorbed MB on the surface of GCE/CMTN without Pb(II) adsorption step (dashed line) and with Pb(II) adsorption step (solid line) and the voltammogram of pre-adsorbed Pb(II) on the surface of bare GCE (dash-dotted line) were shown in Figure7. The voltammogram of pre-adsorbed MB on the surface of GCE/CMTN without Pb(II) adsorption step demonstrated an oxidation peak at the potential of −345 mV vs. SCE (I = 0.745 μA) (dashed line). In presence of Pb(II) adsorption step, a new oxidation peak related to Pb(II) was observed at the potential of −653 mV vs. SCE (I = 3.20 μA) and the peak current of MB decreased (I = 0.538 μA) (solid line). MB on the surface of GCE/CMTN played a part in improving the rate of electron transfer in detection of Pb(II).

Some parameters such as pH, time, agitation rate and MB concentration were studied to acquire the optimum conditions for extraction and detection of Pb(II) (Supplementary data S3). The effect of pH on adsorption of Pb(II) was investigated. The peak current rose with increasing pH values and the best response was gained at pH 5.0. At higher pH, Pb(II) precipitated in the form of $Pb(OH)_2$ and the peak current decreased. So, the pH 5.0 was selected as an optimum pH for adsorption of Pb(II). Different extraction times 2, 4, 6, 10, 15 min were studied. Adsorption process proceeded with increasing time and the response signal was enhanced. However, after 4 min, the peak current started descending. Thus, an adsorption time of 4 min was chose. Agitation rates of 250, 500, 750 and 1000 rpm were studied; the best signal was gained for 1000 rpm. Effect of MB concentration on the peak current of Pb(II) was examined. The best anodic peak current was gained for 1.0 μM MB that was employed for further measurements. The pre-adsorbed MB on the surface of GCE/CMTN (GCE/CMTN/MB) was applied in the detection of Pb(II). The cyclic voltammetric studies for adsorbed Pb(II) in optimized conditions were performed with GCE/CMTN/MB in a buffered solution of pH 7.0 at different υ (Supplementary data S4A). As can be seen in Supplementary data S4B, the peak currents are related to the υ linearly in the range of 10–200 mV s^{-1}. The equations for anodic and cathodic peak current versus υ are:

$$I_{p,a}/\mu A = -0.49(\pm0.311) + (46.4(\pm2.79)\upsilon/(Vs-1)) \quad (R^2 = 0.990) \qquad (5)$$

$$I_{p,c}/\mu A = -0.0230(\pm0.232) - (58.7(\pm2.90)\upsilon/(Vs-1)) \quad (R^2 = 0.998) \qquad (6)$$

G. Analytical Measurements of Pb(II) at GCE/CMTN/MB

DPV was employed as a sensitive method to detect low values of Pb(II). DPV measurements were performed by immersing GCE/CMTN/MB into the solution of various concentrations of Pb(II) under optimum conditions. The consistent increase of peak current of Pb(II) and decrease of peak current of MB by raising the concentration of Pb(II) was observed (Supplementary data S5A). The calibration curve of peak current versus Pb(II) concentration was shown in Supplementary data S5B. The linear calibration curve was obtained for Pb(II) in the range of 5×10^{-4} to 1×10^{-7} M with a slope of 0.00297 μA/μM and a correlation coefficient (R^2) of 0.994. The detection limit for determination Pb(II) was calculated to be 3.0×10^{-8} M (for S/N=3).

$$I/\mu A = 1.73(\pm0.022) + (0.297\times10^{-2}(\pm0.0001)C) \quad (R^2 = 0.994, C \text{ is in } \mu M) \qquad (7)$$

The performance of some modified carbon based electrodes that they have been applied for detecting of Pb(II) were listed in Table 3. In present investigation, GCE/CMTN/MB as a high performance, low cost and environmentally friendly working electrode was suggested for monitoring of Pb(II) with wide dynamic linear range and good limit of detection.

A standard addition method was employed to investigate the performance of GCE/CMTN/MB in determination of Pb(II) in water samples by using DPV under optimum conditions. First sample was collected from tap water and was diluted five times. The slope of the calibration curve was estimated 0.00290 μA/μM with a correlation coefficient of (R^2)

TABLE III
COMPARISON OF THE PERFORMANCE OF SOME MODIFIED CARBON BASED ELECTRODES THAT PREVIOUSLY APPLIED FOR THE DETERMINATION OF Pb(II)

Electrode	Modifier	DLR (M)	LOD (M)	Method	Ref.
GCE	PANI/MMT[a]	0.004×10^{-6}–0.1×10^{-6}	0.001×10^{-6}	DPASV[b]	[26]
GCE	Band	0.4×10^{-6}–1.5×10^{-6}	0.169×10^{-6}	SWASV	28]
CPE	Fe_3O_4/rGO[c] TPP[d]	0.3×10^{-6}–20.0×10^{-6}	0.084×10^{-6}	DPASV	[27]
GCE	$MnFe_2O_4$ NC[e]	0.2×10^{-6}–1.1×10^{-6}	0.054×10^{-6}	SWASV	[53]
GC spheres	2- Hyroxy benzoic acid diazonium tetrafluroborate	1.0×10^{-6}–10.0×10^{-6}	0.18×10^{-6}	DPASV	[53]
GCE	5-Br-PADAP[f]/MWCNT	4.34×10^{-9}–5.5×10^{-7}	4.8×10^{-10}	DPASV	[54]
CPE	α- and β-cyclodextrins	1×10^{-5} – 1×10^{-3}	–	DPASV	[55]
CPE	periodic mesoporous organosilica	9.6×10^{-9}–4.8×10^{-7}	2.4×10^{-9}	SWASV	[56]
GCE	siloxane-crown ether polyamide copolymer	9.6×10^{-8}–3.3×10^{-6}	1.69×10^{-8}	DPASV	[57]
GCE	CMTN/MB	1×10^{-7}–5.0×10^{-4}	3.0×10^{-8}	DPV	This work

[a]Na^+–montmorillonites/polyaniline nanocomposite
[b]Differential pulse anodic stripping voltammetry, SWASV: square□wave anodic voltammetry
[c]Band Fe_3O_4 decorated reduced graphene oxide, TPP: Kaolinite clay modified with tripolyphosphate
[d]Kaolinite clay modified with tripolyphosphate
[e] $MnFe_2O_4$ nanocrystal clusters
[f]2-(5-bromo-2-pyridylazo)-5-diethylaminophenol¦2-(5-bromo-2-pyridylazo)-5-diethylaminophenol

0.984 by spiking standard solution of Pb(II) in the range of 5.0×10^{-6} to 5.0×10^{-4} M. Compared with the standard curve, 0.00297 μA/μM, a recovery of 102.41% was evaluated, which rehearsed the efficiency of this method for determination of Pb(II) in real water samples. The other water sample was collected from local lake (Pankalampi, Mikkeli, Finland). Experimental studies indicated that no Pb(II) was observed with GCE/CMTN/MB. The standard addition method was applied for estimating recovery. A recovery of 101.36% was calculated for this study.

The interference impact of coexisting ions on the determination of Pb(II) was studied on the surface of GCE/CMTN/MB by adding different concentrations of interfering ion to the solution 1.0×10^{-5} M Pb(II) in the pre-adsorption step under optimum conditions. Resulting data from the experiments demonstrated that no interference was detected for ions Ni^{2+}, Co^{2+}, a 100-fold excess of Cr^{2+}, Zn^{2+}, a twofold excess of Cu^{2+}, Mg^{2+} and a one fold excess of Cd^{2+} (Supplementary data, S6).

IV. CONCLUSION

GCE/CMTN was fabricated with a simple and low cost method. This modified electrode rehearsed high efficiency in MB detection in the linear range of 1.0×10^{-8} to 1.0×10^{-3} M. Furthermore, the pre-adsorbed MB on GCE/CMTN introduced a novel modified electrode for sensing of trace amounts of Pb(II). Overall, GCE/CMTN is an excellent mercury-free working electrode with good analytical performance and environment friendly characteristics to detect both of these contaminants by profiting from CMTN which enhanced the electrocatalytic performance and adsorption ability significantly. In future, CMTN can be utilized as an electrode material for detecting low concentrations of bio-labels, contaminants and as an efficient and cost-effective adsorbent in water purification systems.

ACKNOWLEDGMENTS

The authors thank Professor Frank Marken for his valuable comments.

REFERENCES

[1] K. V. Kumar and A. Kumaran, "Removal of methylene blue by mango seed kernel powder," *Biochem. Eng. J.*, vol. 27, no. 1, pp. 83–93, 2005.
[2] J. Lin *et al.*, "Adsorption of basic dye from aqueous solution onto fly ash," *J. Environ. Manage.*, vol. 87, no. 1, pp. 193–200, 2008.
[3] D. Moemen, T. Bedir, E. A. Awad, and A. Ellayeh, "Fungal keratitis: Rapid diagnosis using methylene blue stain," *Egyptian J. Basic Appl. Sci.*, vol. 2, no. 4, pp. 289–294, 2015.
[4] M. Ozm, D. E. Lorke, M. Hasan, and G. A. Petroianu, "Cellular and molecular actions of methylene blue in the nervous system," *Medicinal Res. Rev.*, vol. 31, no. 1, pp. 93–117, 2011.
[5] L. E. Korshoj, A. J. Zaitouna, and R. Y. Lai, "Methylene blue-mediated electrocatalytic detection of hexavalent chromium," *Anal. Chem.*, vol. 87, no. 5, pp. 2560–2564, 2015.
[6] R. García-González, A. Costa-García, and M. T. Fernández-Abedul, "Enzymatic amplification-free nucleic acid hybridisation sensing on nanostructured thick-film electrodes by using covalently attached methylene blue," *Talanta*, vol. 142, pp. 11–19, Sep. 2015.
[7] M. Lin, H. Han, D. Pan, H. Zhang, and Z. Su, "Voltammetric determination of total dissolved iron in coastal waters using a glassy carbon electrode modified with reduced graphene oxide, methylene blue and gold nanoparticles," *Microchimica Acta*, vol. 182, nos. 3–4, pp. 805–813, 2015.
[8] N. Bélaz-David *et al.*, "Spectrophotometric determination of methylene blue in biological fluids after ion-pair extraction and evidence of its adsorption on plastic polymers," *Eur. J. Pharmaceutical Sci.*, vol. 5, no. 6, pp. 335–345, 1997.
[9] J. G. Wagner, "A modern view of pharmacokinetics," *J. Pharmacokinetics Biopharmaceutics*, vol. 1, no. 5, pp. 363–401, 1973.
[10] J.-Z. Xu *et al.*, "Determination of methylene blue residues in aquatic products by liquid chromatography-tandem mass spectrometry," *J. Separat. Sci.*, vol. 32, nos. 23–24, pp. 4193–4199, 2009.
[11] H. Borwitzky, W. E. Haefeli, and J. Burhenne, "Analysis of methylene blue in human urine by capillary electrophoresis," *J. Chromatograp. B*, vol. 826, no. 1, pp. 244–251, 2005.
[12] S. H. de Araujo Nicolai *et al.*, "Electrochemical and spectroelectrochemical (SERS) studies of the reduction of methylene blue on a silver electrode," *J. Electroanal. Chem.*, vol. 527, no. 1, pp. 103–111, 2002.
[13] S. S. Hassan *et al.*, "Ultra-trace level electrochemical sensor for methylene blue dye based on nafion stabilized ibuprofen derived gold nanoparticles," *Sens. Actuators B, Chem.*, vol. 208, pp. 320–326, Mar. 2015.
[14] J. Li *et al.*, "Adsorptive and stripping behavior of methylene blue at gold electrodes in the presence of cationic gemini surfactants," *Electrochimica acta*, vol. 51, no. 2, pp. 297–303, 2005.
[15] I. K. Tonlé *et al.*, "Sorption of methylene blue on an organoclay bearing thiol groups and application to electrochemical sensing of the dye," *Talanta*, vol. 74, no. 4, pp. 489–497, 2008.
[16] M. Tüzen, "Determination of heavy metals in soil, mushroom and plant samples by atomic absorption spectrometry," *Microchem. J.*, vol. 74, no. 3, pp. 289–297, 2003.

[17] S. Dadfarnia, A. M. Salmanzadeh, and A. M. H. Shabani, "A novel separation/preconcentration system based on solidification of floating organic drop microextraction for determination of lead by graphite furnace atomic absorption spectrometry," *Analytica Chim. Acta*, vol. 623, no. 2, pp. 163–167, 2008.

[18] E. J. dos Santos *et al.*, "Determination of lead in sediments and sewage sludge by on-line hydride-generation axial-view inductively-coupled plasma optical-emission spectrometry using slurry sampling," *Anal. Bioanal. Chem.*, vol. 388, no. 4, pp. 863–868, 2007.

[19] Z. Y. Wang, Y. D. Su, S. Li, and L. H. Gan, "A flow injection on-line unequal flow complexation preconcentration procedure coupled with flame atomic absorption spectrometry for determination of lead in tap water," *Guang Pu Xue Yu Guang Pu Fen Xi= Guang Pu*, vol. 28, no. 11, pp. 2695–2698, 2008.

[20] J. dos Santos *et al.*, "Simultaneous determination of Pb and Cd in seafood by ICP OES with on-line pre-concentration by solid phase extraction with amberlite XAD-4 after complex formation with DDTP," *Brazilian Arch. Biol. Technol.*, vol. 56, no. 1, pp. 127–134, 2013.

[21] E. Fischer and C. M. van den Berg, "Anodic stripping voltammetry of lead and cadmium using a mercury film electrode and thiocyanate," *Analytica Chim. Acta*, vol. 385, no. 1, pp. 273–280, 1999.

[22] J. A. Rodrigues *et al.*, "Increased sensitivity of anodic stripping voltammetry at the hanging mercury drop electrode by ultracathodic deposition," *Analytica Chim. Acta*, vol. 701, no. 2, pp. 152–156, 2011.

[23] R. Ouyang, Z. Zhu, C. E. Tatum, J. Q. Chambers, and ÄZ.-L. Xue, "Simultaneous stripping detection of Zn (II), Cd (II) and Pb (II) using a bimetallic Hg–Bi/single-walled carbon nanotubes composite electrode," *J. Electroanal. Chem.*, vol. 656, no. 1, pp. 78–84, 2011.

[24] Z. Bi, P. Salaün, and C. M. van den Berg, "Study of bare and mercury-coated vibrated carbon, gold and silver microwire electrodes for the determination of lead and cadmium in seawater by anodic stripping voltammetry," *Electroanalysis*, vol. 25, no. 2, pp. 357–366, 2013.

[25] Y. Dong, Y. Ding, Y. Zhou, J. Chen, and C. Wang, "Differential pulse anodic stripping voltammetric determination of Pb ion at a montmorillonites/polyaniline nanocomposite modified glassy carbon electrode," *J. Electroanal. Chem.*, vols. 717–718, pp. 206–212, Mar. 2014.

[26] Y. Sun *et al.*, "Controlled synthesis various shapes Fe_3O_4 decorated reduced graphene oxide applied in the electrochemical detection," *J. Alloys Compounds*, vol. 638, pp. 182–187, Jul. 2015.

[27] Y. Wang, Y. Wu, J. Xie, and X. Hu, "Metal–organic framework modified carbon paste electrode for lead sensor," *Sens. Actuators B, Chem.*, vol. 177, pp. 1161–1166, Feb. 2013.

[28] Y. Gómezm, L. Fernández, C. Borrás, J. Mostany, and B. Scharifker, "Characterization of a carbon paste electrode modified with tripolyphosphate-modified kaolinite clay for the detection of lead," *Talanta*, vol. 85, no. 3, pp. 1357–1363, 2011.

[29] I. Rutyna and M. Korolczuk, "Determination of lead and cadmium by anodic stripping voltammetry at bismuth film electrodes following double deposition and stripping steps," *Sens. Actuators B, Chem.*, vol. 204, pp. 136–141, Dec. 2014.

[30] C. Kyrisoglou, A. Economou, and C. E. Efstathiou, "Bismuth-coated Iridium microwire electrode for the determination of trace metals by anodic stripping voltammetry," *Electroanalysis*, vol. 24, no. 9, pp. 1825–1832, 2012.

[31] Y. Li *et al.*, "Electrochemical determination of trace lead(II) with enhanced sensitivity and selectivity by three-dimensional nanoporous gold leaf and self-assembled homocysteine monolayer," *J. Electroanal. Chem.*, vol. 758, pp. 78–84, Dec. 2015.

[32] J.-H. Deng, X.-R. Zhang, G.-M. Zeng, J.-L. Gong, Q.-Y. Niu, and J. Liang, "Simultaneous removal of Cd(II) and ionic dyes from aqueous solution using magnetic graphene oxide nanocomposite as an adsorbent," *Chem. Eng. J.*, vol. 226, pp. 189–200, Jun. 2013.

[33] K. Bubacz, B. Tryba, and A. W. Morawski, "The role of adsorption in decomposition of dyes on TiO_2 and N-modified TiO_2 photocatalysts under UV and visible light irradiations," *Mater. Res. Bull.*, vol. 47, no. 11, pp. 3697–3703, 2012.

[34] A. Di Paola *et al.*, "Photocatalytic activity of nanocrystalline TiO_2 (brookite, rutile and brookite-based) powders prepared by thermohydrolysis of $TiCl_4$ in aqueous chloride solutions," *Colloids Surfaces A, Physicochem. Eng. Aspects*, vol. 317, no. 1, pp. 366–376, 2008.

[35] W. Kangwansupamonkon, V. Lauruengtana, S. Surassmo, and U. Ruktanonchai, "Antibacterial effect of apatite-coated titanium dioxide for textiles applications," *Nanomed., Nanotechnol., Biol. Med.*, vol. 5, no. 2, pp. 240–249, 2009.

[36] S. El-Sherbiny, F. Morsy, M. Samir, and O. A. Fouad, "Synthesis, characterization and application of TiO_2 nanopowders as special paper coating pigment," *Appl. Nanosci.*, vol. 4, no. 3, pp. 305–313, 2014.

[37] C.-Y. Lin and C.-S. Li, "Effectiveness of titanium dioxide photocatalyst filters for controlling bioaerosols," *Aerosol Sci. Technol.*, vol. 37, no. 2, pp. 162–170, 2003.

[38] M. Janus, E. Kusiak, and A. W. Morawski, "Carbon modified TiO_2 photocatalyst with enhanced adsorptivity for dyes from water," *Catal. Lett.*, vol. 131, nos. 3–4, pp. 506–511, 2009.

[39] Z. Tian-Hui, P. Ling-Yu, Z. Su-Ling, X. Zheng, W. Qian, and K. Chao, "Application of TiO_2 with different structures in solar cells," *Chin. Phys. B*, vol. 21, no. 11, p. 118401, 2012.

[40] M. G. Hosseini, M. Faraji, and M. M. Momeni, "Application of titanium oxide nanotube films containing gold nanoparticles for the electroanalytical determination of ascorbic acid," *Thin Solid Films*, vol. 519, no. 11, pp. 3457–3461, 2011.

[41] A. A. Ismail, R. A. Geioushy, H. Bouzid, S. A. Al-Sayari, A. Al-Hajry, and D. W. Bahnemann, "TiO_2 decoration of graphene layers for highly efficient photocatalyst: Impact of calcination at different gas atmosphere on photocatalytic efficiency," *Appl. Catal. B, Environ.*, vol. 129, pp. 62–70, Jan. 2013.

[42] U. Caudillo-Flores *et al.*, "Enhanced photocatalytic activity of MWCNT/TiO_2 heterojunction photocatalysts obtained by microwave assisted synthesis," *Catal. Today*, vol. 266, pp. 102–109, May 2016.

[43] F. Mole, J. Wang, D. A. Clayton, C. Xu, and S. Pan, "Highly conductive nanostructured C-TiO_2 electrodes with enhanced electrochemical stability and double layer charge storage capacitance," *Langmuir*, vol. 28, no. 28, pp. 10610–10619, 2012.

[44] S. Jafari, B. Yahyaei, E. Kusiak-Nejman, and M. Sillanpää, "The influence of carbonization temperature on the modification of TiO_2 in the removal of methyl orange from aqueous solution by adsorption," *Desalination Water Treat.*, vol. 57, no. 40, pp. 18825–18835, 2016.

[45] D. Zhang, X. Ouyang, W. Ma, L. Li, and Y. Zhang, "Voltammetric determination of folic acid using adsorption of methylene blue onto electrodeposited of reduced graphene oxide film modified glassy carbon electrode," *Electroanalysis*, vol. 28, no. 2, pp. 312–319, 2016.

[46] S. Yang, G. Li, R. Yang, M. Xia, and L. Qu, "Simultaneous voltammetric detection of dopamine and uric acid in the presence of high concentration of ascorbic acid using multi-walled carbon nanotubes with methylene blue composite film-modified electrode," *J. Solid State Electrochem.*, vol. 15, no. 9, pp. 1909–1918, 2011.

[47] M. Xiao *et al.*, "Electrochemical study of methylene blue/titanate nanotubes nanocomposite and its layer-by-layer assembly multilayer films," *J. Solid State Electrochem.*, vol. 12, no. 9, pp. 1159–1166, 2008.

[48] Y. Xiao, A. A. Rowe, and K. W. Plaxco, "Electrochemical detection of parts-per-billion lead via an electrode-bound DNAzyme assembly," *J. Amer. Chem. Soc.*, vol. 129, no. 2, pp. 262–263, 2007.

[49] M. Chao and X. Ma, "Simultaneous electrocatalytic determination of lead and cadmium ions employing a poly(methylene blue)/graphene modified glassy carbon electrode," *Russian J. Electrochem.*, vol. 51, no. 1, pp. 39–48, 2015.

[50] X. Ma and M. Chao, "Rapid voltammetric determination of maltol in some foods and beverages using a poly(methylene blue)/graphene-modified glassy carbon electrode," *J. Solid State Electrochem.*, vol. 18, no. 3, pp. 621–628, 2014.

[51] C. Liu, J. Hu, J. Hu, and H. Tanga, "Electrocatalytic oxidation of dopamine at a nanocuprous oxide-methylene blue composite glassy carbon electrode," *Electroanalysis*, vol. 18, no. 5, pp. 478–484, 2006.

[52] X.-J. Han *et al.*, "Mesoporous $MnFe_2O_4$ nanocrystal clusters for electrochemistry detection of lead by stripping voltammetry," *J. Electroanal. Chem.*, vol. 755, pp. 203–209, Oct. 2015.

[53] G. K. Raghu, S. Sampath, and M. Pandurangappa, "Chemically functionalized glassy carbon spheres: A new covalent bulk modified composite electrode for the simultaneous determination of lead and cadmium," *J. Solid State Electrochem.*, vol. 16, no. 5, pp. 1953–1963, May 2012.

[54] A. Salmanipour and M. A. Taher, "An electrochemical sensor for stripping analysis of Pb(II) based on multiwalled carbon nanotube functionalized with 5-Br-PADAP," *J. Solid State Electrochem.*, vol. 15, nos. 11–12, pp. 2695–2702, 2011.

[55] G. R. Morales, T. R. Silva, and L. Galicia, "Carbon paste electrodes electrochemically modified with cyclodextrins," *J. Solid State Electrochem.*, vol. 7, no. 6, pp. 355–360, 2003.

[56] S. Morante-Zarcero, D. Pérez-Quintanilla, and I. Sierra, "A disposable electrochemical sensor based on bifunctional periodic mesoporous organosilica for the determination of lead in drinking waters," *J. Solid State Electrochem.*, vol. 19, no. 7, pp. 2117–2127, 2015.
[57] I. M. Simionca, A. Arvinte, R. Ardeleanu, and M. Pinteala, "Siloxane-crown ether polyamide based electrode for electrochemical determination of lead(II) in aqueous solution," *Electroanalysis*, vol. 24, no. 10, pp. 1995–2004, 2012.

Khadijeh Nekoueian is currently pursuing the Ph.D. degree with the Lappeenranta University of Technology in Finland. Her research interests are electrochemistry, nanotechnology, and sensors.

Shila Jafari received the Ph.D. degree from the Lappeenranta University of Technology, Finland, in 2016. Her Ph.D. research dealing with water treatment by adsorption process. Her major field of study was green environmental chemistry via study onto TiO2 roll in water treatment and air purification. In 2014, she visited the West Pomeranian University of Technology, Poland, to work on air purification by photocatalytic systems. In early 2017, she has been involved in Post-Doctoral Research at Aalto University, Finland, and is currently a Research Scientist at VTT, Technical Research Central of Finland. Her research interests are related to corrosion study and the development of environmental sustainability in term of water and ecosystems.

Mandana Amiri received the Ph.D. degree from the Sharif University of Technology, Tehran, Iran, in 2007. She was a Visiting Scientist at the Marken Group, University of Bath, U.K., from 2006 to 2007, supported by British council. She is currently an Associate Professor of Chemistry with the University of Mohaghegh Ardabili, Ardabil, Iran. Her main area of research is nano-materials in electroanalysis. She is a MRSC member. She received the Roger Taylor Award in 2015 from the British Carbon Group.

Mika Sillanpää is a Professor with the Lappeenranta University of Technology, Finland. He has over 20 years of expertise in green chemistry, analytical chemistry, and environmental engineering and has worked extensively with adsorption, photocatalysis, electrochemical treatment, and advanced oxidation processes and environmental analysis. He has published several books and published over 500 internationally refereed scientific papers. Overall, he has more than 700 publications and 20 000 citations to them. He has also established close collaboration with over 80 research partners from the world's leading laboratories across six continents.

ACTA UNIVERSITATIS LAPPEENRANTAENSIS

824. ZAFARI, SAHAR. Segmentation of partially overlapping convex objects in silhouette images. 2018. Diss.

825. MÄLKKI, HELENA. Identifying needs and ways to integrate sustainability into energy degree programmes. 2018. Diss.

826. JUNTUNEN, RAIMO. LCL filter designs for paraller-connected grid inverters. 2018. Diss.

827. RANAEI, SAMIRA. Quantitative approaches for detecting emerging technologies. 2018. Diss.

828. METSO, LASSE. Information-based industrial maintenance - an ecosystem perspective. 2018. Diss.

829. SAREN, ANDREY. Twin boundary dynamics in magnetic shape memory alloy Ni-Mn-Ga five-layered modulated martensite. 2018. Diss.

830. BELONOGOVA, NADEZDA. Active residential customer in a flexible energy system - a methodology to determine the customer behaviour in a multi-objective environment. 2018. Diss.

831. KALLIOLA, SIMO. Modified chitosan nanoparticles at liquid-liquid interface for applications in oil-spill treatment. 2018. Diss.

832. GEYDT, PAVEL. Atomic Force Microscopy of electrical, mechanical and piezo properties of nanowires. 2018. Diss.

833. KARELL, VILLE. Essays on stock market anomalies. 2018. Diss.

834. KURONEN, TONI. Moving object analysis and trajectory processing with applications in human-computer interaction and chemical processes. 2018. Diss.

835. UNT, ANNA. Fiber laser and hybrid welding of T-joint in structural steels. 2018. Diss.

836. KHAKUREL, JAYDEN. Enhancing the adoption of quantified self-tracking wearable devices. 2018. Diss.

837. SOININEN, HANNE. Improving the environmental safety of ash from bioenergy production plants. 2018. Diss.

838. GOLMAEI, SEYEDMOHAMMAD. Novel treatment methods for green liquor dregs and enhancing circular economy in kraft pulp mills. 2018. Diss.

839. GERAMI TEHRANI, MOHAMMAD. Mechanical design guidelines of an electric vehicle powertrain. 2019. Diss.

840. MUSIIENKO, DENYS. Ni-Mn-Ga magnetic shape memory alloy for precise high-speed actuation in micro-magneto-mechanical systems. 2019. Diss.

841. BELIAEVA, TATIANA. Complementarity and contextualization of firm-level strategic orientations. 2019. Diss.

842. EFIMOV-SOINI, NIKOLAI. Ideation stage in computer-aided design. 2019. Diss.

843. BUZUKU, SHQIPE. Enhancement of decision-making in complex organizations: A systems engineering approach. 2019. Diss.

844. SHCHERBACHEVA, ANNA. Agent-based modelling for epidemiological applications. 2019. Diss.

845. YLIJOKI, OSSI. Big data - towards data-driven business. 2019. Diss.

846. KOISTINEN, KATARIINA. Actors in sustainability transitions. 2019. Diss.

847. GRADOV, DMITRY. Experimentally validated numerical modelling of reacting multiphase flows in stirred tank reactors. 2019. Diss.

848. ALMPANOPOULOU, ARGYRO. Knowledge ecosystem formation: an institutional and organisational perspective. 2019. Diss.

849. AMELI, ALIREZA. Supercritical CO2 numerical modelling and turbomachinery design. 2019. Diss.

850. RENEV, IVAN. Automation of the conceptual design process in construction industry using ideas generation techniques. 2019. Diss.

851. AVRAMENKO, ANNA. CFD-based optimization for wind turbine locations in a wind park. 2019. Diss.

852. RISSANEN, TOMMI. Perspectives on business model experimentation in internationalizing high-tech companies. 2019. Diss.

853. HASSANZADEH, AIDIN. Advanced techniques for unsupervised classification of remote sensing hyperspectral images. 2019. Diss.

854. POPOVIC, TAMARA. Quantitative indicators of social sustainability applicable in process systems engineering. 2019. Diss.

855. RAMASAMY, DEEPIKA. Selective recovery of rare earth elements from diluted aqueous streams using N- and O –coordination ligand grafted organic-inorganic hybrid composites. 2019. Diss.

856. IFTEKHAR, SIDRA. Synthesis of hybrid bio-nanocomposites and their application for the removal of rare earth elements from synthetic wastewater. 2019. Diss.

857. HUIKURI, MARKO. Modelling and disturbance compensation of a permanent magnet linear motor with a discontinuous track 2019. Diss.

858. AALTO, MIKA. Agent-based modeling as part of biomass supply system research. 2019. Diss.

859. IVANOVA, TATYANA. Atomic layer deposition of catalytic materials for environmental protection. 2019. Diss.

860. SOKOLOV, ALEXANDER. Pulsed corona discharge for wastewater treatment and modification of organic materials. 2019. Diss.

861. DOSHI, BHAIRAVI. Towards a sustainable valorisation of spilled oil by establishing a green chemistry between a surface active moiety of chitosan and oils. 2019. Diss.

ISBN 978-952-335-394-7
ISBN 978-952-335-395-4 (PDF)
ISSN-L 1456-4491
ISSN 1456-4491
Lappeenranta 2019